METAL BINDING POLYMERS FROM 4-VINYLPYRIDINE BY CONTROLLED RADICAL POLYMERISATION

By

Nurulsaidah Abdul Rahim, M.Sc.

A Thesis Presented at Dublin City University for the Degree of Doctor of Philosophy

Supervisor

Dr. Andreas Heise

Prof. Johannes G. Vos

School of Chemical Sciences

2013

DECLARATION

I hereby certify that this material, which I now submit for assessment on the programme of study leading to the award of Doctor of Philosophy is entirely my own work, that I have exercised reasonable care to ensure that the work is original, and does not to the best of my knowledge breach any law of copyright, and has not been taken from the work of others save and to the extent that such work has been cited and acknowledged within the text of my work.

Signed : _____

Nurulsaidah Abdul Rahim

ID No : 58124691

Date :

Acknowledgement

First and foremost, all praises be to the exalted One, ALLAH the Almighty for giving me the strength to carry out this challenging task. There are many people that I would like to thank for helping me complete this manuscript.

I would like to sincerely express my gratitude to my supervisor, Dr. Andreas Heise, for his great support, supervision, assistance and guidance over the past four years. I also offer deep appreciation to my co-supervisor, Prof Johannes G. Vos for his support and advice in electrochemistry project. I am very grateful for the opportunity to work with him.

The assistance of all the staff in School of Chemical Sciences, Dublin City University is greatly appreciated. I would like to thank Julie, Veronica, Catherine, Ambrose, John and Vincent for the technical support provided. I would also like to convey my thanks to Dr. Brendan Twamley for operating as well as discussing the FeSEM and EDX. I would like to extend my gratitude to Tuzcu Gozde and Martin, who has greatly helped me during my stay at Eindhoven University of Technology (TU/e).

The polymer research group, past and present members, Paul, Fabrice, Jin, Tushar, Zeliha, Claudia, Marcello, Mark, Antonis and Jaco, I highly appreciate all the emotional support, assistance and valuable discussions especially in dealing with stress and work. Dr. Fabrice Audouin is thanked for assistance at the beginning of this study and for the invaluable input he made in this work. Special thanks also to Dr. Yvonne Halphin and Jane for the assistance, guidance and invaluable discussion in electrochemistry.

No amount of words will ever be enough to thank my family in Malaysia for their support and prayer during my stay in Dublin. To my parents, I thank you for the encouragement and love over the years, and for believing in me. To Dzahir, I am glad I have you as a brother, thanks for everything.

Many thanks to my friends: Aida, Aqida, Asnul, Norain, Siti Norhayati, Tuty Asma, Dr. Aida Hanim, Amalina, Raihana, Zulikha, Aisyah, Anis, Hamiza, Azrilawani, Syara, and Husna. Thank you for everything that you have done for me. Indeed, you are my family here. This journey would not have been the same without all of you and the good times

had made things every bit worthwhile. It is really impossible for me to name each of you who has helped me from the very beginning of my journey here, but I sincerely appreciate all of your kind help and attention. May ALLAH bless all of you and grant you with happiness and prosperity.

And last but not least, I would like to thank Ministry of Higher Education Malaysia (SLAB) and Universiti Pendidikan Sultan Idris (UPSI) for the support.

THANK YOU!!!

Abstract

The metal binding ability of poly(4-vinylpyridine) (P4VP) has extensively been explored in various advanced catalytic applications and nanotechnology. The aim of this study was the synthesis of well-controlled polymer structures containing P4VP blocks employing controlled radical polymerisation (CRP) techniques. Initial results confirmed that atom transfer radical polymerisation (ATRP) can successfully be used in the synthesis of poly(4VP-*b*-MMA) block copolymers but significant interference of the 4-vinylpyridine (4VP) monomer with the catalytic ATRP metal ions hampers the practical applicability of this technique. Better results were obtained with nitroxide-mediated polymerisation (NMP) using BlocBuilder MAMA-SG1 as a commercial initiator/mediator. In these reactions P4VP were used as macroinitiators and chain extended to form poly(4-vinylpyridine-*b*-methyl methacrylate), poly(4VP-*b*-MMA) and poly(4-vinylpyridine-*b*-(methyl methacrylate-*co*-styrene)), P4VP-*b*-P(MMA-*co*-S) block copolymers. The controlled character of the polymerisation was confirmed by kinetic measurements and the linear increase of the molar mass with monomer conversion. These block copolymer spontaneously self-assemble into spherical inverse micelles and could be loaded with copper(II)acetate. Star polymers were synthesised by multiple arm initiators for both polymerisation techniques. New star initiator based on the JEFFAMINE® and dendrimer functionalised with SG1 were introduced. P4VP as supporting catalyst of cobalt(II)hexadecafluorophthalocyanine ($CoPcF_{16}$) was investigated by electrochemistry methods for hydrogen evolution. The interactions between P4VP and $CoPcF_{16}$ in solution were examined *via* UV spectroscopy. It was found that P4VP/$CoPcF_{16}$ produced more H_2 compare to $CoPcF_{16}$ at low overpotential in pH 2 phosphate buffer aqueous solution at glassy carbon electrode under argon atmosphere.

Publication

Nurulsaidah Abdul Rahim, Fabrice Audouin, Brendan Twamley, Johannes G Vos, Andreas Heise, *Synthesis of poly(4-vinyl pyridine-b-methyl methacrylate) by MAMA-SG1 initiated sequential polymerisation and formation of metal loaded block copolymer inverse micelles*, European Polymer Journal 2012;48:990-996

Posters

Nurulsaidah Abdul Rahim, Fabrice Audouin, Johannes G Vos, Andreas Heise, *New synthetic approach and characterization of poly(4-vinylpyridine) through nitroxide-mediated polymerisation*, MACRO Group UK Young Research Meeting 2010, Nottingham UK, April 2010.

Nurulsaidah Abdul Rahim, Fabrice Audouin, Johannes G Vos, Andreas Heise, *Amphiphilic poly(4-vinylpyridine-b-methyl methacrylate) block copolymers for metal binding application*, European Polymer Congress 2011, Granada Spain, June 2011.

Nurulsaidah Abdul Rahim, Fabrice Audouin, Johannes G Vos, Andreas Heise, *Amphiphilic poly(4-vinylpyridine-b-methyl methacrylate) block copolymers for metal binding application*, MACRO Group UK International Conference of Polymer Synthesis and UKPFC International Conference of Colloids 2012, Warwwick UK, July 2012.

Abbreviation

4VP	4-vinylpyridine
A	Ampere
Ag/AgCl	Silver/silver chloride
ATRP	Atom Transfer Radical Polymerisation
BA	*n*-butyl acrylate
CO_2	Carbon dioxide
CRP	Controlled radical polymerisation
CV	Cyclic voltammetry
$CoPcF_{16}$	Cobalt(II) hexadecafluorophtalocyanine
DMF	Dimethylformamide
DLS	Dynamic light scattering
EBiB	Ethyl 2-bromoisobutyrate
FTIR	Fourier transform infrared
FRP	Free radical polymerisation
GC	Glassy carbon electrode
H_2	Hydrogen
HMTETA	1,1,4,7,10,10-hexamethyltriethylenetetramine
J	Current density
MAMA-SG1	2-({tert-butyl[[1-(diethoxyphosphoryl)-2,2-dimethylpropyl]amino}oxy)-2-methylpropanoic acid
MALS	Multi angle light scattering
Me_6TREN	Tris[2-(dimethylamino)ethyl]amine
MMA	Methyl methacrylate
NMP	Nitroxide mediated polymerisation
NMR	Nuclear magnetic resonance
O_2	Oxygen
Pc	Phthalocyanine
P4VP	Poly 4-vinylpyridine

PBA	Poly butyl acrylate
PMMA	Poly methyl methacrylate
PPI	Polypropylene imine
PT-Br	Pentaerythritol tetrakis (2-bromoisobutyrate)
RAFT	Radical addition fragmentation chain transfer
sPMMA	Star poly methyl methacrylate
SEC	Size exclusion chromatography
SEC	Saturated calomel electrode
SG1	*N*-tert-butyl-*N*-[1-diethylphosphono-(2,2-dimethylpropyl)] nitroxide
SHE	Standard hydrogen electrode
TEMPO	2,2,6,6-tetramethylpiperidinyl-1-oxyl
TIPNO	2,2,5-tri-methyl-4-phenyl-3-azahexane-3-nitroxide
TN	Turnover number
UV-Vis	Ultraviolet-visible spectroscopy
V	Volt

Contents

List of Figures

List of Tables

List of Schemes

1 Introduction

Abstract

Controlled Radical Polymerisation (CRP) methods and the synthesis of the structure of star and block copolymer are discussed. Moreover, several examples of poly(4-vinylpyridine) and its applications as templates for nanoparticles, electrocatalysis, drug delivery and pH responsive material are provided. In addition, an introduction into the theory of electrochemistry is presented.

1.1 Radical Polymerisation

Free radical polymerisation (FRP) is widely used in industry due to its versatility, synthetic ease, compatibility with a wide variety of functional groups, and its tolerance to water and protic media. There are three steps in FRP namely initiation, propagation and termination as illustrated in Scheme 1.1. In FRP, the slow and continuous initiation process, together with the fast propagation results in formation of polymers with a broad molar mass distribution and little control over chain length and chain end functionality. Termination reactions occur *via* coupling of two active radical centres or atomic transfer between active chains (disproportionation). Therefore, in conventional FRP it is essentially impossible to control molecular weight distribution and polymers with well-defined microstructures such as block copolymers.[1]

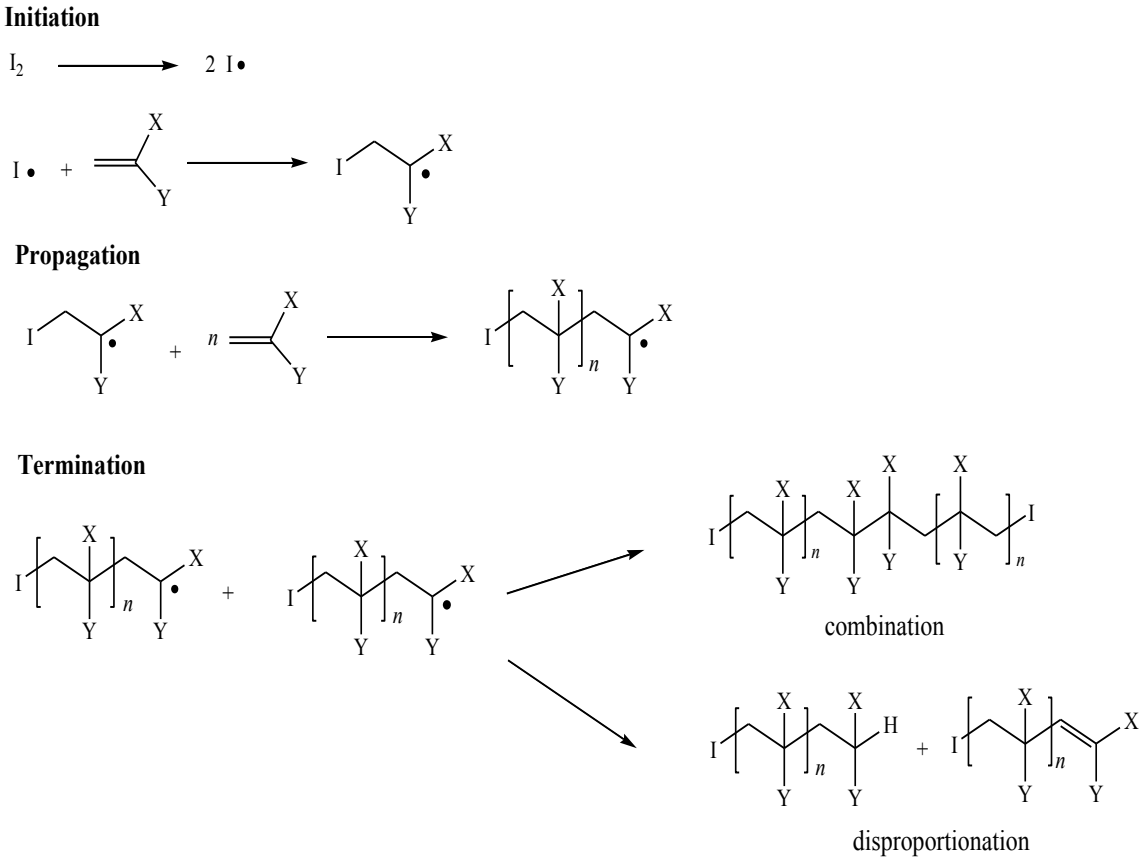

Scheme 1.1: Mechanism of free radical polymerisation.

1.2 Controlled Radical Polymerisation

The discovery of living anionic polymerisation by Michael Szwarc[2] in 1950s opened the possibility to synthesis well-defined polymers in terms of size, functionality and architectures. However, ionic polymerisation techniques are not applicable to the rapid synthesis of a wide variety of functional vinyl monomers. In addition, ionic polymerisation required rigorous exclusion of oxygen and water, ultrapure reagents and solvents.[3,4] Thus, polymer chemist have developed new polymerisation strategies to overcome these limitations and combine the chemical strengths of FRP with a high level of control over polymer composition and architectures. Consequently, controlled radical polymerisation (CRP) became extremely attractive in polymer synthesis and for kinetic studies.[1,3] CRP and FRP proceed *via* the same basic radical mechanism, exhibit similar chemo-, regio-, and stereo- selectivities and can polymerise a similar range of monomers. However, several important differences exist and are summarised in Table 1.1.[3]

Table 1.1: Summary on the differences between radical polymerisation and control radical polymerisation

Free Radical Polymerisation (FRP)	**Controlled Radical Polymerisation (CRP)**
• Continuous initiation and free radical initiator left unconsumed at the end of polymerisation • Almost all chains dead (terminated) during polymerisation • Most propagation are fast • Steady-state radical concentration is established with similar rates of initiation and termination	• Fast initiation and all chain start essentially at the same time • The proportion of dead chains is ≤ 10% • Polymerisations are slow (depend on the target molecular weight) • Steady-state radical concentration is reached by balancing the rates of activation and deactivation, based on persistent radical effect (PRE) • In the early stage, all chains are short but as they become much longer, the termination rate decrease significantly

The mechanisms employed in CRP include catalytic atom transfer represented by atom transfer radical polymerisation (ATRP)[5,6], dissociation-combination represented by nitroxide mediated polymerisation (NMP)[7-9] and degenerative chain transfer represented by radical addition fragmentation chain transfer (RAFT)[10,11] polymerisation. Both NMP and ATRP are controlled by the persistent radical effect (PRE)[12] in which every radical-radical termination leads to an irreversible accumulation of deactivator. The equilibrium shifts towards the dormant species and decreases the probability of termination reactions. The difference between NMP and ATRP is that stoichiometric amounts of mediating agent (*e.g.* nitroxide) are required to cap all dormant chains in the NMP system. In contrast, the amount of transition metal catalyst added to an ATRP can be sub-stoichiometric because the catalytic process in ATRP employs an atom as capping group, which transfers between growing chains and a redox active catalyst.[13] Meanwhile, RAFT not based on the persistent radical effect, is kinetically similar to FRP process with slow initiation and fast termination reaction.[14] General methods for ATRP, NMP and RAFT are shown in Scheme 1.2 and Table 1.2 summarises the advantages and limitations of ATRP, NMP and RAFT.

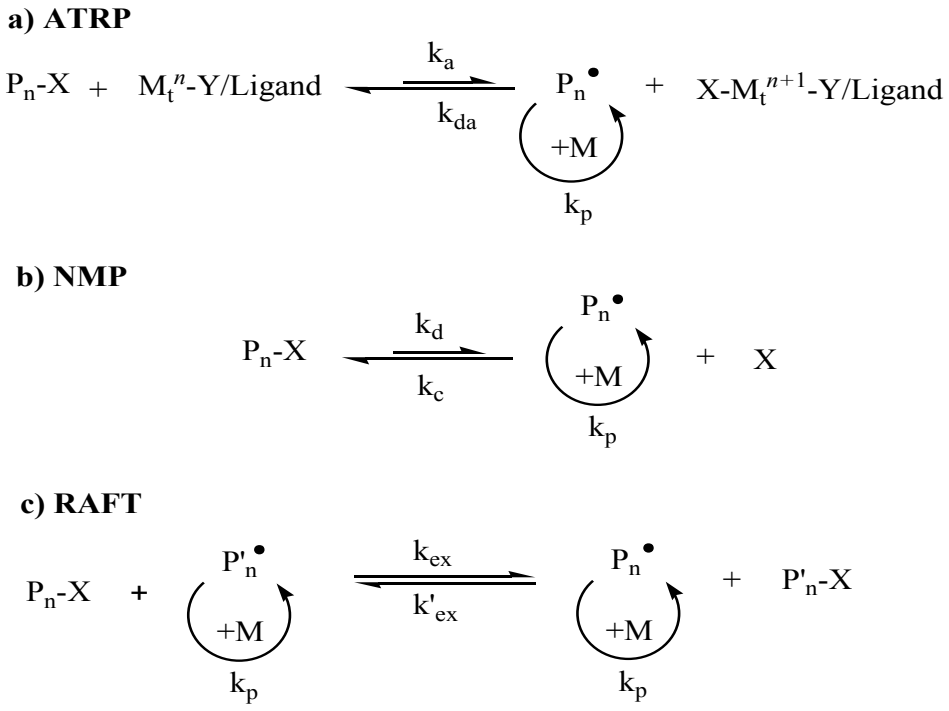

Scheme 1.2: General methods for Atom Transfer Radical Polymerisation (ATRP), Nitroxide Mediated Polymerisation (NMP) and Radical Addition Fragmentation Chain Transfer (RAFT).[5]

Table 1.2: Advantages and limitations of ATRP, NMP and RAFT polymerisations.[15]

	ATRP	**NMP**	**RAFT**
Advantages	• only catalytic amounts of transition metal complexes are necessary • initiator commercially available • large range of monomers (except unprotected acids) • easy end functionalisation • large range of polymerisation temperature	• purely organic system • tolerant to many functional group including acids • commercial initiator under developments	• large range of monomers • minimal perturbation to FRP system • applicable in protic media (emulsion polymerisation)
Limitations	• transition metal catalyst must often be removed • acidic monomer require protection	• relatively expensive moderators must be used in stoichiometric amounts to the chain end • difficult to control polymerisation of disubstituted alkenes such as metacrylates • difficult to introduced end functionality • relatively high temperatures are required	• only some transfer agents are commercially available • dithio ester and other end groups should be removed due to colour, toxicity and potential odour • amine-containing monomers decompose dithio ester • functionalisation is usually difficult

In the past ten years, a lot of research has been carried out to overcome specific limitation in CRP. For examples, methacrylate monomers are the major problem in NMP. Therefore, addition of the small amount of styrene[16-19] or acetonitrile[20] can deliver control to the polymerisation, hence, allowing formation of block copolymers. Besides that, development of alkoxyamines with labile C-ON bond such as MAMA-SG1 makes it possible to polymerise at low temperature compare to TEMPO.[21,22] For ATRP, improvements allowing reactions with the low concentration of copper catalyst at 1-100 ppm levels by ARGET (activators regenerated by electron transfer) and ICAR (initiators for continuous activator regeneration) ATRP. Both techniques were regenerated the catalyst with employed the copper(II) complexes that continuously reduced to copper (I) complexes by reducing agents such as glucose and tin(II) 2-ethylhexanoate for ARGET, and radical initiator for ICAR ATRP.[23,24]

One of the most interesting aspects of different CRP is the possibility to synthesis polymers of composition, topology and functionality as illustrated in Figure 1.1. Copolymers such as block, gradient, random, graft or alternate composition are possible. Macromolecular structure such as star, network and hyperbranched are also attractive structures to explore due to multiple active sites present in molecules.[3,6,8]

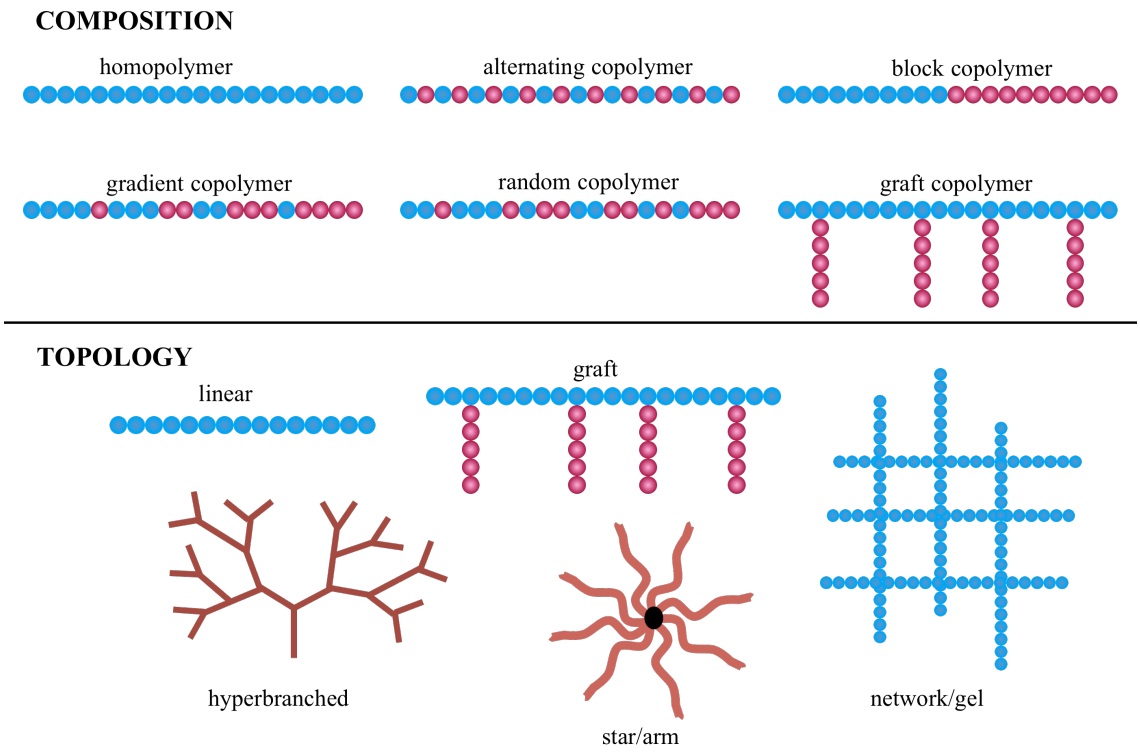

Figure 1.1: Composition and topology of polymer structure synthesised by CRP methods.[3]

1.3 Star polymers

Star polymers provide one of the simplest arrangements of linked chains, because star polymer contains only one central branching point (core) and emanating arms. Therefore, for star polymers it is possible to rearrange into core-shell microstructures with multiple radiating arms and chain-end functionalities. Generally, star polymers can be classified into two categories (Figure 1.2). Homoarm star polymers consist of arms having the same molecular weight and chemical composition with a symmetric structure. Miktoarms star polymers contain different (two or more) arms species with different molecular weight and/or chemical composition. Star polymers have attracted considerable attention due to their potential application as encapsulates[25], drug carriers[26], membranes[27] and catalysis[28].

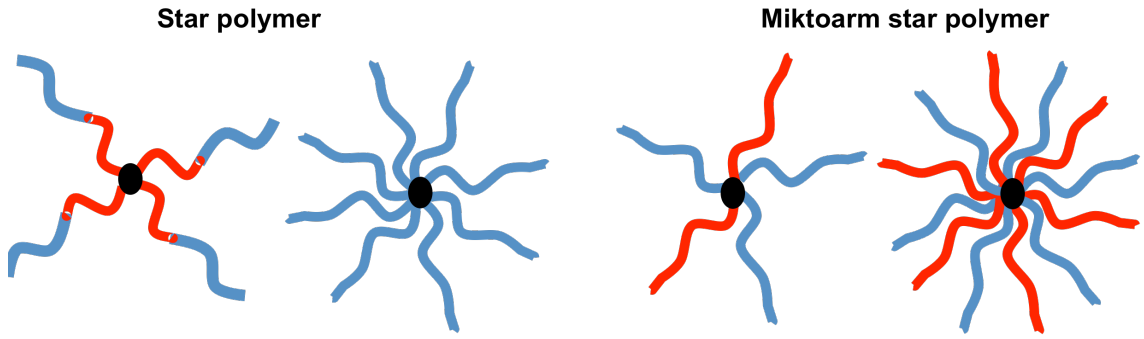

Figure 1.2: Categories of star polymers.

Star polymers *via* CRP have been mainly synthesised using a "core-first" and "arm-first" approach.[29,30] In the "core-first" method, a multifunctional initiator is used to initiate the CRP of monomer to obtain star polymers with a constant number of arms and identical arm structures. Meanwhile, the "arm-first" method are synthesised with the attachement of terminally reactive linear arms in the core by multifunctional coupling agents.

Due to the preserved initiating site at the end of the arms in "core first" method, a second monomer could be introduced to produce block copolymers. This proved the living properties of the macroinitiator (Scheme 1.3a). Star macroinitiators were developed for ATRP from organic[31,32], hybrid inorganic/organic[33,34], dendritic

moieties[35,36] and porphyrins[37]. These were used in the synthesis of styrenic, methacrylate or (meth)acrylic star polymer. In NMP, Hawker reported the first tri-alkoxyamine initiator based on TEMPO with well-controlled polystyrene (PS) arms.[38] Then, varieties of 3, 6 and 12 arms multifunctional initiator based on TEMPO were prepared from mesitylene[39], porphyrin[40], dendrimer[41] or polyhedral oligometric silsesquioxane (POSS) cores[42]. Robin *et al.* has designed star macroinitiators based on *N*-tert-butyl-1-diethylphosphono-2,2-dimethylpropyl nitroxide (SG1) and successfully polymerised poly (butyl acrylate) (PBA) block copolymer.[43] The octafunctional alkoxyamine initiator was prepared by resorcinarene with TEMPO and SG1 as nitroxide free radicals.[44] Development of star initiators was continued with the introduction of alkoxyamine MAMA-SG1 onto olefin *via* intermolecular radical addition approach to have 3 and 4 arms.[45] Examples of the macroinitiators are shown in Figure 1.3.

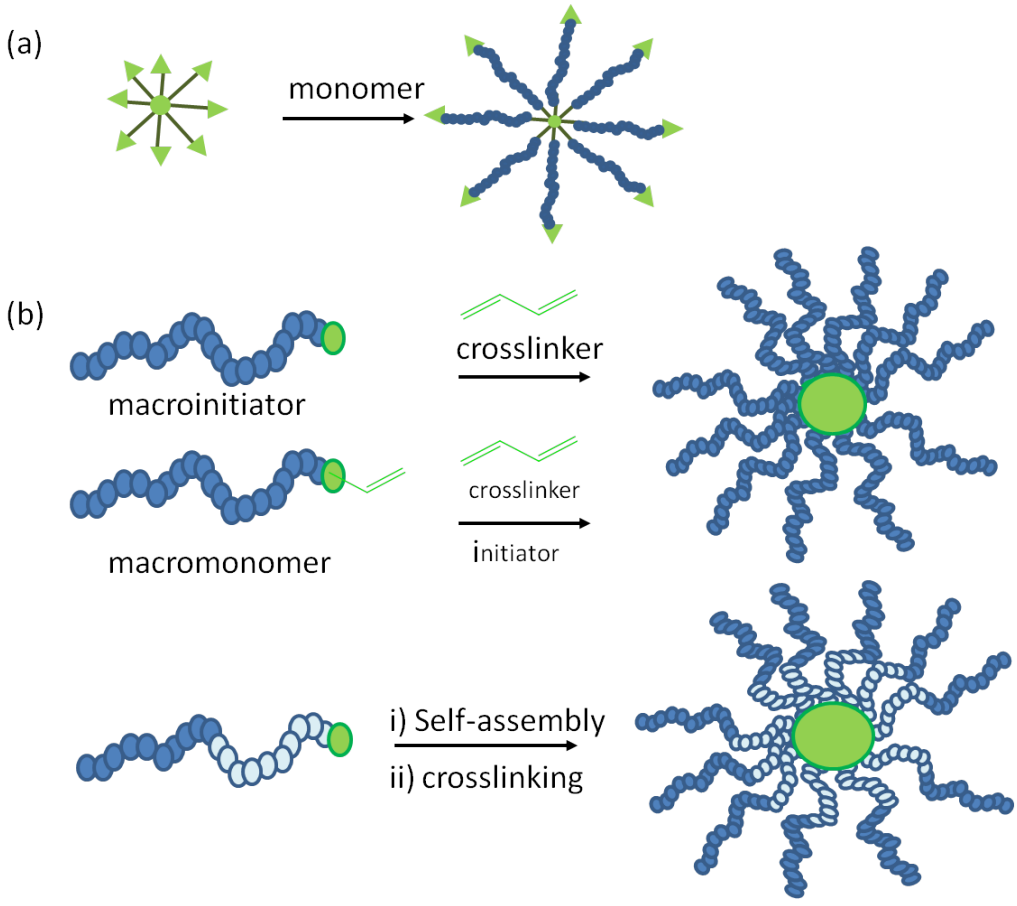

Scheme 1.3: Synthetic approaches for star polymers via CRP techniques; (a) "core-first"; (b) "arm-first".[30]

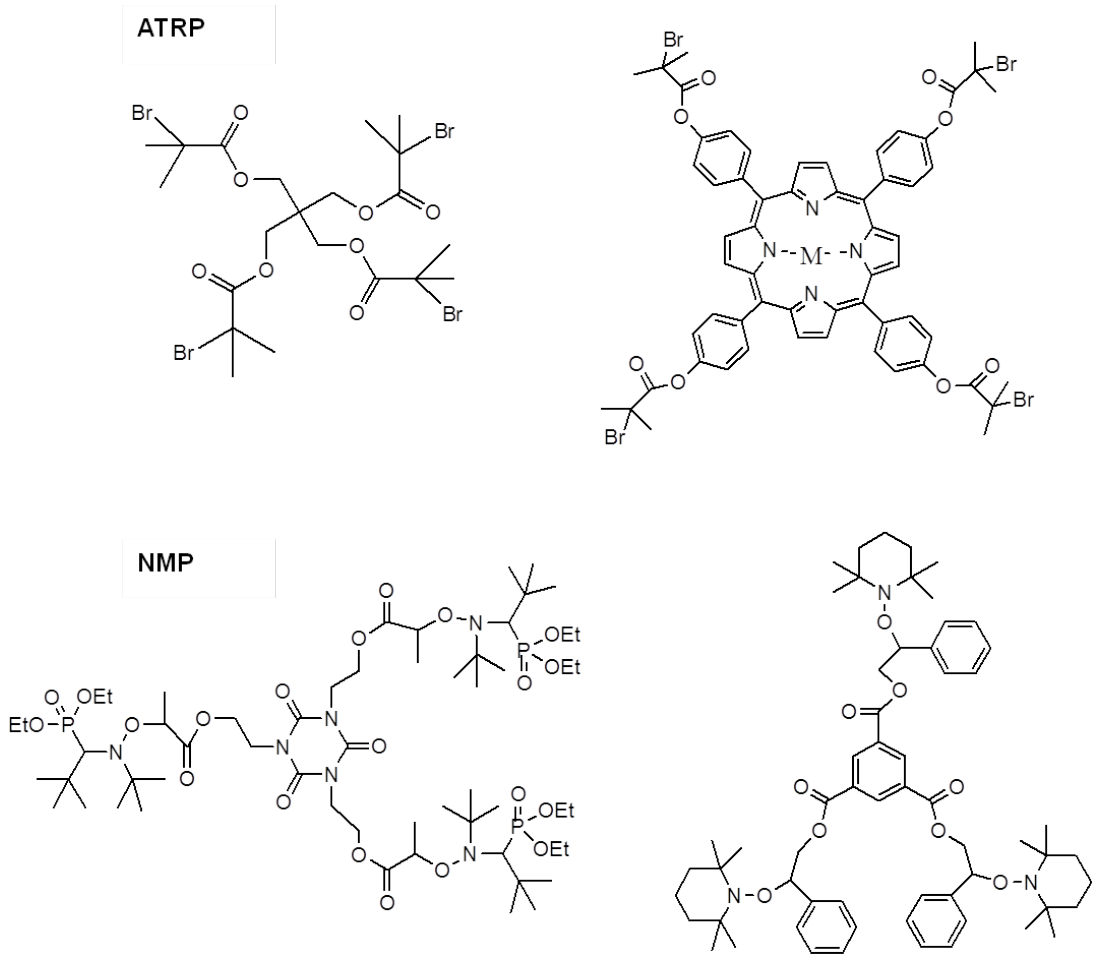

Figure 1.3: Some examples of multifunctional initiators used in ATRP and NMP.[24,28,29,34]

For the "arm-first" method as shown in Scheme 1.3b, the terminally reactive linear arms are synthesised first and then attached to a core by the reaction of the arms using multifunctional coupling agents such as divinylbenzene (DVB) and ethylene glycol dimethacrylate (EDGMA). Matyjaszewski *et al*. reported the arm first methods of PS[46] and PtBA[47] with DVB, EDGMA and 1,4-butanediol diacrylate (BDDA) using the copper catalyst system in ATRP. For a PS macroinitiator, DVB was shown lead to soluble polymer, whereas EDGMA and BDDA formed a gel. Similar results were obtained for PtBA except that BDDA formed a soluble polymer with high molecular weight and broad dispersity. Sawamoto and co-workers investigated the PMMA star polymer synthesis by "arm-first" approach with various divinyl and diacrylamide compounds.[48,49] The cross-linkers **1-4** resulted in star polymers with high yield, whereas **5** and **6** showed poor conversion (Figure 1.4). This was attributed to the rigid

hydroquinone spacer presence in **5**, while the flexible trioxyethylene spacer **6** formed the most stable structure in position two vinyl groups were close to each other that would be facilitated intramolecular cyclisation.[48] Several groups employed PS-TEMPO with DVB to produce star structure.[50,51] Hawker and co-workers presented core cross linked polymers of PS-TIPNO through a high-throughput combinatorial technique. This provided libraries for macromolecular 3-D structures.[52]

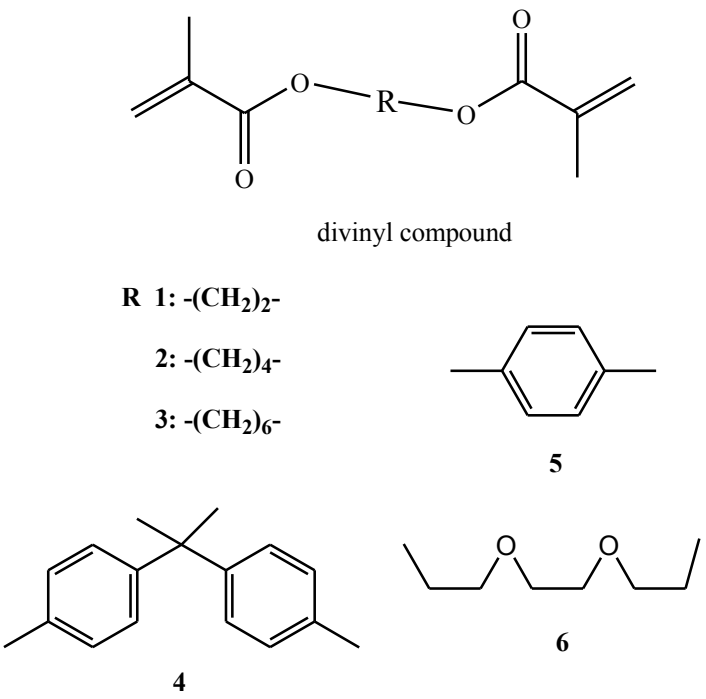

Figure 1.4: Divinyl compound employed for star polymer synthesis by the arm-first method.[48]

1.4 Block copolymer

Recently, block copolymers have also received a great interest among researchers. The importance of block copolymers is based on the fact that a single molecule contains two (or more) different segments. Therefore, it may exhibit the characteristics of both components and would offer the possibility of tuning or combining properties, in between the extremes of the pure components. If the polymer blocks are thermodynamic incompatibility they may undergo microphase separation. Microphase separation occurs when the block of one block type segregates into domains that have

dimension on the length scale of the blocks themselves. Then, these polymers could self-assembly to produce particular nanostructures. The most important synthetic system for nanostructures are amphiphilic block copolymers. Amphiphilic block copolymers combine hydrophilic and hydrophobic segments that are capable of self-aggregation into microdomains in selective solvents. The morphology of nanostructures depends on the concentration and volume ratio between soluble and insoluble blocks. CRP techniques were extensively employed to design amphiphilic copolymers to form varieties of colloidal objects such as micellar spheres, vesicles and cylinders.[53] Thus, it opens applications in biomedical, nanocomposites and nanoporous membrane.[54,55] Figure 1.5 shows the examples of the assemblies of block copolymers in selective solvents.

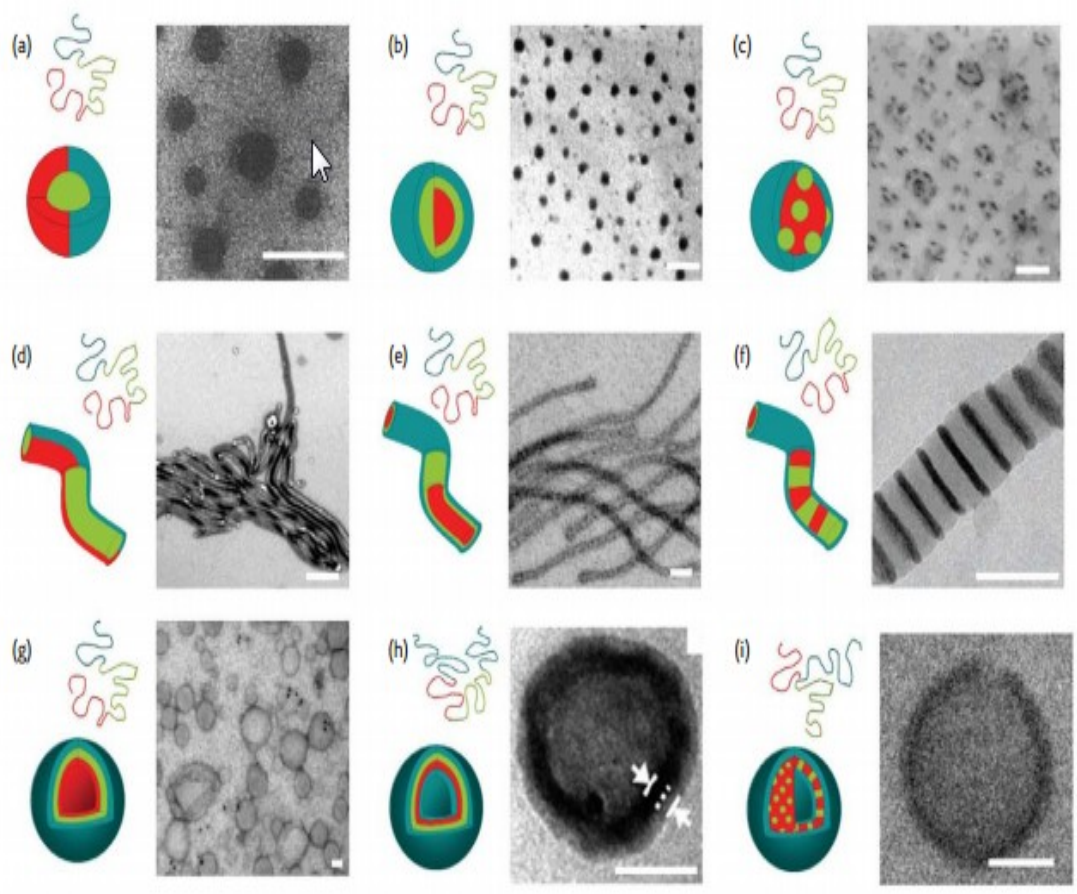

Figure 1.5: Assemblies formed in selective solvent conditions by multiblock copolymers: (a) Janus spheres, (b) core-shell spheres, (c) raspberry-like spheres, (d)Janus cylinders, (e) core-shell cylinders, (f) segmented cylinders, (g) asymmetric (Janus) membrane vesicles, (h) double-layer membrane vesicles, and (i) vesicles with hexagonally packed cylinders. Scale bar 50nm.[54]

The most widely applied synthetic pathway to form block copolymers is sequential polymerisation of different monomers. After the polymerisation of the first monomer, the resulting macroinitiator can either be used *in-situ* or purified before further chain-extension. The purified macroinitiator is the best way to get the pure block copolymer. However, the synthesis of well-defined block copolymers can be difficult because not all monomers can be polymerised in a controlled fashion with the functionality required for chain extension. It also depends on the monomer sequences in the polymerisation step. Sometimes, it is possible to chain extend from a specific "A" block to the desired "B" block, but it may be not to possible to chain extend from a performed "B" block to the same "A" block.[5] For example, polyacrylonitrile macroinitiators are capable to polymerise *n*-butyl acrylate but not *vice versa*.[56] In all cases of CRP systems, the polymerisation should be stopped before total consumption of monomer to preserve the end-functionality and to prevent 'dead' blocks.

Alternatively, double-headed initiators either with the similar end-functionality or a combination with an initiator group from other polymerisation methods could be used in designing block copolymers or complex macromolecular structures.[8,57,58] For examples, Tunca and co-workers successfully synthesised block copolymers by combining ATRP and NMP polymerisation.[59,60] This bifunctional initiator contains two reactive sites which are TEMPO end-group for NMP and a 2-bromopropionate or 2-bromo isobutyrate end-group for ATRP. Well-controlled diblock copolymers with low dispersity were prepared from this bifunctional initiator either by ATRP-NMP or NMP-ATRP pathway as shown in Scheme 1.4. Since they have a reactive end-group, the extension to ABC-triblock copolymer is possible. However, the authors found that the ATRP-ATRP-NMP pathway was less efficient than the NMP-ATRP-ATRP pathway due to the loss of TEMPO end-groups in the first two ATRP sequences. Besides that, the compatibility of the NMP initiator with the ring opening polymerisation (ROP) of lactones and NCA has been widely investigated to form bifunctional initiator. For instance, Vinas *et al.* reported that MAMA-SG1 has been modified with ethanolamine, **(7)** to make polystyrene-*b*-polylactide.[21] On the other hand, Habraken *et al*. synthesised dual initiator MAMA-SG1 with diaminoethane, **(8)** to polymerise polypeptide block copolymers with styrene or *n*-butyl acrylate.[61] Both of these initiators accommodate MAMA-SG1 with OH- and NH_2- end functional group that are useful for ROP (Figure 1.6).

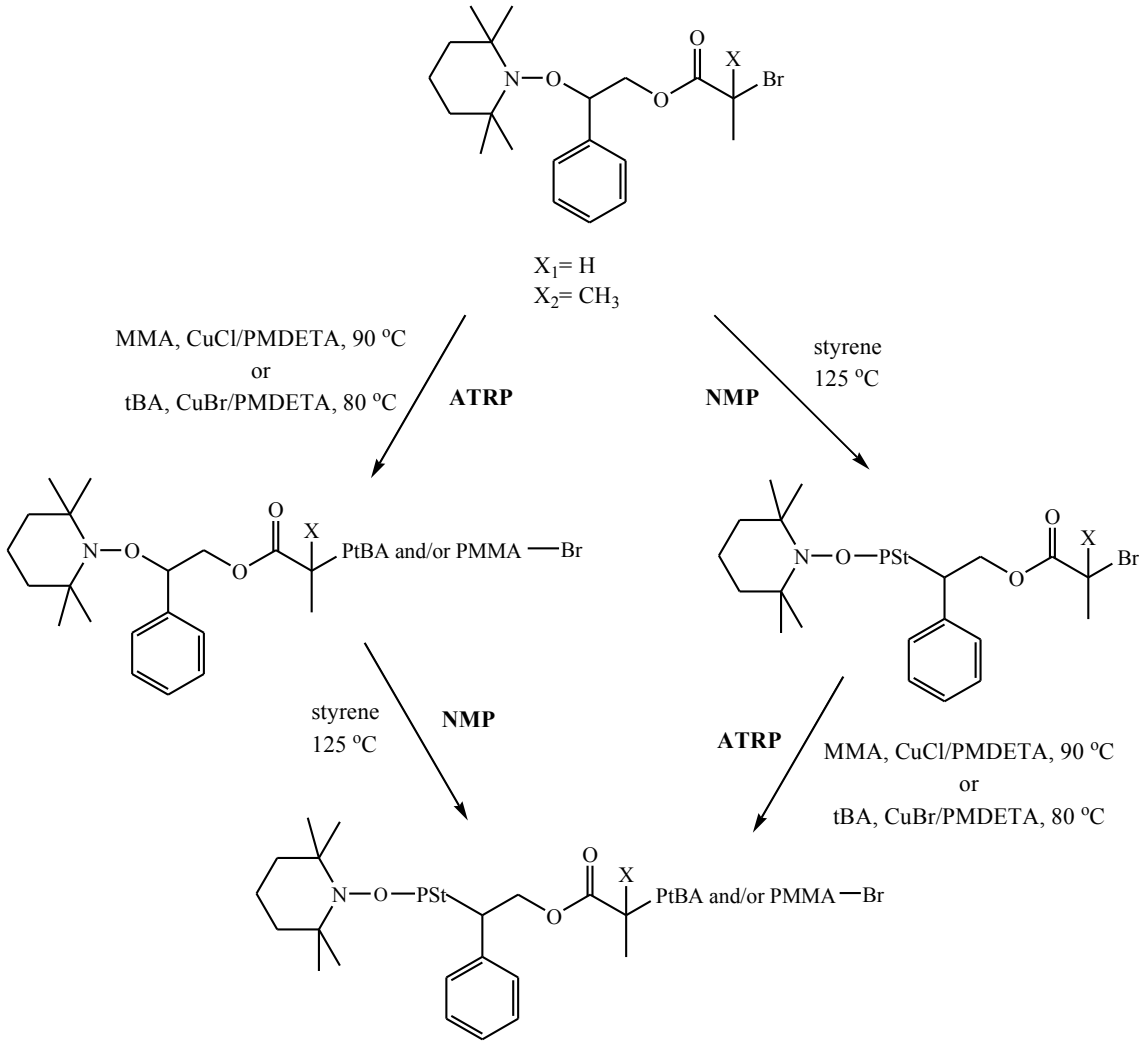

Scheme 1.4: Diblock copolymer from bifunctional initiator combining ATRP and NMP polymerisation.[59]

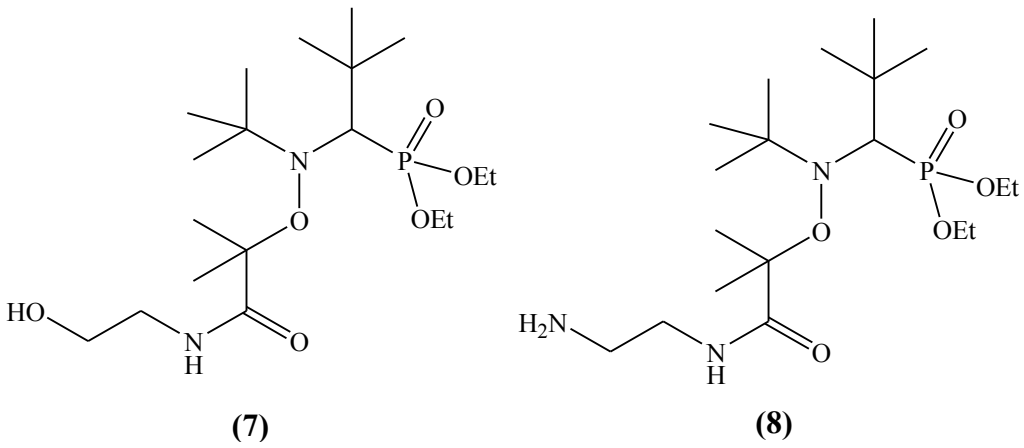

Figure 1.6: Dual initiator for NMP-ROP polymerisation.[21,61]

In the work reported in this thesis, block copolymers of poly(methyl methacrylate-*b*-4-vinylpyridine), poly(MMA-*b*-4VP) were investigated through sequential polymerisation by ATRP and NMP. Based on our knowledge, very little research on poly(MMA-*b*-4VP) was reported by CRP methods. Matyjaszewski reported a problem with nitrogen-containing vinyl monomer, such as 4VP, in the synthesis of poly(MMA-*b*-4VP) by ATRP because the monomers could directly coordinate to and deactivate the copper catalyst.[62] Therefore, a new copper catalyst with stronger binding-ligand was introduced. Furthermore, the ATRP of 4VP employs polar solvents, which limit the molecular weight of the formed PMMA block due to poor solubility.[62,63] While, NMP is well-known with their limitation to certain monomer such as methacrylates due to β-hydrogen elimination from the propagating radicals. This reaction is leading to termination reaction and dead chains.[64] Therefore, Shoji *et al*. tried to combine NMP and ATRP using a bifunctional initiator for preparing block copolymers.[65] The polymerisation of PMMA could be well controlled by ATRP, while 4VP could be polymerised with NMP. NMP of 4VP is usually performed without any complicated additives and any solvent could be used in polymerisation (Scheme 1.5).[65]

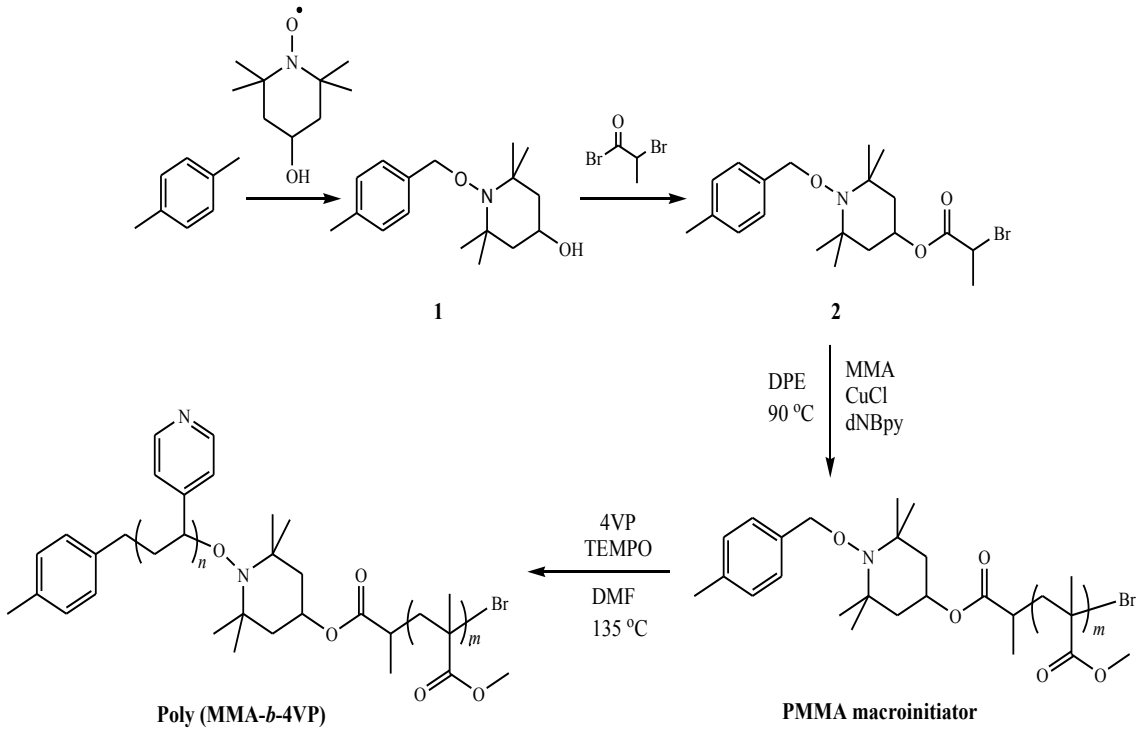

Scheme 1.5: Preparation route of the poly(MMA-*b*-4VP) block copolymer by ATRP and NMP using 1-N-[(4-methylbenzyl)oxy-4-(2-bromopropanoyl)-2,2,6,6-tetramethylpiperidine **(2)** as the bifunctional initiator.[65]

1.5 4-vinylpyridine and its metal binding applications

1.5.1 Polymerisation of 4-vinylpyridine

Controlled radical polymerisations (CRP) techniques are receiving great attention because they are powerful tool for macromolecular design. These include the potential to synthesis homopolymers and block copolymers with narrow molecular weight distribution, the synthesis of different architectures of polymer (star, comb and dendritic) and easy to end-functionalised polymers with the selective end-group.[3,8,11] Pyridine containing polymer have attracted much interest due to their potential applications, especially in coordination with metal.[66] It is well-known that living anionic polymerisation has been one of the best way to prepare poly(4-vinylpyridine) (P4VP).[67,68] Recently, the polymerisation of 4VP by CRP such as ATRP, NMP and RAFT were investigated and discussed in the following.

Xia *et al*. was the pioneer in exploring the polymerisation of 4VP by ATRP.[62] Firstly, they investigated the polymerisation of 4VP using 1-phenylethyl bromide (1-PEBr)/CuBr/2,2'-bipyridine (bpy) as the initiation system at 40 °C and found only 10% monomer conversion after 25 hours polymerisation. However, when a strong coordinating ligand was used such as *N,N,N',N'',N''*-pentamethyldiethylenetriamine (PMDETA), a faster polymerisation rate was observed. A linear increase in the kinetic plots with time and molecular weight with conversion was obtained when the polymerisation was conducted in solution with 1-phenylethyl chloride (PECl)/CuCl/tris[2-(dimethylamino)ethyl]amine (Me_6TREN). The livingness of P4VP was confirmed by the chain extension with MMA. This study showed that the choice of ligand is important to control the polymerisation of 4VP. Therefore, Wang and co-workers introduced macrocyclotetraamine (Me_6[14]aneN_4) as a ligand, PECl as initiator and CuCl as catalyst for P4VP in 2-propanol solution.[69] As a result, the polymerisation reached 90% conversion in 3 hours with controlled molecular weight and narrow dispersity. Then, PMMA-Cl was used as macroinitiator to synthesise amphiphilic block copolymers with styrene. Furthermore, Jiang *et al*. studied the effect of different catalyst system for copolymerisation of diisopropyl-p-vinylbenzyl phosphonate (DIPVBP) and 4VP in DMF solution and ethyl-2-bromoisobutyrate (EBiB) as initiator. Three catalyst systems of CuCl/PMDETA, CuCl/Me_6TREN and CuCl/HMTETA at 90 °C were compared. They found that CuCl/HMTETA catalyst

system gave high conversion and reaction rates than other system.[70] It was concluded that the polymerisation of 4VP is very challenging because of its ability to coordinate and thus compete for the binding of the metal catalyst in the polymer system. Two factors should be considered in designed the polymerisation of 4VP: (1) multidentate ligands must be used due to their stable complex with Cu(I) and Cu(II) and (2) protic solvents like 2-propanol is preferable because it can minimise the contamination of catalyst.

For RAFT, the choice of chain transfer agents is very important because they are specific for certain monomers. Since 2003, a few literature examples have reported the successful polymerisation of 4VP with different chain transfer agents (CTA) as shown in Figure 1.7. The first attempt was by McCormick employing cumyl dithiobenzoate **(9)** as the chain transfer agent and azoisobutyronitrile (AIBN) as initiator at 60 °C to polymerise 2- and 4-vinylpyridine.[71] Besides that, P4VP with high conversion (95%) and low dispersity was obtained by S-dedocyl-S'-(isobutyric acid) trithiocarbonate (DBTTC) **(10)** as CTA. The resulting macrointiator was used for chain extension with azeotropic mixture of styrene and acetonitrile in solution and emulsion condition.[72] Other research groups used **(10)** to design triblock copolymer poly(S-*b*-4VP-*b*-S) and poly(4VP-*b*-S-*b*-4VP) from PS- and P4VP-CTA macroinitiator.[73] P4VP has also been synthesised by seven-membered ring cyclic trithiocarbonate **(11)**.[74] This cyclic RAFT agent undergoes a ring opening process to incorporate a trithiocarbonate moiety, which functions as a RAFT agent and can be used to prepare block copolymers. However, the problem with RAFT is the contamination with thiol group and the need to synthesise specific CTA for the polymerisation.

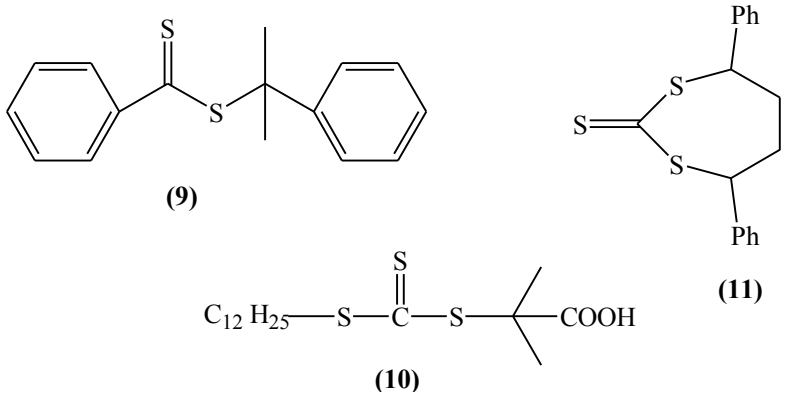

(9) **(11)** **(10)**

Figure 1.7: Chain transfer agents (CTA) for polymerisation of 4VP.[71-74]

In comparison, NMP can polymerise 4VP without any contamination of catalyst or sulphur. It is also the simplest method as only addition of alkoxyamine and heat is required.[3] However, most of the polymerisations were conducted at high temperature around 120 °C. Bohrisch *et al*. started to explore 4VP as potential monomer for NMP in 1997 using 2,2,6,6-tetramethylpiperidin-1-oxyl (TEMPO) as capping agent and benzoyl peroxide as initiator.[75] Further research of 4VP with TEMPO was conduct by Lonchon's research groups to study the influence of temperature and nitroxide concentration on the kinetics of the reaction.[76] They reported that P4VP using the bimolecular system AIBN and free SG-1 provide faster polymerisation rate and very well controlled molecular weight distributions at high conversion.[77] Not only TEMPO, but also 2,2,5-trimethyl-4-phenyl-3-azahexane-3-nitroxide (TIPNO) was investigated for the polymerisation of 4VP.[78,79] According to Maria *et al*., P4VP initiated by TIPNO reached the optimum condition of high conversion and low dispersity when the polymerisation was conducted in anisole solution compare to bulk.[79] Recently, the homopolymerisation of P4VP based on the ([tert-butyl[1-(diethoxyphosphoryl)-2,2-dimethylpropyl] amino] oxy)-2-methyl propionic acid (MAMA-SG1) was reported.[80-82] Rahim *et al*. successfully synthesised P4VP to full conversion (99%) with good controlled dispersity (D=1.1). It was proven by the clean shift of SEC traces to higher molecular weights as the reaction proceded with no significant termination reaction detected. The livingness of the polymer was confirmed by chain extension with MMA.[82] Meanwhile, Lessard and Marić studied the effect of initiator protection and complexation with fullerene in P4VP. They showed that a protected alkoxyamine (MAMA-NHS) and MAMA-SG1 initiator produce a well controlled P4VP with low dispersity. However, additions of C_{60} acted as inhibitor and prevented the polymerisation to exceed 40% conversion.[81]

In summary, P4VP has been synthesised from variety methods of polymerisation especially CRP methods. Thus, complex macromolecular structures can be designed by polymer chemists/engineers to develop a variety of applications such as templates for nanoparticles, catalysis, drug delivery and sensors as discussed further.

1.5.2 Self-assembly of P4VP block copolymer as a template for nanoparticles

Self-assembly of block copolymers is defined as the arrangement of the hydrophobic and hydrophilic segments of copolymer in selective solvent which must be a good solvent for one of the blocks but a poor one for the other. Therefore, in solution the insoluble segments of the block copolymer collapse to form the core of a micelle, while soluble segments are solvated by the solvent. In the fabrication of nanoparticles, block copolymer micelles provide good control of shape, dispersion, size distribution and alignment of nanoparticles which have been selectively incorporated in a specific domain.[83] Poly(styrene-*b*-4-vinylpyridine), poly(S-*b*-4VP) are widely investigated as template for nanoparticle such as Au[84-86], Co[87], Cu[88], Ag[89] *etc*. Nanoparticles were prepared by self-assembly in colloidal solution or surfaces.

Antonietti and his co-workers studied the preparation of nanoparticles in micelles of poly(S-*b*-4VP) in toluene and THF solution.[84,87] The poly(S-*b*-4VP) were dissolved in toluene and mixed with metal salt. Then, the metal salt containing micelles were then reduced with reducing agents such as $NaBH_4$ and hydrazine, resulting in metal colloid formation inside the micelles core. This metal colloids can easily be precipitated, isolated and redissolved in good solvents for PS. Reduction of gold salt containing micelles in solution with $NaBH_4$ or superhydride leads to the formation of gold nanoparticles in the micelle core. Based on the assemblies of the particles after the reduction process, they proposed two morphologies of metal colloids called “raspberry-like” and “cherry-like”. “Cherry-like” architectures were obtained by slow nucleation, in contrast “raspberry-like” architectures were obtained by fast nucleations that simultaneously start at many sites (Figure 1.8).

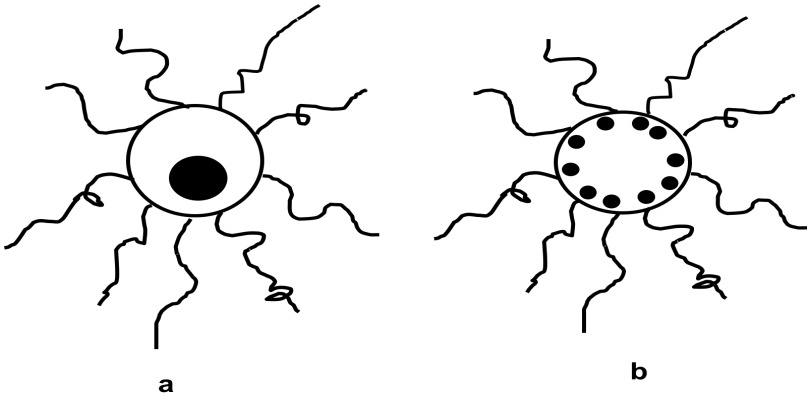

Figure 1.8: Sketch of the "cherry-like" (a) and "raspberry-like" (b) morphology of block copolymer supported metal colloids.[84]

Not only linear copolymer, but also star block copolymers were used as nanoreactor templates for preparing nanoparticles. Star block copolymer poly(S-*b*-4VP) were synthesised using ATRP by Li and co-workers.[90] Self-assembly of this star copolymer formed reverse micelles with P4VP as the core and PS as the shell in toluene solution. In the closed shell structure, resembling a petal shape, PS chains spread from the P4VP core and join at one point (Scheme 1.6). Then, the P4VP core was coordinate with $HAuCl_4.3H_2O$, followed by reduction with hydrazine to form gold nanoparticles. The core size of the reverse micelles increased with the chain length of P4VP, such as 26.4, 44.3 and 74 nm for PS_{25}-*b*-$P4VP_{17}$, PS_{25}-*b*-$P4VP_{37}$ and PS_{25}-*b*-$P4VP_{63}$, respectively. After incorporating gold complex into the core, the micelle size of PS_{25}-*b*-$P4VP_{17}$ and PS_{25}-*b*-$P4VP_{37}$ increased, while PS_{25}-*b*-$P4VP_{63}$ decreased. The difference is owed to the electron repulsion and chelation. The morphology for all the micelles was spherical because the petal shells efficiently stabilised the core and prevented the aggregation of micelles and complexes.

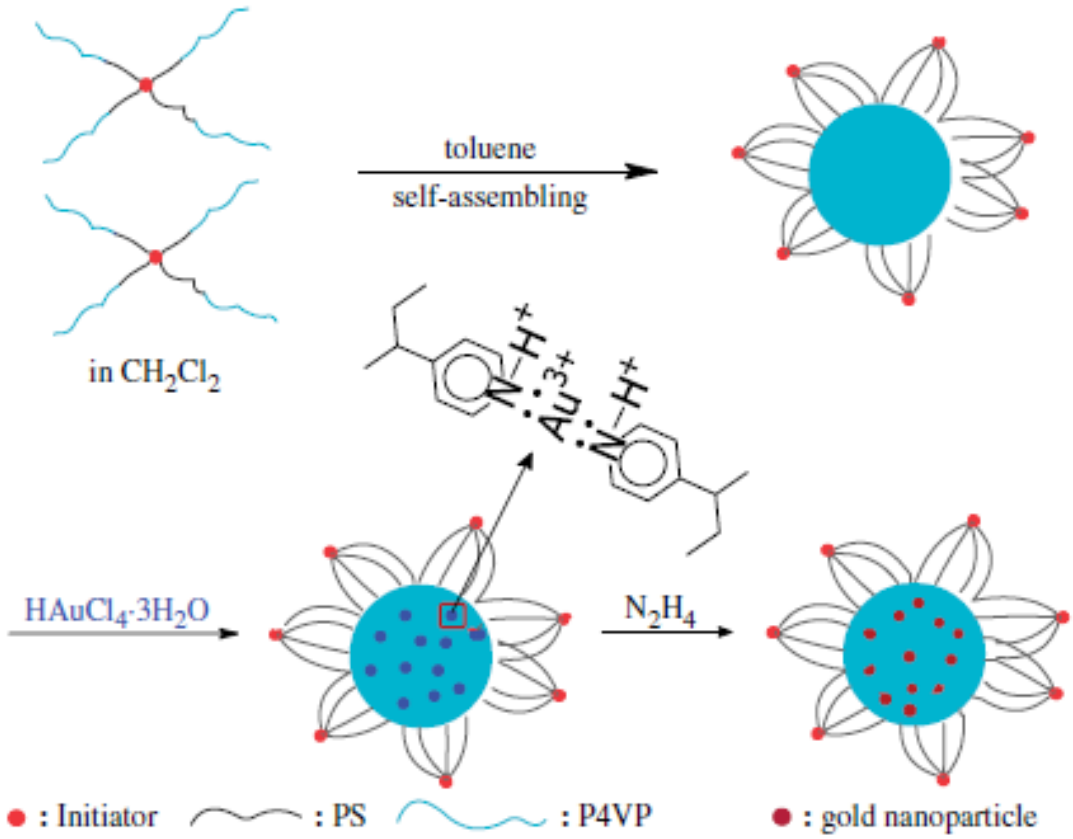

Scheme 1.6: Preparation of reverse micelles star block copolymer poly(S-*b*-4VP) and gold nanoparticles.[90]

On the other hand, well-controlled polymeric micelles with an aqueous core (PMAC) of poly(S-*b*-4VP) were also introduced as nanoreactors for nanoparticles.[89] This PMAC formed *via* biphase diffusion of HCl at the top phase into the bottom phase poly(S-*b*-4VP) solution. The micelles formed with PS as a shell and P4VP as a core after protonated by HCl. The authors prepared silica, Fe and Ag nanoparticles in the PMAC.

The morphology of block copolymers is sensitive to the environment, incompatibility between different block and degree of polymerisation. Cheng and Chan reported that the attachment of rhenium to poly(S-*b*-4VP) block copolymer changed the solid state morphology from spherical to cylindrical micelles compare to the metal free poly(S-*b*-4VP).[91-93] The size of micelles was measured to be around 20 nm. The poly(S-*b*-4VP) cylindrical shape depends on the preparation conditions and nature of the substrate surface. Semiconducting nanoparticles, CdS could be deposited on the film by electrostatic interaction, which accommodated two particles (size 10 nm) for a

cylindrical domain. On the other hand, gold nanoparticles 2-4 nm were prepared with poly(S-*b*-4VP) template mediated by Cu^{2+} ions.[94]

1.5.3 P4VP in electrocatalysis

In electrocatalysis, polymers such as P4VP and Nafion® are utilised for supporting catalysts. According to Kaneko and Abe, a complex incorporated into a polymer backbone can be suppressed the coagulation of catalyst and formed a molecular aggregate which improving the catalytic activity. Besides that, polymer matrix may be inhibited the diffusion of the substrate (CO_2, O_2, H^+) from the solution phase to the active site in the polymer backbone, then slowing the overall kinetics in the catalysis.[95] In the following, electrocatalyst incorporated into P4VP for reduction of oxygen, carbon dioxide and protons are discussed.

1.5.3.1 Reduction of oxygen

Liu and co-workers developed layer by layer (LBL) assembly of Pd particles for the reduction of oxygen as illustrated in Scheme 1.7.[96] Firstly, a GC surface was functionalised with 4-aminobenzoic acid (4-ABA). Quaternised P4VP complexed with $Os(bpy)_2Cl_4^{2-}$ were alternately assembled by electrostatic interaction. Electrochemical reduction of the multilayer film resulted in Pd particles (average diameter, 3~7 nm). The Pd particles-modified electrode can reduce O_2 into hydrogen peroxide in 1 M sulphuric acids, where QP4VP-Os acts as a mediator of the catalytic reduction. This LBL method is suitable for other metal systems for the reduction of O_2.

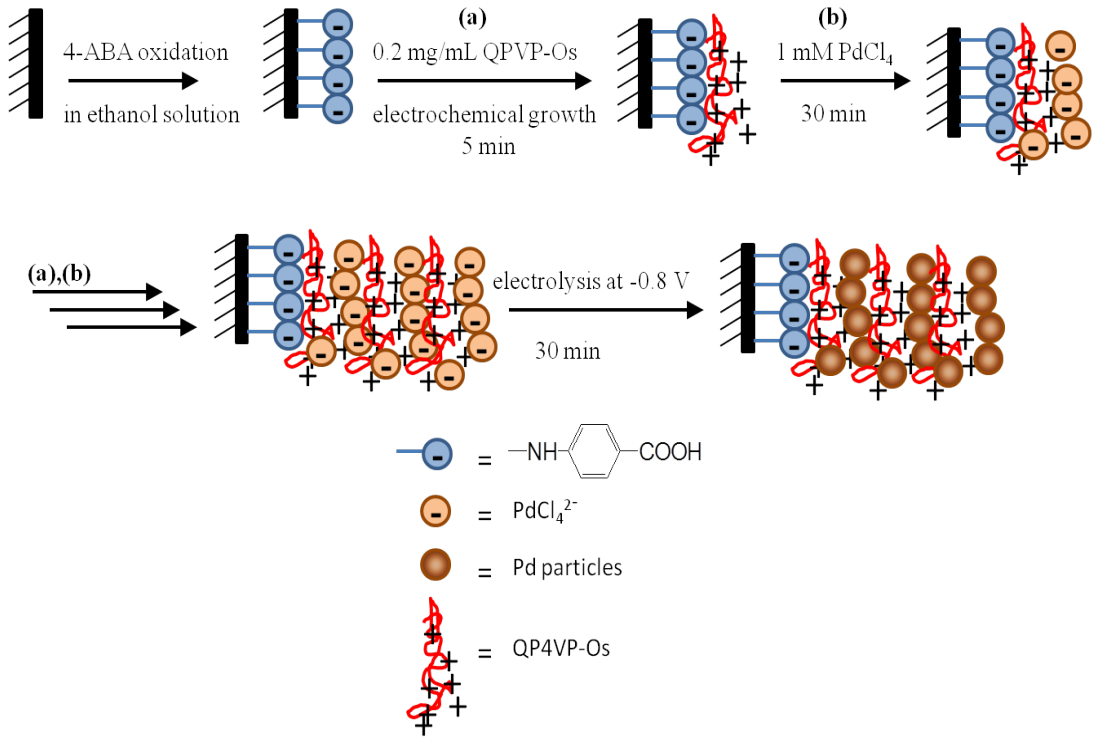

Scheme 1.7: Illustration of the formation Pd particles by multi-layer films for reduction of O_2.[96]

1.5.3.2 Hydrogen evolution

Kaneko *et al*. have reported the electrocatalytic proton reduction by metal centre phthalocyanine (Pc) derivatives, such as cobalt(II) phthalocyanine (CoPc), cobalt(II) octacyanophthalocyaanine ($CoPc(CN)_8$) and cobalt(II) tetrasulphonatophthalocyanine ($CoPc(SO_3H)_4$) incorporated in a poly (4-vinylpyridine-*co*-styrene) (P4VP-St) films coated on the graphite electrode (Figure 1.9).[97] Turnover numbers (*TN*) are important in electrocatalytic study as indicator of the performance of the complex. *TN* can describe as number of moles of product generated per mole of immobilised, electrochemically active catalyst over the duration of the experiment.[98] The highest *TN* value of $2x10^5$ h^{-1} was obtained for CoPc when the electrolysis was applied at -0.9 V vs Ag/AgCl at pH 1, 0.1 M aqueous phosphate buffer solution. The catalytic efficiency increases in the following order CoPc > $CoPc(CN)_8$ > $CoPc(SO_3H)_4$. This electrocatalytic efficiency depends on the rate of electron transfer within the catalyst incorporated in the polymer matrix. Redox states of CoPc derivatives also influences the electrocatalytic activity. For P4VP-St/CoPc and P4VP-St/$CoPc(SO_3H)_4$, proton reduction occurred at second reduction, while P4VP-St/$CoPc(CN)_8$ catalysed the H_2

formation at the third reduction wave. Generally, this reduction is considers to occur at the macrocyclic ring of the Pc.

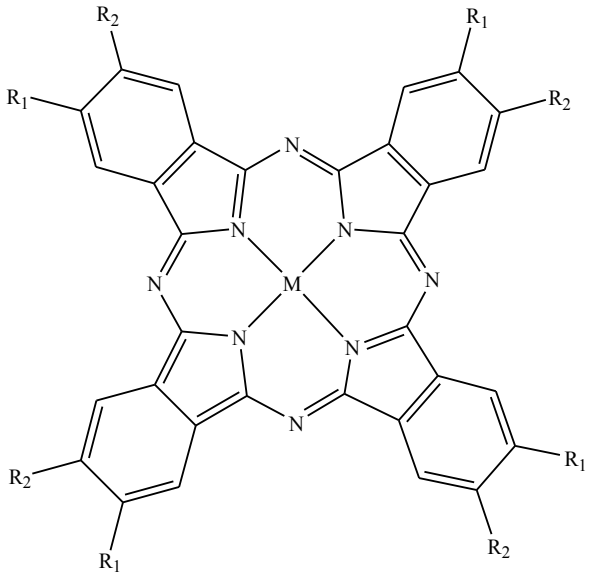

M = Co

R_1=R_2: H (CoPc)

R_1=R_2: CN ($CoPc(CN)_8$)

R_1: H, R_2: SO_3H ($CoPc(SO_3H)_4$)

M = Zn

R_1=R_2:H (ZnPc)

Figure 1.9: Structure of cobalt(II) metallophthalocyanine and its derivatives.

The zinc phthalocyanine (ZnPc) complex also acts as catalyst for electrochemical hydrogen production.[99] ZnPc embedded in Nafion® and P4VP-St absorbed at a graphite electrode displayed reduction at macrocyclic Pc ring. After 1 hour electrolysis at -0.9 V (Ag/AgCl), the *TN* values were $4.3x10^4$ and $2.9x10^4$ for Nafion/ZnPc and P4VP-St/ZnPc, respectively. The difference was ascribed to the interaction of the redox species with the polymer matrix and counterion migration. For P4VP-St/ZnPc, the electron transfer is slower than Nafion® because of the axial coordination of complexes and 4VP although many of the 4VP is protonated at pH 1. This protonate polymer would prevent the proton from the solution coming into electrode surface, which decreased electron propagation through the matrix.

1.5.3.3 Reduction of carbon dioxide (CO_2)

Reduction of CO_2 in water involved a multi-electron reduction process, producing multiple products, such as formic acid, hydrocarbon, methanol and oxalic acid.

However, the product is selective to the catalyst. For instance, Kaneko *et al*. studied the electrocatalytic reduction of CO_2 in 0.1 M aqueous phosphate buffer solution by P4VP-bound CoPc and cobalt(II) octabutoxyphthalocyanine, ($CoPc(BuO)_8$) coated on graphite electrode.[100-102] The catalyst membrane exhibited more active and selective CO_2 reduction than the neat CoPc coating. The degree of selectivity is defined as the ratio of CO to H_2 produced and it is affected by pH, applied potential and CoPc concentration immobilised in the polymer. P4VP-St/CoPc showed maximum selective CO_2 reduction (CO/H_2) at pH 4.4 was 3.4 at -1.2 V vs SCE. At pH 2.3, the selectivity was not as good with the maximum value ~1 at -1.1 V (SCE), while at pH 6.8 the maximum ratio CO/H_2 almost 4.7 at -1.3 V (SCE).[100] In addition, they proved that the more efficient catalytic CO_2 reduction proceeds under higher concentration of CoPc in P4VP membrane. The selectivity reached 6 at applied potential -1.2 V vs SCE by 5.3 mM CoPc (pH 4.4).[101] P4VP with pyridine groups would facilitate CO_2-coordinate species by increasing the electron density of the central Co ion by axial coordination. Due to weakly basic properties, P4VP should act as H^+ sources for dehydration process in producing CO from CO_2 (Scheme 1.8).

1.5.4 Other applications

Redox polymers are electroactive polymer which the redox centres covalently attached to a polymer backbone. The materials can be obtained by electropolymerisation or chemical synthesis. The molecular weight and the concentration of the electroactive centre can be controlled compared to electropolymerisation method. Forster and Vos synthesised P4VP containing redox active centre such as ruthenium and osmium-based polypyridyl complexes[103] (Figure 1.10), potentially used for an electrochemical sensor, for example a glucose sensor [104-106].

Doherty and co-workers developed an electrochemical sensor for nitrite from $[Ru(bpy)_2(P4VP)_{10}Cl]Cl$ coated on the glass carbon electrode.[105] The modified electrode showed efficient electrocatalyst for oxidation of nitrate with 4.8 μA which are greater by at least a factor of 3 compare to bare electrode, 1.3 μA. This sensor was applied to detect the composition of nitrate in commercial fertiliser compound using a flow injection analysis protocol. They also showed the potential of $[Os(bpy)_2(P4VP)_{10}Cl]Cl$ as sensor for the detection of nitrite in saliva.[104]

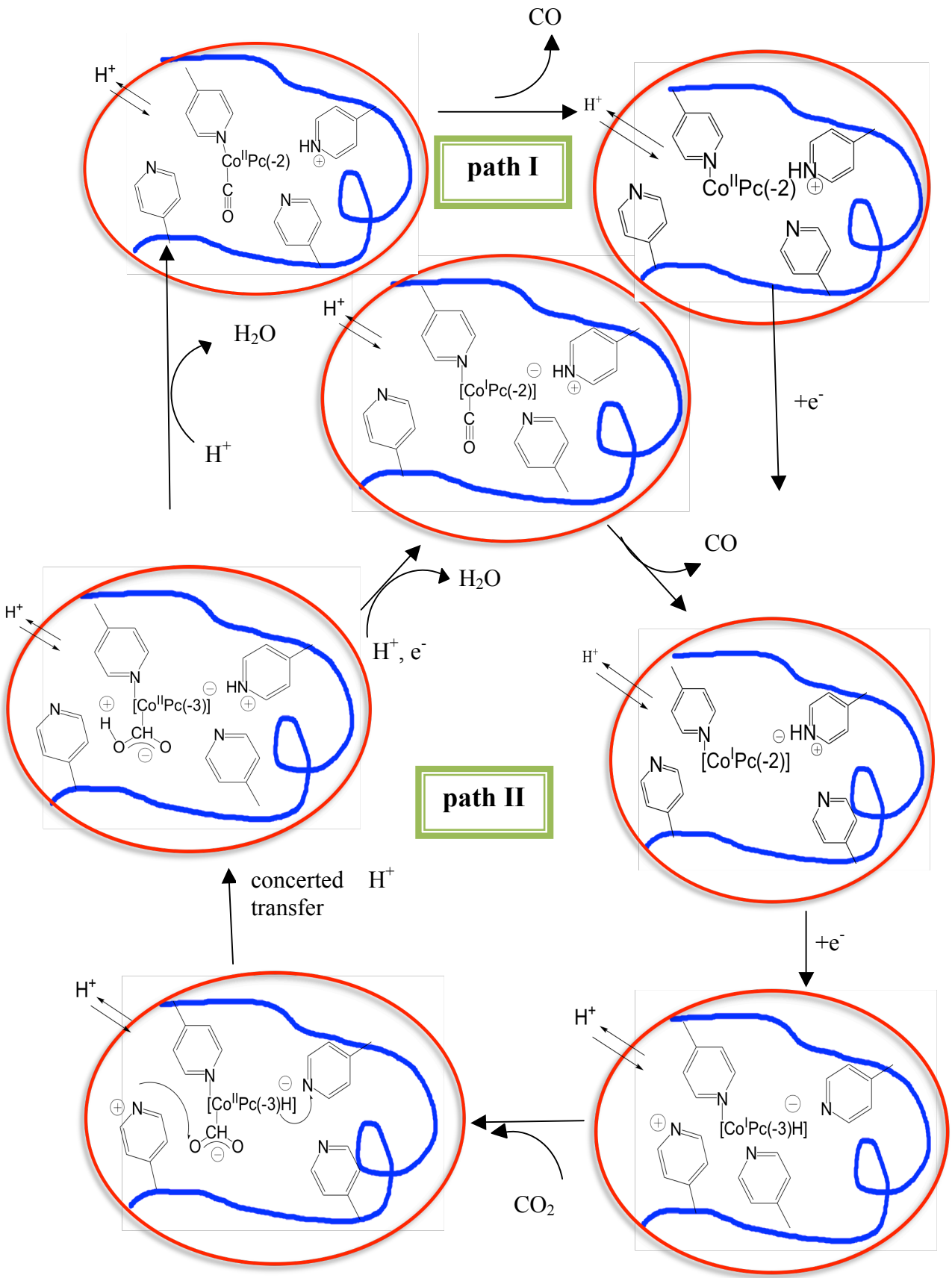

Scheme 1.8: The mechanism for electrochemical CO_2 reduction catalysed by CoPc-P4VP.[101]

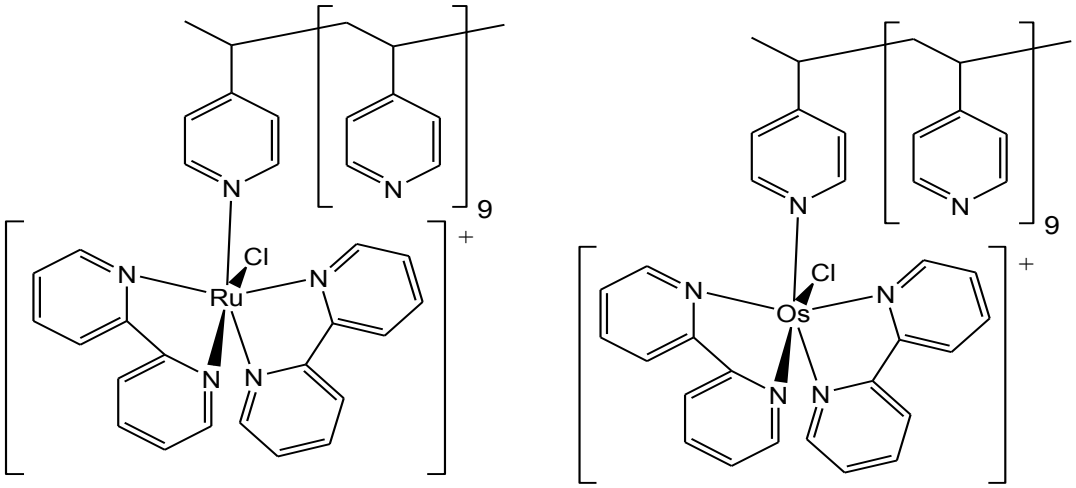

$[Ru(bipy)_2(P4VP)_{10}Cl]Cl$ $[Os(bipy)_2(P4VP)_{10}Cl]Cl$

Figure 1.10: Sturucture of redox polymer based Ru and Os-based polypyridyl complexes.

Studies of P4VP nanoparticles and magnetic nanoparticles prepared by microemulsion polymer and modified with various bromoalkane describe the effect of the quaternisation and potential use in biomedical and environmental application.[107-110] In general, the longer the chain length of the quaternising agents the smaller the particles size, because of the increase in hydrophobicity of the particles. The charges of the particles also decreased with the increase of quaternised chain length. For example, Table 1.3Table 1.3 showed the size of P4VP particles and zeta potential values before and after quaternisation with HCl, bromoethane (E), 1-bromobutane (B) and 1-bromohexane (H). In drug delivery application, naproxene sodium was used as a drug model with P4VP nanoparticles and P4VP magnetic nanoparticles. As a result, P4VP nanoparticles alone are not encapsulate the drug, while higher loading of the drug was obtained for modified P4VP nanoparticles and magnetic nanoparticles.[107,108] In addition, P4VP nanoparticles can adsorb organic pollutants (phenol, 4-nitrophenol) and carcinogenic pollutant (arsenic) from aqueous environment. Sahiner *et al*. reported that P4VP-HCl nanoparticles removed 95% of arsenate from the stock solution 10 mg/L in 15 minutes, whereas bulk hydrogel removed >82% of arsenate from an equivalent solution in ~12 h. The P4VP-HCl nanoparticles can be reused up to 5 times with around 90% absorption/desorption for each cycle at medium of 2 M NaOH.[109] Uranium and Thorium also can be removed from aqueous solution by P4VP nanoparticles and its

magnetic nanoparticles.[110] Therefore, P4VP nanoparticles materials are promising to use as removal of toxic species from the contaminated environment.

Table 1.3: The dimension and zeta potentials of P4VP nanoparticles before and after quaternised with hydrochloric acid (HCl), bromoethane (E), 1-bromobutane (B) and 1-bromohexane (H).[107]

Particle	Diameter (nm)	Zeta potential (mV)
P4VP	370 ± 6	1.8 ± 0.4
P4VP-HCl	562 ± 19	39.8 ± 2.1
P4VP-E	501 ± 15	29.6 ± 1.7
P4VP-B	463 ± 14	35.9 ± 2.8
P4VP-H	420 ± 12	21.9 ± 2.3

P4VP is a pH-sensitive polymer which is soluble in the water when the pH value below 4.7 and becomes insoluble at high pH. Therefore, it is possible to design pH-responsive polymer. However, addition of poly(*N*-isopropyl acrylamide) (PNIPAM) to the P4VP segment added thermoresponsive properties. The block copolymer of poly(NIPAM-*b*-4VP) was thus expected to respond to both temperature and pH changes. Xu *et al*. reported that poly(NIPAM-*b*-4VP) formed spherical core-shell micelles in solution. At pH 2.8 under 25 °C, the copolymer existed as unimers. When the temperature increased to 50 °C at pH 2.8, the micelles formed with PNIPAM as a core and P4VP as a shell. However, the micelles with P4VP as a core and PNIPAM as a shell obtained by the increasing the pH from 2.8 to 6.5 at 25 °C.[111] Scheme 1.9 shows the pH and thermoresponsive of poly(NIPAM-*b*-4VP) in aqueous solution. The critical aggregation of temperature and pH of poly(NIPAM-*b*-4VP) are 36 °C and 4.7, respectively.

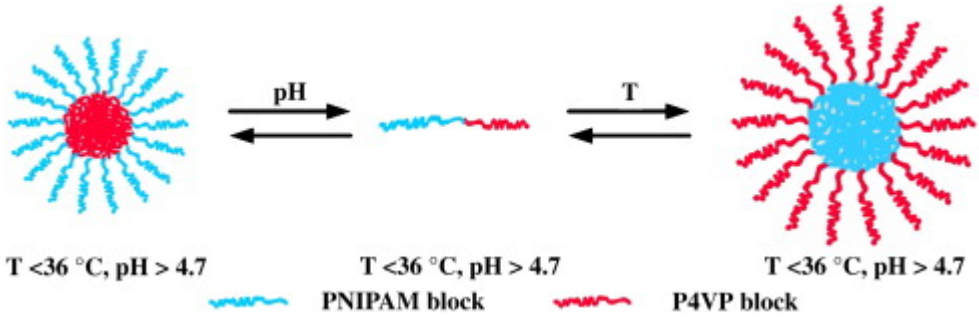

Scheme 1.9: The formation of micelles and reverse micelles of poly(NIPAM-*b*-4VP) in aqueous solutions.[111]

Double hydrophilic block copolymers were first introduced by Armes and co-workers.[112] Self-assembly of these block copolymers in solution formed two type of micelles. The individual block copolymer easily changed the behaviour just by changing the pH. For instance, poly(*tert*-butyl acrylate-*b*-4-vinylpyridine) were synthesised using ATRP, followed by hydrolysis to formed poly(acrylic acid-*b*-4-vinylpyridine). This block copolymer was associated to poly acrylic acid (PAA) as a core micelles and P4VP as a shell at pH 2.8, while micelles with P4VP as a core and PAA as corona micelles observed at pH 10. The average size measured by TEM were 12 nm and 20 nm for PAA core and P4VP core, respectively.[113] Further encapsulation application by zinc and cobalt tetraphenylporphyrin were studied. The P4VP core loads more metalloporphyrin than the PAA core due to the axial coordination between pyridine of the polymer and transition metal. The metalloporphyrin encapsulate in the core P4VP can be released by pH decrease, while metalloporphyrin entrapped in the PAA core was released by pH increase. The pH sensitivity opens possibilities to design polymers for drug delivery application.[114]

1.6 Introduction of Electrochemistry

1.6.1 Electrochemical cell

The fundamental apparatus used in electrochemical techniques is the electrochemical cell either as a two or three electrode system. Typical three-electrode cells consist of working electrode, reference electrode and counter electrode as shown in Figure 1.11.

The working electrode is the terminal which the electrochemical reaction under investigation occurs. It makes contact with the electrolyte and the charge is transferred to or from the electrolyte. The electrolyte is a chemical compound which is salt, acid or base that dissociates into electrically charged ions when dissolved in a solvent. In order to apply potential or current to the working electrode, a counter electrode and a reference electrode are required to complete the system. The reference electrode is important as reference in measuring and controlling the working electrode potential by comparing it to their known reduction potential. The counter electrode passes a current to balance the potential at the working electrode, thus providing the potential stability to the reference electrode during the experiment. This cell is used throughout the experiments in Chapter 5.

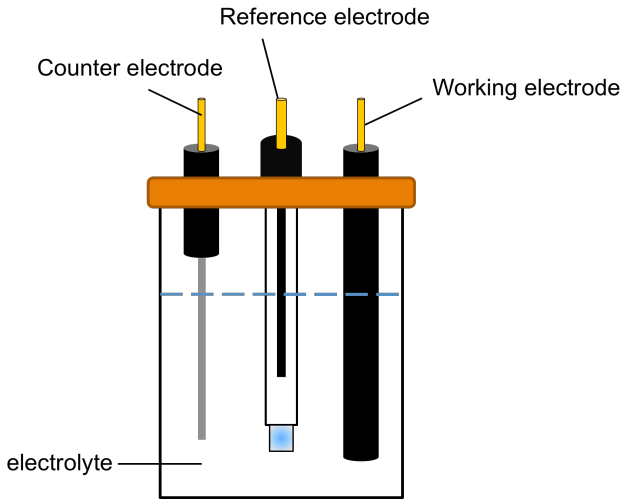

Figure 1.11: Three electrode system in electrochemical cell.

1.6.2 Cyclic voltammetry

Cyclic voltammetry (CV) is the most versatile electroanalytical technique for the study of electroactive species. CV measures the current as a function of electrical potential in an unstirred solution. The potential applied produces pulse excitation signals in triangular waveform such as shown in **Error! Reference source not found.**. In a forward scan, the potential increases linearly from initial potential (point a) to a predetermined limit (point b). At point b, the voltage is sufficient enough to reduce or

oxidise the analyte. Then, the reverse scan occurred to be at the same potential as the initial and the turning point is called 'switching potential'. The scan rate is measured by the slope of potential versus time, *e.g.* 50 mV/s for Figure 1.12. This cycle can be repeated many times and have different scan rates.

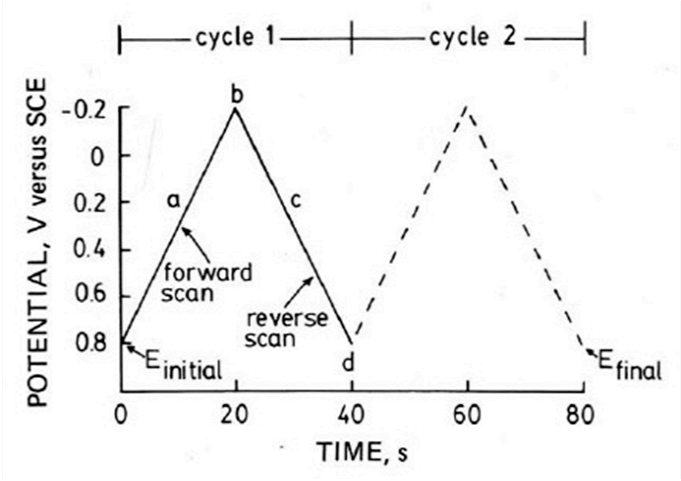

Figure 1.12: Typical excitation signal for cyclic voltammetric-a triangular potential with switching potentials at 0.8 and -0.2 V vs SCE.[115]

A CV is obtained by measuring current at the working electrode during potential scans. For example, Figure 1.13**Error! Reference source not found.** shows the voltammogram of the reduction process of potassium ferricyanide.[115] At initial potential (**a**), no current is observed until the cathodic current (i_{pc}) begins to developed (**b**) at the potential applied sufficient enough to reduced $Fe^{III}(CN)_6^{3-}$. The cathodic current increase rapidly from (**b**) to (**d**) as the concentration becomes diminished at (**d**) performed cathodic peak (E_{pc}). Then, the current decays from (**d**) to (**g**) due to the fact that the diffusion layer is expanded farther and farther away from electrode surface. The scan direction is switched to the reverse scan at (**f**) performed anodic current (i_{pa}). This anodic current (**i**) to (**k**) obtained the oxidation process of $Fe^{II}(CN)_6^{4-}$ and the ions completely oxidise at the anodic peak (E_{pa}). The first cycle of redox reaction is complete when the original potential given below is reached.

$$Fe(CN)_6^{3-} + e^- \rightleftharpoons Fe(CN)_6^{4-}$$

Overall, two processes are involved during the CV which are the diffusion of the electroactive materials in bulk solution to the surface and electron transfer reaction.

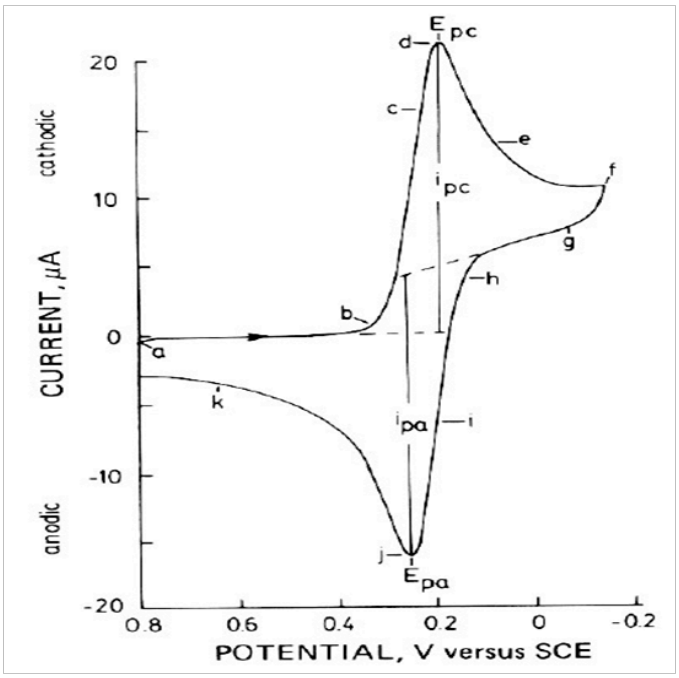

Figure 1.13: Cyclic voltammogram of 6 mM $K_3Fe(CN)_6$ in 1 M KNO_3, scan rate 50 mV/s at 0.8 V versus SCE.[115]

The important characterisations of the CV are peak potentials (E_{pc}, E_{pa}) and peak currents (i_{pc}, i_{pa}). If the electron transfer is fast, the reaction is called electrochemically reversible. Theoretically for the CV at 25°C, the formal reduction potential ($E°$) for a reversible couple is given below:

$$E° = \frac{E_{pa} + E_{pc}}{2}$$

The number of electron transferred in the electrode reaction (n) for a reversible couple can be determined from separation between the peak potentials:

$$\Delta E_p = E_{pa} - E_{pc} \cong \frac{0.0592}{n}$$

For reversible redox reaction, the peak current is related to the concentration according to Randles-Sevcik equation as follow:

$$i_p = 2.69 \times 10^5 \, n^{3/2} \, A D^{1/2} C v^{1/2}$$

where i_p is peak current (A), n is number of electron by stoichiometry, A is the area (cm^2), D is diffusion coefficient (cm^2/s), C is concentration (mol/cm^3) and v is scan rate (V/s). It should be noted that the ratio of anodic and cathodic peak current equal to 1 for reversible redox reaction. Analysis of CV offers information about the chemical processes, properties and the amount of electroactive materials that may occur in the system.

1.6.3 Bulk electrolysis

Generally, electrolysis is the process where the chemical compound decomposes to its elements or produced a new product driven by electrical currents. For example, electrolysis of water producing hydrogen (H_2) and oxygen (O_2) gases when electric current were passed through it.

In bulk electrolysis, the current flow is measured with a constant potential applied at working electrode throughout the reaction. The constant potential is carried for long enough time to fully reduce or oxidise all the substrate in the bulk solution. Thus, the concentration and current is decreasing with time during the electrolysis as the substrate is consumed. The quantity of electricity, Q consumed in the electrolysis can be expressed as follow:

$$Q = i\,t$$

where, i is current and t is time of reaction. Coulombs, Q represent the quantity of the charge transported in one seconds by a constant current of one Ampere. Analysis of bulk electrolysis offers information about the quantities of materials or number of electrons involved in the electrode reaction by applying Faraday's Law:

$$Q = nFN_A$$

where, n is number of electron by stoichiometry, F is Faraday constant (96485 C mol^{-1}) and N_A is the moles of the analyte present.

1.7 Objectives of the work

The aims of this project were:

1. To compare two methods of controlled radical polymerisation for the synthesis of linear block copolymers, poly(MMA-*b*-4VP)
2. To synthese original polymer architectures such as star homopolymers and star block copolymers, poly(MMA-*b*-4VP)
3. To investigate the metal binding of P4VP materials in selected applications, such as with in micelles and during electrocatalysis processes

1.8 Outline

The first chapter of this dissertation deals with the introduction of the controlled radical polymerisation and the architectures of polymer. In addition, the synthesis and optimum condition of P4VP from ATRP, NMP and RAFT are reviewed. As known, the nitrogen atom in the pyridine ring has an electron pair that easily coordinates with the metal centres and quaternises at acidic pHs. Therefore, selected examples of application such as drug delivery, sensors, electrocatalysis and templates for fabricating nanoparticles are discussed.

Chapter 2 will describe the synthesis of linear and star architectures of PMMA and poly(MMA-*b*-4VP) block copolymer by ATRP. Different ratios of Cu(I)/Cu(II) and ligand such as HMTETA and Me_6TREN were explored. Polymerisation of PMMA is well-controlled with low dispersity, in contrast to star PMMA, which suffered from termination reactions. Manipulation of the ratio of monomer to initiator is considered for reducing the termination reaction.

In Chapter 3, the polymerisation of 4VP and poly(4VP-*b*-MMA) block copolymer by NMP will be discussed. MAMA-SG1 is used as initiator for synthesising P4VP. However, the extension of MMA to the P4VP segments is challenging. Introduction of 10% styrene at the initial polymerisation can improve the control of the polymerisation. Self-assembly of poly(4VP-*b*-MMA) in a selective solvents for PS resulted in inverse micelles with P4VP as a core and PS as a corona. Then, metal binding application are studied with addition of metal salts at different ratios of [pyridine]:[Cu].

Chapter 4 addresses the approach to synthesis of star P4VP using NHS functionalised MAMA-SG1. Firstly, MAMA-NHS is grafted to the JEFFAMINE® and PPI dendrimer to form star initiator. Then, P4VP were synthesised and characterised.

In Chapter 5, the application of P4VP as an electrocatalys will be discussed. P4VPs was complexed with cobalt(II) hexadecafluorophthalocyanine and the interaction between pyridine and metal were investigated. The electrocatalytic potential for hydrogen evolution from P4VP/Co is discussed and compared with the results obtained from the neat P4VP and Co films. In addition, the potential of P4VP film as electrocatalyst for CO_2 reduction are assessed.

Chapter 6 deals with general finding and conclusion of the work reported in the dissertation. Recommendation for further studies are also provided.

References

1. Matyjaszewski, K.; Davis, T. P., Eds. Handbook of radical polymerisation; John Wiley & Sons, Inc. Publications: Haboken, 2002.

2. Szwarc M, Nature 1956;178:1168.

3. Braunecker WA, Matyjaszewski K, Prog Polym Sci 2007;32:93.

4. Hadjichristidis N, Iatrou H, Pitsikalis M, Mays J, Prog Polym Sci 2006;31:1068.

5. Matyjaszewski K, Xia J, Chem Rev 2001;101:2921.

6. Matyjaszewski K, Macromolecules 2012;45:4015.

7. Hawker CJ, Bosman AW, Harth E, Chem Rev 2001;101:3661.

8. Nicolas J, Guillaneuf Y, Lefay C, Bertin D, Gigmes D, Charleux B, Prog Polym Sci 2012;38:63.

9. Grubbs RB, Polymer Review 2011;51:104.

10. Moad G, Rizzardo E, Thang SH, Acc Chem Res 2008;41:1133.

11. Moad G, Rizzardo E, Thang SH, Polymer 2008;49:1079.

12. Fischer H, Chem Rev 2001;101:3581.

13. Gromada J, Matyjaszewski K, Macromolecules 2001;34:7664.

14. Goto A, Fukuda T, Prog Polym Sci 2004;29:329.

15. Matyjaszewski K, Gnanou Y, Leibler L, Molecular Engineering: Precise Synthesis, Materials Properties, Applications ; Wiley-VCH Verlaq GmbH & Co.: Weinheim, Germany, 2007.

16. Charleux B, Nicolas J, Guerret O, Macromolecules 2005;38:5485.

17. Nicolas J, Dire C, Mueller L, Belleney J, Charleux B, *et al*. Macromolecules 2006;39:8274.

18. Nicolas J, Couvreue P, Charleux B, Macromolecules 2008;41:3758.

19. Nicolas J, Mueller L, Dire C, Matyjaszewski K, Charleux B, Macromolecules 2009;42:4470.

20. Nicolas J, Brusseau S, Charleux B, J Polym Sci Part A:Polym Chem 2010;48:34.

21. Vinas J, Chagneux N, Gigmes D, Trimaille T, Favier A, Bertin D. Polymer 2008; 49:3639.

22. Guillaneuf Y, Couturier JL, Gigmes D, Marque SRA, Tordo P, Bertin D, J Org Chem 2008;73:4738.

23. Pintaeur T, Matyjaszewski K, Chem Soc Rev 2008;37:1087.

24. Jakubowaki W, Min K, Matyjaszewski K, Macromolecules 2006;39:39.

25. Bosman AW, Vestberg R, Heunmann AJ, Fréchet JM, Hawker CJ, J Am Chem Soc 2003; 125:715.

26. Liu H, Li S, Zhang M, Shao W, Zhao Y, J Polym Sci Part A: Polym Chem 2012;50:4705.

27. Kim DG, Hyo Kang H, Han S, Lee JC, ACS Appl Mater Interfaces 2012;4:5898.

28. Terashima T, Kamigaito M, Baek KY, Ando T, Sawamoto M, J Am Chem Soc 2003; 125:5288.

29. Gao H, Matyjaszewski K, Prog Polym Sci 2009;34:317.

30. Blencowe A, Tan JF, Goh KT, Qiao GG, Polymer 2009;50:5.

31. Moschogianni P, Pispas S, Hadjichristidis N, J Polym Sci Part A:Polym Chem 2001;39:650.

32. Strandman S, Tenhu H, Polymer 2007;48:3938.

33. Matyjaszewski K, Miller PJ, Pyun J, Kickelbick G, Diamanti S, Macromolecules 1999;32: 6526.

34. Costa ROR, Vasconcelos WL, Macromolecules 2001;34:5398.

35. Zhao Y, Chen Y, Chen C, Xi F. Polymer 2005; 46:5808; b)

36. Hedrick JL, Trollsås M, Hawker CJ, Atthoff B, Claesson H *et al*. Macromolecules 1998; 31:8691.

37. High LRH, Holder SJ, Penfold HV, Macromolecules 2007;40:7157.

38. Hawker CJ, Angew Chem Int Ed 1995;34:1456.

39. Miura Y, Yoshida Y, Macromol Chem Phys 2002;203:879.

40. Beil JB, Zimmerman SC, Macromolecules 2004;37:778.

41. Miura Y, Dote H, J Polym Sci Part A:Polym Chem 2005;43:3689.

42. Lu CH, Wang JH, Chang FC, Kuo SW, Macromol Chem Phys 2010;211:1339.

43. Robin S, Guerret O, Couturier JL, Gnanou Y, Macromolecules 2002; 35:2481.

44. Abraham S, Choi JH, Ha CS, Kim I, J Polym Sci Part A:Polym Chem 2007;45:5559.

45. Dufils PE, Chagneux N, Gigmes D, Trimaille T, Marque SRA, Bertin D, Tordo P, Polymer 2007;48:5219.

46. Xia J, Zhang X, Matyjaszewski K, Macromolecules 1999;32: 4482.

47. Zhang X, Xia J, Matyjaszewski K, Macromolecules 2000;33:2340.

48. Baek KY, Kamigaito M, Sawamoto M, Macromolecules 2001;34:215.

49. Baek KY, Kamigaito M, Sawamoto M. Macromolecules 2001;34:7629.

50. Pasquale AJ, Long TE, J Polym Sci Part A:Polym Chem 2001;39:216.

51. Tsoukatos T, Pispas S, Hadjichristidis N, J Polym Sci Part A:Polym Chem 2001;39:320.

52. Bosman AW, Heumann A, Klaener G, Benoit D, Fréchet JM, Hawker CJ. J Am Chem Soc 2001; 123:6461.

53. O'Reilly RK, Hawker CJ, Wooley KL, Chem Soc Rev 2006;35:1068.

54. Smart T, Lomas H, Massignani M, Flores-Merino MV, Perez LR *et al*. Nanotoday 2008;3-4:38 reference therein.

55. Riess G, Prog Polym Sci 2003;28:1107.

56. Tang C, Kowalewski T, Matyjaszewski K, Macromolecules 2003;36:1465.

57. Jérôme R, Macromol Symp 2002;177:43.

58. Bernaerts KV, Du Prez FE, Prog Polym Sci 2006;31:671.

59. Tunca U, Karliga B, Ertekin S, Ugur A L, Sirkeciogiu O, Hizal G, Polymer 2001;42:8489.

60. Tunca U, Erdogan T, Hizal G, J Polym Sci Part A:Polym Chem 2002;40:2025.

61. Habraken GJM, Peeters M, Thornton PD, Koning CE, Heise A, Biomacromolecules 2011;12:3761.

62. Xia J, Zhang X, Matyjaszewski K, Macromolecules 1999;32:3531.

63. Tsarevsky NV, Braunecker WA, Brooks SJ, Matyjaszewski K, Macromolecules 2006;39:6817.

64. Burguière C, Dourges MA, Charleux B, Vairon JP. Macromolecules 1999;32:3883.

65. Shoji M, Eguchi M, Layman JM, Cashion MP, Long TE, Nishide H, Macromol Chem Phys 2009;210:579.

66. Antonietti M, Golner C, Angew Chem Ed Engl 1997;36:910.

67. Creutz S, Teyssié P, Jérome R. Macromolecules 1997;30:1.

68. Lee J, Hogen-Esch TE, Macromolecules 2001;34:2805.

69. Yang R, Wang, Y, Wang X, He W, Pan C, Eur Polym J 2003;39:2029.

70. Jiang F, Kaltbeitzel A, Meyer WH, Pu H, Wegner G, Macromolecules 2008;41:3081.

71. Convertine AJ, Sumerlin BS, Thomas DB, Lowe AB, McCormick CL, Macromolecules 2003;36:4679.

72. Vukić JB, Manon HT, Meuldijk J, Koning C, Klumperman B. Macromolecules 2007;40:7132.

73. Yuan JJ, Ma R, Gao Q, Wang YF, Cheng SY *et al*. J App Polym Sci 2003;89:1017.

74. Zhang L, Wang Q, Lei P, Wang X, Wang C, Cai L, J Polym Sci Part A:Polym Chem 2007; 45:2617.

75. Bohrisch J, Wendler U, Jaeger W, Macromol Rapid Commun 1997;18:975.

76. Fisher A, Brembilla A, Lochon P, Macromolecules 1999;32:6069.

77. Diaz T, Fischer A, Jonquiéres A, Brembilla A, Lochon P, Macromolecules 2003;36:2235.

78. Lohmeijer BGG, Schubert US, J Polym Sci Part A:Polym Chem 2005;43:6331.

79. Maria S, Susha AS, Sommer M, Talapin DV, Rogach AL, Thelakkat M, Macromolecules 2008;41:6081.

80. Polakova L, Lokaj J, Holler P, Starovoytova L, Pelkarek M, Stepanek P, e-Polymers 2010;65:1.

81. Lessard BH, Marić M, e-Polymers 2012;63:1.

82. Rahim NA, Audouin F, Twamley B, Vos JG, Heise A, Eur Polym J 2012;48:990.

83. Bockstaller MR, Mickiewiez RA, Thomas EL, Adv Mater 2005;17:1331.

84. Antonietti M, Wenz E, Bronstein L, Seregina M, Adv Mater 1995;7:1000.

85 Mendoza C, Pietsch T, Gutmann JS, Jehnichen D, Gindy N, Fahmi A, Macromolecules 2009;42:1203.

86. Huang CM, Wei KH, Macromolecules 2007;40:5067.

87. Platonova OA, Bronstein LM, Solodovnikov SP,Yanovskaya IM, Obolonkova ES *et al*., Colloid Polym Sci 1997;275:426.

88. Liu Y, Lor C, Fu Q, Pan D, Ding L, et al. J Phys Chem C 2010;114:5767.

89. Cheng F, Yang X, Peng H, Chen D, Jiang M, Macromolecules 2007;40:8007.

90. Li J, Shi l, An Y, Li Y, Chen X, Dong H, Polymer 2006;47:8480.

91. Cheng KW, Chan WK, Langmuir 2005;21:5247.

92. Hou S, Man KYK, Chan WK, Langmuir 2003;19:2485.

93. Hou S, Chan WK, Macromol Rapid Commun 1999;20:440.

94. Zhang J, Wang J, Xu X, Zhu H, Wang Z *et al*., Nanotechnology 2009;20:1.

95. Abe T, Kaneko M, Prog Polym Sci 2003;28:1441.

96. Liu J, Cheng L, Song Y, Liu B, Dong S, Langmuir 2001;17:6747.

97. Zhao F, Zhang J, Abe T, Wöhrle D, Kaneko M, J Mol Catal A: Chem 1999;145:245.

98. Inglis JL, Maclean BJ, Pryce MT, Vos JG, Coord Chem Rev 2012;256:2571.

99. Zhao F, Zhang J, Wöhrle D, Kaneko M, J Porphy Phthalocyan 2000;4:31.

100. Yoshida T, Kamato K, Tsukamoto M, Iida T, Schlettwein D *et al*. J Electroanal Chem 1995;385:209.

101. Abe T, Yoshida T, Tokita S, Taguchi F, Imaya H, Kaneko M, J Electroanal Chem 1996;412:125.

102. Abe T, Taguchi F, Yoshida T, Tokita S, Schnurpfeil G *et al*. J Mol Catal A: Chem 1996;112:55

103. Forster RJ, Vos JG, Macromolecules 1990;23:4372.

104. Doherty AP, Forster RJ, Smyth MR, Vos JG, Analytica Chimica Acta 1991;255:45.

105. Doherty AP, Stanley MA, Leech D, Vos JG, Analytica Chimica Acta 1996;319:111.

106. Heller A, Feldman B, Chem Rev 2008;108:2482.

107. Sahiner N, Ozay O, React Funct Polym 2011;71:607.

108. Sahiner N, Ozay O, Colloids Surf A:Physiochem Eng Aspects 2011;378:50.

109. Sahiner N, Ozay O, Aktas N, Blake D, John VT, Desalination 2011;279:344.

110. Ozay O, Ekici S, Aktas N, Sahiner N, J Environ Manage 2011;92:3121.

111. Xu Y, Shi L, Ma R, Zhang W, An Y, Zhu XX, Polymer 2007;48:1711.

112. Bütün V, Liu S, Weaver JVM, Bories-Azeau X, Cai Y, Armes SP, React Funct Polym 2006;66:157.

113. Bo Q, Zhao Y, J Polym Sci Part A: Polym Chem 2006;44:1734.

114. Li G, Guo L, Ma S, Liu J, J Polym Sci Part A: Polym Chem 2009;47:1804.

115. Kissinger PT, Heineman WR, J Chem Edu 1983;60:702.

2 Poly (methyl methacrylate-*b*-4 vinylpyridine) linear and star polymers by Atom Transfer Radical Polymerisation

Abstract

Poly(methyl methacrylate) (PMMA) macroinitiators were synthesised by Atom Transfer Radical Polymerisation (ATRP) using ethyl 2-*bromoisobutyrate (EBiB) as initiator, CuCl as catalyst and 1,1,4,7,10,10-hexamethyltriethylenetetramine (HMTETA) as ligand at 90 °C. The controlled polymerisation followed a first-order kinetics with respect to the monomer conversion. The molecular weights of the resulting polymers were very close to their theoretical value and increased with conversion. The star PMMA polymerisation also showed a similar trend in results. Furthermore, PMMA terminated with chloride were used as macroinitiator, to obtain diblock copolymer of poly(MMA-b-4VP). Spectroscopy methods confirmed the structures of polymers, however, the strong metal complexing character of the 4VP was shown to interfer with the ATRP catalytic system.*

2.1 Introduction

Atom Transfer Radical Polymerisation (ATRP) is an extensively studied controlled radical polymerisation (CRP) method.[1-4] The main components in this system include a monomer, an initiator and a catalyst. Typically, catalysts are composed from a transition metal and a ligand, and modulate the activated and deactivated species of equilibrium during polymerisation. Other factors that need to be understand in order to achieve for a successful reactions are solvent, temperature, concentration and solubility of all components.[3] The advantage of ATRP is the tolerance to functional groups of monomers and initiators which makes it suitable for a wide range of monomers, such as styrene[5-7], acrylates[8,9], methacrylates[10,11] and their derivatives. This also allows for the synthesis of controlled architectures (stars, comb, branched), compositions (block, alternating) and end functionalities.[12,13]

As shown in Scheme 2.1, the propagating species P_n* is generated through a reversible redox process catalysed by a transition metal complex (activator, M_t^n-Y/Ligand where Y may be another ligand or a counter ion). The transition metal complex undergoes oxidation by abstraction of a halogen atom, X, from the dormant species, P_n-X. Then, radicals react reversibly with the oxidized metal complexes X-M_t^{n+1}/Ligand, the deactivator, to reform the dormant species and the activator. This process occurs with a rate constant of an activation, k_a, and deactivation, k_{da}. Polymer chains grow by the addition of monomers to free radicals with the rate propagation, k_p. Termination reaction, k_t, occur through radical coupling and disproportionation. In this stage, the deactivators, which behave likes persistent radicals, reduced the stationary concentration of growing radicals and thereby minimize the contribution of termination. In other words, the contribution of termination becomes insignificant due to the persistent radical effect.[14,15] Several transition metal such as Cu, Ru, Fe and Ni are used as catalyst in ATRP.[16,17]

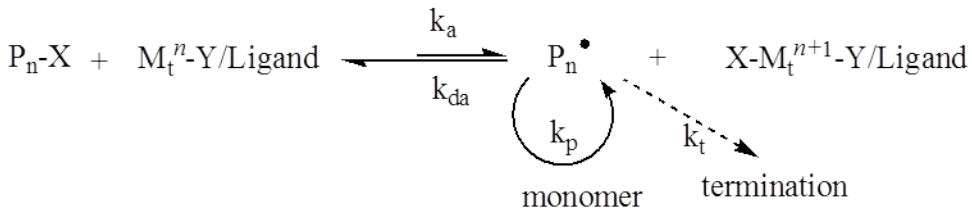

Scheme 2.1: General scheme of transition-metal-catalysed ATRP.

Methyl methacrylate (MMA) has been extensively investigated in ATRP catalytic systems based on copper[10,11], ruthenium[18,19], nickel[20,21] and iron[22,23]. Polymerisation of MMA by copper mediated catalysts has been explored by Matyjaszewski and his groups. Since 1995, they studied the effect of ligand/Cu(I) ratio on the rate of polymerisation, the dependence of polymerisation rate on the concentrations of initiator, involvement of Cu(I) and Cu(II) species in the polymerisation system, effect of temperature on polymerisation and improvement of polymerisation by choice of the initiator and experimental procedure.[10,24] For example, high molecular weight of PMMA was reported by Xue *et al*. of 367000 g/mol and dispersity, 1.2 using 2-bromo-2-methyl propionate.[11] While, at different concentration of initiator *p*-toluenesulfonyl chloride (*p*-TsCl) under sealed tube condition, high molecular weight ranging from 83900 to 183000 g/mol was obtained.[10]

However, 4-vinylpyridine (4VP) and its polymerisation poses a very challenging problem for ATRP because it is a strong coordinating ligand that can compete for the binding of the metal catalyst in these system. Therefore, if the monomer is present in large excess over the employed ligand, there is the possibility of the formation of pyridine-coordinated metal ion complexes in the polymerisation solution. Xia *et al*. showed that by addition of 5% (v/v) of pyridine to the styrene polymerisation solution catalysed CuBr complexed by 4,4'-di(5-nonyl)-2,2'-bipyridine (dNbpy) the polymerisation rate significantly slowed down.[25] The successful ATRP of 4VP was reported using chloride-ATRP initiator/catalyst system in protic media, *e.g*. polymerisation of 4VP in 2-propanol with 1-phenylethyl chloride (PECl) as initiator and CuCl/ tris[2-(dimethylamino)ethyl]amine (Me_6TREN) catalyst system.[26]

Because of the potential metal binding abilities of 4VP, integration of P4VP into polymers structures is of great interest. For example, amphiphilic poly (methyl methacrylate-block-4-vinylpyridine), poly(MMA-*b*-4VP) was synthesised successfully by sequential anionic polymerisation.[27-29] However, anionic polymerisation requires rigorous exclusion of oxygen and water, ultrapure reagent and solvent, and low temperature. Moreover, only a limited number of monomer can be polymerised and the presence of functional monomers can cause undesired side reaction. CRP is the convenient methods to overcome these limitations. Notably, ATRP polymerisation of 4VP can be conducted with CuCl/Me_6TREN. However, because this catalyst system is relatively poor for MMA, Cu(II)Cl needs to be introduced at the beginning of the reaction at high concentration.[26,30]

This chapter reports our investigations into the use of PMMA-Cl macroinitiator for chain extension with 4VP for the synthesis of amphiphilic block copolymer poly(MMA-*b*-4VP). To the best of our knowledge, only a few research reports on this sequential block copolymer have been published.[31] We were also interested in the development of star polymer due to their higher degree of chain end functionality compared to linear polymers.[32,33] In this chapter we provided the kinetic study of PMMA and poly(MMA-*b*-4VP) polymerisation. Moreover, the structure of PMMA and poly(MMA-*b*-4VP) was confirmed by spectroscopy methods.

2.2 Experimental

2.2.1 Materials

All solvents employed were HPLC grade or better and used directly as received unless otherwise stated. Methyl methacrylate, MMA (Aldrich, 99%) and 4-vinylpyridine, 4VP (Aldrich, 95%) were distilled from calcium hydride before used. Ethyl 2-bromoisobutyrate (Aldrich, 98%) was used as a monofunctional initiator. CuCl (Sigma Aldrich, 99.995%) and $CuCl_2$ (Aldrich, 99.995%) was used as combination catalyst according to the ratio needed for ATRP. The ligand used in this experiment was 1,1,4,7,10,10-hexamethyltriethylenetetramine, HMTETA (Aldrich, 97%).

2.2.2 Synthesis of ligand tris[2-(dimethylamino)ethyl]amine (Me_6TREN)

This compound was synthesised following a literature procedure involving 2 steps [34]; *i.e.* preparation of ammonium salt and Me_6TREN. To prepare the salt $(ClNH_3CH_2CH_2)_3NHCl$, 30 mL of 3.0 M HCl in methanol was added dropwise to 4.0 mL (0.027 mol) of tris(2-aminoethyl)amine in 50 mL of methanol. After stirring at room temperature for 1 hour, the precipitate was filtered and washed with 50 mL methanol three times to yield 5.65 g (0.019 mol). To prepare Me_6TREN, 5.65 g of $(ClNH_3CH_2CH_2)_3NHCl$, 10 mL of water, 50 mL of formic acid, and 46 mL of a formaldehyde aqueous solution were mixed. The mixture was heated under stirring in a 120 °C oil bath for 6 hours before volatile components were removed by rota-evaporation. To the solid residue (yellow) was then added 100 mL of 10 wt% NaOH aqueous solutions (pH 10-11). After shaking, the aqueous phase was extracted 4 times with 100 mL diethyl ether. The organic phases were combined, dried over anhydrous magnesium sulphate, and evaporated by rotary evaporation to produce the yellow oil.

^{1}H NMR (400 MHz, $CDCl_3$) (ppm): 2.20 (s, 18H, CH_3), 2.33–2.37 (m, 6H, CH_2), 2.56–2.60 (m, 6H, CH_2). Yield: 2.26 g.

2.2.3 Synthesis of tetrafunctional initiator pentaerythritol tetrakis (2-bromoisobutyrate), (PT-Br)

A literature method was followed to prepare PT-Br.[35] A 100 mL round-bottom flask with a magnetic stirring bar was charged with pentaerythritol (1.0 g, 7.3 mmol) and kept under nitrogen before the addition of 20 mL of toluene (degassed with nitrogen before used) and triethylamine (4.8 mL, 35 mmol) *via* syringe transfer. The reaction medium was cooled with an ice bath under stirring. A solution of 2-bromoisobutyryl bromide (3.7 mL, 30 mmol) was slowly added. The flask was kept at room temperature for overnight under stirring. Then, it was filtered and the salt washed with toluene until the bromine colour disappeared. The filtrate was added with water (100 mL) and saturated $NaHCO_3$ aqueous solution (50 mL) three times. The organic layers were then dried over

anhydrous magnesium sulphate, filtered, concentrated, dried in vacuum oven overnight and recrystallised in diethyl ether three times to produce light yellow crystals.

^{1}H NMR (400 MHz, $CDCl_3$), (ppm): 4.25 (s, 8H, C–**CH_2**–O), 1.85 (s, 24H, C(Br)–**CH_3**). ^{13}C NMR (100 MHz, $CDCl_3$), δ ppm: 30.6 (**C**$(CH_3)_2$Br), 43.7 (**C**$(CH_2O)_4$), 55.2 (**C**$(CH_3)_2$Br), 62.9 (**C**H_2), 170.9 (**C**=O).Yield: 1.7 g.

2.2.4 Typical procedure for the synthesis of polymerisation of methyl methacrylate (MMA)

A dry Schlenk flask with a stirring bar was charged with MMA (11.16 g, 110 mmol), ethyl 2-bromoisobutyrate (0.1 g, 0.56 mmol), CuCl (0.044 g, 0.46 mmol), $CuCl_2$ (0.015 g, 0.11 mmol), toluene (10.8 mL, 100 mmol) and DMF (1.2 mL, 15.5 mol). The flask was sealed with a rubber septum and was degassed by bubbling nitrogen about 20 minutes to remove the oxygen. HMTETA (0.15 mL, 0.56 mmol) was then added using a syringe, imparting green colour to the solution. The flask was immersed in an oil bath held by a thermostat at 90 °C and timing was started. Samples were taken periodically from the flask using degassed syringes and quenched in ice bath for the kinetic studies. The polymer was recovered by removing the solvent by rotary evaporation, redissolving the polymer in dichloromethane, passing the polymer solution through alumina column to remove metal containing residues and precipitation in methanol. The polymer was dried at 40 °C under vacuum overnight to obtain white PMMA powder.

^{1}H NMR (400 MHz, $CDCl_3$) (ppm): 3.59 (s, -OCH_3), 2.10-1.50 (m, -CH_2 polymer backbone), 1.10-0.80 (s, -CH_3). FTIR (cm^{-1}): 3100-2900 (-CH_2-), 1731 (C=O), 1449 (CH_3), 1145 (O-CH_3). Precipitated yield: 8.90 g.

2.2.5 Typical procedure for the synthesis of poly (MMA-*b*-4VP)

A dry Schlenk flask with a magnetic stirring bar was charged with PMMA-Cl, (M_n 5000 g/mol; 1.20 g, 0.21 mmol), CuCl (17.2 mg, 0.17 mmol), $CuCl_2$ (5.8 mg, 0.04 mmol) and 4VP (4.4 g, 0.04 mol). Then, flask was sealed and bubbled with nitrogen for 30

minutes. 0.36 mL (1.31 mmol) HMTETA was added *via* syringe and the flask was immersed in oil bath at 90 °C. Samples were withdrawn from the flask using degassed syringe for kinetic studies. The polymer was recovered by removing the solvent by rotary evaporation, redissolving the polymer in dichloromethane, passing the polymer solution through an alumina column to remove the metal containing residues. Then, sample was precipitated in diethyl ether, filtered using a vacuum filtration and dried in vacuum at 40 °C to obtain a light yellow powder.

^{1}H NMR (400 MHz, $CDCl_3$) (ppm): 8.3-8.1 (m, CH-N-CH), 6.3-6.1 (m, CH-C-CH), 3.6 (s, -OCH_3), 2.1-1.5 (m, -CH_2-), 1.1-0.8 (s, -CH_3). FTIR (cm^{-1}): 3023, 1598, 1557, 1416, 993 (pyridine ring), 2938 (-CH_2-), 1726 (C=O), 1449 (CH_3), 1145 (O-CH_3). Precipitated yield: 1.90 g.

2.2.6 Typical procedure for the synthesis of star polymerisation of methyl methacrylate (sPMMA)

MMA (11.16 g, 110 mmol), PT-Br (0.1 g, 0.14 mmol), CuCl (0.04 g, 0.45 mmol), $CuCl_2$ (0.02 g, 0.11 mmol), toluene (10.8 mL, 0.10 mol) and DMF (1.2 mL, 15.5 mol) were added into a Schlenk flask with a magnetic stirrer. The flask was then sealed with a rubber septum and degassed for 30 minutes. 0.15 mL (0.56 mol) HMTETA was then added using syringe, imparting green colour to the solution. The flask was immersed in an oil bath held by a thermostat at 90 °C and timing was started. Samples were taken periodically from the flask using degassed syringes and quenched in ice bath for the kinetics studies. The polymer was recovered by removing the solvent by rotary evaporation, diluted the polymer in dichloromethane, passing the polymer solution through alumina column to remove metal containing residues and precipitated in methanol. The polymer was dried at 40 °C under vacuum overnight to obtain white 4-arm star PMMA powder.

^{1}H NMR (400 MHz, $CDCl_3$) (ppm): 3.59 (s, -OCH_3), 2.10-1.50 (m, -CH_2 polymer backbone), 1.10-0.80 (s, -CH_3). FTIR (cm^{-1}): 3100-2900 (-CH_2-), 1731 (C=O), 1449 (CH_3), 1145 (O-CH_3). Precipitated yield: 8.20 g.

2.2.7 Typical procedure for the synthesis of star block copolymer poly(MMA-*b*-4VP)$_4$

A dry Schlenk flask with a magnetic stirring bar was charged with sPMMA-Cl, (M_n 20,000 g/mol; 0.3 g, 0.015 mmol), CuCl (4.8 mg, 0.05 mmol), $CuCl_2$ (1.6 mg, 0.02 mmol) and 4VP (1.3 g, 12 mmol). Then, flask was sealed and bubbled with nitrogen for 30 minutes. 0.1 mL (0.36 mmol) HMTETA was added *via* syringe and the flask was immersed in oil bath at 90 °C. Samples were withdrawn from the flask using degassed syringe for kinetic studies. The polymer was recovered by removing the solvent by rotary evaporation, redissolving the polymer in dichloromethane, passing the polymer solution through an alumina column to remove the metal containing residues. Then, sample was precipitated in diethyl ether, filtered using a vacuum filtration and dried in vacuum at 40 °C to obtain a light yellow powder.

^{1}H NMR (400 MHz, $CDCl_3$) (ppm): 8.3-8.1 (m, CH-N-CH), 6.3-6.1 (m, CH-C-CH), 3.6 (s, -OCH_3), 2.1-1.5 (m, -CH_2-), 1.1-0.8 (m, -CH_3). FTIR (cm^{-1}): 3023, 1598, 1557, 1416, 993 (pyridine ring), 2938 (-CH_2-), 1726 (C=O), 1449 (CH_3), 1145 (O-CH_3). Precipitated yield: 0.18 g

2.2.8 Characterisation methods

^{1}H NMR and ^{13}C NMR analyses were performed in $CDCl_3$ solution, at 25 °C using a Bruker Avance 400 (400 MHz) spectrometer. The chemical shift was calibrated using the solvent peak (δ = 7.26 ppm). Fourier Transform InfraRed (FTIR) spectroscopy was carried out in the solid state on a Perkin Elmer Spectrum 100. For measured molecular weight and dispersity of the polymer, two eluent system were used on SEC, THF and DMF. SEC analysis using THF as eluent (elution rate: 1min/mL) was performed using two PL gel 5 µm mixed-C (300 x 7.5 mm) and PL gel 5 µm mixed-C guard (50 x 7.5 mm) columns on an Agilent 1200 series apparatus equipped with a refractive index and UV detector thermostat at 35 °C. Calibration was based on PMMA standards. For block copolymer, SEC analysis using DMF (0.1 M LiBr) as eluent (elution rate: 1min/mL) was performed using two PSS GRAM analytical (300 and 100 Å, 10 L) columns on an Agilent 1200 series apparatus equipped with a Wyatt Optilab rEX refractive index

detector thermostat at 40 °C and a Wyatt DAWN HELEOS-II multi angle light scattering (MALS) detector. Molecular weights and dispersities were calculated from the MALS signal using the ASTRA software (Wyatt) and a *dn/dc* value of 0.059 mL/g (PMMA)[36] and 0.225 mL/g (P4VP)[37] in DMF. Before analysis, samples were filtered through a 0.45 µm PTFE filter (13 mm, PP housing, Whatman). For block copolymer *dn/dc* was estimated by composition according to the block ratio;

$$(dn/dc)_{AB} = \text{Molar fraction}_A\ (dn/dc)_A + \text{Molar fraction}_B\ (dn/dc)_B$$

where, AB is the copolymer and A, B denote the homopolymers A and B.

2.3 Results and discussion

2.3.1 Polymerisation of methyl methacrylate (PMMA)

PMMA was synthesised using ethyl 2-bromoisobutyrate (EBiB) as the initiator, CuCl and $CuCl_2$ as a combination catalyst and HMTETA as the ligand at 90 °C in toluene. The synthetic route of the polymerisation is shown in

Scheme 2.2 and the summary of experiments in Table 2.1.

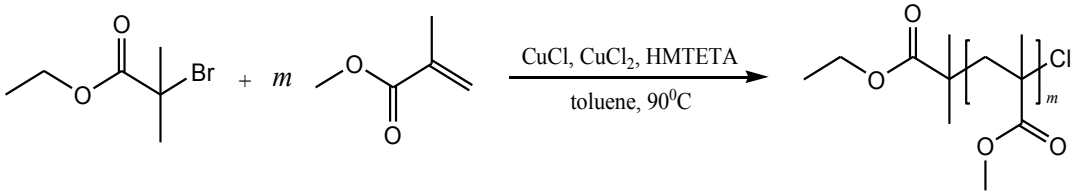

Scheme 2.2: Synthesis of PMMA by ATRP.

Table 2.1: Polymerisation of MMA by ATRP at 90 °C in toluene.

Sample	time (min)	Conv. [a] (%)	$M_{n\ theo}$ [b] (g/mol)	$M_{n\ SEC}$ [c] (g/mol)	D [c]	Ratio $[I]_0:[HMTETA]_0:[CuCl]_0:[CuCl_2]_0:[M]_0$
PMMA-6	60	87	4000	6000	1.1	1:1:0.8:0.2:40
PMMA-2	95	95	4000	6000	1.3	1:1:0.8:0.2:40
PMMA-3	95	74	3000	6000	1.3	1:1:0.7:0.3:40
PMMA-5	360	90	18000	19000	1.2	1:1:0.8:0.2:200

[(a)]Conversion calculated by ^{1}H NMR through integration of PMMA (5.4 ppm, 6.13 ppm) and DMF (2.8 ppm) peaks. [(b)]$M_{n\ theo}$ was calculated using the equation: M_n = conversion x $[M]_0/[I]_0$ x $M_{monomer}$. [(c)] D and M_n measure by THF SEC with PMMA standards calibration.

The effect of the reaction condition on the PMMA synthesis was investigated and the semilogarithmic kinetics plot is shown in Figure 2.1. PMMA-5 was prepared using a high ratio of $[M]_0/[I]_0$ of 200 compare to 40 for PMMA-6 with expected molecular weights (M_n) of 20000 and 5000 g/mol, respectively. The kinetic profiles were first order with respect to monomer and initiator concentration and increased linearly with time. Thus, the concentration of propagating radicals was thought to be constant throughout the reaction.[3,38,39]. Figure 2.1b shows that the M_n increases linearly with conversion in accordance to the theoretical value with good control of the dispersity (D) (< 1.2). PMMA-6 with a high concentration of initiator and ligand (0.11 M) displayed a fast reaction within 1 hour, resulting in a higher conversion of 87% and narrow D of 1.14. Meanwhile, PMMA-5 with low concentration of initiator and ligand (0.02 M) needs a longer reaction time to reach 90% conversion and a D of 1.15.

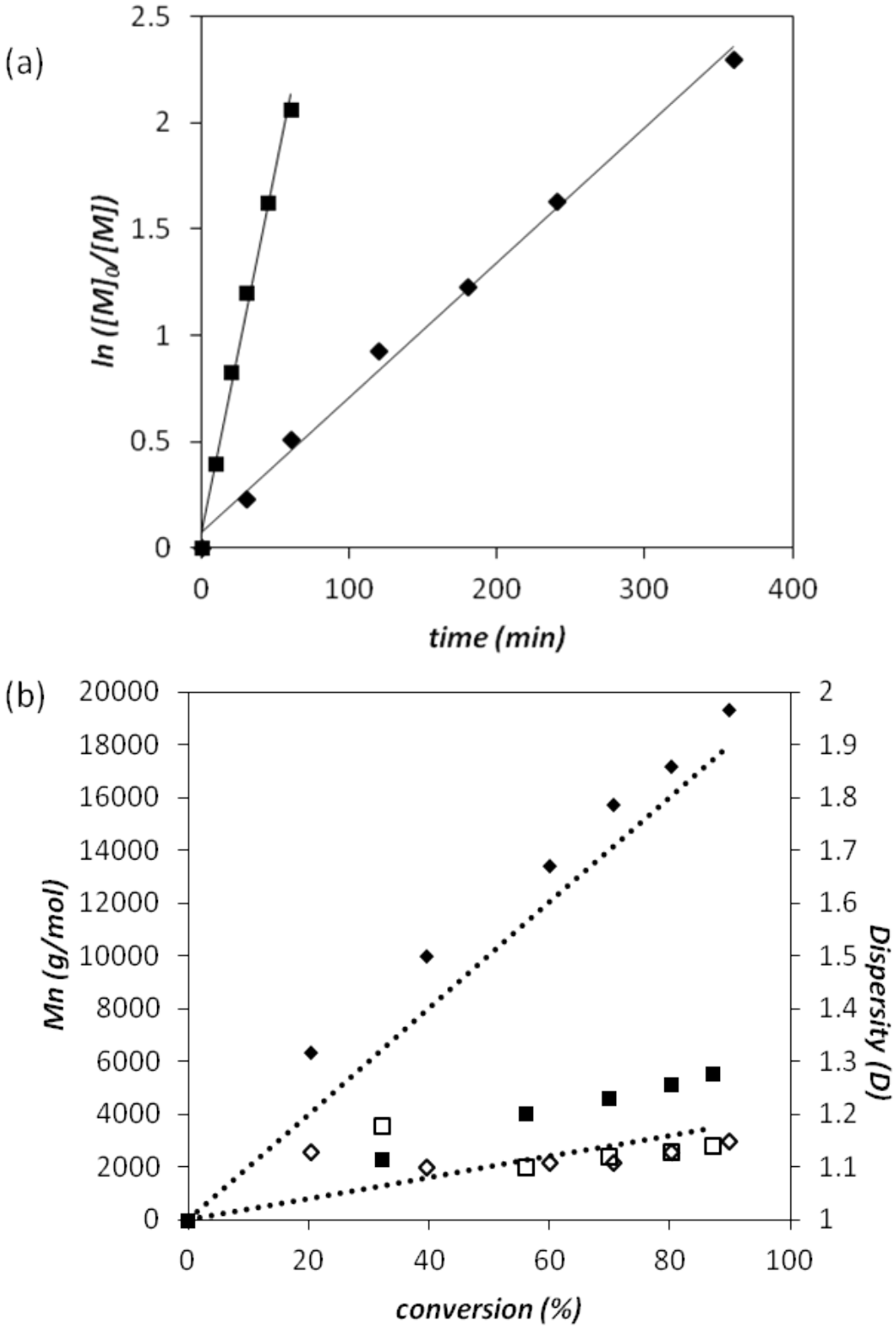

Figure 2.1: ATRP of MMA at 90 °C with different ratio of $[M]_0/[I]_0$: (a) Evolution of $\ln([M]_0/[M])$ versus time; (b) Dependence of M_n (filled symbols) and D (open symbols) on monomer conversion from SEC analysis (PMMA standards) (line plotted represent the M_n theoretical); ◆ PMMA-5 ($[M]_0/[I]_0$=200) and ■PMMA-6 ($[M]_0/[I]_0$=40).

According to Matyjaszewski, this EBiB/CuCl initiation system provides good control of molecular weight and dispersity at high conversion due to the halogen exchange that occurs at 90 °C, causing a sufficiently fast deactivation process.[40] They obtained molecular weights in agreement with the theoretical value and low dispersity throughout the reaction, similar to our results. This indicates that EBiB/CuCl minimises side reaction by a sufficiently fast deactivation process. Halogen atoms exchange rapidly between carbon and copper centres for polymer end group capped with chloride in a short time. A study of *p*-TsCl/CuBr (ratio 2/1) showed that approximately 90 % of PMMA chains are end-capped with chloride group measured by MALDI-TOF MS and ES analysis. This system also provided low dispersity at high conversion of MMA.[10,24] Besides that, Ru-based ATRP also shows halogen exchange for MMA.[18] Recently, Peng *et al*. proposed a mechanism of halogen exchange *via* radical pathway or ionic pathway.[41]

SEC chromatogram displayed a monomodal molar mass distribution as depicted in **Error! Reference source not found.**. The small shoulders on the higher molar mass side of the peak might be attributes to termination reaction. It is probably due to the low concentration of deactivator at initial stage of polymerisation. Therefore, M_n obtained by SEC is higher than theoretical values.

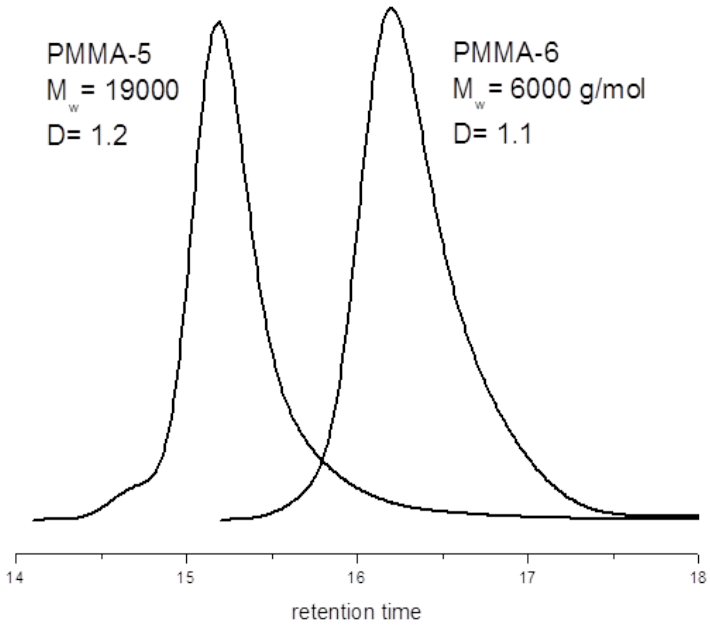

Figure 2.2: SEC chromatogram of PMMA-5 ($[M]_0/[I]_0$=200) and PMMA-6 ($[M]_0/[I]_0$=40).

2.3.1.1 Effect of Cu(II) concentration

PMMA-2 and PMMA-3 were introduced to study the relation of Cu(I) and Cu(II) in the system where ratio $[Cu(II)]_0/[Cu(I)]_0$ are 0.25 and 0.43, respectively. Cu(I) is faster activating while Cu(II) is slower deactivating. The evolution of $\ln([M]_0/[M])$ versus reaction time of PMMA-2 displayed in Figure 2.3 indicate a constant concentration of growing radical and that shows first order reaction with respect to monomer concentration. Similar results were reported by Wang for MMA polymerisation conducted in toluene.[42] The polymerisation rate increases due to a higher than expected radical concentration in solution because of the low solubility of Cu(II) in this non-polar solvent. For PMMA-3, a slow initiation reaction was observed in the early stage of the polymerisation (around 30 min) before increasing linearly with time. At the start of the polymerisation, because 30% of Cu(II) was added purposely to accelerate the deactivation reaction. However, the concentration of Cu(II) continuously increases by contribution from Cu(I) and the initiator/dormant species. Cu(II) not only decreases the polymerisation rate but also deactivates the active Cu(I) species, thus reducing the polymerisation progress. Therefore, the radical concentration is large and the the rate of deactivation is much slower than the rate of termination. Consequently, termination of radicals preferably occurs through combination or disproportionation. Similar results were reported in that by the addition of 40% Cu(II) of the initial $[Cu(I)]_0$ the polymerisation rate was decelerated more than 10-folds.[38] Zhang *et al.* study the effect of Cu(II) concentration on the kinetic of MMA polymerisation.[43] The results showed that the addition of $[Cu(II)]_0/[Cu(I)]_0 \geq 0.1$ effectively diminished the radical termination with linear kinetic plots of $\ln([M]_0/[M])$ against time, t, which is similar to the PMMA-2 results. Besides that, this plotted graph fitted with the equation proposed by Matyjaszewski, $\ln([M]_0/[M]) \propto t$ showing that the polymerisation rate is almost first order with respect to concentration of initiator and Cu(I).[44] This "persistent radical effect" has been describe by Fisher [14,15] and radical termination during the ATRP process become unimportant when enough Cu(II) is added at beginning of the reaction.

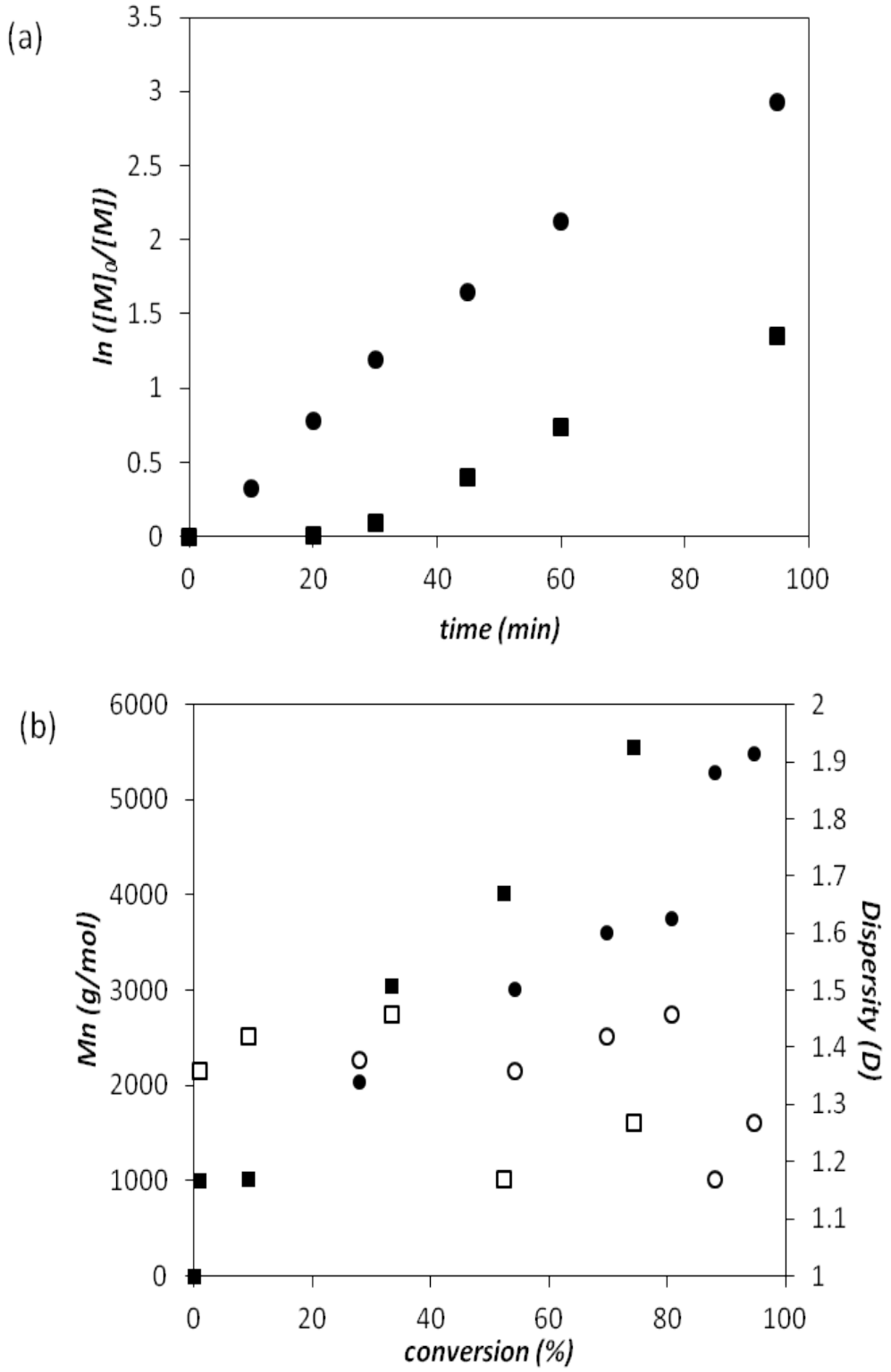

Figure 2.3: ATRP of MMA at 90 °C with different ratio of $CuCl/CuCl_2$: (a) Evolution of $\ln([M]_0/[M])$ versus time; (b) Depedence of M_n (filled symbols) and D (open symbols) on monomer conversion from SEC analysis (PMMA standards); ● PMMA-2 ($CuCl/CuCl_2$=0.8:0.2), ■ PMMA-3 ($CuCl/CuCl_2$=0.7:0.3). Experiment conducted in ratio $[M]_0/[I]_0 = 200$.

In all cases, M_n increase linearly with conversion but are much higher than theoretical values (Figure 2.3b and Table 2.1). PMMA-2 at 95% conversion shows a small peak at higher molar mass in the SEC chromatogram due to the termination reaction with a dispersity 1.27 (Figure 2.4). This indicates that termination reaction occurred at the early stage of polymerisation as discuss above. Meanwhile, PMMA-3 displayed a symmetric chromatogram with a molecular weight of 6000 g/mol at 74% conversion and low dispersity (1.15). Although the M_n increases linearly with monomer conversion, it is noted that the experimental value departs from the theoretical line especially in the low molecular weight region. Angot *et al*.[45] and Sawamoto *et al*.[46] also exhibited a similar trend in their experiments. The initiator efficiency for PMMA-2 is 69% and PMMA-3 is 53%. Besides that, Matyjaszewski *et al*. reported that slow initiation of EBiB relates to back strain effects, *i.e.* the release of the steric strain of dormant species during the rehybridisation from sp^3 to sp^2 configurations.[24]

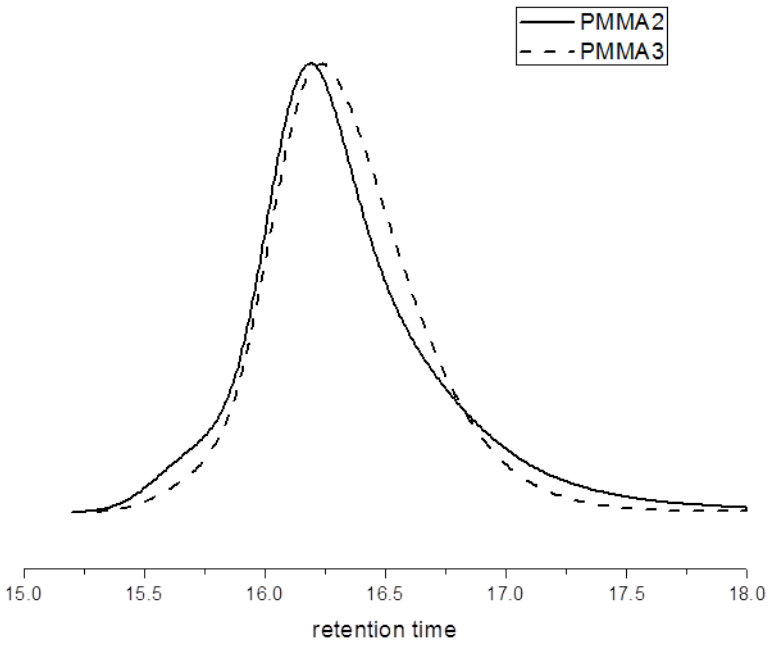

Figure 2.4: SEC chromatograms of PMMA-2 and PMMA-3 ($[M]_0/[I]_0$=40).

2.3.2 Poly(MMA-*b*-4VP) diblock copolymer

PMMA-Cl at different molecular weight which are PMMA-2 (5500 g/mol) and PMMA-5 (19400 g/mol) were used as macroinitiator in the polymerisation of 4VP at 90 °C with different ligand (Scheme 2.3). HMTETA and Me_6TREN were used in excess as ligands to reduce the possibility of forming pyridine-copper complexes. ^1H NMR was also employed to analyse the structure of poly(MMA-*b*-4VP) with chemical shifts for pyridine ring (8.3 and 6.3 ppm), methyl proton of ester group MMA (3.6 ppm), methylene (2.1-1.5 ppm) and methyl proton (0.8-1.1 ppm) clearly visible in the spectrum as shown in Figure 2.5. For FTIR, the pyridine signals appear at 1414, 1557 cm^{-1} (C=C stretch) and 1596 cm^{-1} (C=N stretch), while, MMA bands can be assigned at 2928 cm^{-1} (C-H stretch), 1727 cm^{-1} (C=O stretch), 1448 cm^{-1} (CH_3 stretch) and 1148 cm^{-1} (-O-CH_3 stretch) (Figure 2.6). Conversion and composition (molar fraction) for the second blocks of the copolymers was calculated using ^1H NMR by comparing the ratio of the pyridyl proton of P4VP to carbonyl proton of PMMA (Appendix 1). Table 2.2 contains the summary of experiments conducted.

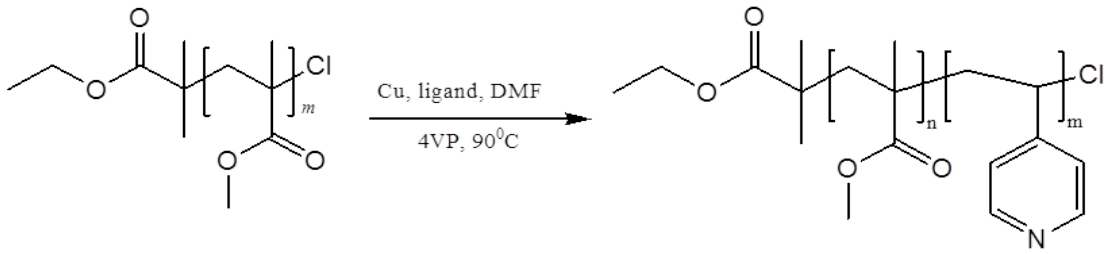

Scheme 2.3: Synthetic route of linear block copolymer, poly(MMA-*b*-4VP).

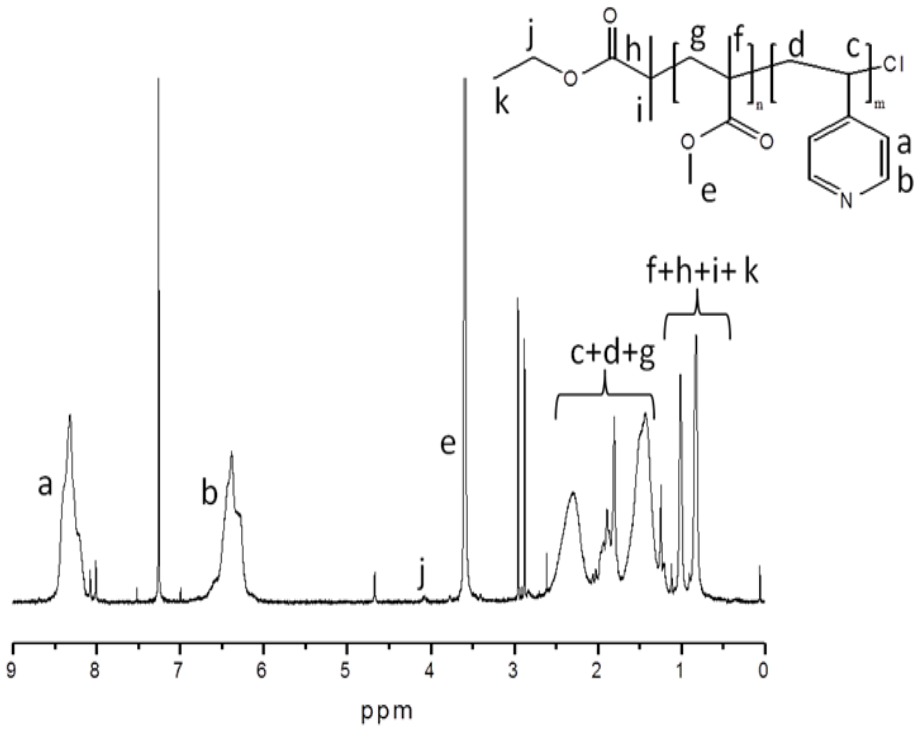

Figure 2.5: ^{1}H NMR spectrum of poly(MMA-*b*-4VP), ($CDCl_3$: 7.26 ppm).

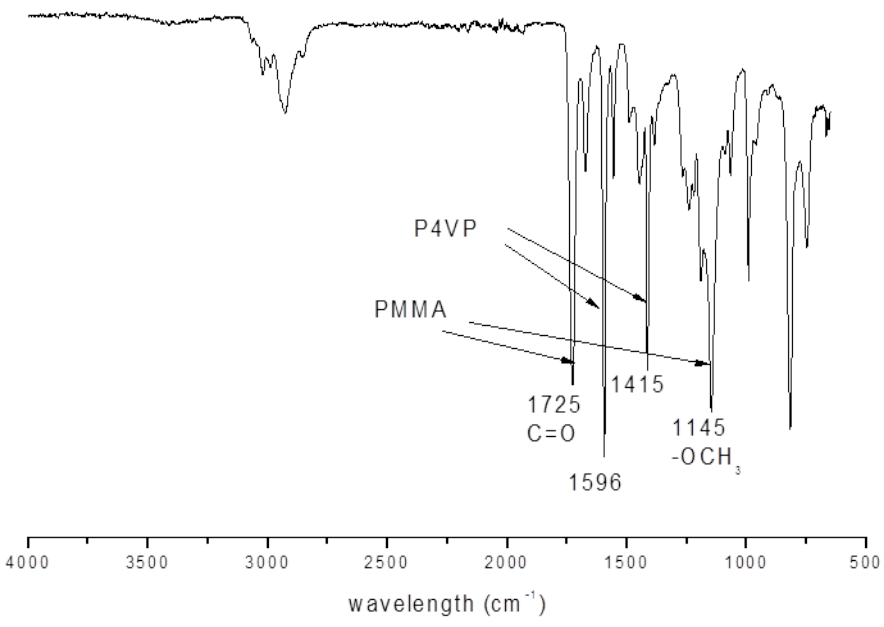

Figure 2.6: FTIR spectrum of poly(MMA-*b*-4VP).

Table 2.2: Polymerisation of linear diblock copolymer poly(MMA-*b*-4VP) by ATRP using PMMA as a macroinitiator.

Macro initiator	Sample	time (min)	Conv. [a] 4VP (%)	$M_{n\ theo}$ [b] (g/mol)	$M_{n\ SEC}$ [c] (g/mol)	$M_{w\ SEC}$ [c] (g/mol)	D [c]
PMMA-2	BC1 [d]	1440	89	23000	54000	71000	1.3
	BC2 [e]	1440	31	12000	56000	87000	1.6
	BC3 [d]	120	40	14000	39000	53000	1.4
PMMA-5	BC4 [d]	180	19	23000	30000	38000	1.2
	BC5 [d]	1440	40	28000	38000	52000	1.4

[(a)]Conversion calculated by ^{1}H NMR through integration of PMMA (3.65 ppm) and P4VP (8.14 and 6.21 ppm) peaks. [(b)]$M_{n\ theo}$ was calculated using the equation: M_n = (conversion x $[M]_0/[I]_0$ x $M_{monomer}$) + M_n macroinitiator. [(c)]D, M_n and M_w measure by DMF SEC with multi angle light scattering detector (MALS). [(d)]Experimental condition: $[I]_0/[HMTETA]_0/[CuCl]_0/[CuCl_2]_0/[4VP]_0$ = 1/6/0.8/0.2/192. [(e)]Experimental condition: $[I]_0/[Me_6TREN]_0//[CuCl]_0/[CuCl_2]_0/[4VP]_0$= 1/6/0.8/0.2/192

BC1, 2 and 3 were prepared with PMMA-2 macroinitiator, while BC4 and 5 with the PMMA-5 macroinitiator. The level of control of polymerisation using HMTETA and Me_6TREN as ligands was investigated. Figure 2.7 shows the evolution of $\ln([M]_0/[M])$ of the block copolymer BC1-5 with time and with the ligand used. BC1 and 3 with HMTETA as the ligand display an almost linear increase of the kinetic plot indicating constant radical concentration during the reaction. However, BC2 (Me_6TREN) does not shows any linearity in the kinetic profile and displays a plateau region around 30% conversion. Consequently, the M_n deviates from the theoretical value with broad dispersity of 1.6 and low macroinitiator efficiency, 21% (Table 2.2, Figure 2.8, BC2). The polymerisation of 4VP from PMMA-5 macroinitiator by HMTETA showed good efficiency, between 75-77 %, but yielded block copolymers with M_n higher than the theoretical values (Table 2.2, BC4 and 5) and the dispersities around 1.2-1.4. Termination reaction occurred due to the possible coordination of copper to 4VP. The Cu(II)-X bond in protic media is significantly weaker than in non-protic media and the complex easy to dissociate. As a result, polymerisation shows fast polymerisation rate, inefficient deactivation and poorly controlled polymers.[26] These experiments demonstrate that HMTETA is the better suited ligand compare to Me_6TREN in protic

solvent. This is because HMTETA forms more stable complex with Cu(I) and Cu(II).[47]

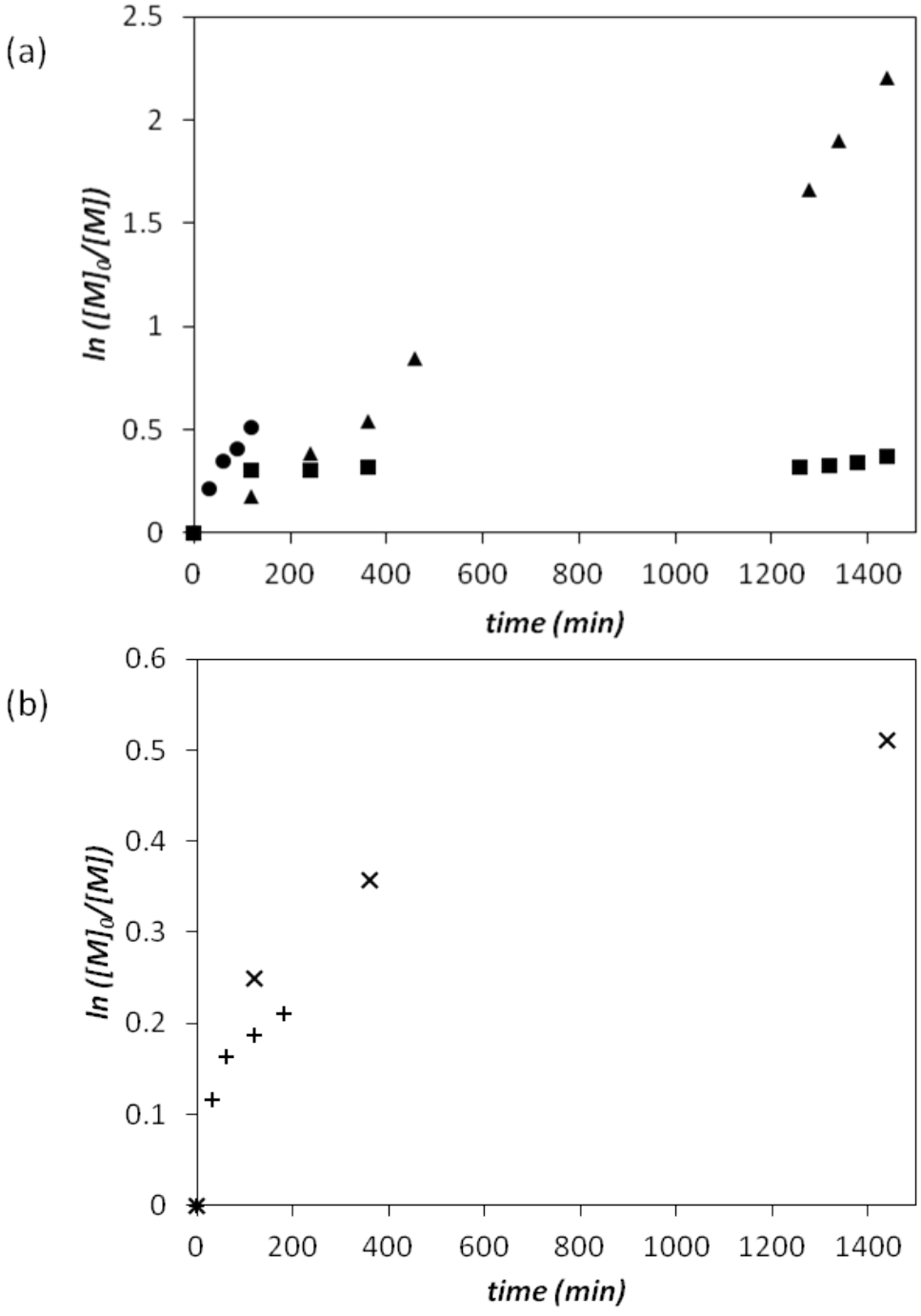

Figure 2.7: Evolution of $\ln([M]_0/[M])$ versus time for 4VP segments with different macroinitiator (a) PMMA-2, 5500 g/mol; (b) PMMA-5, 19400 g/mol; and different ligand, ▲ BC1, ● BC3, + BC4 and **X** BC5 (HMTETA), ■ BC2 (Me_6TREN).

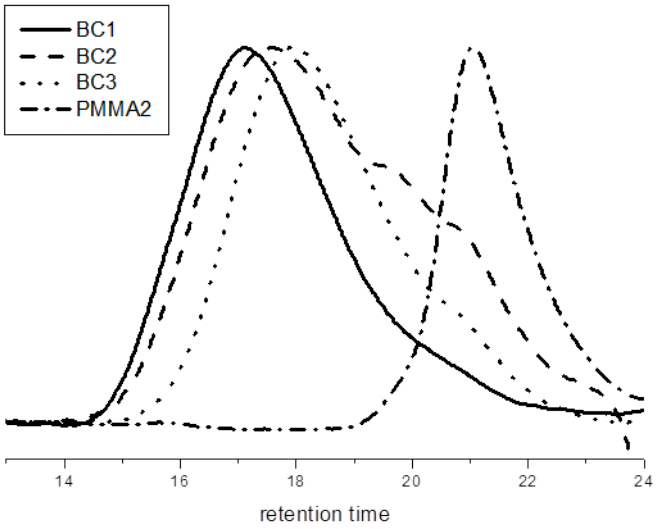

Figure 2.8: SEC traces (RI signals) of poly(MMA-*b*-4VP) initiated by macroinitiator PMMA-2 (5500 g/mol).

2.3.3 Polymerisation of star (methyl methacrylate), sPMMA

For the synthesis of tetrafunctional initiator pentaerythritol tetrakis (2-bromoisobutyrate), PT-Br, an excess 2-bromoisobutyryl bromide was added to pentaerythritol (PT) in a condensation reaction (Scheme 2.4), and triethylamine was added to capture the HBr condensate. The structure of PT-Br was confirmed by ^{1}H NMR, ^{13}C NMR and FTIR (Appendix 1). In the proton NMR spectra, the signals at 4.3 and 1.9 ppm are representative of C-CH_2-O and C(Br)-CH_3, respectively. In the ^{13}C-NMR, peak shows the presence of carbonyl group, -O-CH_2-C-, -C$(CH_3)_2$-Br, -$(CH_2)_4$-C- and methyl groups at 170.9, 62.9, 55.2, 43.7 and 30.6 ppm, respectively. Moreover, carbonyl stretching bands appeared at 1733 cm^{-1} in FTIR. The four arm macroinitiator was first used for the synthesis of star PMMA in toluene at 90 °C. ^{1}H NMR was employed to analyse the structure of star PMMA. The methyl proton connected to the ester group can be attributed to 3.60 ppm, while, methylene and methoxy group exhibit signal at 0.8-1.1 and 1.5-2.1 ppm, respectively (Appendix 1). The data of molar mass and dispersity of the obtained sPMMA, synthesised using different ratios of monomer to initiator and varying amounts of additional Cu(II) at the beginning of reaction are listed in Table 2.3.

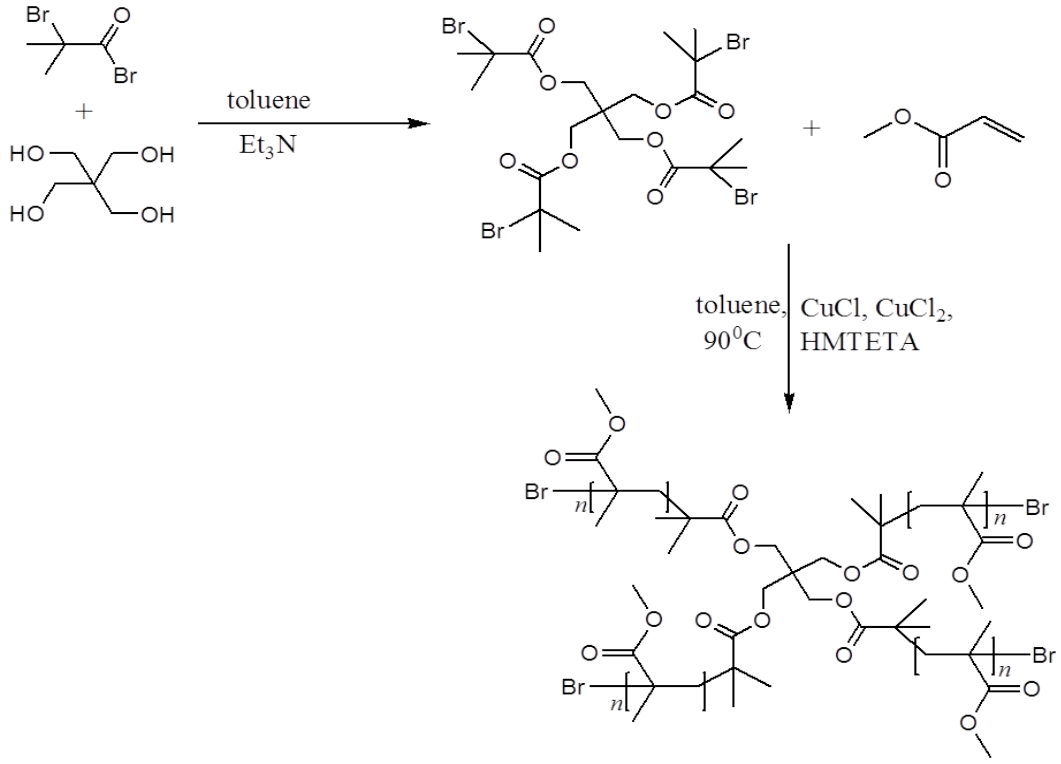

Scheme 2.4: Synthetic route of four arm star poly (methyl methacrylate), sPMMA.[35]

Table 2.3: Polymerisation of star MMA at 90 °C in toluene by ATRP.

Sample	**time (min)**	**Conv.**[a] **(%)**	$M_{n\ theo}$[b] **(g/mol)**	$M_{n\ SEC}$[c] **(g/mol)**	D[c]	**Ratio $[I]_0$:[ligand]$_0$: $[Cu(I)]_0$:$[Cu(II)]_0$:$[M]_0$**
sPMMA-1	60	90	18000	29000	1.4	1:1:0.8:0.2:40
sPMMA-2	300	85	68000	64000	1.2	1:1:0.8:0.2:200
sPMMA-4	300	62	99000	88000	1.2	1:1:0.8:0.2:400
sPMMA-5	180	39	78000	75000	1.2	1:1:0.8:0.2:500
sPMMA-6	100	34	69000	67000	1.1	1:1:0.8:0.2:500
sPMMA-3	360	87	70000	77000	1.2	1:1:0.7:0.3:200

[(a)]Conversion calculated by ^{1}H NMR through integration of PMMA (5.4 ppm, 6.13 ppm) and DMF (2.8 ppm) peaks (see details in Appendix 1). [(b)]$M_{n\ theo}$ = (conversion x $[M]_0/[I]_0$ x 100.12)4 + M initiator. [(c)]D and M_n measure by THF SEC with PMMA standards.

Figure 2.9 shows that the semilogaritmic kinetic plots, molecular weight and molecular weight distribution of different ratios of $[MMA]_0/[PT\text{-}Br]_0$, namely 40/1, 200/1, 400/1 and 500/1 per arms. These represents targeted molecular weight were between 16000 to 200000 g/mol. In all cases for sPMMA-1,2,4 and 5, the kinetic profiles linearly increase with time showing that the radical concentrations are constant throughout the reaction. Meanwhile, the M_n increases gradually with the monomer conversion and close to the theoretical value. For example, sPMMA-1 with an initiator concentration of 0.022 M shows the faster kinetic profile reaching 90% conversion in 60 minutes. However, the M_n higher than the theoretical value with a broad D, 1.4 probably due to the star-star coupling in termination reaction (Table 2.3, Figure 2.10**Error! Reference source not found.**). This is also supported by the appearance of a high molecular weight shoulder in SEC (Figure 2.10). On the other hand, sPMMA-5 displays a narrow dispersity of 1.2 at 39% conversion after 180 minutes (Figure 2.10). Therefore, similar condition of sPMMA-5 were used in the purpose to reduce termination reactions at low conversion. As a result, there are no significant different of M_n and dispersity for sPMMA-6 observed at 35% conversions in 100 minutes (Table 2.3). From these experiments, termination reaction seems possible to decrease by keeping the conversion below 60%. Moreover, to obtain the target degree of polymerisation, DP_n, it is necessary to adjust the initial experimental condition, in other words, to adjust $[M]_0/[I]_0$ and stay below 60% conversion. Generally, the dispersity of all polymers increased with conversion which is indicative of a higher rate of termination at high monomer conversion in agreement with literature reports.[48]

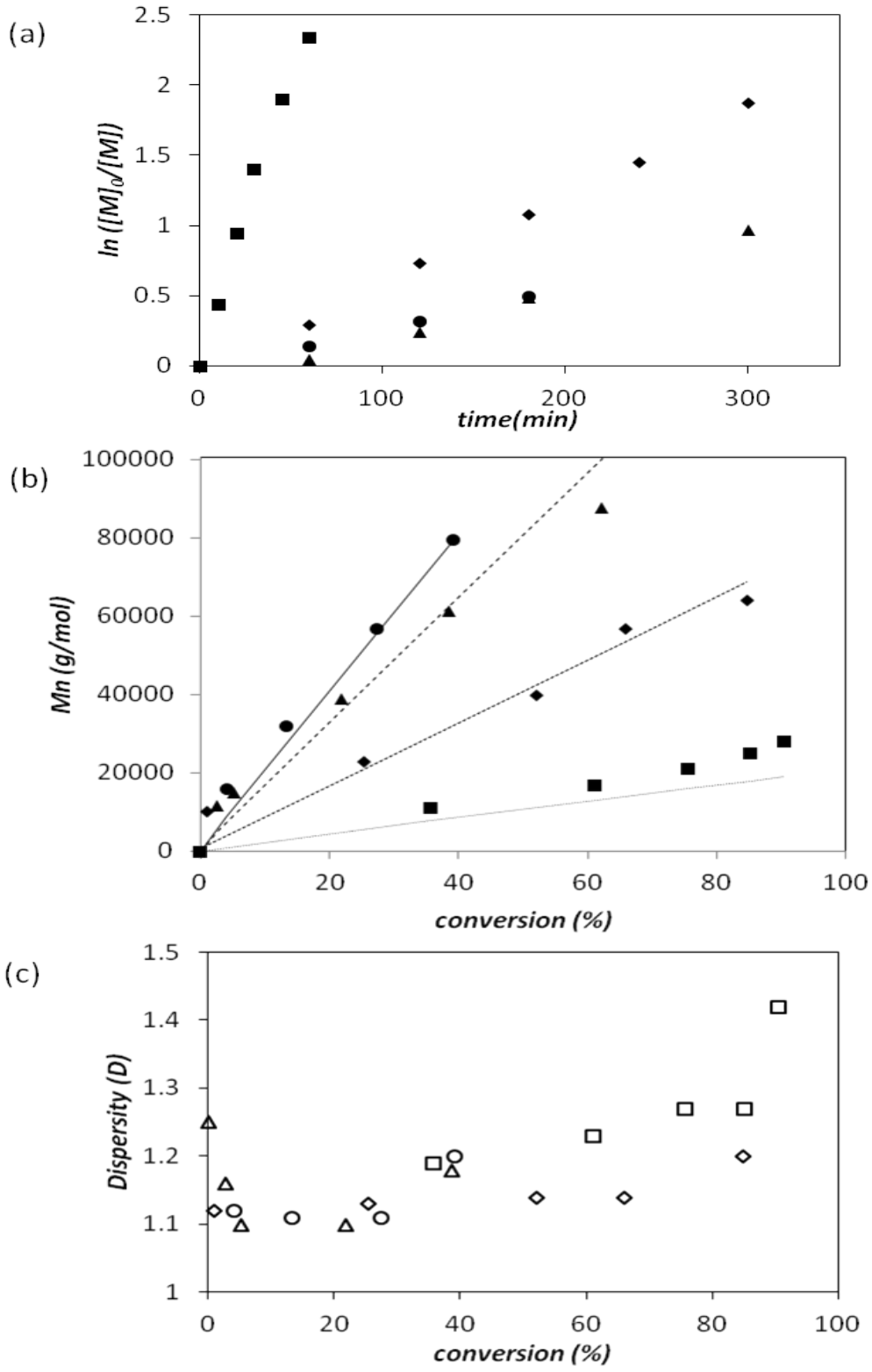

Figure 2.9: ATRP of MMA with the PT-Br as initiator with different ratios of $[M]_0/[I]_0$: (a) Evolution of $\ln([M_0]/[M])$ versus time, (b) Dependences of M_n on monomer conversion, (c) Dependeces of D on monomer conversion from GPC analysis (PMMA standards) (line plotted represent M_n theoretical); ■ sPMMA-1 (40/1), ◆ sPMMA-2 (200/1), ▲ sPMMA-4 (400/1) and ● sPMMA-5 (500/1).

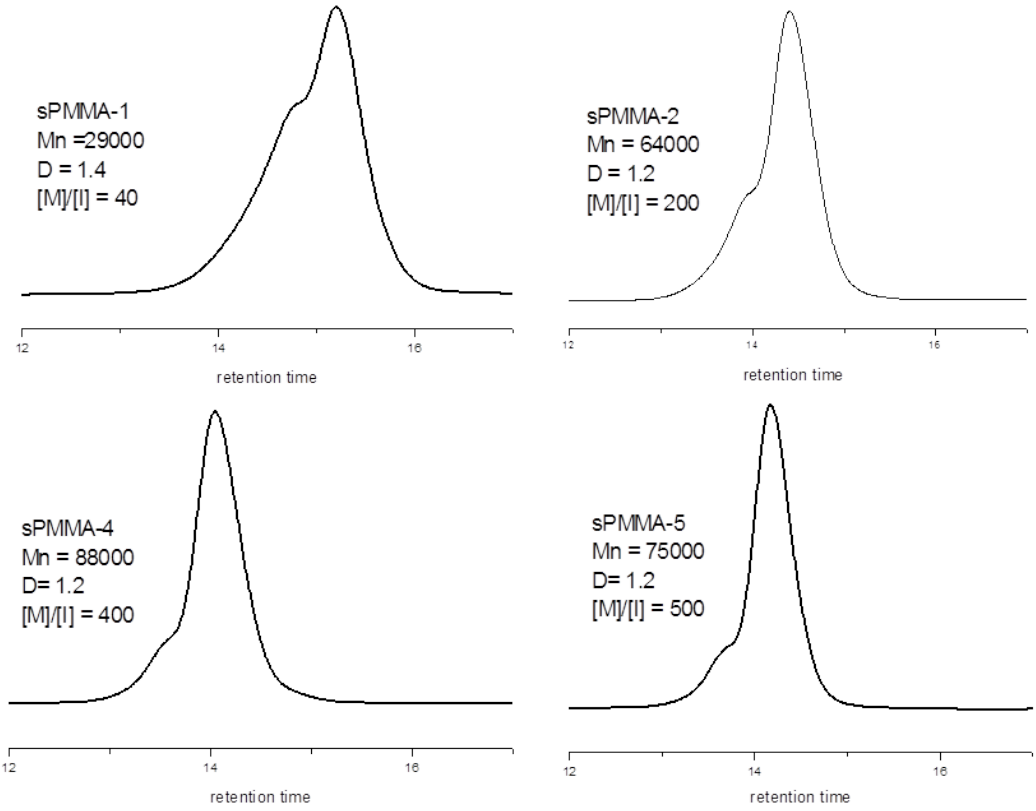

Figure 2.10: SEC chromatograms of sPMMA in different concentration of MMA in ratio $[M]_0/[I]_0$ range from 40 to 500.

In ATRP of star polymers, the termination reaction is a critical issue because of more active sites that should be effectively start the polymerisation at the same time. In the experiments reported in the thesis, termination products could be expected from disproportionation of MMA and/or radical combination called star-star coupling. This termination may be occurring at only one or multiple chains. If the propagating species terminate at one of the chains, the chains cease participating in the ATRP process while other active chains continue growing from the polymer to achieve high molecular weight. If the termination is significant, the kinetic plots will shows a curve pattern with decreasing slope. This was proven by Matyjaszewski and his co-workers for the polymerisation of styrene, *n*-butyl acrylate and MMA with varying arms number of initiator from organic and hybrid inorganic multifunctional initiators.[35]

Angot *et al*. claimed that star-star coupling of PMMA is prominent compare to styrene and acrylates, resulting in a shoulder of high molecular weight detected in SEC even at

25% conversion.[45] Meanwhile, Costa and Vasconcelos reported that termination product depends on the initiator and catalyst concentration. They obtained not only star-star coupling, but also low molecular weight species when high CuCl concentration was used in their polymerisation system with octafunctional silesquioxane initiator for MMA polymerisation.[48] However, it is well-documented that star polymer of di-, tetra-, hexa- or octafunctional initiator are controllable in agreement between measured and theoretical molecular weight when the conversion below 20%.[35,49]

2.3.3.1 Effect of Cu(II) concentration

Then, the amount of Cu(II) added at the initial polymerisation was investigated for sPMMA-2 and sPMMA-3. The linear evolution of $\ln([M]_0/[M])$ with time was obtained for sPMMA-2, while sPMMA-3 shows a slow initiation step with addition of 30% of Cu(II) as shown in Figure 2.11a. Besides that, the M_n linearly increases with conversion, around 85% and is close to the theoretical values with a narrow D for both star polymers (Table 2.3, Figure 2.11**Error! Reference source not found.**b). As discuss earlier in linear PMMA, slow initiation occurred due to high concentration of Cu(II) present in the system, resulting in deactivation the Cu(I) species and promoting high radical concentration.

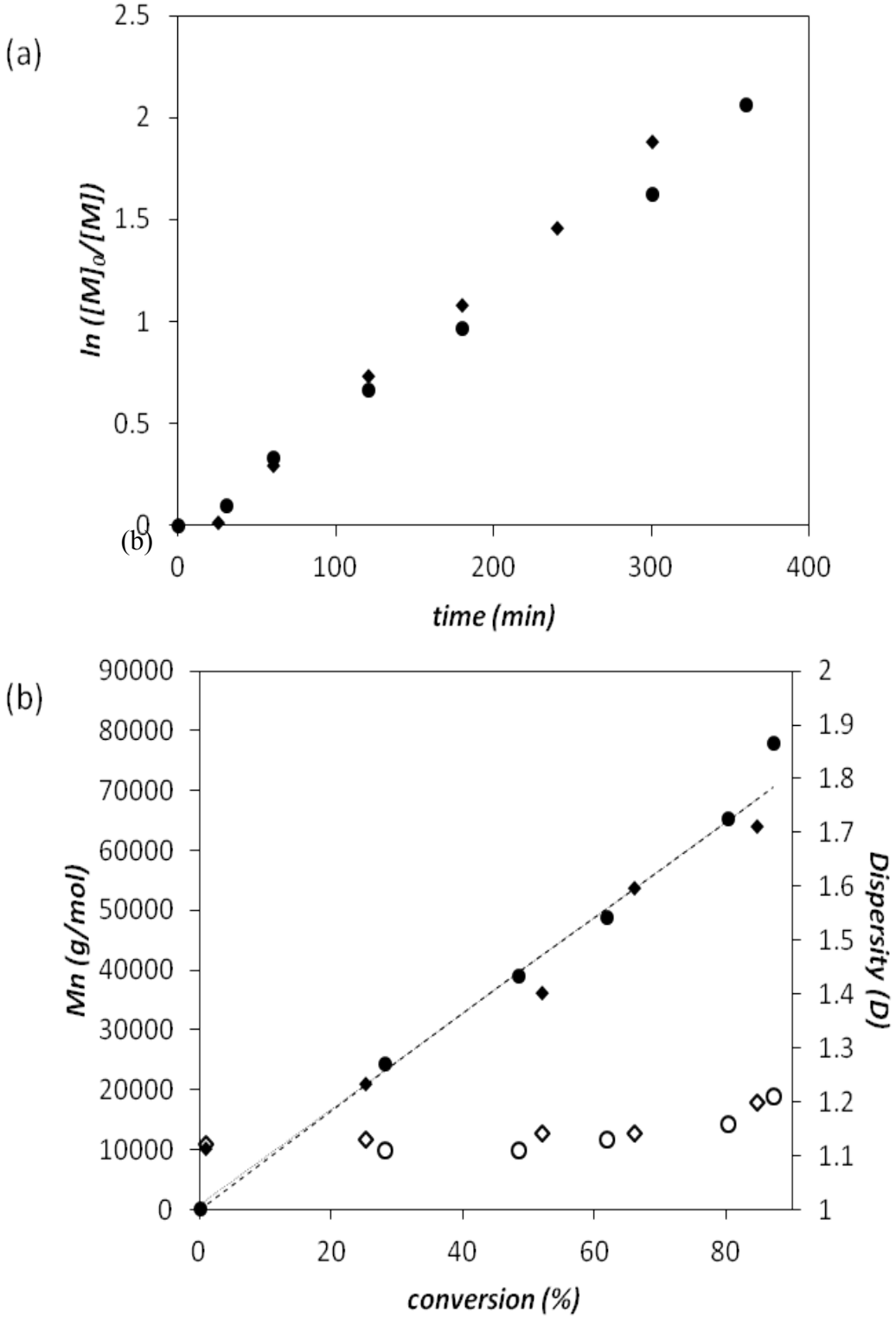

Figure 2.11: ATRP of MMA with the PT-Br as initiator with different ratios of $CuCl/CuCl_2$: (a) Evolution of $\ln([M_0]/[M])$ versus time; (b) Dependences of M_n (filled symbols) and D (open symbols) on monomer conversion from SEC analysis (PMMA standards) (line plotted represents M_n theoretical); ◆ sPMMA-2 ($CuCl/CuCl_2$=0.8:0.2), ● sPMMA-3 ($CuCl/CuCl_2$=0.7:0.3). Experiment conducted in ratio $[M]_0/[I]_0 = 200$.

2.3.4 Star poly(MMA-*b*-4VP)$_4$ diblock copolymer

The sPMMA-Cl polymers were subsequently used as macroinitiators in the polymerisation of 4VP at 90 °C (Scheme 2.5). The level of control of polymerisation of two different macroinitiator sPMMA-1 and sPMMA-5 were investigated and listed in Table 2.4.

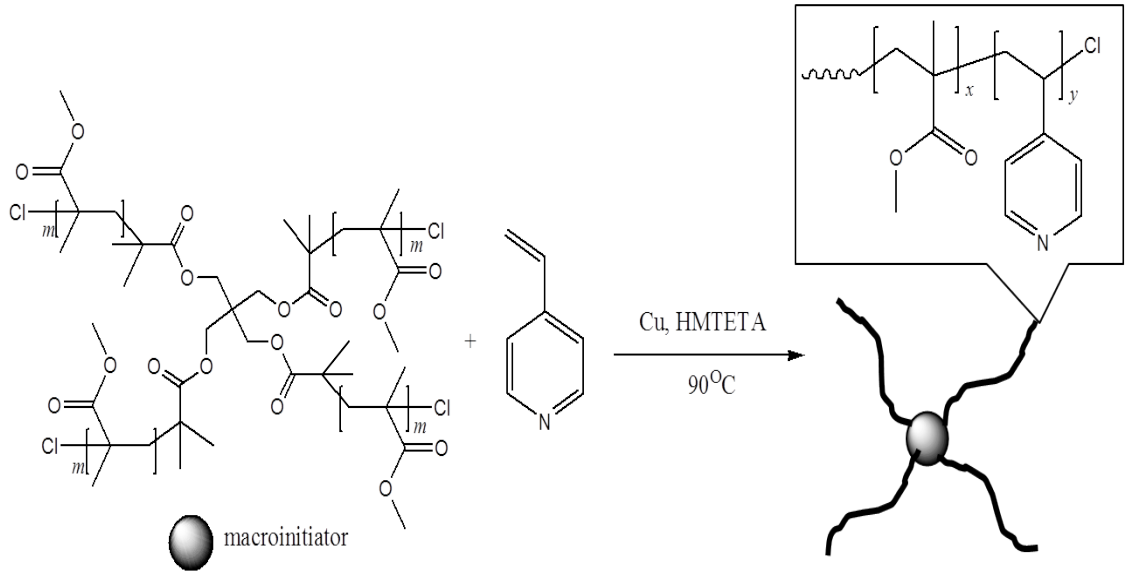

Scheme 2.5: Synthetic route of star block copolymer poly(MMA-*b*-4VP)$_4$.

Table 2.4: Experimental summary of star block copolymer poly(MMA-*b*-4VP)$_4$ by ATRP.

Initiator	Sample	time (min)	Conv.[a] 4VP (%)	$M_{n\ theo}$ [b] (g/mol)	$M_{n\ SEC}$ [c] (g/mol)	$M_{w\ SEC}$ [c] (g/mol)	D [c]
sPMMA1	sBC1	1440	46	57000	83000	99000	1.2
sPMMA5	sBC2	510	18	94000	173000	171400	1.3
	sBC3	1440	40	112000	2639000	3220000	1.2

[(a)]Conversion calculated by ^{1}H NMR through integration of PMMA (3.65 ppm) and P4VP (8.14 and 6.21 ppm) peaks, [(b)]$M_{n\ theo}$ = (conversion x $[M]_0/[I]_0$ x M_w monomer)4 + M_n macroinitiator, [(c)]D, M_n and M_w measure by DMF SEC with multi angle light scattering detector (MALS). Experimental condition: $[I]_0/[HMTETA]_0/[CuCl]_0/[CuCl_2]_0/[4VP]_0$ = 1/6/0.8/0.2/200.

The polymerisation of 4VP from sPMMA-1 macroinitiator showed 46% conversion with higher M_n than the theoretical value due to the star-star coupling termination reaction as shown in Figure 2.12 and Table 2.4. Moreover, the D is narrow at 1.2 showing that the polymer is growing from the active site. This chain extension was confirmed by the SEC traces, where the monomodal peak of sBC1 shifted to high molar mass side (Figure 2.13). When, the polymerisation was carried out using sPMMA-5, we also obtained the M_n higher than the theoretical value with 18% and 40% of conversion for sBC2 and sBC3, respectively (Table 2.4). sBC3 showed low efficiency, 4%, after 24 hours reaction with M_n (2639000 g/mol) which is 23 times higher than theoretical (112000 g/mol). It can be explained by the occurrence of star-star coupling resulting from inevitable termination reaction. The tendency for coupling increases with time, as monomer concentration is depleted and the number of active site is decreased. The formation of block copolymers from ATRP chains with 4VP monomer is difficult due to possibility of coordination copper to 4VP and the stable complex formed between HMTETA and Cu.[31,47] In order to have control star block copolymer, it is important to keep the polymerisation at low conversion and higher number of active sites.

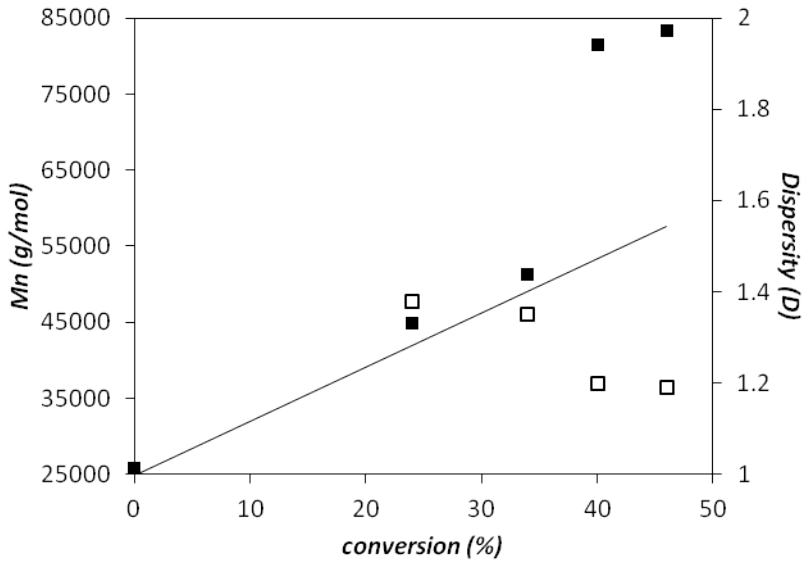

Figure 2.12: Dependences of M_n (filled symbols) and PDI (open symbols) on monomer conversion of star block copolymer, sBC1 from GPC analysis with MALS detector (line plotted represent M_n theoretical).

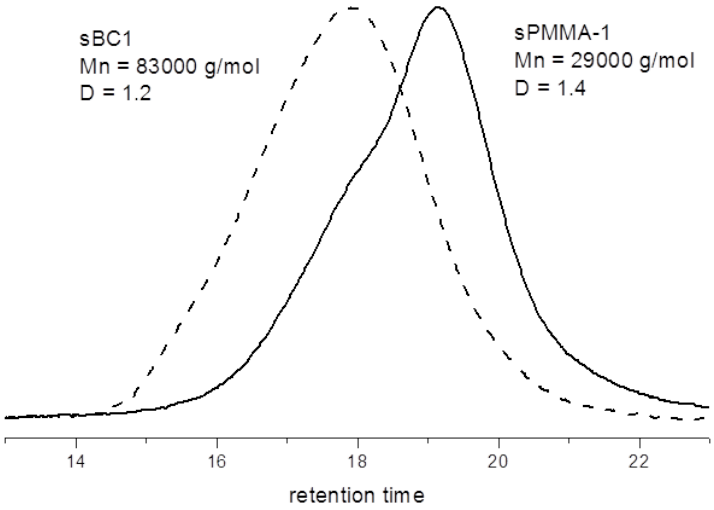

Figure 2.13: SEC traces (RI signals) of star block copolymer poly(MMA-*b*-4VP), sBC1.

2.4 Conclusion

We were successfully synthesised the linear and star poly (methyl methacrylate) architecture from α-bromoester and CuCl/HMTETA catalyst system. In all PMMA polymerisation, the linear increase of molecular weights with conversion has been observed, and polymers with low dispersity (D = ~1.1-1.2) were obtained. Meanwhile, slow initiation process were observed with introducing 30% of Cu(II) in the beginning of the polymerisation. For star poly (methyl methacrylate), linear kinetic profiles were obtained. However, the M_n is higher than theoretical value due to the termination reaction. This termination reaction can be controlled when excess monomer to initiator ratio was used and the reaction is stopped whilst still below 60% conversion. AB block copolymers of MMA and 4VP were prepared by PMMA-Cl or sPMMA-Cl macroinitiation. HMTETA and Me6TREN were used as a ligand in combination with CuCl. As a results, both ligand indicated high molecular weight than theoretical values and large dispersity, due to the potential coordinating of 4VP with Cu. For star block copolymers, the termination is prominent resulting in star-star coupling as end-products. There are many factors to be considered such as ratio of monomer to initiator, amount

of catalyst, type of initiator, solvent and ligand in order to have a good controlled of polymer.

References

1. Matyjaszewski K, Macromolecules 2012;45:4015.

2. Tsarevsky NV, Matyjaszeski K, Chem Rev 2007;107:2270.

3. Matyjaszewski K, Xia J, Chem Rev 2001;101:2921.

4. Braunecker WA, Matyjaszewski K, Prog Polym Sci 2007;32:93.

5. Matyjaszewski K, Patten TE, Xia J, J Am Chem Soc 1997;119:674.

6. Wang JS, Matyjaszewski K, Macromolecules 1995;28:7901.

7. Percec V, Barboiu B, Macromolecules 1995;28:7970.

8. Davis KA, Paik HJ, Matyjaszewski K.Macromolecules 1999;32:1767.

9. Wang JS and Matyjaszewski K, J Am Chem Soc 1995;117:5614.

10. Grimaud T and Matyjszewski K, Macromolecules 1997;30:2216.

11. Xue L, Agarwai US, Lemstra PJ, Macromolecules 2002;35:8650.

12. Gao H, Matyjaszewski K, Prog PolymSci 2009;34:329.

13. Coessens V, Pintaeur T, Matyjaszewski K, Prog Polym Sci 2007;26:337.

14. Fisher H, J Polym Sci Part A:Polym Chem 1999;37:1885.

15, Fisher H, Chem Rev 2001;101:3581.

16. Ouchi M, Terashima Takaya, Sawamoto M, Chem Rev 2009;109:4963.

17. di Lena F, Matyjaszewski K, Prog Polym Sci 2010;35:959.

18. Ando T, Kamigaito M, and Sawamoto M, Macromolecules 2000;33:2819.

19. Kato M, Kamigaito M, Sawamoto M, Higashimura T, Macromolecules 1995;28:1721.

20. Uegaki H, Kotani Y, Kamigaito M, Sawamoto M, Macromolecules 1997;30:2249.

21. Moineau G, Minet M, Dubois P, Teyssié P, Senninger T, Jérôme R, Macromolecules 1999;32:27.

22. Wang Yu and Matyjaszewski K, Macromolecules 2010;43:4003.

23. Ando T, Kamigaito M, Sawamoto M, Macromolecules 1997;30:4507.

24. Matyjaszewski K, Wang JL, Grimaud T, Shipp DA, Macromolecules 1998;31:1527.

25. Matyjaszewski K, Pattern TE, Xia J, J Am Chem Soc 1997;119:674.

26. Tsarevsky NV, Braunecker WA, Brooks AJ, Matyjaszewski K, Macromolecules 2006;39:6817.

27. Nugay N, Hosotte C, Nugay T, Riess G, Eur Polym J 1994;30:1187.

28. Nugay N and Nugay T, Eur Polym J 2000;36:1027.

29. Kuo SW, Tung PH, Chang FC, Eur Polym J 2009;45:1924.

30. Queffelec J, Gaynor SG, Matyjaszewski K, Macromolecules 2000;33:8629.

31. Xia J, Zhang X, Matyjaszewski K, Macromolecules 1999;32:3531.

32. Heise A, Nguyen C, Malek R, Hedrick JL, Frank CW, Miller RD, Macromolecules 2000;33:2346.

33. Becer CR, Hoogenboom R, Fournier D, Schubrt US, Macromol Rapid Commun 2007;28:1161.

34. Feng L, Hu J, Liu Z, Zhao F, Liu G, Polymer 2007;48:3616.

35. Matyjaszewski K, Miller PJ, Pyun J, Kickelbick G, Diamanti S, Macromolecules 1999;32:6526.

36. Shimura Y, Bull Chem Soc Jpn 1967;40:273.

37. Convertine AJ, Sumerlin BS, Thomas DB, Lowe AB, McCormick CL, Macromolecules 2003;36:4679.

38. Wang JL, Grimaud T, Matyjaszewski K, Macromolecules 1997;30:6507.

39. Xia J and Matyjaszewski K, Macromolecules 1997;30:7697.

40. Matyjaszewski K, Shipp DA, Wang J, Grimaud T, Patten TE, Macromolecules 1998;31:6836.

41. Peng CH, King J, Seeliger F, Matyjaszewski K, Macromolecules 2011;44:7546.

42. Wang T, Liu Y, Jeng B,Cai Y, J Polym Res 2005; 12:67.

43. Zhang H, Klumperman B, Ming W, Fischer H, van der Linde R, Macromolecules 2001;34:6169.

44. Matyjaszewski K, Patten TE, Xia J, J Am Chem Soc 1997; 119:674.

45. Angot S, Murthy KS. Taton D, Gnanou Y, Macromolecules 2000;33:7261.

46. Ueda J, Kamigaito M, Sawamoto M, Macromolecules 1998;31:6762.

47. Pintaeur T, Matyjaszewski K, Coord Chem Rev 2005;249:1155.

48. Costa ROR and Vasconcelos WL, Macromolecules 2001;34:5398.

49. Stradman S, Pulkkinen P, Tenhu H, J Polym Sci A:Polym Chem 2005;43 3349.

3 Amphiphilic block copolymer P4VP by Nitroxide Mediated Polymerisation

Abstract

Well-defined poly(4-vinylpyridine) (P4VP) was synthesised by nitroxide-mediated radical polymerisation using the BlocBuilder MAMA-SG1. The controlled character of the polymerisation was confirmed by kinetic measurements and linear increase of the molar mass with monomer conversion. Poly(4-vinylpyridine) terminated with SG1 was then used as macroinitiator and chain extended to form block copolymer with methyl methacrylate and n-butyl acrylate. Block copolymer of poly(4-vinylpyridine-b-methyl methacrylate) and poly(4-vinylpyridine-b-(methyl methacrylate-co-styrene)) spontaneously organised into spherical inverse micelles in THF. The critical micelle concentrations was measured at 0.1 mg/mL for poly($4VP_{190}$-b-MMA_{91}) and 0.01 mg/mL for poly($4VP_{190}$-b-(MMA_{57}-co-S_{18})) and sizes of 70 and 130 nm (DLS), respectively. The inverse micelles were loaded with copper(II)acetate leading to a slight increase in micelle size. The uniform structure of the inverse micelles was confirmed by FeSEM images, while the presence of copper in the micelle core was established by energy-dispersive X-ray spectroscopy (EDX) and FTIR spectroscopy.

3.1 Introduction

In the recent years there has been a continuing interest in the preparation, investigation and application of nano-structured materials for metal templation. Of interest are the generation of self-organised assemblies with well defined size and properties, aimed at producing materials with potential application in areas such as photocatalysis[1], catalytic selectivity[2,3] and non-linear optics[4]. One promising approach is the application of block copolymers, where by design of the polymer composition the construction and manipulation of structured domains can be achieved. Because of the well known ability of poly(4-vinylpyridine) (P4VP) to coordinate metal ions[5-8] it has been widely used and has shown to be a material suitable for the introduction into devices such as biosensors and chemical sensors.[9,10] Therefore, block copolymers containing a P4VP block represent an interesting development in this field as they allow the defined spatial control of the coordinated metal ion *via* polymer self assembly. For example, localisation of metal ions or nanoparticles in the P4VP phase of phase separated block copolymer thin films has been reported.[11-16] Another area of interest is the self-organisation of amphiphilic P4VP block copolymers in conventional and inverse micelles.[17-20] Noticeably, is that almost exclusively it has been poly(styrene-*b*-4VP) block copolymers which have been reported in those examples due to the readily synthetic accessibility of this block copolymer. Both styrene and 4VP are very similar in their polymerisation behaviour and block copolymer synthesis by sequential controlled radical polymerisation such as nitroxide-mediated polymerisation (NMP) thus been straightforward. Attempts to introduce a larger variety of comonomers such as methacrylates usually cause significant synthetic difficulties due to the limitations of NMP in the polymerisation of this class of monomers. This is caused by the β-hydrogen elimination from the propagating radicals, which leads to the formation of ω-unsaturated dead chains.[21] Other controlled radical polymerisation techniques like atom transfer radical polymerisation (ATRP) are very well suited for the polymerisation of methacrylates, but in this case the polymerisation of 4VP poses some limitations owing to the competitive binding of the catalytic metal by 4VP.[22] In order to circumvent these difficulties Nishide and Long combined both ATRP and NMP for the synthesis of poly(4VP-*b*-MMA). Using a bifunctional initiator with an ATRP as well as an NMP initiating unit allowed the sequential polymerisation of MMA and 4VP in a

controlled fashion.[16] However, this approach requires a multi-step initiator synthesis. Reversible addition-fragmentation chain transfer (RAFT) polymerisation also provides an alternative to widen the range of P4VP block copolymer and has been reported for the synthesis of various homo and block copolymers.[23-27]

Here, we investigate the use of the NMP initiator MAMA-SG1 (Blocbuilder) for the synthesis of poly(4VP-*b*-MMA) and poly(4VP-*b*-BA). The commercial initiator MAMA-SG1 has been shown to be highly versatile in the polymerisation of styrenes and acrylates [28-30] but to our knowledge has not been investigated for the sequential synthesis of P4VP/methacrylate block copolymers. In this report we provide a kinetic investigation of the synthesis of these block copolymers using SG1-MAMA initiator. Our results show the versatility of this initiator for the 4VP polymerisation and the subsequent polymerisation of MMA under the addition of styrene. Moreover, the resulting block copolymers were formulated into inverse micelles in THF and loaded with copper salts.

3.2 Experimental

3.2.1 Materials

The monomers 4-vinylpyridine (4VP, Aldrich, 95%), methyl methacrylate (Aldrich, 99%) and styrene (Aldrich, 99%) were distilled under reduced pressure over calcium hydride. *n*-butyl acrylate (Aldrich, 99%) purified by passing through a column of alumina. 2-({Tert-butyl [1-(diethoxyphosphoryl)-2,2-dimethylpropyl]amino}oxy)-2-methylpropanoic acid (MAMA-SG1) was gifted from TU Eindhoven. Copper (II) acetate hydrate ($Cu(OAc)_2$) was purchased from Merck. All solvents were analytical grade and used directly as received unless otherwise noted.

3.2.2 Typical procedures for the polymerisation of 4-vinylpyridine (4VP)

4VP (2.62 g, 25 mmol), MAMA-SG1 (0.05 g, 0.13 mmol) and DMF (1.36 mL) were sealed in a Schlenk flask and degassed for 15 min by nitrogen bubbling. The reaction mixture was then immersed in a pre-heated oil bath at 110 °C. During the reaction, a small amount of the reaction mixture was sampled at time intervals to monitor the reaction kinetics. After the polymerisation, the reaction was stopped by quenching in an ice bath. The reaction mixture was precipitated in diethyl ether as a brownish powder and dried under vacuum at 40 °C.

^{1}H NMR (400 MHz, $CDCl_3$) (ppm): 8.54–8.11 (m, CH–N–CH), 6.89–6.18 (m, CH–C–CH), 2.08–1.14 (m, $–CH_2–CH–(C_5H_5N)$), 0.792–0.629 (m, $–CH_3$ from MAMA-SG1). FTIR (cm^{-1}): 3023, 1596, 1556, 1414, 993 (pyridine ring), 2927 ($–CH_2–$). Precipitated yield: 1.35 g.

3.2.3 Typical procedures for the synthesis of poly(4VP-*b*-MMA)

P4VP-SG1 macroinitiator (M_n 17,000 g/mol; 0.4 g, 0.02 mmol), MMA (0.47 g, 4.70 mmol) and DMF (3.60 mL) were sealed in a Schlenk flask and degassed for 15 min by nitrogen bubbling. Then, the flask was immersed in a pre-heated oil bath at 80 °C for 5 h. The polymerisation was stopped by quenching in an ice bath. The reaction mixture was precipitated in diethyl ether as a brownish powder and dried under vacuum at 40 °C.

^{1}H NMR (400 MHz, $CDCl_3$) (ppm): 8.54–8.11 (m, CH–N–CH), 6.89–6.18 (m,CH–C–CH), 3.59 (s, $–OCH_3$), 2.08–1.14 (m, $–CH_2–CH–(C_5H_5N)$), 1.05–0.80 (m, $–CH_3$ from MAMA-SG1). FTIR (cm^{-1}): 3023, 1598, 1557, 1416, 993 (pyridine ring), 2938 ($–CH_2–$), 1726 (C=O), 1449 (CH_3), 1145 ($O–CH_3$). Precipitated yield: 0.15 g.

3.2.4 Typical procedures for the synthesis of poly(4VP-*b*-MMA) with 10% styrene

P4VP-SG1 macroinitiator (M_n 17,000 g/mol; 0.4 g, 0.02 mmol), MMA monomer (0.47 g, 4.70 mmol), styrene (0.05 g, 0.47 mmol) and DMF (3.60 mL) were sealed in a Schlenk flask and degassed for 15 min by nitrogen bubbling. The flask was immersed in a pre-heated oil bath at 80 °C for 6 h. The polymerisation was stopped by quenching in an ice bath. The reaction mixture was precipitated in diethyl ether as a brownish powder and dried under vacuum at 40 °C.

^{1}H NMR (400 MHz, $CDCl_3$) (ppm): 8.62–8.11 (m, CH–N–CH), 7.06–6.94 (m, phenyl) 6.70–6.18 (m, CH–C–CH), 3.59 (s, $–OCH_3$), 2.08–1.14 (m, $–CH_2–CH–(C_5H_5N)$), 1.05–0.80 (m, $–CH_3$ from MAMA-SG1). FTIR (cm^{-1}): 3025, 1597, 1557, 1415, 993 (pyridine ring), 2933 ($–CH_2–$), 1725 (C=O), 1449 (CH_3), 1145 ($O–CH_3$), 1493, 1452 (phenyl ring). Yield: 0.24 g.

3.2.5 Typical procedure for the synthesis of poly(4VP-*b*-BA)

P4VP-SG1 macroinitiator (M_n 17,000 g/mol; 0.17 g, 0.01 mmol), BA (0.26 g, 2 mmol) and DMF (2 mL) were sealed in a Schlenk flask and degassed for 15 min by nitrogen bubbling. Then, the flask was immersed in a pre-heated oil bath at 120 °C for 5 h. The polymerisation was stopped by quenching in an ice bath. The reaction mixture was precipitated in diethyl ether as a brownish powder and dried under vacuum at 40 °C.

^{1}H NMR (400 MHz, $CDCl_3$) (ppm): 8.38–8.18 (m, CH–N–CH), 6.42–6.27 (m, CH–C–CH), 4.40 (s, $–OCH_2$), 2.27–1.83 (m, $–CH_2$ and –CH polymer backbone), 1.60-1.36 (m, $–CH_2$ for BA). FTIR (cm^{-1}): 1597, 1557, 1415 (pyridine ring), 1729 (C=O), 1453 ($–CH_2–$), 1161 (C-O). Precipitated yield: 0.1 g.

3.2.6 Typical procedure for the synthesis of poly(4VP-*b*-BA) with 10% styrene

P4VP-SG1 macroinitiator (M_n 17,000 g/mol; 0.17 g, 0.01 mmol), BA monomer (0.26 g, 2 mmol), styrene (0.03 g, 0.2 mmol) and DMF (2 mL) were sealed in a Schlenk flask and degassed for 15 min by nitrogen bubbling. The flask was immersed in a pre-heated oil bath at 120 °C for 3 h. The polymerisation was stopped by quenching in an ice bath. The reaction mixture was precipitated in diethyl ether as a brownish powder and dried under vacuum at 40°C.

^{1}H NMR (400 MHz, $CDCl_3$) (ppm): 8.62–8.11 (m, CH–N–CH), 7.06–6.94 (m, phenyl) 6.70–6.18 (m, CH–C–CH), 3.59 (s, $–OCH_3$), 2.08–1.14 (m, $–CH_2–CH–(C_5H_5N)$), 1.05–0.80 (m, $–CH_3$ from MAMA-SG1). FTIR (cm^{-1}): 3025, 1597, 1557, 1415, 993 (pyridine ring), 2933 ($–CH_2–$), 1725 (C=O), 1449 (CH_3), 1145 ($O–CH_3$), 1493, 1452 (phenyl ring). Yield: 0.24 g.

3.2.7 Preparation of block copolymer micelles loaded with metal salts

P($4VP_{190}$-b-MMA_{91}) was dissolved in THF at a concentration range of 0.2 mg/mL. The metal salt, copper(II)acetate hydrate $(Cu(OAc))_2$, was added to the block copolymer micellar solution using molar Cu:4VP ratios of 0.1:1, 0.5:1, 1:1, 2:1 and 5:1, respectively, and stirred overnight to coordinate Cu with P4VP units at room temperature. The particle size was measured by DLS and morphological effects after loading were characterised by field emission scan electron microscopy (FeSEM) using EDX spectroscopy.

3.2.8 Characterisation methods

^{1}H NMR analyses were performed in $CDCl_3$ solution, at 25 °C using a Bruker Avance 400 (400 MHz) spectrometer. The chemical shift was calibrated using the solvent peak (δ = 7.26 ppm). Fourier Transform InfraRed (FTIR) spectroscopy was carried out in the solid state on a Perkin Elmer Spectrum 100. SEC analysis using DMF (0.1 M LiBr) as

eluent (elution rate: 1 min/mL) was performed using two PSS GRAM analytical (300 and 100 Å, 10 L) columns on an Agilent 1200 series apparatus equipped with a Wyatt Optilab rEX refractive index detector thermostat at 40 °C and a Wyatt DAWN HELEOS-II multi angle light scattering (MALS) detector. Molar mass and dispersity (*D*) were calculated from the MALS signal using the ASTRA software (Wyatt) and a dn/dc value of 0.059 mL/g (PMMA) [31], 0.225 mL/g (P4VP) [23] and 0.041 mL/g (PBA) [32] in DMF. For block copolymer dn/dc was estimated by composition according to the block ratio $(dn/dc)_{block} = w_{P4VP}(dn/dc)_{P4VP} + w_{PMMA}(dn/dc)_{PMMA}$) [33,34]. Before analysis, samples were filtered through a 0.45 μm PTFE filter (13 mm, PP housing, Whatman). DLS experiments were conducted on a Malvern Zetasizer Nano ZS equipped with a He–Ne laser with a wavelength, $k = 632.8$ nm. The temperature was set to 25 °C and the angle of measurement was 173°. Samples were filtered through 0.45 μm Milipore before analysis. Field emission scanning electron microscopy (FeSEM) was conducted by using a Hitachi S5500 at an acceleration voltage of 20.0 kV equipped with an energy dispersive X-ray spectrometer. EDX was performed using a Nickel grid that had been carbon coated. Analysis was undertaken using a 25 kV accelerating voltage. Data was processed using the INCA Oxford Instruments software package.

3.3 Results and discussion

3.3.1 Polymerisation of 4-vinylpyridine (P4VP)

The synthetic strategy for the synthesis of poly(4VP-*b*-MMA) using MAMA-SG1 is depicted in Scheme 3.1. It involved the preparation of a P4VP first block followed by the chain extension with MMA. Nitroxides have been demonstrated to provide very satisfactory results with 4VP [35-38], but to our knowledge MAMA-SG1 has not been studied for the polymerisation of this monomer to date. The polymerisation of 4VP using MAMA-SG1 alkoxyamine was conducted in solution at 110 °C. In this process the unimolecular initiator MAMA-SG1 is dissociating into initiating C-radicals and reversibly terminating nitroxyl radicals in a 1:1 molar ratio. The data of molecular weight and dispersity of the obtained P4VP, using two different initial ratio

$[4VP]_0/[MAMA\text{-}SG1]_0$, namely 190/1 and 48/1 are listed in Table 3.1. Both polymerisations yielded polymers with low dispersities (*D*) of 1.1 and molecular weights (M_n) of 17000 and 4100 g/mol, respectively. These values were close to the theoretical values at high monomer conversion.

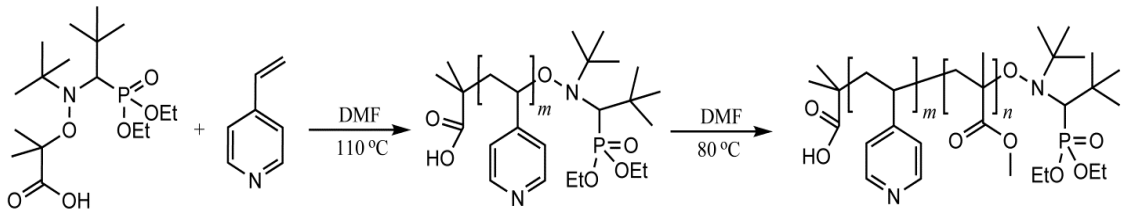

Scheme 3.1: Synthesis of poly(4VP-*b*-MMA) by sequential polymerisation using the alkoxyamine MAMA-SG1 as an initiator.

Table 3.1: Molar mass and dispersity (*D*) of P4VP obtained at 110 °C with MAMA-SG1 at different ratio of $[4VP]_0/[I]_0$ (subscript numbers).

Entry	**time (min)**	**Conversion** [a] **(%)**	$M_{n\ theo}$ [b] **(g/mol)**	$M_{n\ SEC}$ [c] **(g/mol)**	$M_{w\ SEC}$ [c] **(g/mol)**	D [c]
$P4VP_{190}$	300	99	19700	17000	18400	1.1
$P4VP_{48}$	210	99	5000	4100	4400	1.1

[(a)]Conversion calculated by ^{1}H NMR integration using monomer peaks at 5.93 and 5.49 ppm and polymer peaks at 1.20 - 2.00 ppm. [(b)]$M_{n\ theo}$ = conversion x $[M]_0/[I]_0$ x $M_{monomer}$. [(c)]Measured in DMF with multi angle light scattering detector (MALS).

The controlled character of the polymerisation was further demonstrated by kinetic measurements shown in Figure 3.1. For both monomer to initiator ratios $\ln([M]_0/[M])$ as a function of time is linear after an induction period confirming a constant number of propagating polymeric radicals during the polymerisation. **Error! Reference source not found.** depicts the dependences of molecular weight (M_n) and dispersity (*D*) on monomer conversion. In both cases, the plots of M_n *vs*. conversion follow a linear trend up to full conversion. Interestingly, the *D* for both polymers remains low around 1.1. The excellent control of the polymerisation is also manifested in the clear shift of the size exclusion chromatography (SEC) traces as the reaction proceeds (**Error!**

Reference source not found.). No remaining peaks or thermal polymerisation, which is sometimes observed in NMRP, was detected in SEC.[39]

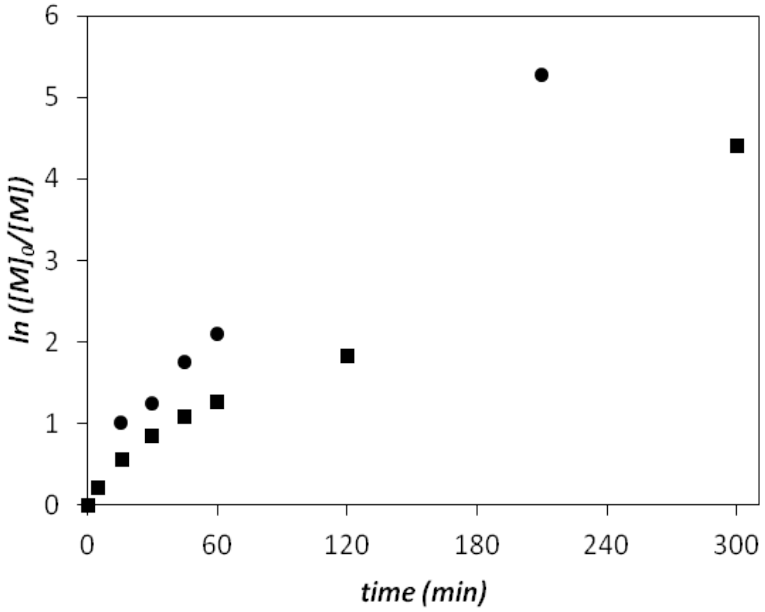

Figure 3.1: Kinetic plot ln($[M]_0/[M]$) versus time of 4VP polymerisation with MAMA-SG1 (110 ºC) at $[M]_0/[I]_0$ ratio 190 (■) and 48 (●).

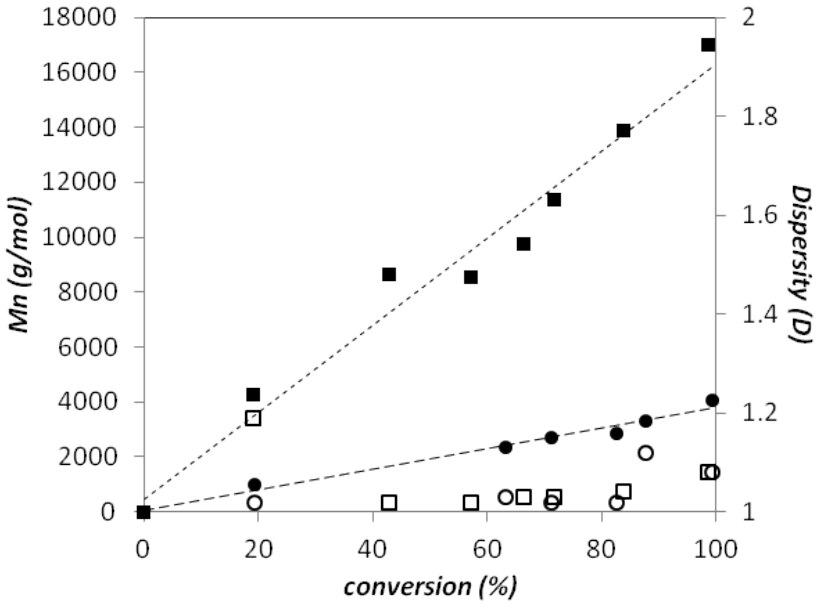

Figure 3.2: Number-average molar mass (M_n) and dispersity (D) of the P4VP chains as a function of monomer conversion ($[M]_0/[I]_0$ = 190: ■ M_n; □ D), ($[M]_0/[I]_0$) = 48: ● M_n; ○ D). Dotted lines added to guide the eye.

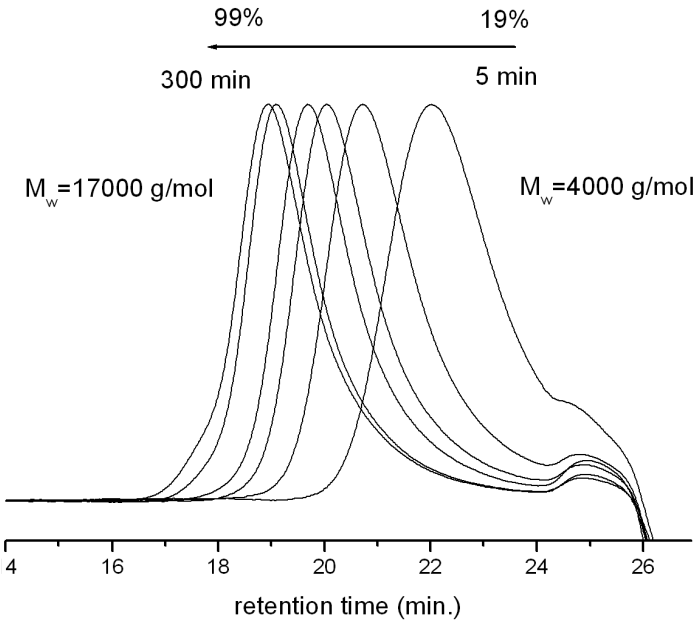

Figure 3.3: SEC chromatograms of the evolution of molar mass at different conversion and reaction time for $P4VP_{190}$.

3.3.2 Poly(4VP-*b*-MMA) diblock copolymer

The SG1-terminated 4VP polymers were subsequently used as macroinitiators in polymerisation of MMA (with and without the addition of styrene) at 80 °C (**Error! Reference source not found.**). ^{1}H NMR and FTIR confirmed the successful polymerisation of MMA. In addition to the 1596 cm^{-1} vibration assigned to the C=N stretch and the 1556 cm^{-1} for C=C stretch of the P4VP pyridine ring, new bands assigned to PMMA (1725 cm^{-1} for C=O stretching, 1449 cm^{-1} for CH_3 stretching and 1145 cm^{-1} for O-CH_3 stretching) appeared in FTIR spectra (**Error! Reference source not found.**). The ^{1}H NMR spectra (**Error! Reference source not found.**) of the obtained polymers also confirmed the presence of both pyridyl groups from the P4VP segment (8.23 and 6.28 ppm) and methoxy groups from PMMA segment (3.56 ppm).

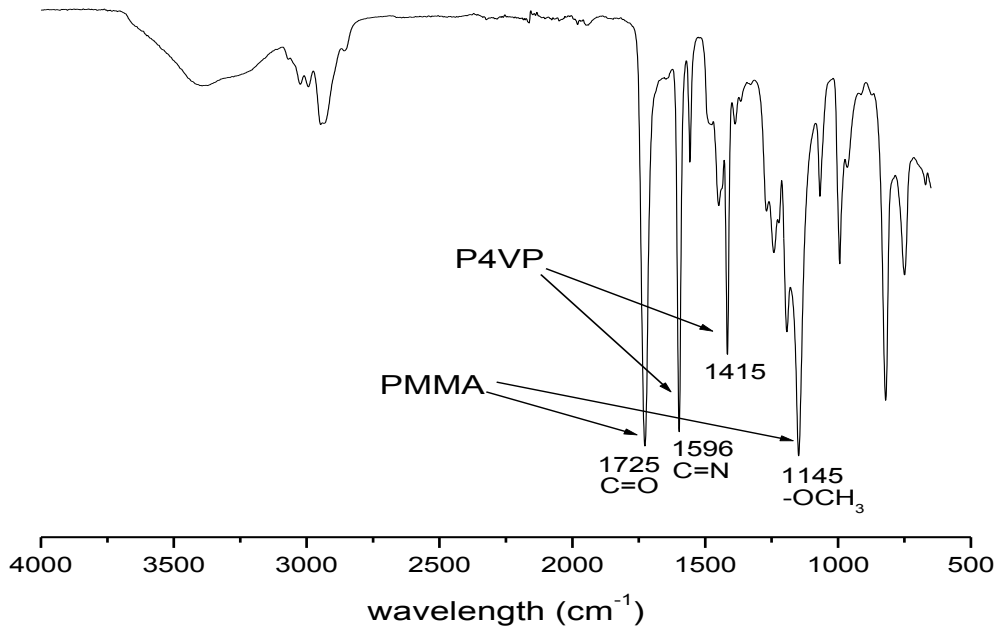

Figure 3.4: FTIR spectrum of poly(4VP-*b*-MMA) block copolymer.

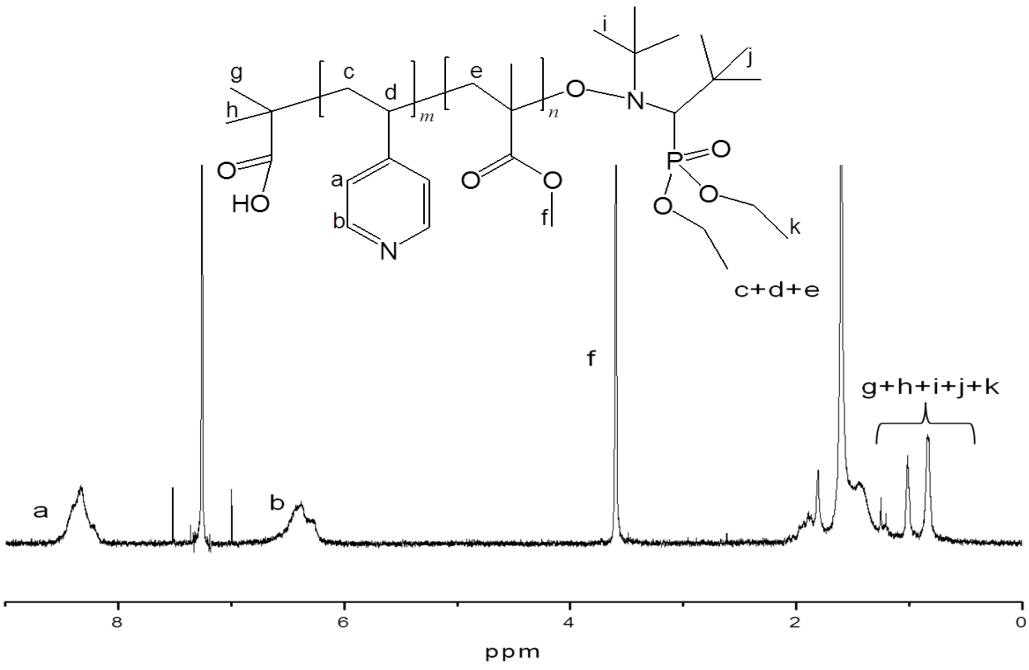

Figure 3.5: ^{1}H NMR spectrum of poly(4VP-*b*-MMA) block copolymer (peak at 7.14 ppm: $CDCl_3$).

While the formation of block copolymers by NMP chain extension with MMA was reported in the literature, the polymerisation has been described as difficult and uncontrolled in the reported cases.[40,41] The level control of the polymerisation and indeed the block structure of the polymers were thus carefully investigated. The direct polymerisation of MMA from both P4VP macroinitiators showed good efficiency, between 75-80 %, but yielded block copolymers with an M_n slightly higher than the theoretical values (Table 3.2, BC1 and 2). Moreover, an increased D in the range of 1.2-1.5 was observed, probably due to cross-disproportionation side reactions. In similar studies with SG-1 the loss of control in MMA polymerisation has been attributed solely to the large activation-deactivation equilibrium constant.[42] An alternative route avoiding this problem involves the copolymerisation of a small percentage of styrene (4-10%) with MMA to form copolymers with a methacrylate functionality.[43-46] When the macroinitiation from P4VP was carried out in the presence of 10 mol% styrene, the polymerisation drastically slowed down (approximately half conversion of MMA for the same reaction time) due to the formation of more thermally stable styrene-SG1 alkoxyamine bonds during the activation-deactivation process. As a consequence, the M_n values of the final block copolymer (Table 3.2, BC3 and 4) were much closer to the theoretical values with lower dispersity and better macroinitiator efficiency of 79-89%. (Note: dispersities were determined by MALS and could be underestimated) because of the inaccuracy measurements at low molecular weight region. This is explained by a dramatic reduction of the concentration of propagating polymeric radicals leading to a decrease of the irreversible termination rate. As an example **Error! Reference source not found.** shows a clear shift of the SEC traces toward higher molar masses with respect to that of the P4VP macroinitiator upon macroinitiation confirming that block copolymers were indeed obtained. Analysis of the block copolymer composition by ^{1}H NMR confirms a much larger incorporation of styrene than present in the monomer feed, *i.e.* 31% for BC3 (conversion MMA 30%) and 38% for BC4 (conversion MMA 38%), respectively. Under the different reaction conditions of a bulk polymerisation initiated by SG1, Charleux reported 12 mol% of styrene at 64% conversion of MMA for initial molar fraction of styrene of 8.8%.[43]

Table 3.2: Molecular characteristics of block copolymers obatined with and without 10% of styrene in the monomer feed (denoted by (S)). BC: blockcopolymer.

Block ratio [a]	$[M]_0/[I]_0$	**time (min.)**	**Conv.**[b] **MMA (%)**	$M_{n\ theo}$ [c] **(g/mol)**	$M_{n\ SEC}$ [d] **(g/mol)**	$M_{w\ SEC}$ [d] **(g/mol)**	D [d]	**Micelle size (nm)**
BC1 $P4VP_{190}$-*b*-MMA_{91}	200	360	48	27300	36000	50600	1.5	70
BC2 $P4VP_{48}$-*b*-MMA_{33}	50	180	69	7400	9800	11300	1.2	-
BC3 $P4VP_{190}$-*b*-$P(MMA_{57}$-*co*-$S_{18})$	200 (S)	360	30	22000	28000	30900	1.1	130
BC4 $P4VP_{48}$-*b*-$P(MMA_{18}$-*co*-$S_7)$	50 (S)	180	38	5900	6600	7000	1.1	-

[(a)]Ratio calculated from ^{1}H NMR integrated peak ratios using the pyridyl peak of P4VP (6.40 ppm) of the macroinitiator, $-OCH_3$ peak of PMMA (3.57 ppm) and aromatic styrene peaks at 6.89-7.20 ppm. [(b)] Conversion calculated by ^{1}H NMR integration using the pyridyl peaks of P4VP (6.40 ppm) of the macroinitiator and $-OCH_3$ peaks of MMA (3.57 ppm). [(c)]$M_{n\ theo}$ calculated using the equation: M_n = (conversion x $[M]_0/[I]_0$ x $M_{monomer}$) + $M_{n\ macroinitiator}$. [(d)] Measured in DMF with multi angle light scattering detector (MALS).

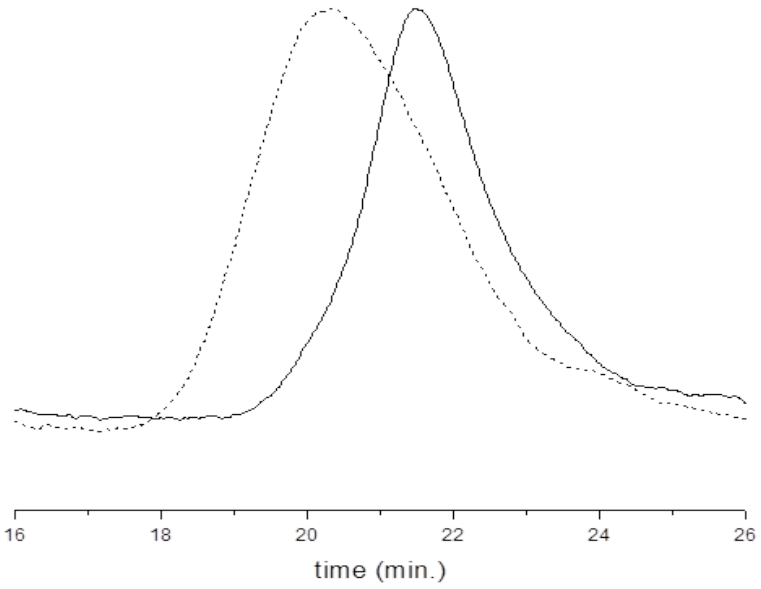

Figure 3.6: SEC trace (MALS signals) of block copolymer BC4 (Table 3.2; dotted line)) block copolymer resulting from chain extension of poly(4-vinylpyridine) ($P4VP_{48}$; solid line).

3.3.3 Poly(4VP-*b*-BA) diblock copolymer

For acrylates monomer, the main challenge in NMP is to control the side product due to the extensive chain transfer to polymer during polymerisation. Thus, the polymer will lose their living functionality leading to the formation of branched polymers. Several investigation either experimental and simulation have reported this phenomenon.[47-50] Therefore, initially addition of excess nitroxide [51,52] or styrene [53] into a polymer system to help in enhanced deactivation process to control polymerisation of butyl acrylate (BA).

The extensions with butyl acrylate (BA) from the macroinitiator, $P4VP_{190}$ was carried out at 120 °C both with and without the addition of styrene (**Error! Reference source not found.**). **Error! Reference source not found.** shows the ^1H NMR of synthesised block copolymer poly(4VP-*b*-BA). The presence of signals at 8.33 and 6.40 ppm was attributed to the protons of the pyridinyl P4VP segment and those at 4.02 ppm to the $-OCH_2$ group of the PBA segment. The characteristic absorption of C=N stretch and C=C stretch for the P4VP ring appeared at 1597 and 1557 cm^{-1} in the FTIR spectrum, respectively. After chain extension new bands of PBA assigned at 1729 cm^{-1} for C=O

stretching and 1161 cm^{-1} for C-O stretching could be detected in the FTIR spectra (**Error! Reference source not found.**).

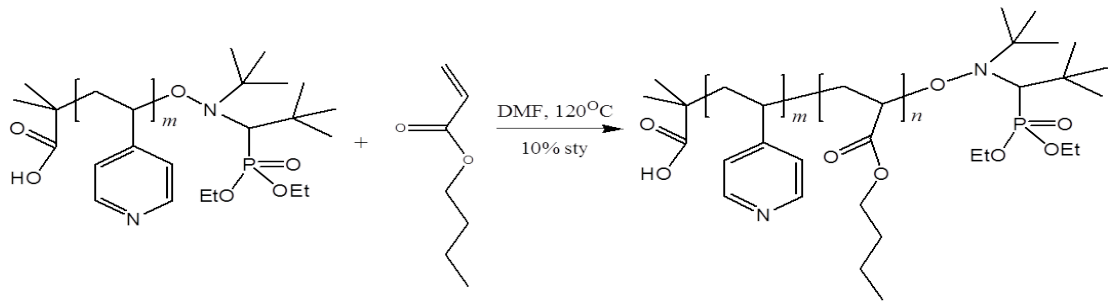

Scheme 3.2: Synthesis of poly(4VP-*b*-BA) by sequential polymerisation using the alkoxyamine MAMA-SG1 as an initiator.

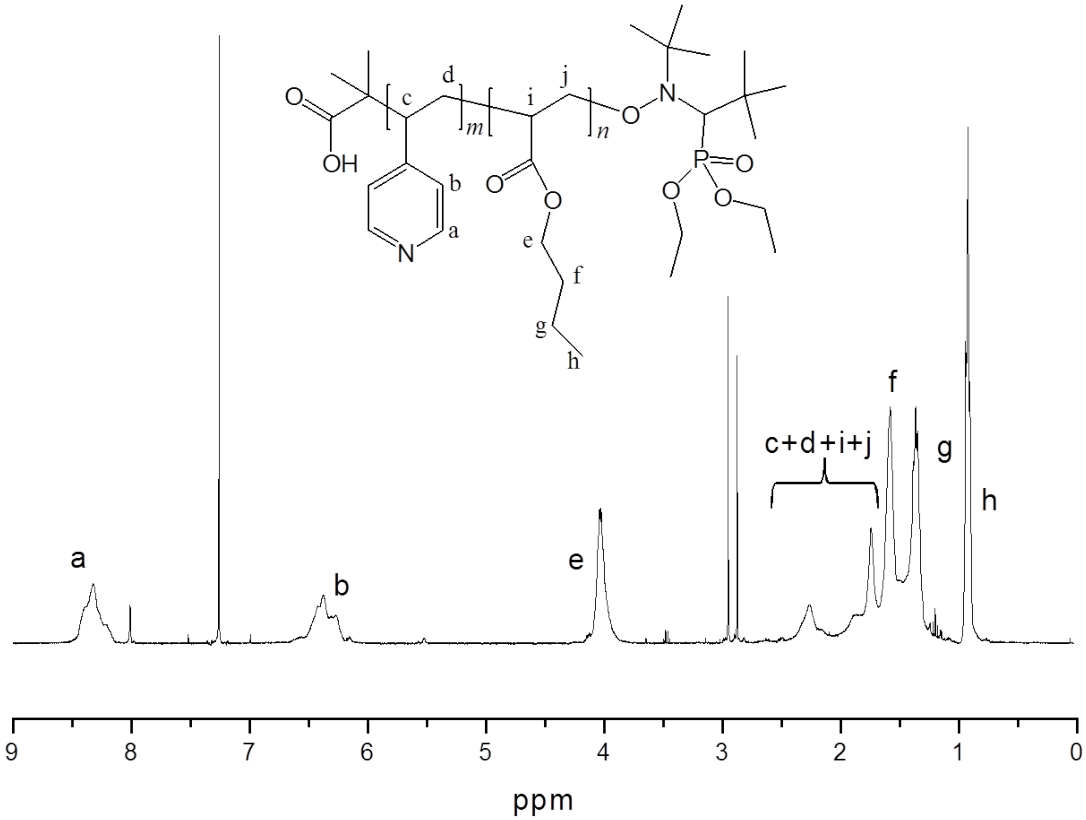

Figure 3.7: ^{1}H NMR spectrum of poly(4VP-*b*-BA) block copolymer (peak at 7.26 ppm: $CDCl_3$).

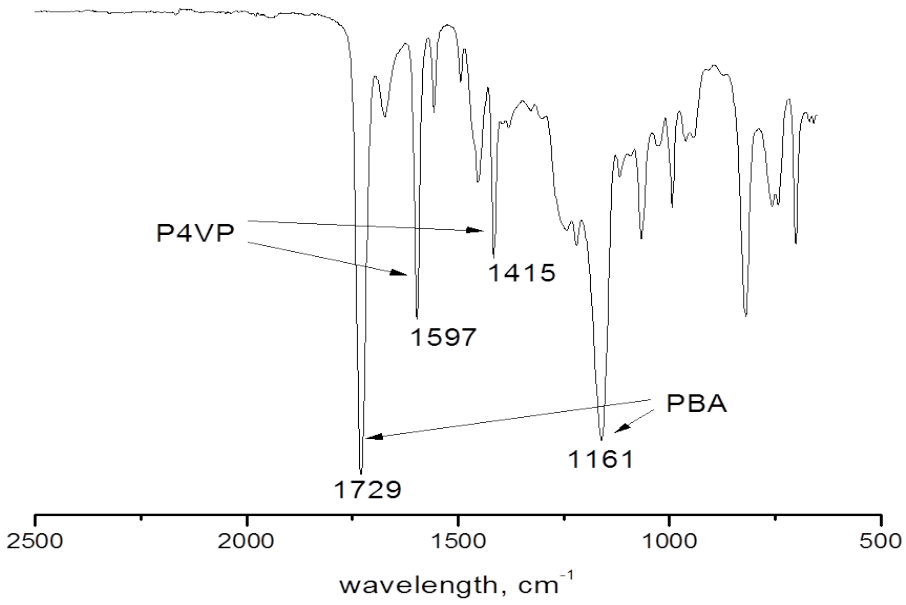

Figure 3.8: FTIR spectrum of poly(4VP-*b*-BA) block copolymer.

As for MMA, polymerisation of BA by NMP is a difficult and uncontrolled process.[54,55] The kinetic plots of BA3 show faster polymerisation rate and reach a plateau stage after 200 minutes of reaction due to termination reaction during polymerisation (**Error! Reference source not found.Error! Reference source not found.**). This agreed with the observation that the polymer had a higher M_n value compare to the theoretical value and the high dispersity of 1.23 as shown in **Error! Reference source not found.** (a, b) and Table 3.3. Meanwhile, addition of 10% styrene (BA1) into the system slowed down the polymerisation rate and halved the conversion similar to MMA. This is because the formation of thermally stable bond between styrene-SG1. However, the M_n value of the final block is lower than the theoretical value and does not increase with conversion. This might be because of chain transfer reaction by hydrogen abstraction from the polymer backbone at the end of polymer chains.[56,57] For extended reaction time, the M_n of both systems doubled with respect to the theoretical value and dispersity broadened. In all cases, termination reaction occurred as evident from the broad tailing of SEC chromatograms at low molecular mass side (**Error! Reference source not found.**). In addition, no clean shift of the polymer peak from macroinitiators was observed which might suggest the presence of two individual polymer rather than a block copolymer. Acrylate monomers are also

known to undergo extensive chain transfer to polymer reaction during polymerisation, in which the second propagating chain ends of a macroradical are transformed into more stabilised tertiary radicals (also called mid-chains) that are located on the polymer backbone. Addition of monomer or termination at this tertiary radicals, leads to the formation of chain branches. From this point of tertiary radicals, Hlalele and Klumperman suggested that nitroxide radicals can attach to this mid-chain radical along the polymer backbone during polymerisation and formed branched polymer which would also result in a broadening of the SEC traces.[58,59] However, Guillaneuf *et al*. reported that midchain radicals do not significantly influence the livingness of polymer because disporportionation (*β*-scission) is more favourable than termination.[50] Fercet *et al*. showed that intramolecular chain transfer presumably backbiting was the prominent mechanism at high temperature.[60] Another possibility is the autoinitiation of PBA at high temperature of polymerisation or our P4VP macroinitiator might be not suitable as macroinitiator for BA extension. Nevertheless, successfully control polymerisation of BA was reported experimentally supported by simulation by the initial addition of excess nitroxide.[51,52]

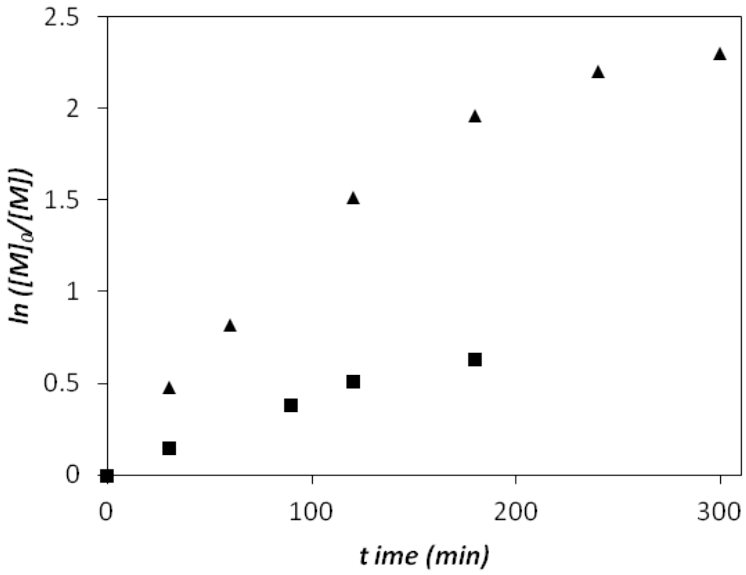

Figure 3.9: Kinetic plot ln ($[M]_0/[M]$) versus time of BA polymerisation with P4VP macroinitiator (120 ºC) at $[M]_0/[I]_0$ ratio 200; ■ = BA1 and ▲= BA3.

(a)

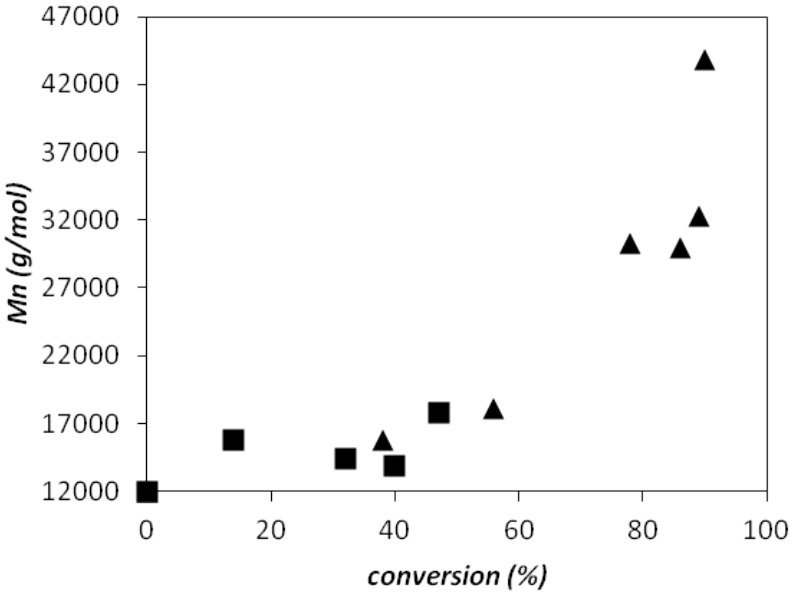

(b)

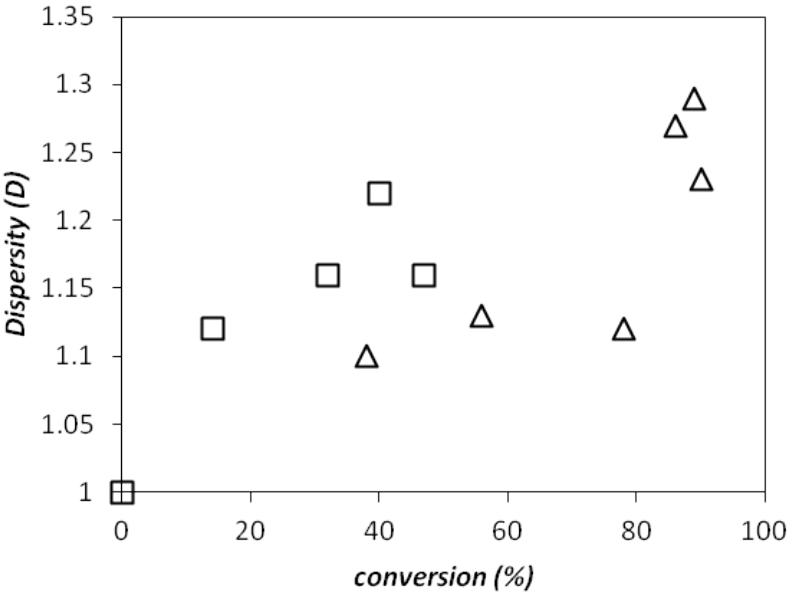

Figure 3.10: (a) Number-average molar mass, M_n (filled symbols) and (b) dispersity, D (open symbols) of the BA chains as a function of monomer conversion at $[M]_0/[I]_0$ = 200; ■ = BA1 and ▲= BA3.

Table 3.3: Molecular characteristics of block copolymers obtained with and without 10% of styrene in the monomer feed (denoted by (S)). BC: block copolymer

Entry[a]	time (min.)	Conv.[b] BA (%)	$M_{n\ theo}$[c] (g/mol)	$M_{n\ SEC}$[d] (g/mol)	$M_{w\ SEC}$[d] (g/mol)	D[d]
BA1	180	47 (S)	24000	17700	20600	1.16
BA3	300	90	35100	43900	53200	1.23
BA4	1440	92	35600	61000	84100	1.38
BA5	1440	69 (S)	29700	80000	101000	1.26

[(a)]Ratio calculated from ^{1}H NMR integrated peak ratios using the pyridyl peak of P4VP (6.40 ppm) of the macroinitiator, –OCH_2 peak of PBA (3.57 ppm) and aromatic styrene peaks at 6.89-7.20 ppm. [(b)]Conversion calculated by ^{1}H NMR integration of CH_2 monomer peaks of BA (5.6 and 5.8 ppm) and CH_2 polymer (1.5-2.3 ppm). [(c)]$M_{n\ theo}$ calculated using the equation: M_n = (conversion x $[M]_0/[I]_0$ x $M_{monomer}$) + $M_{w\ macroinitiator}$. [(d)] Measured in DMF with multi angle light scattering detector (MALS).

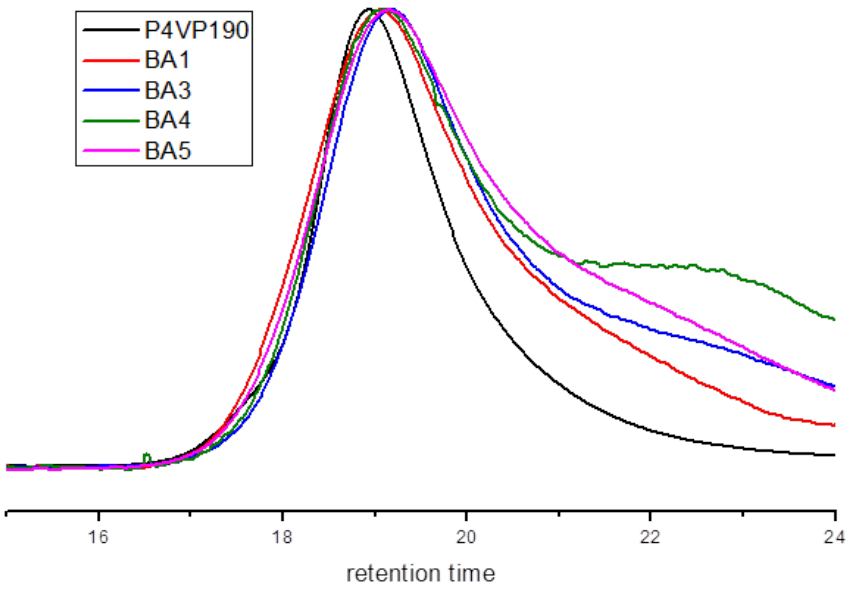

Figure 3.11: SEC trace of block copolymer with addition of styrene (BA1, BA5) and block copolymer without styrene (BA3, BA4) resulting from chain extension of $P4VP_{190}$.

3.3.4 Formation of inverse micelles and metal binding

The self-assembly of poly(4VP-*b*-MMA) block copolymers into inverse micelles in THF consisting of a soluble PMMA corona and insoluble P4VP core was then invistigated. Different concentrations of all block copolymers listed in Table 3.2 were prepared in order to determine the critical micelle concentration (CMC) using DLS. For both block copolymers with a short P4VP block, namely BC2 and BC4, micelle formation could not be achieved probably due to the improper hydrophobic–hydrophilic balance. DLS results for BC2 in **Error! Reference source not found.** shows that P4VP chains were not assembled to form micelles core even at higher concentration of 5 mg/mL. On the other hand, all block copolymers with 190 4VP units formed inversed micelles in THF. The size of particles remained constant around 70 nm for BC1 (CMC: 0.1 mg/ mL) and 130 nm for BC3 (CMC: 0.01 mg/mL), respectively (Figure 3.13). The different size might be due to a slight difference in block length ratio as well as the presence of 30% styrene in the hydrophobic block of BC3.

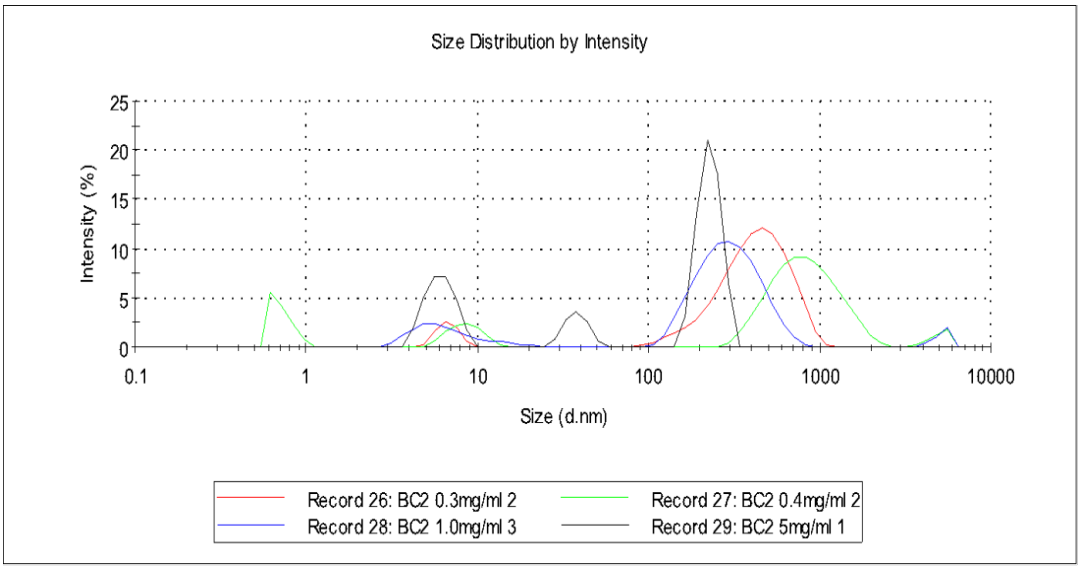

Figure 3.12: DLS measurement for BC2 ($P4VP_{48}$-*b*-$PMMA_{33}$) micelles at concentration 5.0, 1.0, 0.4 and 0.3 mg/mL.

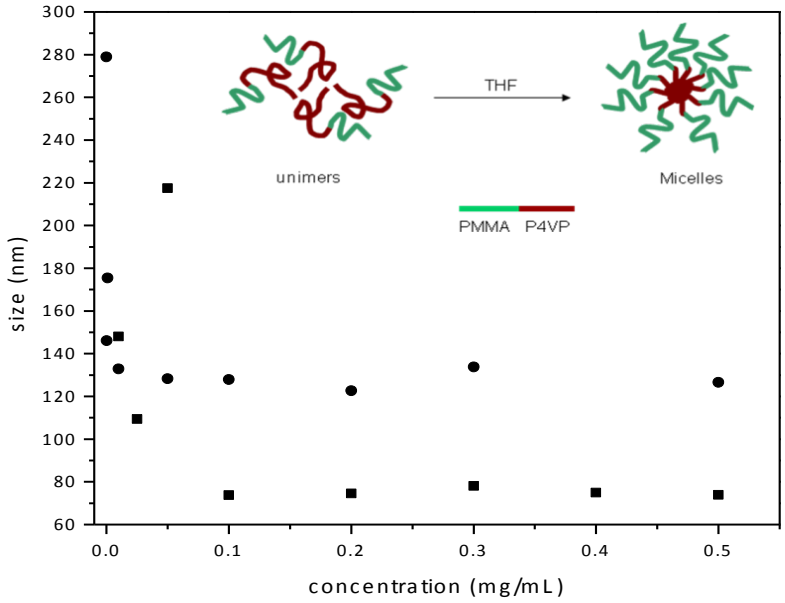

Figure 3.13: Hydrodynamic diameter measured by DLS at 25 °C versus the concentration of $P4VP_{190}$-*b*-$PMMA_{91}$ (■ BC1, Table 3.2) and $P4VP_{190}$-*b*-P(MMA_{57}-co-S_{18}) (● BC3, Table 3.2).

The ability of 4VP to coordinate metal ions can be used to load the core of block copolymer micelles.[19,20] This was investigated by the addition of copper(II)acetate in different ratios with respect to pyridine units in the micelle solution of BC1 (0.2 mg/mL, $P4VP_{190}$-b-$PMMA_{91}$) at room temperature. DLS measurements showed that the micelles size increased from 75 nm for the unloaded micelle to 85-95 nm with increasing ratio Cu:P4VP up to 1:1 (Note: the concentration of 4VP in the sample was calculated using the M_n of the P4VP block implying an uncertainty in the calculation of suggesting the formation of undefined polymer clusters (Table 3.4). There is a well-established coordination chemistry for metal ions in solution. For example, Cu(II) will form generally 4, 5 or 6 coordinated complexes with a wide range of ligands. However, these coordination modes are normally not observed in a polymer matrix mostly because of steric hindrance issues and in general a mixture of lower coordination numbers were observed for many metal ions including Fe(II) and Fe(III)[8], Ru (III)[7] and Cu(II)[61]. The maximum micelle loading at a 1:1 ratio must thus be a combination of metal coordination and the preference of the copper ions for the hydrophilic environment of the micelle core. FeSEM images (Figure 3.14) taken from the micellar solution showed dispersed micelles in a size range of 55-65 nm (BC1, Table 3.2). The

smaller size as compared to the DLS measurement is most likely owed to the effect of drying in the SEM sample preparation. Energy-dispersive X-ray spectroscopy (EDX) spectra clearly show the presence of copper (Figure 3.15). Finally, the coordination of the metal salts could directly be confirmed by IR-spectroscopy.[62] Distinctive evidence for the metal coordination could be obtained from the disappearance of the bands characteristic for the pyridine units (1597, 1557 and 1415 cm^{-1}, Figure 3.4) and the appearance of a new band at 1614 cm^{-1}, caused by the metal coordination of the pyridine units (Figure 3.16). This validates that the copper ions are indeed located in the core of the inverse micelles.

Table 3.4: Particles size of $P4VP_{190}$-*b*-$PMMA_{91}$ micelles (0.2 mg/mL in THF) after loading with Cu (II) acetate by DLS measurement (average of three measurements). The 4VP concentration was calculated from the polymer M_n (0.28 x 10^{-4} mol)

Ratio Cu:P4VP	**Cu(II) (x 10^{-4} moles)**	**Size (nm)**	**Dispersity (*D*)**
0	-	75 ±0.77	0.05 ±0.02
0.1:1	0.03	86 ±0.20	0.07 ±0.01
0.5:1	0.14	95 ±0.17	0.15 ±0.01
1:1	0.28	85 ±0.16	0.10 ±0.01
2:1	0.56	105 ±1.76	0.20 ±0.01
5:1	1.39	182 ±1.10	0.28 ±0.02

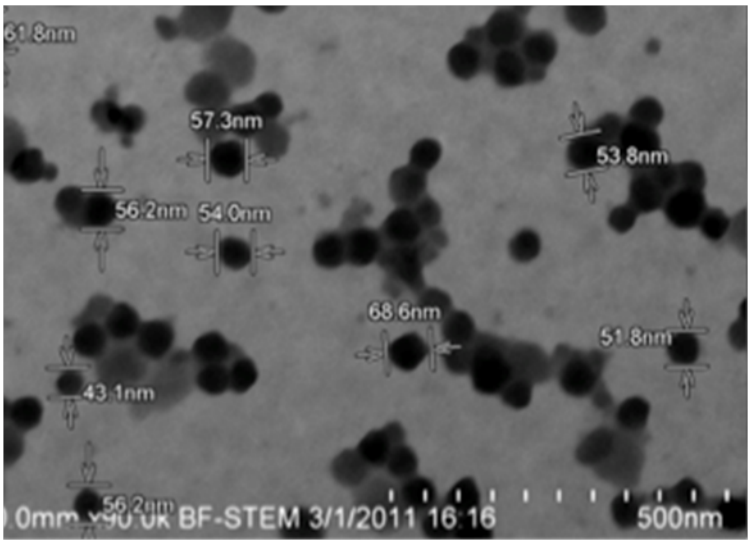

Figure 3.14: FeSEM images of $P4VP_{190}$-*b*-$PMMA_{91}$ inverted micelles in THF loaded with copper(II)acetate (Cu: P4VP 1:1,Table 3.4).

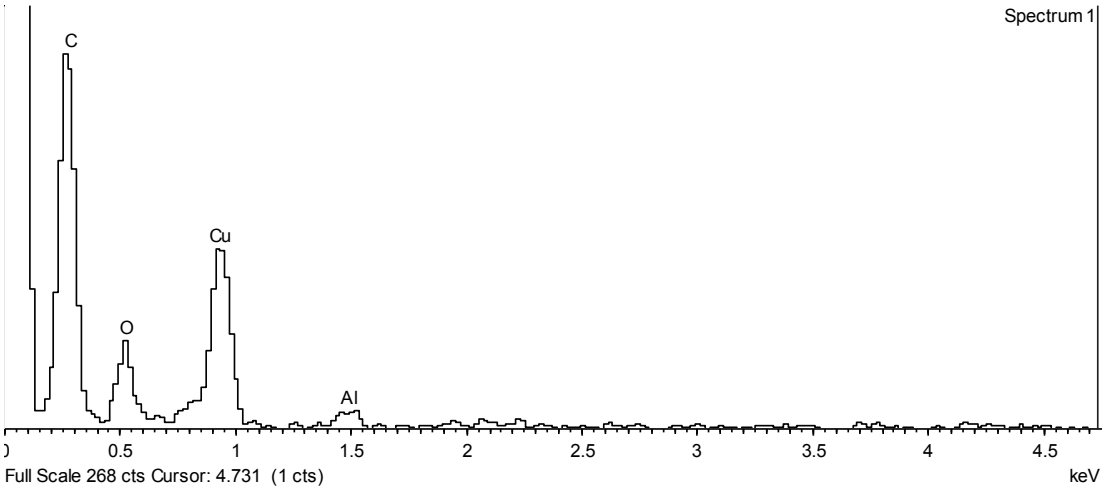

Figure 3.15: EDX measurement of atomic presence in $P4VP_{190}$-*b*-$PMMA_{91}$ inverted micelles in THF loaded with copper (II)acetate (Cu: P4VP 1:1, Table 3.3).

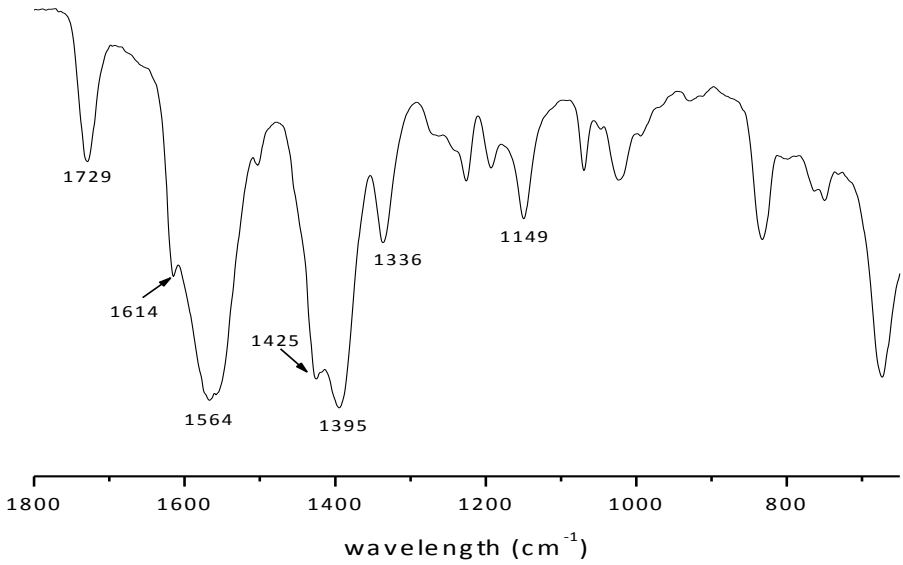

Figure 3.16: FTIR spectrum of precipitated copper coordinated P4VP-*b*-PMMA) inverse micelle at a ratio of copper(II)acetate to 4VP of 1:1 (BC1,Table 3.4).

3.4 Conclusion

Well defined poly(4-vinylpyridine) by NMRP using the BlocBuilder MAMA-SG1 have been synthesized for the first time. The P4VP terminated SG1 were used as macroinitiator and chain extended to form poly(4VP-*b*-MMA) and P4VP-b-(PMMA-co-S) block copolymers. The kinetic and SEC results confirm that the polymerisations are well controlled. These block copolymers spontaneously organised into spherical inverse micelles in THF, which were core loaded with copper(II)acetate as confirmed by DLS, FeSEM image, EDX and FTIR spectroscopy. The versatility of the synthetic approach opens possibilities for the synthesis of other well-defined P4VP block copolymers from a range of methacrylic monomers thereby increasing the range of metal binding polymers. However, P4VP as macroinitiator for BA is not good control. The block copolymer of poly(4VP-*b*-BA) and P4VP-*b*-(PBA-*co*-S) showed termination reaction. There also have a possibility two individual homopolymer of P4VP and PBA presence as the product based on SEC results.

References

1. Lehn JM, Sauvage JP, Ziessel R, Nouv J Chem 1980;4:623.

2. Kishida M, Fugita T, Umakoshi K, Ishiyama J, Nagata H, Wakabayashi KJ, Chem Soc Chem Commun 1995;763.

3. Lewis JN, Chem Rev 1993;93:2693.

4. Ogawa S, Hayashi Y, Kobayashi N, Tokazaki T, Nakamura A, Jpn J Appl Phys 1994;33:331.

5. Agnew JH, J Polym Sci 1976;14:2819.

6. Forster RJ, Vos JG, Macromolecules 1990;23:4372.

7. Clear JM, Kelly JM, Vos JG, Makromol Chem 1983;184:613.

8. Coey JMD, Meagher AP, Kelly JM, Vos JG, J Polym Sci Polym Chem Ed 1984;22:303.

9. Heller A, Acc Chem Res 1990;23:128.

10. Doherty AP, Forster RJ, Smyth MR, Vos JG, Anal Chem 1992;64:572.

11. Aizawa M, Buriak JM, Chem Mater 2007;19:5090.

12. Zhao Y, Thorkelsson K, Mastroianni AJ, Schilling T, Luther JM, Rancatore BJ, Matsunaga K, Jinnai H, Wu Y, Poulsen D, Frechet JMJ, Alivisatos AP, Xu T, Nat Mater 2009;8:979.

13. Kim B J, Bang J, Hawker CJ, Kramer EJ, Macromolecules 2006;39:4108.

14. Fahmi AW, Stamm M, Langmuir 2005;21:1062.

15. Kuila BK, Rama MS, Stamm M, Adv Mater 2011;23:1797.

16. Shoji M, Eguchi M, Layman JM, Cashion MP, Long TE, Nishide H, Macromol Chem Phys 2009;210:579.

17. Cho H, Park H, Park S, Choi H, Huang H, Chang T, J Colloid Interfacial Sci 2011;356:1.

18. Zhang M, Rene-Boisneuf L, Hu YW, Moozeh K, Hassan Y, Scholes G, Winnik, MA, J Mater Chem 2011;21:9692.

19. Athony SP, Kim JK, Chem Commun 2008;1193.

20. Jang YH, Kochuveedu ST, Cha MA, Jang YJ, Lee JY, Lee J, Lee J, Kim J, Ryu DY, Kim DH, J Colloid Interfacial Sci 2010;345:125.

21. Burguière C, Dourges MA, Charleux B, Vairon JP, Macromolecules 1999;32:3883.

22. Xia J, Zhang X, Matyjaszewski K, Macromolecules 1999;32:3531.

23. Convertine AJ, Sumerlin BS, Thomas DB, Lowe AB, McCormick CL, Macromolecules 2003;36:4679.

24. Wan W-M, Pan C-Y, Polym Chem 2010;1:1475.

25. Zhao D, Chen X, Liu Y, Wu C, Ma R, An Y, Shi L, J Col Interface Sci 2009;331:104.

26. Zhang L, Wang Q, Lei P, Wang X, Wang C, Cai L, J Polym Sci A: Polym Chem 2007;45:2617.

27. Bozovic-Vukic J, Manon HT, Meuldijk J, Koning C, Klumperman B, Macromolecules 2007;40:7132.

28. Charleux B, Nicolas J, Polymer 2007;48:5813.

29. Trimaille T, Mabrouk K, Monnier V, Charles L, Bertin D, Gigmes D, Macromolecules 2010;43:4864.

30. Karaky K, Billon L, Pouchan C, Desbrières J, Macromolecules 2007;40:458.

31 Shimura Y. Bull Chem Soc Jpn 1967;40:273.

32 Alb AM, Enohnyaket P, Drenski MF, Shunmugam R, Tew GN, Reed WF, Macromolecules 2006;39:8283.

33 Ke F, Mo X, Yang R, Wang Y, Liang D, Macromolecules 2009;42:5339.

34 Mya KY, Lin EMJ, Gudipati CS,, Gose HBAS, He C, J Phys Chem B 2010;114:9128.

35. Fischer A, Brembilla A, Lochon P, Macromolecules 1999;32:6069.

36. Bohrisch J, Wendler U, Jaeger W, Macromol Rapid Commun 1997;18:975.

37. Chen Z, Cai J, Jiang X, Yang C, J App Polym Sci 2002;86:2687.

38. Diaz T, Fischer A, Jonquieres A, Brembilla A, Lochon P, Macromolecules 2003;36:2235.

39. Polakova L, Lokaj J, Holler P, Starovoytova L, Pelkarek M, Stepanek P, e-Polymers 2010;65:1.

40. Ruzette A-V, Tencé-Girault S, Leibler I, Chauvin F, Bertin D, Guerret O, Géranrd P. Macromolecules 2006;207:1278

41. Chauvin F, Dufils P-E, Gigmes D, Guillaneuf Y, Marque SRA, Tordo P, et al. Macromolecules 2006;39:5238.

42. Guillaneuf Y, Gigmes D, Marque SRA, Tordo P, Bertin D, Macromol Chem Phys 2006;207:1278.

43. Charleux B, Nicolas J, Guerret O, Macromolecules 2005;38:5485.

44. Nicolas J, Dire C, Mueller L, Belleney J, Charleux B, Marque SRA, Bertin D, Magnet S, Couvreur L, Macromolecules 2006;39:8274.

45. Nicolas J, Couvreur P, Charleux B, Macromolecules 2008;41:3758.

46. Nicolas J, Mueller L, Dire C, Matyjaszewski K, Charleux B, Macromolecules 2009;42:4470.

47. Chiefari J, Jeffery J, Mayadunne RRTA, Moad G, Rizzardo E and Thang SH, Macromolecules 1999;32:7700.

48. Roos SG, Müller AHE, Macmol Rapid Commun 2000;21:864.

49. Ahmad NM, Heatley F, Lovell PA, Macromolecules 1998; 31:2822.

50. Guillaneuf Y, Gigmes D, Junkers T, Macromolecules 2012;45:5371.

51. Benoit D, Grimaldi S, Robin S, Finet JP, Tordo P, Gnanou Y. J Am Chem Soc 2000;122:5929.

52. Becer CR, Paulus RM, Hoogenboom H, Schubert US, J Polym Sci Part A: Polym Chem 2006;44:6202.

53. Hlale L, Klumperman B, Macromolecules 2011;44:6683.

54. Chauvin F, Dufils P-E, Gigmes D, Guillaneuf Y, Marque SRA, Tordo P, et al. Macromolecules 2006;39:5238.

55. Tang C, Kowalewski T, Matyjaszewski K, Macromolecules 2003;36:1465.

56. Junker T and Banner-Kowollik C, J Polym Sci Part A:Polym Chem 2008;46:7585.

57. Ahmad NM, Charleux B, Farcet C, Ferguson CJ, Gaynor S et al. Macromol Rapid Commun 2009;30:2002.

58. Hlalele L, Klumperman B, Macromolecules 2011;44:5554.

59 Hlalele L, Klumperman B, Macromolecules 2011;44:7100.

60. Fercet C, Belleney J, Charleux B, Pirri R, Macromolecules 2002;35:4912.

61. Lin T, Li CL, Ho RM, Ho JC, Macromolecules 2010;43:3383.

62. Antonietti M, Wenz E, Bronstein L, Seregina M, Adv Mater 1995;7:1000.

4 Star Poly(4-vinylpyridine) architecture by Nitroxide Mediated Polymerisation

Abstract

This study produced multifunctional alkoxyamine 2-({tert-butyl [[1-(diethoxyphosphoryl)-2,2-dimethylpropyl]amino}oxy)-2-methylpropanoic acid (MAMA-SG1) initiators for the 'grafting-from' method to obtain star architecture of poly 4-vinylpyridine (P4VP) from JEFFAMINE® and second generation dendrimer polypropylenediamine (PPI). The structure of macroinitiators was confirmed by identifying the amide bond present in NMR and FTIR spectroscopy. Furthermore, the macroinitiators were used to polymerise 4VP. P4VP from JEFFAMINE-SG1 shows a monomodal peak in the SEC chromatogram, indicating more control polymerisation process than PPI-SG1.

4.1 Introduction

Nitroxide-mediated polymerisation (NMP) is a powerful tool for the synthesis of macromolecular architectures.[1,2] NMP is well-documented for the design of new initiators[3], kinetic investigation[4,5] and preparation of new materials[6]. Block[7,8,], graft[9] copolymer and star shaped copolymers[10-13] prepared from NMP indeed show good structural control producing polymers with narrow molar mass distribution at high conversion. The synthetic approaches to producing star polymers are classified by two methods which are "arm-first" methods and "core-first" methods. The "arm-first" method involves living macromonomers or macroinitiators which link together in the core with vinylic cross linker such as divinylbenzene (DVB).[14] On the other hand, the "core-first" methods employs multifunctional initiators that simultaneously initiate the polymerisation of monomers to form the arms of the star polymer.[10]

MAMA-SG1 is an alkoxyamine nitroxide for use with a wide range of monomer systems. It has a high dissociation rate constant and a terminal carboxylic acid group. This functional group can then be used for further modification or transformation processes to open new possibilities for complex molecules that are not accessible with TEMPO nitroxide.[15] In 2008, Vinas *et al*. reported the preparation of MAMA-SG1 bearing a *N*-succinimidyl ester group **(1)** (Scheme 4.1).[16] This alkoxyamine initiator can be attached to OH- and NH_2- functional groups, the later used as macroinitiator for block copolymer preparation.[16,17] Silica nanoparticles were also grafted with activated MAMA-SG1 **(1)** to polymerise styrene from the surface.[18]

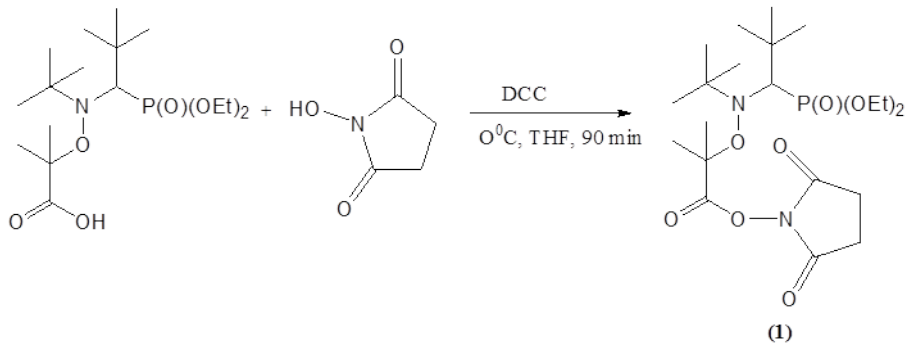

Scheme 4.1: Synthetic route to activated MAMA-SG1 with NHS.[16]

Star polymer production with MAMA-SG1 was explored by Dufils and his co-workers by intermolecular radical addition of alkoxyamine onto olefins.[19] They controllably synthesised 3- and 4-arms initiators and star polystyrene from this reaction, which exhibited dispersities not exceeding 2. Meanwhile, Robin *et al*. synthesised trifunctional alkoxyamine SG1 with 1,3.5-tris(2-hydroxyethyl)-1,3,5-triazine-2,4,6(1H,3H,5H)-trione.[20] Furthermore,well-defined star polymers of n-butyl acrylate (*n*BuA), styrene (S) and block copolymers poly(BuA-*b*-PS) were reported as products from this trialkoxyamine initiator.[20]

In this chapter, star macroinitiator with SG1 such that it contains an end functionality has been synthesised. The first approach is using polyetheramine JEFFAMINE® T-403 grafted with NHS activated MAMA-SG1. The second propose macroinitiator with 8 arms was obtained by coupling a second generation dendrimer polypropyleneimine (PPI) with MAMA-SG1. Then, P4VP was prepared by core first method. The chemical structure were characterised with FTIR and ^{1}H NMR.

4.2 Experimental

4.2.1 Materials

All solvents employed were HPLC grade or better and used directly as received unless otherwise stated. Methyl methacrylate, MMA (Aldrich, 99%) and 4-vinylpyridine, 4VP (Aldrich, 95%) were distilled from calcium hydride before used. 2-({tert-butyl [[1-(diethoxyphosphoryl)-2,2-dimethylpropyl]amino}oxy)-2-methylpropanoic acid (MAMA-SG1) and JEFFAMINE® T-403 were kindly gifted of TU/e, Eindhoven and HUNSTMAN, UK respectively. PPI (polypropylene imine) dendrimers, generations 2, were purchased from SyMO-Chem BV (The Netherlands). 2-(1H-benzotriazol-1-yl)-1,1,3,3-tetramethyluronium hexafluorophosphate (HBTU) and *N*,*N*-Diisopropylethylamine (DIPEA) were purchased from Sigma-Aldrich.

4.2.2 Synthesis of activated alkoxyamine, 2-methyl-2-[N-tert-butyl-N-(1-diethoxyphosphoryl-2,2-dimethylpropyl) aminoxy]-N-propionyloxysuccinimide (MAMA-NHS (1))

This compound was synthesised following a literature procedure.[16] MAMA-SG1 (0.5 g, 1.31 mmol) and *N*-hydroxysuccinimide (NHS) (0.18 g, 1.57 mmol) were dissolved in 2 mL THF and deoxygenated by nitrogen bubbling for 15 minutes. Then, a degassed solution of 0.3 g *N,N'*-dicyclohexylcarbodiimide (DCC) in 0.5 mL THF was added. After stirring at 0 °C for 1.5 hours, the precipitated *N,N'*-dicyclohexylurea (DCU) was removed by filtration and washed with a minimum of cool THF. The filtrate volume was reduced under vacuum to one third and kept at -20 °C for 2 hours in order to precipitate the residual DCU. After filtration, the precipitation was performed in pentane. The obtained solid was further washed with water to remove NHS and dried under vacuum. The alkoxyamine was obtained as a white powder.

^{1}H NMR (400 MHz, $CDCl_3$) (ppm): 1.17–1.33 (m, 24H), 1.82 (s, 3H), 1.88 (s, 3H), 2.82 (s, 4H), 3.31 (d, 1H), 3.95–4.35 (m, 4H). Mixture with DCU 2.00-1.15 (m, 8H). ^{31}P NMR (400 MHz, $CDCl_3$) (ppm): 24.89. Yield: 200mg (0.40 mmol).

4.2.3 Synthesis of P4VP from JEFFAMINE functionalise MAMA-SG1

Activated alkoxyamine **(1)** (24 mg, 0.05 mmol) and JEFFAMINE® T-403 (20 mg, 0.045 mmol) were added to a Schenk flask and degassed for 15 minutes by nitrogen bubbling. Then, degassed 0.05 mmol DCC in 2 mL DMF was added and stirred at room temperature for 3 days. The precipitated DCU was removed by filtration. Then, the filtrate solution was precipitated in pentane and dried in vacuum oven overnight. The end product was obtained as a yellow sticky material, grafted JEFFAMINE **(2)**.

^{1}H NMR (400 MHz, $CDCl_3$) (ppm): 0.85 (s, **CH_3**-CH_2- from JEFFAMINE), 1.01-1.36 (m, -**CH_3** from MAMA-SG1), 1.57-1.86 (m, **CH_3**-C-C(O)), 2.61 (m, -N-**CH**-P from MAMA-SG1), 3.3-4.12 (m, -**CH_2**- from JEFFAMINE and MAMA-SG1), 8.14 (s, **NH**(CO)) .

Grafted JEFFAMINE **(2)** (30 mg; 0.02 mmol) and 4VP (1.21 g, 11.5 mmol) was added to a Schlenk flask and immersed in a pre-heated oil bath at 110 °C for 24 hours. The reaction was quenched by cooling the mixture in an ice-water bath and the polymer was precipitated in diethyl ether and allowed to dry in a vacuum oven overnight. Solid white polymer was obtained. Yield: 500 mg; M_n: 119000 g/mol; D: 1.4

4.2.4 Synthesis P4VP from MAMA-SG1 functional PPI

A solution of MAMA-SG1 (0.13 g, $3.3x10^{-4}$ mol), HBTU (0.14g, $3.6x10^{-4}$ mol) and DIPEA (0.05g, $3.6x10^{-4}$ mol) were mixed in DMF (2 mL). The solution was left to pre-activate for 20 minutes before added to the dendrimer, PPI (0.03 g, $4.1x10^{-5}$ mol) under N_2 atmosphere. After 3 days stirring at room temperature, the mixture was diluted with ethyl acetate before washing with 50% v/v with water and brine. Then, the organic phase was dried with ($MgSO_4$), filter and concentrate under vacuum pressure.

^{1}H NMR ($CDCl_3$), δ ppm: 1.03-1.38 (-**CH_3** from MAMA-SG1), 1.54 (O-C(**CH_3**)-CO from MAMA-SG1), 1.68 (–CH_2-**CH_2**-CH_2- from PPI), 2.42 (-**CH_2**-N- from PPI), 3.00 (-**CH_2**-NH(CO) from PPI), 3.34 (-N-**C**H-P from MAMA-SG1), 4.0-4.20 (m, from MAMA-SG1), 8.35 (-**NH**(CO))

A mixture of 4VP (0.9 g, $6.5x10^{-5}$ mol), PPI-SG1 (0.03 g, $8.2x10^{-6}$ mol) and DMF (0.7 mL) was poured into a Schlenk and degassed with N_2 bubbling for 20 minutes and then immersed in pre-heated oil bath at 110 °C for 5 hours. Polymerisation was stopped by quenching the flask in an ice bath. The polymer solution was precipitated in diethyl ether and dried in vacuum oven at 40 °C until constant weight obtained. Yield: 600 mg; M_n: 343000 g/mol; D: 1.7

4.2.5 Characterisation methods

^{1}H NMR analyses were performed in $CDCl_3$ solution, at 25 °C using a Bruker Avance 400 (400 MHz) spectrometer. The chemical shift was calibrated using the solvent peak (δ = 7.26 ppm). Fourier Transform InfraRed (FTIR) spectroscopy was carried out in the solid state on a Perkin Elmer Spectrum 100. SEC analysis using DMF (0.1 M LiBr) as eluent (elution rate: 1 min/mL) was performed using two PSS GRAM analytical (300 and 100 Å, 10 l) columns on an Agilent 1200 series apparatus equipped with a Wyatt

Optilab rEX refractive index detector thermostat at 40 °C and a Wyatt DAWN HELEOS-II multi angle light scattering (MALS) detector. Molecular weights and D were calculated from the MALS signal using the ASTRA software (Wyatt) and a dn/dc value of 0.225 mL/g (P4VP) [21] in DMF. Before analysis, samples were filtered through a 0.45 μm PTFE filter (13 mm, PP housing, Whatman).

4.3 Results and discussion

4.3.1 Star polymerisation of 4-vinylpyridine (sP(4VP)$_3$) from JEFFAMINE®-SG1

The synthesis of sP(4VP)$_3$ was carried out according to Scheme 4.2. It involves (1) functionalisation of MAMA-SG1 with NHS, (2) Grafting the activated alkoxyamine (MAMA-NHS) to JEFFAMINE® and (3) polymerisation.

For MAMA-NHS **(1)**, the reaction of MAMA-SG1 with NHS in the present of *N,N'*-dicyclohexylcarbodiimide (DCC) was carried out at 0 °C in THF for 1.5 hours. Then, the product was precipitated in pentane as a white powder. ^{1}H NMR confirmed the structure of MAMA-NHS with the peaks of the methyl (**b**, **c**, **e**, **g**), methylene (3.95-4.35 ppm) and –CH (3.31 ppm) from MAMA-SG1 as well as the methylene of the succinimidyl ester appearing at 2.82 ppm (Figure 4.1a). In addition, the carbonyl band in FTIR spectra shifted from the free acid MAMA-SG1 at 1718 cm^{-1} to the NHS ester 1741 cm^{-1}. The succinimidyl C=O group appears at 1816 and 1781 cm^{-1} (Figure 4.2a). Then, the activated alkoxyamine was grafted to JEFFAMINE® at room temperature in DMF to form star initiator **(2)** as a yellow sticky material. The ^{1}H NMR spectrum shows characteristic peaks of both the JEFFAMINE® bands (0.85 ppm for free –CH_3, 3.20 – 4.20 ppm for CH and CH_2) and the SG1 (**h**, **i**, **k**, **m** for -CH_3 groups). Moreover, the amide linker can be identified in the spectrum at 8.14 ppm (Figure 4.1b). The FTIR spectrum in Figure 4.2b shows the new band at 1625 and 1572 cm^{-1} assigned to the amide bond (-CONH-) *i.e.* the C=O stretching and N-H bending vibration band.

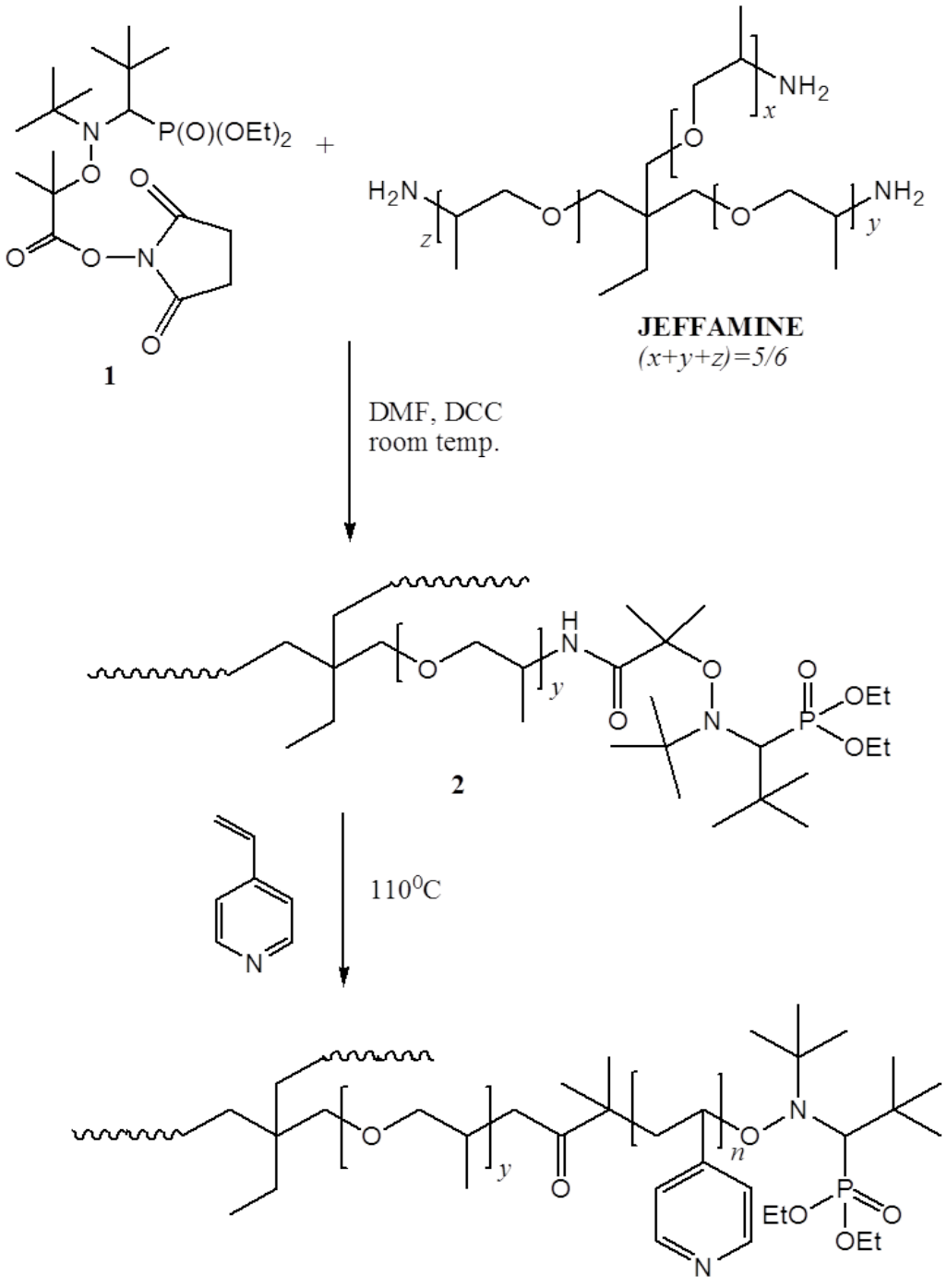

Scheme 4.2: Schematic route of star poly 4-vinylpyridine with JEFFAMINE®.

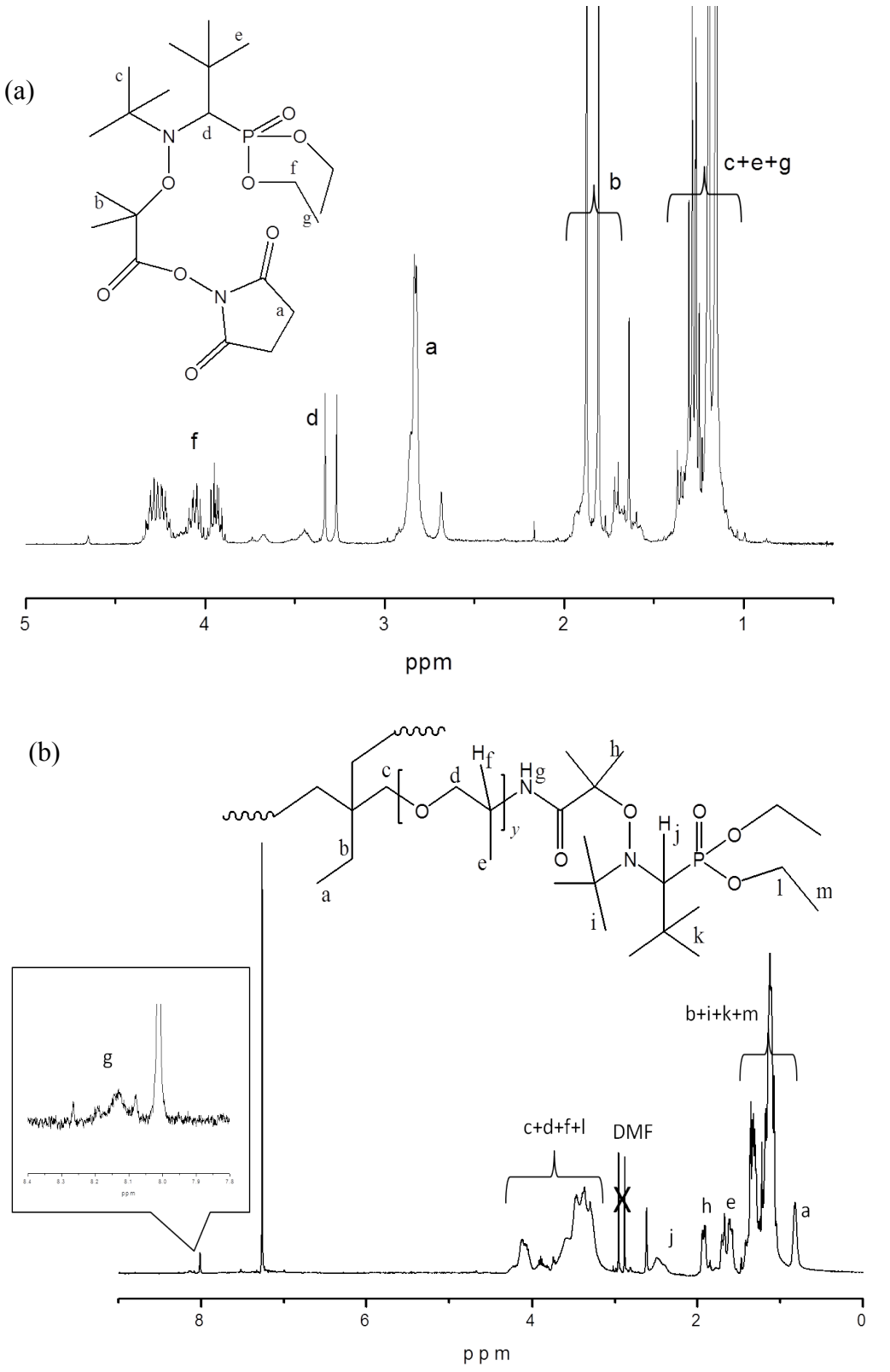

Figure 4.1: ^{1}H NMR of activated alkoxyamine MAMA-NHS (a) and JEFFAMINE® functionalised with NHS-alkoxyamine (b).

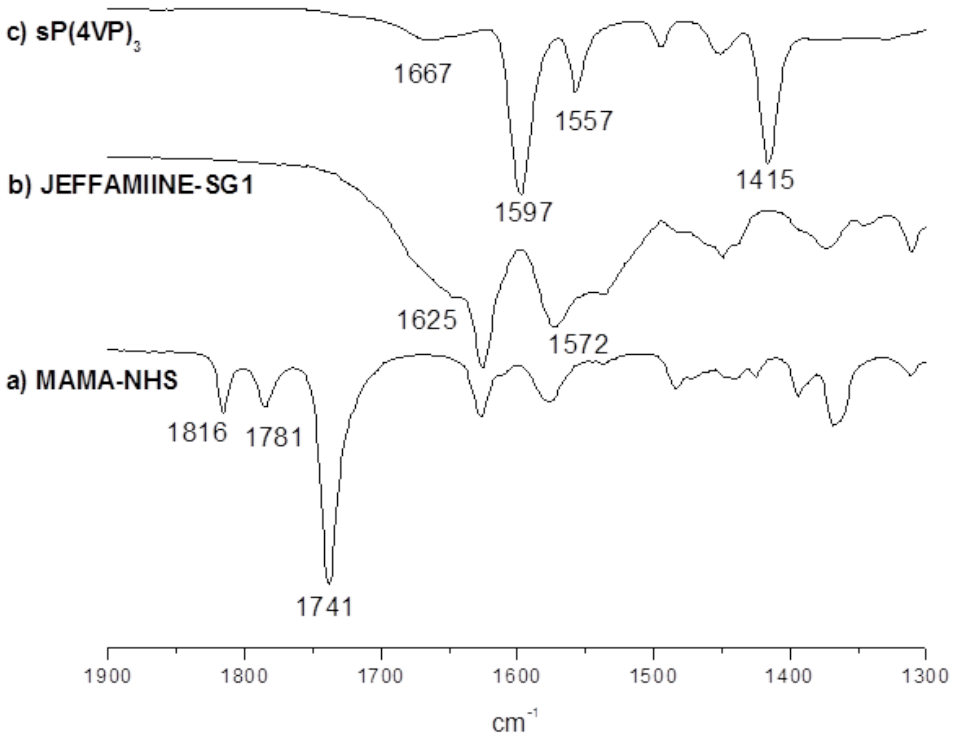

Figure 4.2: FTIR spectrum of (a) activated alkoxyamine, MAMA-NHS (1816, 1781, 1741 cm^{-1}); (b) JEFFAMINE® functionalise SG-1 (1625,1592 cm^{-1}) (c) star polymer 4-vinylpyridine, $sP(4VP)_3$ (1667,1597, 1556 cm^{-1}).

P4VP with the functionalised JEFFAMINE®-SG1 macroinitiator **(2)** was synthesised at 110 °C yielding white polymer product at 98% conversion. Figure 4.2c shows the position of the amide bond in $sP(4VP)_3$ shifted from 1625 to 1666 cm^{-1} with the presence of P4VP bands at 1597, 1557 and 1451 cm^{-1}. A molecular weight of 170000 g/mol, M_w, measured by SEC equipped with a MALS detector was obatiend compare to the M_n theoretical of 106000 g/mol (Figure 4.3). The SEC chromatogram shows a monomodal peak with a dispersity of 1.4. Termination reaction are never inhibit during NMP leading to disproportionation and combination reactions between radicals. According to Vinas *et al*., the dissociation rate constant (k_{d1}) of C-ON bond homolysis in **(1)** is 5 s^{-1} (E_a = 103 kJ mol^{-1}) which is 15 times higher than MAMA-SG1 (k_{d1} = 0.32s^{-1}, E_a = 112 kJ mol^{-1}).[16,22] The higher k_{d1} value can be ascribe to a long-range polar effect of NHS moiety in the activated MAMA-NHS. A summary of the experiments is provided in Table 4.1.

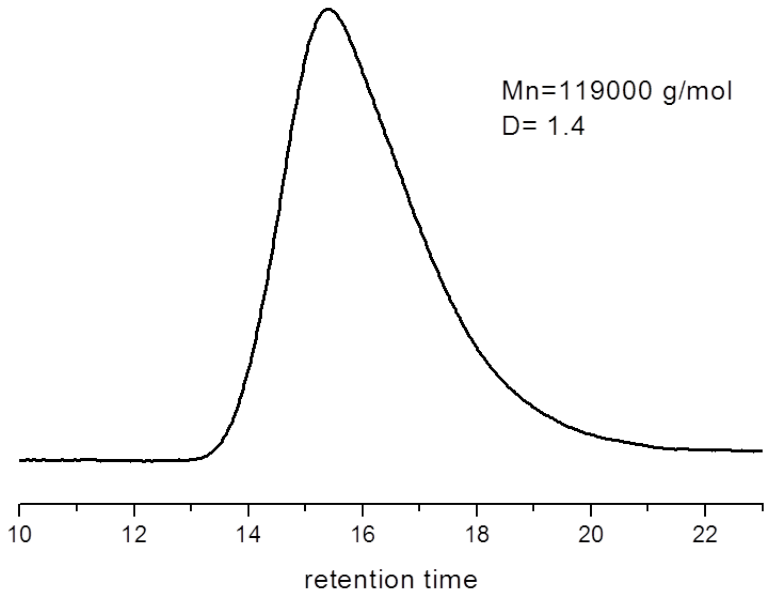

Figure 4.3: SEC traces (RI signals) of $P(4VP)_3$ with JEFFAMINE® star initiator at a ratio $[M]_0/[I]_0$=370.

Table 4.1: Experimental results of star polymerisation of 4-vinylpyridine.

Entry	Time (min)	Conv. [a] (%)	$M_{n\ theo}$ [b] (g/mol)	$M_{n\ SEC}$ [c] (g/mol)	$M_{w\ MALLS}$ [c] (g/mol)	D [c]
$sP(4VP)_3$ [d]	300	98	106000	119000	170000	1.4
$S(P4VP)_8$ [e]	300	98	210000	343000	602000	1.7

[(a)]Conversion calculated by ^{1}H NMR through integration of CH_2 peaks of 4VP (5.94 and 5.46 ppm) and P4VP (2.10-1.41 ppm). [(b)]$M_{n\ theo}$ = (conversion x $[M]_0/[I]_0$ x *M*monomer) + M_n macroinitiator. [(c)]Measured by DMF GPC with multi angle light scattering detector (MALS). [(d)]Experimental condition: $[I]_0/[4VP]_0$ = 1/370 per arms. [e] Experimental condition: $[I]_0/[4VP]_0$ = 1/150 per arms.

4.3.2 Star polymerisation of poly 4-vinylpyridine, $sP(4VP)_8$ from polypropyleneimine dendrimer (PPI-SG1)

Polypropyleneimine (PPI) was functionalised with MAMA-SG1 using HBTU and DIPEA at room temperature. The structure was confirmed by the presence of amide peak at 8.40 ppm and methylene group attached to the nitrogen atom of PPI at 2.42 ppm in ^{1}H NMR spectra. The peak of SG1 is present at 4.25-4.05 (methylene, **n**), 3.34 (-CH, **m**) and 1.03-1.38 (methyl, **k, l** and **o**) ppm (Figure 4.4). Moreover, the presence of the amide linker is confirmed by a broad band N-H stretch at 3283 cm^{-1} compare to two bands for primary PPI (3280 cm^{-1}) in FTIR. A new band of C=O ester and N-H for amide bond appeared at 1656 and 1526 cm^{-1}, respectively, as shown in Figure 4.5.

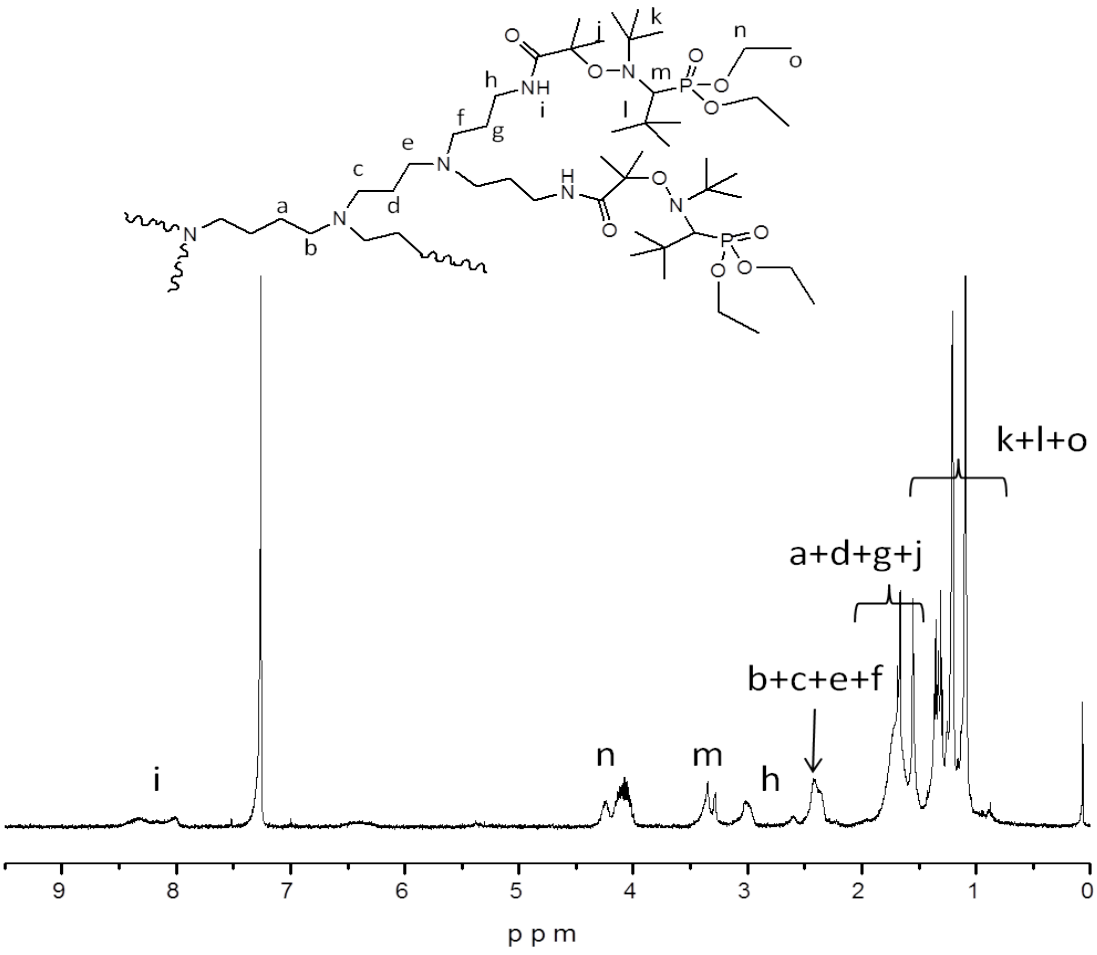

Figure 4.4: ^{1}H NMR of polypropyleneimine functionalised with alkoxyamine (PPI-SG1).

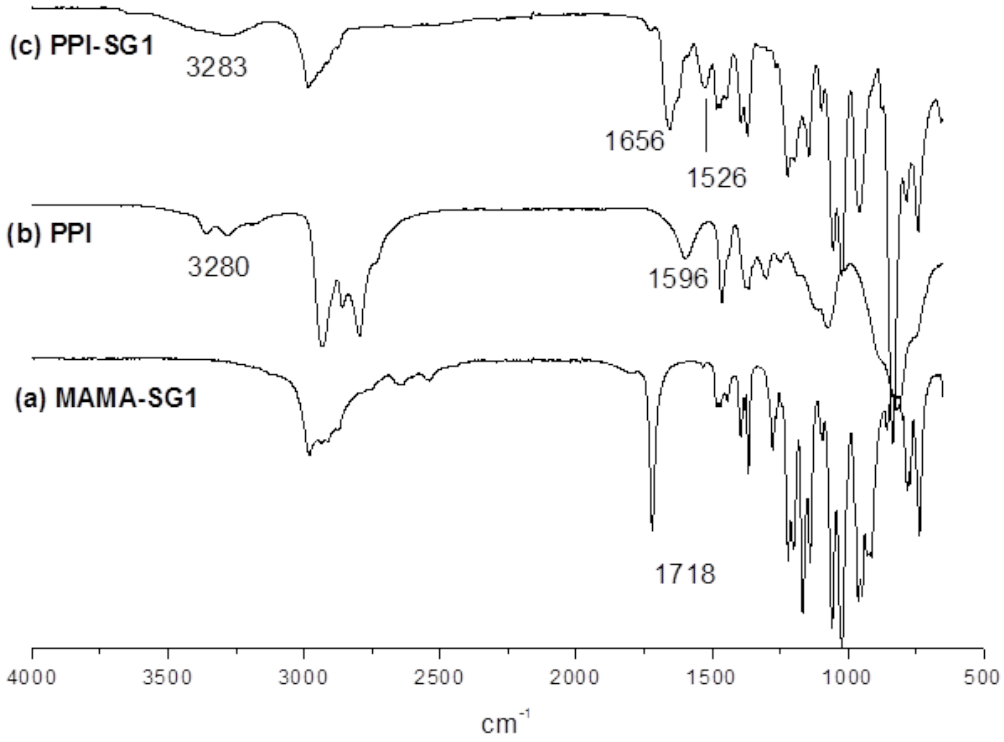

Figure 4.5: FTIR spectrum of (a) MAMA-SG1; (b) dendrimer polypropyleneimine, PPI; (c) functionalise PPI with SG1 macroinitiator, PPI-SG1.

Polymerisation of 4VP with PPI-SG1 was carried out at 110 °C in DMF solution (Scheme 4.3). The polymerisation kinetics of 4VP was followed by ^{1}H NMR and it shows nearly linear growth with time with a deviation from linearity only at longer reactions time (higher conversion) (Figure 4.6). The SEC chromatogram in Figure 4.6Figure 4.7 shows a clearly shifted peak from the initiator, PPI-SG1 at low molar mass side to high molar mass side of sP(4VP)$_8$. However, the polymerisation shows only moderate control with a broad dispersity of 1.7. Moreover the molecular weight measured by SEC, M_w (602000 g/mol) is much higher than theoretical value, M_n (210000 g/mol) noted in Table 4.1 . Besides that, a broad tailing at the low molar mass side of the chromatogram was obtained probably due to autopolymerisation of 4VP at high temperature. Baumann and Schmidt observed that the rate of autopolymerisation of 4VP is in order 11%/h at 125 °C.[23]

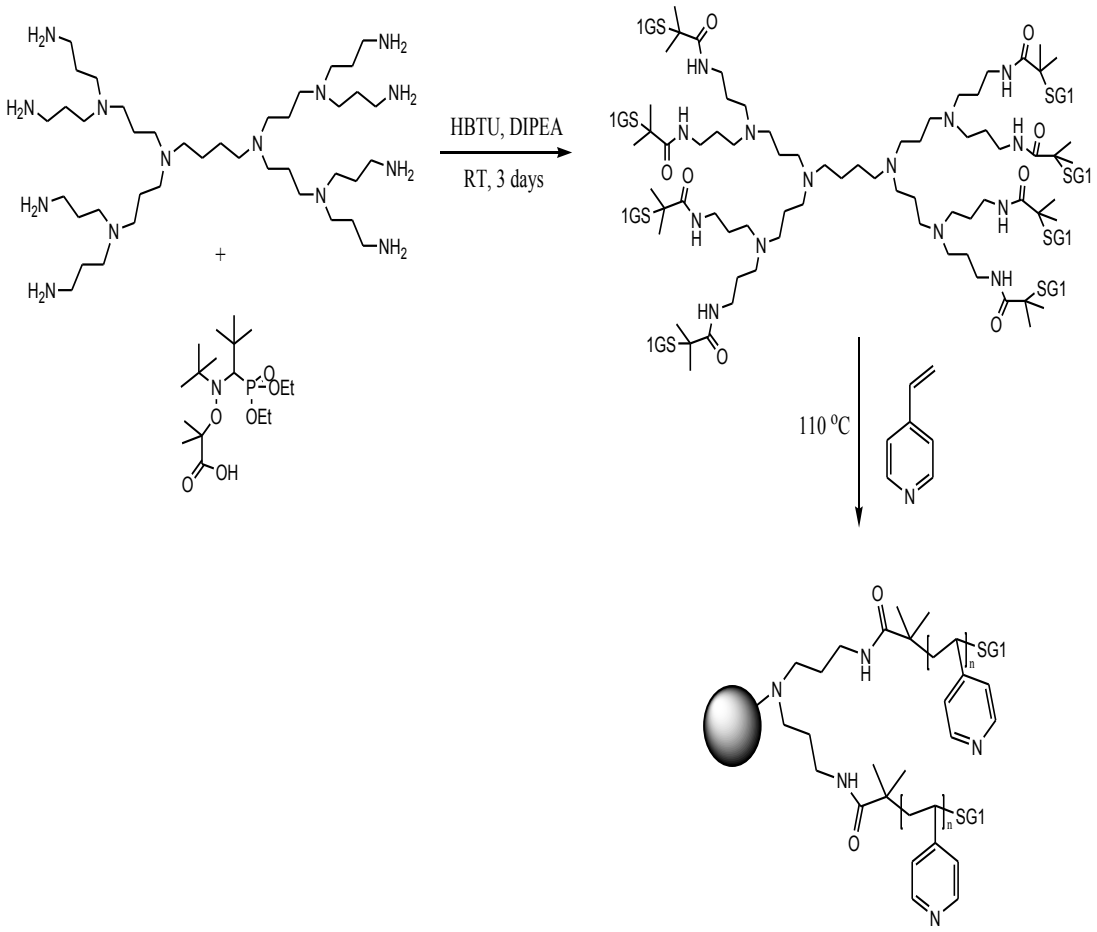

Scheme 4.3: Schematic route of star poly 4-vinylpyridine with PPI-SG1 macroinitiator.

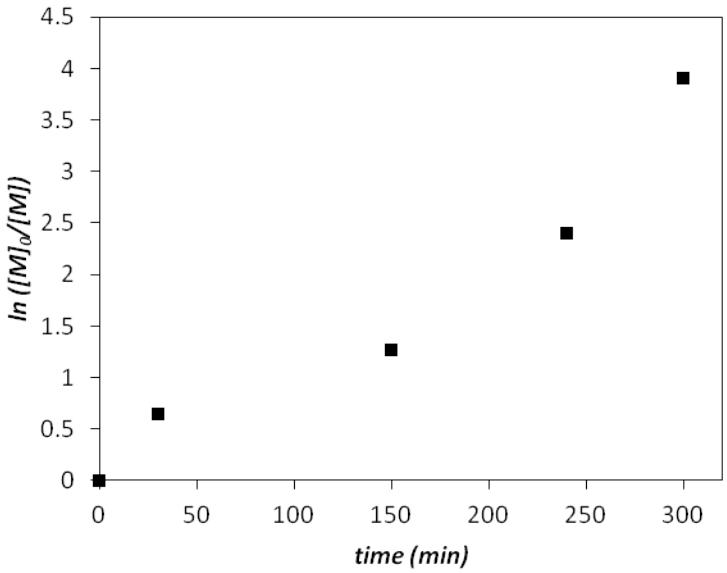

Figure 4.6: Semilogarithmic plots of conversion ln ($[M]_0/[M]$) versus time of 4-vinylpyridine by PPI-SG1 macroinitiator.

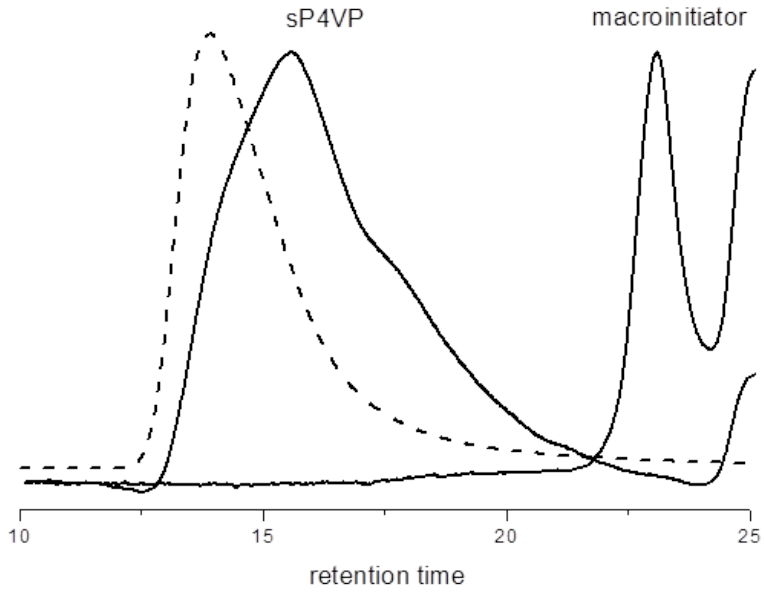

Figure 4.7: SEC chromatogram of sP(4VP)$_8$ initiate by PPI-SG1detected by RI detector. (Dotted line in LS detector as comparison).

4.4 Conclusion

Multifunctional initiators core molecules were synthesised from JEFFAMINE® and PPI to obtain 3- and 4- arms for the polymerisation of 4VP. This structure of the alkoxyamines was confirmd spectroscopically. s(P4VP)$_3$ and s(P4VP)$_8$ were synthesised from the macroinitiator with high molecular weight (~10^5 g/mol). However, low molecular weight products were obtained in both polymerisation either due to autopolymerisation or termination reactions at the early stage of the polymerisation. Further investigation to control the rate of polymerisation and to synthesise well-defined polymer will be necessary to optimise this procedure.

References

1. Hadjichristidis N, Iatrou H, Pitsikalis M, Mays J, Prog Polym Sci 2006;31:1068.

2. Nicolas J, Guillaneuf Y, Lefay C, Bertin D, Gigmes D, Charleux B, Prog Polym Sci 2012;38:63 .

3. Benoit D, Chaplinski V, Braslau R, Hawker CJ, J Am Chem Soc 1999;121:3904.

4. Gigmes D, Bertin D, Lefay C, Guillaneuf Y, Macromol Theory Simul 2009;18:402.

5. Bertin D, Gigmes D, Marque SRA, Tordo, Chem Soc Rev 2011;40:2189.

6. Hawker CJ, Bosman AW, Harth E, Chem Rev 2001;101:3661.

7. Rahim NA, Audouin F, Twaley B, Vos JG, Heise A, Eur Polym J 2012;48:990.

8. Benoit D, Harth E, Fox P, Waymouth RM, Hawker CJ, Macromolecules 2000;33:363.

9. Flakus S and Schmidt-Naake, G. Macromol Symp 2009;43:275.

10. Miura Y and Yoshida Y, Polymer 2002;34:748.

11. Abraham S, Choi JH, Ha CS, Kim I, J Polym Sci Part A: Polym Chem 2007;45:5559.

12. Lu CH, Wang JH, Chang FC, Kuo SW, Macromol Chem Phys 2010;211:1339.

13. Li J, Zhang Z, Zhu X, Zhu J, Cheng Z, e-Polymers 2010;145:1.

14. Tsoukatos T, Pispas S, and Hadjichristidis N, J Polym Sci Part A: Polym. Chem 2001;39:320.

15. Diaz T, Fischer A, Jonquières A, Brembilla A, Lonchon P, Macromolecules 2003;36:2235.

16. Vinas J, Chagneu N, Gigmes D, Trimaille T, Favier A, Bertin D, Polymer 2008;49:3639.

17. Habraken GJM, Peeters M, Thornton PD, Koning CE, Heise A, Biomacromolecules 2011;12:3761.

18. Chevigny C, Gigmes D, Bertin D, Jestin J, Boué F, Soft Matter 2009;5:3741.

19. Dufils PE, Chagneux N, Gigmes D, Trimaille T, Marque SRA, Bertin D, Tordo P, Polymer 2007; 48:5219.

20. Robin S, Guerret O, Couturier JL, Gnanou Y, Macromolecules 2002; 35:2481

21. Convertine AJ, Sumerlin BS, Thomas DB, Lowe AB, McCormick CL, Macromolecules 2003; 36:4679.

22. Ananchenko G, Beaudoin E, Bertin D, Gigmes D, Lagarde P, Marque SRA, Revalor E, Tordo P, J Phys Org Chem 2006;19:269.

23. Baumann M, Schmidt-Naake G, Macromol Chem Phys 2000;201:2751

5 Investigation of Electrocatalytic Hydrogen Generation by Carbon Electrodes Modified with P4VP/$CoPcF_{16}$ Layers

Abstract

Electrochemical hydrogen generation is catalysed by cobalt(II) hexadecafluorophthalocyanine ($CoPcF_{16}$) incorporated in poly(4-vinylpyridine) (P4VP) or poly(4-vinylpyridine-b-methyl methacrylate) (P(4VP-b-MMA)) films coated on glassy carbon electrodes. The P4VP/$CoPcF_{16}$ layers show reduced overpotential for hydrogen production with respect to bare electrodes. The turnover number (TN) and current density (J) of the P4VP/$CoPcF_{16}$ complex for H_2 evolution depend on the concentration of $CoPcF_{16}$ and molecular weight of P4VP. The highest TN and J were obtained with P4VP-2/$CoPcF_{16}$ at low Co concentration (6 μM) at -1.2 V values of $8x10^5$ h^{-1} and 16 mA/cm^2 were obtained respectively with a Faradaic efficiency of 33%. The potential of coordination of $CoPcF_{16}$ to the P4VP backbone and aggregation was studied by electronic spectroscopy.

5.1 Introduction

The expected human population rise to 9 billion in 2015 demands a high increase in energy production to meet its need of this number of people. Consequently, it has been estimated that, world energy consumption will increase by 53% from 505 quadrillion British thermal unit (Btu) needed in 2008 to 770 quadrillion Btu by 2035. Currently, renewable energy only generates electricity at 3.1% per year of the overall need, while coal remains the primary sources of electricity (Figure 5.1).[1] In addition, our world's largest energy source, oil, may be depleted by the middle of the 21st century.[2,3] Importantly combustion of fossil fuels releases carbon dioxide (CO_2) which is playing a significant role in climate change. The concentration of CO_2 increased to 390 ppm (or 39%) above pre-industrial levels by the end of 2010, as a result with global temperatures expected to rise by 6 °C at the end of the 21st century.[4] Therefore, new environmentally friendly renewable energy sources are required to replace fossil fuels such as wind, solar, hydro and biomass generated energy.[1,3]

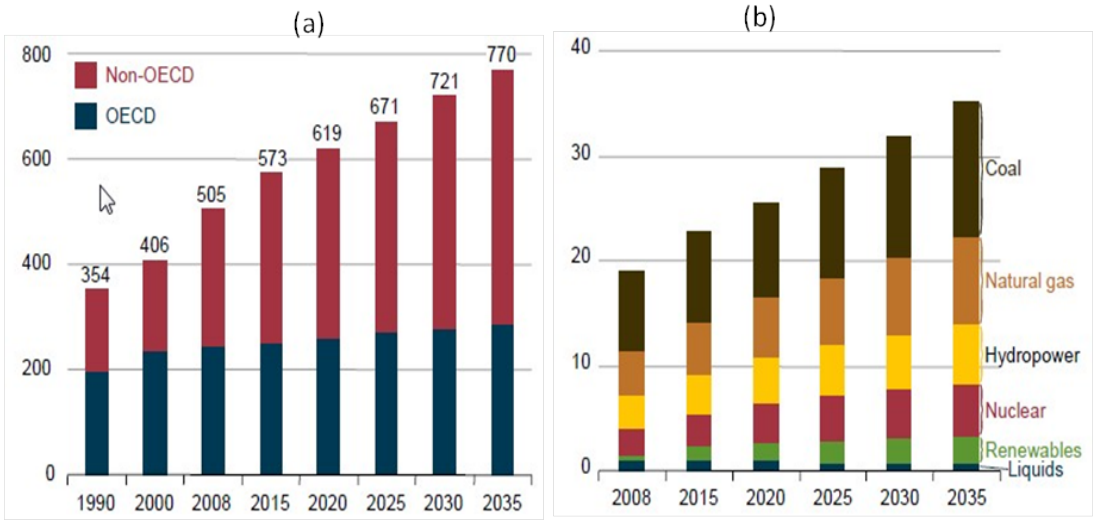

Figure 5.1: (a) World energy consumption, 1990 - 2035 (quadrillion Btu), (b) World net electricity generation by fuel type, 2008-2035 (trillion kilowatt hours).[1]

Solar energy is a promising energy source for the future due to the unlimited solar energy available in day time, even though it depends on the region and the weather. Recently systems that mimick the natural photosynthesis have been investigated where a metal centred complex adsorbs sunlight energy and subsequently transfers an electron

to a catalyst. These process have been used to the generate of solar fuels, such as of the hydrogen, or the reduction of carbon dioxide to hydrocarbon liquids through thermochemical or electrochemical pathways.[5-7] For thermal use of solar energy, temperatures greater than 1200 °C are required to produce hydrogen (H_2) from water and CO from CO_2. This results in problems such as low productivity, high production cost and material instability. However, water electrolysis can produce H_2 at the cathode directly in solution at lower temperatures. But, the storage and transportation of H_2 are the critical issues and are linked to its physical and chemical properties. H_2 is a very volatile gas which is need to be compresses at high pressure (350-370 bar) or liquefied by cryonic temperature (-253 °C) to have a viable volumetric energy density. **Error! Reference source not found.** shows the role of renewable technologies in energy production.

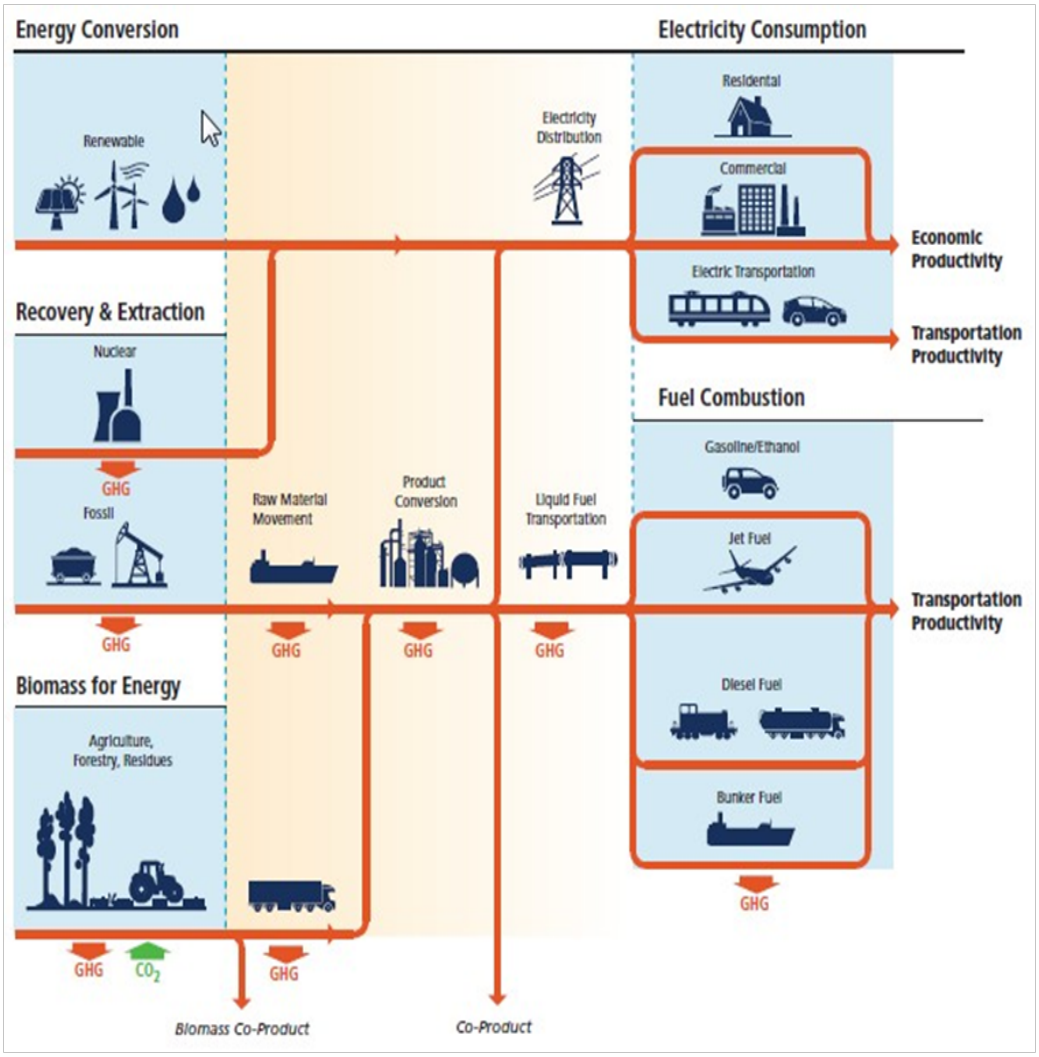

Figure 5.2: Illustration of the different systems for energy production showing the role of renewable energy along with other energy production options.[4]

Electrolysis is a well-establish method of water splitting whereby a direct current is applied to water to separate it into hydrogen and oxygen. Since water covers 71% of the earth's surface, water electrolysis may be a promising method of supplying part of the world's energy and reducing the impact of climate change. Importantly the level of CO_2 in the atmosphere has increased of late as a result of ever increasing industrial operation and as a by-product of the burning of fossil fuels. Thus, research on water electrolysis as a sustainable, carbon neutral energy production in the form of hydrogen is expanding.[6-79] The process of splitting water to provide hydrogen is environmentally "clean" with no carbon by-products. Therefore, hydrogen is a promising energy carrier for use either in homes, transport or industry. The on-site generation and consumption of hydrogen at oil refineries or in vehicles is a promising step in the efforts to relieve the storage and transportation issues of H_2 drawbacks.[10]

For electrocatalytic CO_2 reduction, the major problem is the low solubility of the gas in water at standard temperature and pressure and this must be increased to accelerate the reaction rate.[6] Theoretically, conversion of CO_2 involves multiple electron, proton transfer processes resulting in the formation of a variety of hydrocarbon products. Formic acid, methanol and oxalic acid are often the main products of electrolysis in aqueous solution.[11] The electrode material has a major role in determining the products and selectivity. For example, reduction of CO_2 by a copper electrode in aqueous electrolyte favoured to produce methane, ethylene, formate and formic acid.[11] While, hydrogen evolution is more favourable than hydrocarbon generation in the case of Pt, Ni, Ti, Co, Rh, Ir and Fe electrodes due to their low hydrogen overpotential and strong CO adsorption characteristics.[7] The choice of electrode is crucial and can be costly. Therefore, an alternative approach in the use of a transition metal catalyst at room temperature is needed and this approach is explored in this chapter.

Research into the development of metallophthalocyanine (MPc) complexes based on abundant transition metals has greatly increased of late due to their attractive features including a rich redox behaviour, the potential to bind with metals or non-metals in the central cavity. They can also easily modified by substitution of the ring and importantly

their chemically stability.[12,13] Hence, MPcs are used in many applications from dyes in the paper/textile industries, photoconductors in photocopy machines,[14] environmental sensors for heavy metals,[15,16] organic solar cells,[5,6] through to catalysts for water splitting to produce hydrogen.[17-19] In the electrochemical area, MPcs and other similar compounds are utilised as potential catalyst for many reactions.[20,21] Artero *et al.* reviewed the potential of electrodes modified with complexes such as cobaloximes, diimine-dioximes, porphyrins and phthalocyanines in electrocatalytic and photocatalytic water splitting systems. In particular, Co complexes are receiving great interest due to their efficient catalytic activity such as low overpotentials and higher turnover numbers. This type of activity is dependent on their molecular structure, the electrode material and experimental conditions.[19]

Recently, several workers reported the synthesis and electrocatalytic activity for hydrogen generation of phthalocyanines.[22-25] As an electron-withdrawing group, fluorines are known to enhance the solubility of phthalocyanine in polar, aprotic organic solvents.[25] The electrochemical properties of the Pc type compounds are also dependent on the number and position of electron-withdrawing groups and the nature of the electrolyte/solvent.[23,24] For example, Koca *et al*. reported that MPc with tetra-pentafluorobenzyloxy substituents shifted the onset of the electrocatalytic process to more positive potentials when comparing to phenoxy substituted MPc compounds.[22]

Various methods were applied in the preparation of MPc modified electrodes: 1) direct deposition with drop casting methods or soaking the electrode in a MPc solution,[26,27] 2) mixing of MPc with carbon paste to make MPc conductive cement,[28] 3) electropolymerisation [26]. The first method is the simplest procedure and forms a thin layer film. This approach uses minimal amount of catalyst and it is easy to remove the layer from the surface. Polymer matrices can enhance the immobilisation of catalysts onto a surface. Poly 4-vinylpyridine (P4VP) and Nafion® are commercially available polymers that are used to immobilise the catalyst. Kaneko has reported that the use of a polymer may improve catalytic activity by binding of the MPc to the polymer backbone. However, diffusion/permeation of reactants such as H^+ or CO_2 from solution to the active site may be inhibited by the presence of a polymer layer.[2] For examples, P4VP can bind the catalyst *via* the nitrogen in pyridine ring.

In this chapter, the potential of cobalt(II) hexadecafluorophthalocyanine ($CoPcF_{16}$) as a electrocatalysts for hydrogen in combination with P4VP is investigated. It has been reported that P4VP-co-Styrene can be used as polymer support for other CoPc derivatives.[17,27,29] From a survey of the literature, there does not appear to be any investigation about the use of this catalyst for hydrogen evolution. The details of P4VP/$CoPcF_{16}$ concerning the aggregation, cyclic voltammetry and catalytic activity are reported. In addition, the potential of P4VP as a catalyst for reduction of CO_2 in aqueous solution is also investigated.

5.2 Experimental

5.2.1 Materials

All solvents employed were HPLC grade or better and used directly as received unless otherwise stated. Cobalt(II) hexadecafluorophthalocyanine ($CoPcF_{16}$) and poly 4-vinylpyridine 160,000 g/mol (**P4VP-2**) were purchased from Aldrich and Merck, respectively. Poly 4-vinylpyridine (5,000 g/mol (**P4VP-1**) and poly (4-vinylpyridine-*b*-methyl methacrylate) (**P4VP-3**) were synthesised by NMP and ATRP as reported in Chapter 3 and Chapter 2, respectively.

5.2.2 UV/Vis spectroscopy

3.0 x 10^{-5} mol/L $CoPcF_{16}$ and 4.5 x 10^{-5} mol/L **P4VP-1** Mw 5,000 g/mol or 4.5 x 10^{-5} mol/L **P4VP-2** (M_w=160,000 g/mol) or **P4VP-3** were prepared in dimethylformamide (DMF) solution. For the aggregation studies, these two solutions were mixed at different ratios to a total volume 5 mL. The ratio and resulting concentration for $CoPcF_{16}$ and P4VP are listed in Table 5.1.

Table 5.1: Concentration and selected electronic data of P4VP/$CoPcF_{16}$ solvent mixtures at different ratios.

4.5 x 10^{-5} M P4VP-2 (mL)	**3.0 x 10^{-5} M $CoPcF_{16}$ (mL)**	**Concentration P4VP (x10^{-5} M)[a]**	**Concentration $CoPcF_{16}$ (x10^{-5} M)[a]**	**Q λ_{max} (nm)**	**Absorbance**
0	5	0	3.0	628	1.71
1	4	0.9	2.4	705	1.37
2	3	1.8	1.8	717	1.59
3	2	2.7	1.2	727	1.35
4	1	3.6	0.6	730	0.56

[a] Concentration after mixing the solution was calculated using equation $M_1V_1 = M_2V_2$; where M_1 =stock concentration of P4VP or $CoPcF_{16}$, V_1 =volume of P4VP or $CoPcF_{16}$ taken from stock solution, M_2 =new concentration, V_2 =total volume after mixed the solution.

5.2.3 Electrode preparation

These different polymer were used in the experiments. The polymers were dissolved in 25 mL DMF to prepare different concentrations as listed in the Table 5.2.:

a) P4VP 0.5% w/w (Mw= 5,000 g/mol, 4VP units per mol=50) called as **P4VP-1**
b) P4VP 0.75% w/w (Mw=160,000g/mol, 4VP units per mol=1500) called as **P4VP-2**
c) P(4VP-b-MMA) 0.5% w/w (Mw=54 000 g/mol, composition=10% MMA and 90% 4VP, 4VP units per mol=170) called as **P4VP-3**

For the preparation of the various P4VP/$CoPcF_{16}$ mixtures, $CoPcF_{16}$ was added to the polymer solution in different ratios for total volume 5 mL as shown in Table 5.1. The actual concentrations of the components in the final solution are given in Table 5.1 and Table 5.2. Later, the prepared solution was used in electrode modification for both the aggregation and the cyclic voltammetry experiments.

Table 5.2: Concentration and the moles of **P4VP-1**, **P4VP-2** and **P4VP-3** used in the preparation of electrode.

Polymer	Concentration prepared in 25 mL (mM)	Mol of polymer (mol)	Active polymer in 1.5 µL (mol)	Mol of 4VP unit (mol)	Active 4VP unit in 1.5 µL (mol)
P4VP-1	0.940	2.35×10^{-9}	1.41×10^{-9}	1.17×10^{-3}	7.02×10^{-8}
P4VP-2	0.045	1.12×10^{-6}	6.68×10^{-11}	1.67×10^{-3}	1.00×10^{-7}
P4VP-3	0.088	2.20×10^{-6}	1.32×10^{-10}	3.74×10^{-4}	2.24×10^{-8}

The glassy carbon electrode (GC) was polished with alumina paste and cleaned thoroughly with sonification before used. 1.5 µL of the prepared solution was cast on the GC electrode (effective area $0.07 cm^2$) and the electrode was dried at room temperature in the dark. The slow evaporation of DMF was expected to allow the catalyst/polymer mixture to adsorb on the electrode surface. As an example, the amount of electroactive material of **P4VP-2**/$CoPcF_{16}$ coated on the electrode surface is given in Table 5.3. For comparison, a GC electrode was also modified by P4VP or $CoPcF_{16}$.

Table 5.3: Electroactive species of P4VP and $CoPcF_{16}$ on the modified electrode surface (1.5 µL).

4.5×10^{-5} M P4VP-2 (mL)	**3.0×10^{-5} M $CoPcF_{16}$ (mL)**	**Concentration P4VP-2 ($x10^{-5}$ M)[(a)]**	**Concentration $CoPcF_{16}$ ($x10^{-5}$ M)[(a)]**	**Active P4VP-2 on surface ($x10^{-11}$ mol)**	**Active $CoPcF_{16}$ on surface ($x10^{-11}$ mol)**
0	5	0	3.0	0	4.5
1	4	0.9	2.4	1.4	3.6
2.5	2.5	2.3	1.5	3.5	2.3
4	1	3.6	0.6	5.4	0.9

[(a)]Concentration after mixing the solution was calculated using equation $M_1V_1 = M_2V_2$; where M_1 =stock concentration of P4VP or $CoPcF_{16}$, V_1 =volume of P4VP or $CoPcF_{16}$ taken from stock solution, M_2 =new concentration, V_2 =total volume after mixed the solution.

5.2.4 Electrochemical methods

Electrochemical studies were performed using a single-compartment electrochemical cell equipped with a modified GC electrode as the working electrode, a platinum wire counter electrode and an Ag/AgCl reference electrode, all measurements were carried out at room temperature. The electrolyte was a phosphate buffer solution (0.1 M NaH_2PO_4/H_3PO_4) at pH 2 unless stated otherwise. The cell was deaerated with argon or carbon dioxide for 20 minutes before performing the measurements and a blanket of gas was maintained throughout the experiment in order to exclude the oxygen from the system. Cyclic voltammetry was recorded at different scan rates and bulk electrolysis was carried out at a constant potential for an hour. All electrochemical measurements were performed on a CHI Instruments potentiostat (CHI 604C). The H_2 evolved in the headspace of the cell was measured by gas chromatography (Varian) with a molecular sieve 5 Å column and argon carrier gas.

5.3 Results and discussion

5.3.1 Investigation of the structural features of $CoPcF_{16}$ within the P4VP matrix

In this study $CoPcF_{16}$ is immobilised in a polymer matrix in order to investigate its potential as electrocatalyst for the generation of hydrogen. In these studies a polymer/MPc solution is added drop wise on a glassy carbon electrode surface and the solvent is left to evaporate. For a full understanding of the behaviour of such a matrix, the nature of the MPc molecules within the polymer layer needs to be considered as two important chemical processes may take place in the polymer/MPc matrix. These are coordination of $CoPcF_{16}$ to the polymer backbone and aggregation of CoPc molecules in solution. Aggregation of MPcs is a widely reported feature for these compounds and is caused by extensive π-π stacking. Kobayashi *et al.* reported that substitution of phthalocyanine at *α*-, *β*- or hexadeca position influences the electronic spectra in solution and films. For some MPc compounds bulky substituted groups at α- position prevent the cofacial aggregation so their Q band remains at similar wavelength either in

solution or film. When substituted at the *β*- position, MPcs tend to aggregate cofacially in polar solvents and in films show broad Q band compare to the solution Q band. For hexadeca substituted compounds, the Q bands exhibit at similar wavelength in solution and film.[30] Stacking of these molecules often results in extensive assemblies of these molecules rather than single molecular units. This process has been investigated using electronic spectroscopy.[31,32] General observations are that apart from the expected Q band an additional broad feature is formed up as a result of aggregation. The feature is found at higher energy than the Q band. The latter will be not only dependent of the interaction between the metal ion in the centre of the PC ring and potential ligands, but also on the solvent present.

Coordination of the MPc to other ligands, in this case a polyvinyl pyridine polymer is driven by the presence of free axial coordination sites. For this particular case the CoPc may be coordinated to either one or two pyridine units as has been observed for other metal complexes. For the purpose of this study this behaviour is favoured since single molecules are expected to be more effective as electrocatalysts than large aggregates. In the 1980s and 1990s many studies on aggregation and coordination of ligands at the axial positions have been reported. However, the results reported are often unclear and open to discussion, as a result many questions remain while it is clear that aggregation does occur readily. In this section, the effect of the mixing of $CoPcF_{16}$ with the polymer in different rations as a function of time using UV/Vis spectroscopy was investigated and considering the aggregation and coordination effects.

The ultraviolet-visible (UV-Vis) spectra observed for these compounds reveal discrete bands arising from transitions within the phthalocyanine (Pc) ring system. They exhibited a strong Q band in the visible region around 650-750 nm due to the $\pi - \pi^*$ transition from the highest occupied molecular orbital (HOMO) to the lowest unoccupied molecular orbital (LUMO) of the macrocyclic phthalocyanine ring.[12] In addition, they also showed an absorption peak in the 400 nm region, the so called B band. For the free base derivatives, a split Q band is observed as a result of their lower symmetry (D_{2h}) because of the presence of the two hydrogen atoms carried by isoindole nitrogen, whereas the other two nitrogen atoms are iminic in nature and as a result two absorption maxima are observed for the Q band between 650-720 nm depending on the nature of the compound.[13] The binding of the metal inside the central cavity leads to

changes in the electronic spectra from the spectra observed for the free PCs. Torres *et al*. reported that the shift of Q band within the range 620 and 720 nm is influenced by metal size, coordination and oxidation state. The presence of closed-shell cations such as *e.g*., lithium (I), magnesium (II) or zinc (II) leads to maximum absorption values for the Q band around 670 nm, whereas for complexes containing open-shell metal ions such as iron (II), cobalt (II) or ruthenium (II) this absorbance feature is observed at around 630-650 nm.[13]

Electronic spectra obtained for a number of reaction mixtures of $CoPcF_{16,}$ and **P4VP-2** are shown in **Error! Reference source not found.**, 5.4, 5.5, 5.7 and 5.8. A $CoPcF_{16}$ solution in DMF was homogenously blue in colour and its electronic spectrum is shown in Figure 5.3Figure 5.3. The absorption maximum of the Q band of $CoPcF_{16}$ lies in the visible region at 628 nm with the B band at 440 nm. The electronic spectra obtained for mixtures of **P4VP-2** and $CoPcF_{16}$ were investigated in DMF solution using different molecular ratios of $CoPcF_{16}$ and **P4VP-2** with concentration changes for the MPc compound from $6.0x10^{-6}$ to $2.4x10^{-5}$ M as shown in Figure 5.4 and Table 5.1. The ratios shown in Table 5.1 indicate that there is a considerable excess of pyridine groups available for interaction with the MPc compounds in the matrix. The blue colour solution changes to green as the concentration of $CoPcF_{16}$ decreases. Typically, a broad peak is observed around 650 to 750 nm. This peak showed a hypsochromic shift and increased absorbance in concentrated solution. When the concentration of $CoPcF_{16}$ increased, the intensity of this peak was increased. This may be a result of the formation of dimers and aggregation of the monomeric species [33] or interaction between **P4VP-2** and the Co centre [34]. Li and co-workers reported similar UV/Vis spectra with the film of $CuPcF_{16}$ in DMF solution and aggregates formed easily at concentrations higher than $2.2x10^{-5}$ mol/L.[35] At a high concentration, an increased number of aggregates form which absorb in the same regions as the dimer Q band, but with broader, lower intensity bands.[32,36]

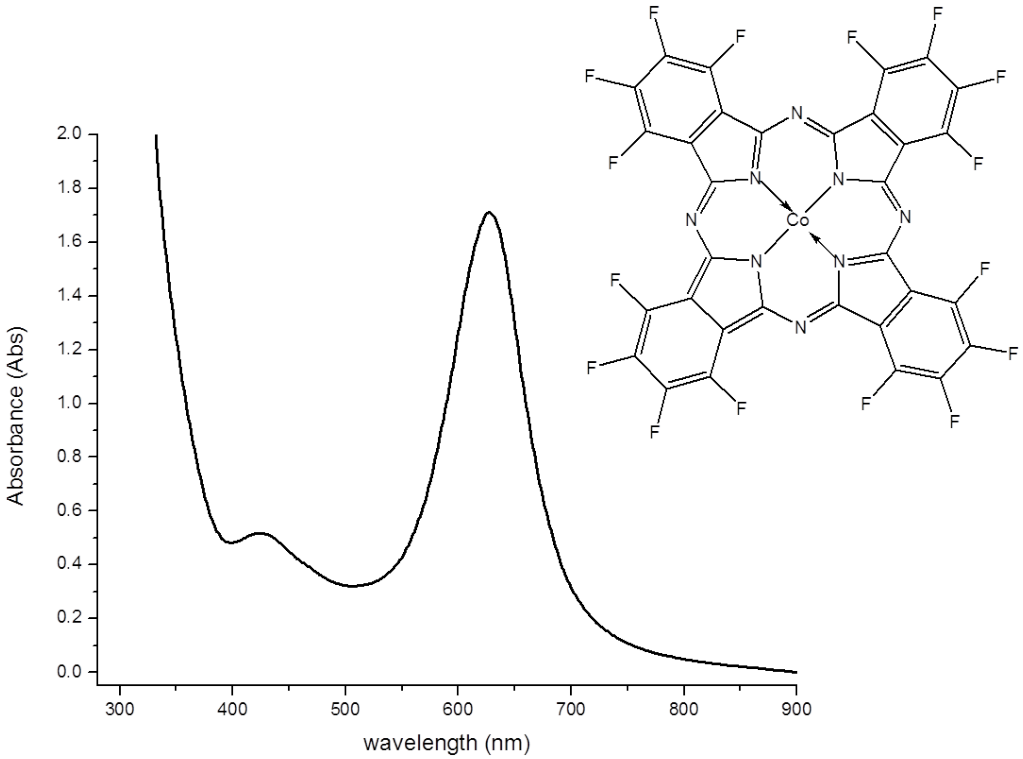

Figure 5.3: UV/vis spectrum of $CoPcF_{16}$ in DMF solution. Inset: Structure of cobalt(II) hexadecafluorocaphtalocyanine ($CoPcF_{16}$),

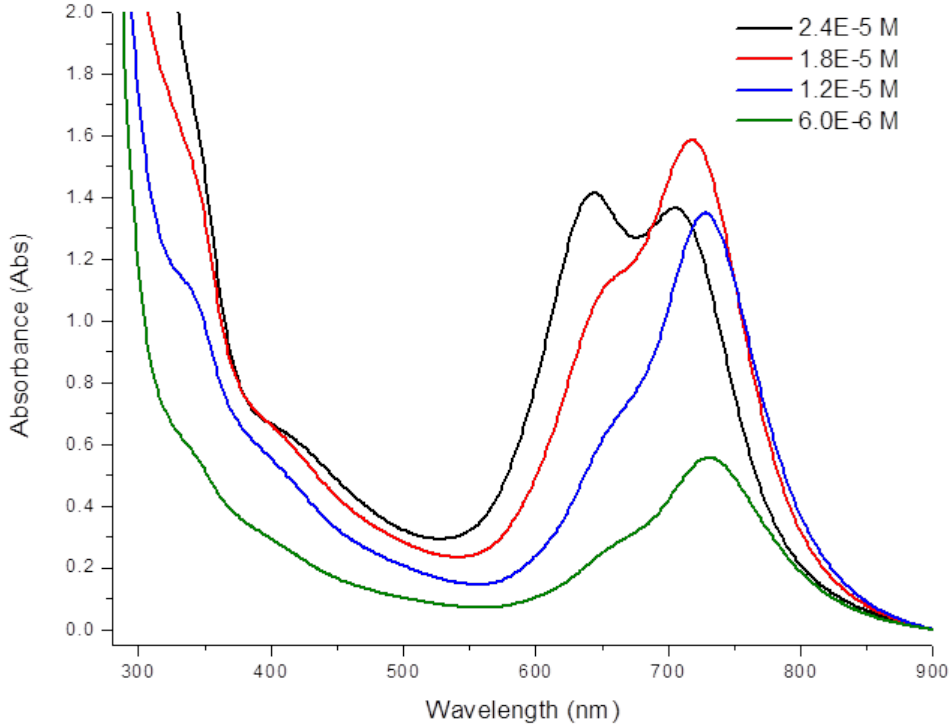

Figure 5.4: Electronic absorption of **P4VP-2**/$CoPcF_{16}$ complexes at different concentration of $CoPcF_{16}$ after 30 days.

The spectroscopic study of the interaction between low concentration mixtures of $CoPcF_{16}$ and **P4VP-2** in DMF (approximately $6.0x10^{-6}$ M) was carried out for 7 days and the results are shown in Figure 5.5. At the beginning of the experiment, the UV/Vis spectra showed a broad peak at about 636 nm. After 30 minutes, the Q band splits into two peaks of lower intensity and a new band was formed at 673 nm. Later, the intensity of this new band increased until day 7. The observations suggest that the peaks corresponds to a mixture compounds formed in solution, such as dimeric structures, which lead to aggregation [33] and the axial coordination of a pyridine residue of **P4VP-2** to the central cobalt ion of $CoPcF_{16}$.[34,37,38] It is expected that the polymer binds with one or two pyridines either from the same or different polymer chains (Figure 5.6). Typically, the formation of dimeric species of more general aggregation results in the appearance of an "extra" Q band absorption at 30-50 nm and to the blue of the monomer Q band, due to coupling between aggregates.[36] Similar adduct formation of CoPcs with P4VP has been reported previously.[39] Ghani and co-workers reported the maximum solubility of unsubstituted CoPc in DMF is 1.74×10^{-4} M, are not stable in solution and for aggregates as shown by the broadening and shifted Q band in UV/Vis spectrum.[40] These general observations, suggest that $CoPcF_{16}$ is dispersed homogenously in DMF at the beginning and forms aggregates at longer times and at higher concentration.

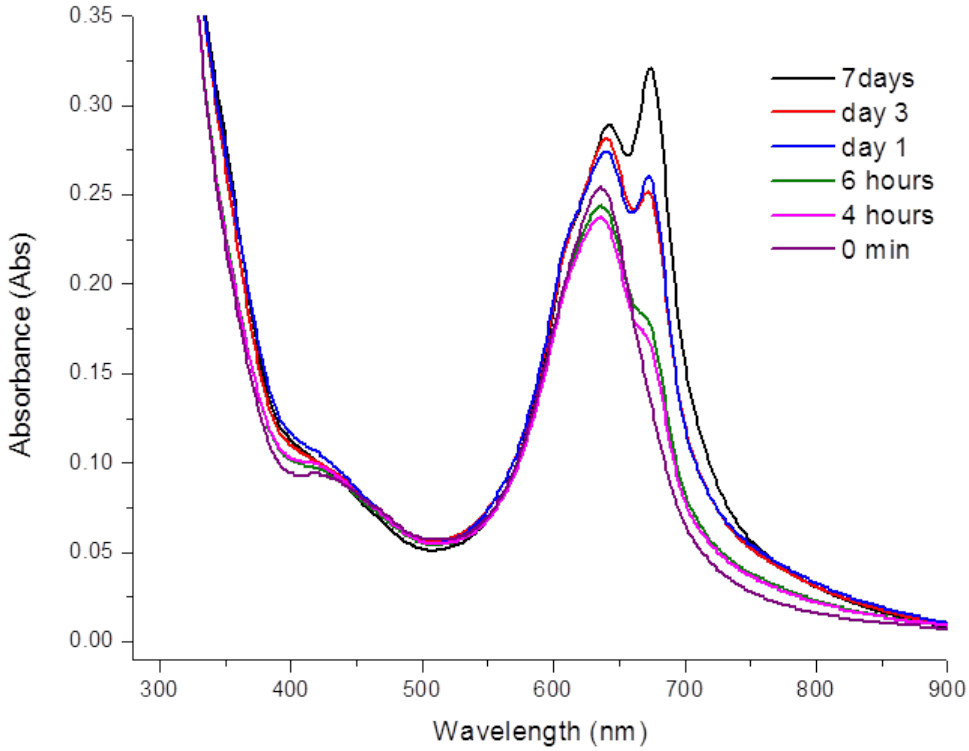

Figure 5.5: Electronic absorption of **P4VP-2**/$CoPcF_{16}$ *via* time at $6.0x10^{-6}$ M of $CoPcF_{16}$.

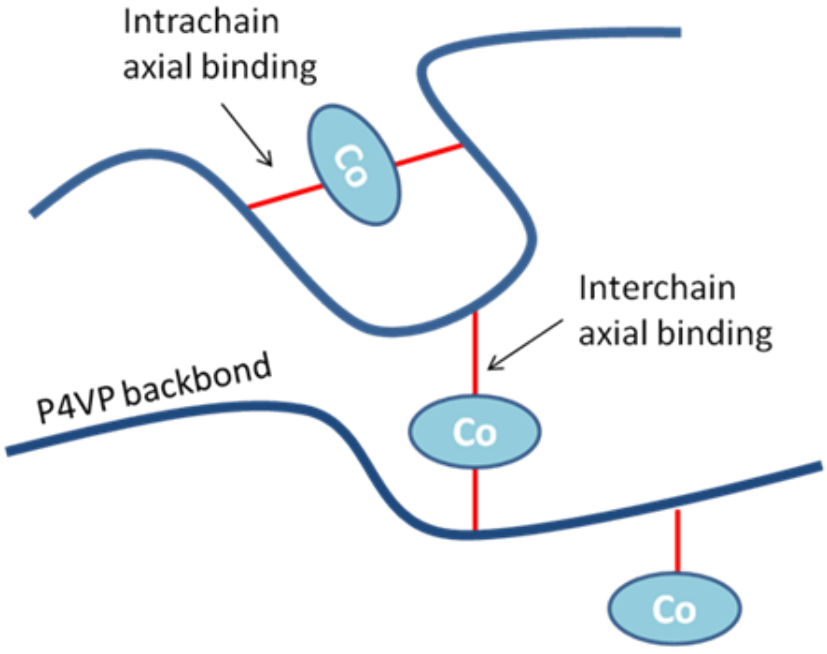

Figure 5.6: Cartoon illustration of axial binding possibility between $CoPcF_{16}$ and a P4VP backbone in polymer solution.

To explore the effect of axial coordination of the Pc compound to **P4VP-2** as shown in Figure 5.6, the interaction of the compound with pyridine was investigated. Solutions containing 0.1% (v/v) pyridine added to $3.0x10^{-5}$ M $CoPcF_{16}$ in DMF and 0.1% $CoPcF_{16}$ in pyridine were prepared. The electronic spectra obtained over 7 days are shown in Figure 5.7 and Figure 5.8. The electronic spectrum of $CoPcF_{16}$ in DMF shows an absorption maximum at 635 nm as shown in Figure 5.3b, in the presence of 0.1% pyridine (Figure 5.7). The Q band is seen at about 650 nm and increases in intensity while the B band is reduced with time. Figure 5.8 shows that in pure pyridine an electronic feature is observed at 665 nm with a shoulder at 600 nm. Both spectroscopic features reach a maximum intensity after 300 minutes provide evidence for coordination of the pyridine in the complexes. Importantly the spectra show no evidence for excessive aggregation of the Pc compounds is observed in the presence of pyridine. The shoulder observed in Figure 5.8 would suggest the formation of dimeric species as shown for other phthalocyanines by Snow and Jarvis.[31] Adduct formation of CoPc in pyridine solution or a CoPc film in pyridine has been reported previously (Table 5.4).

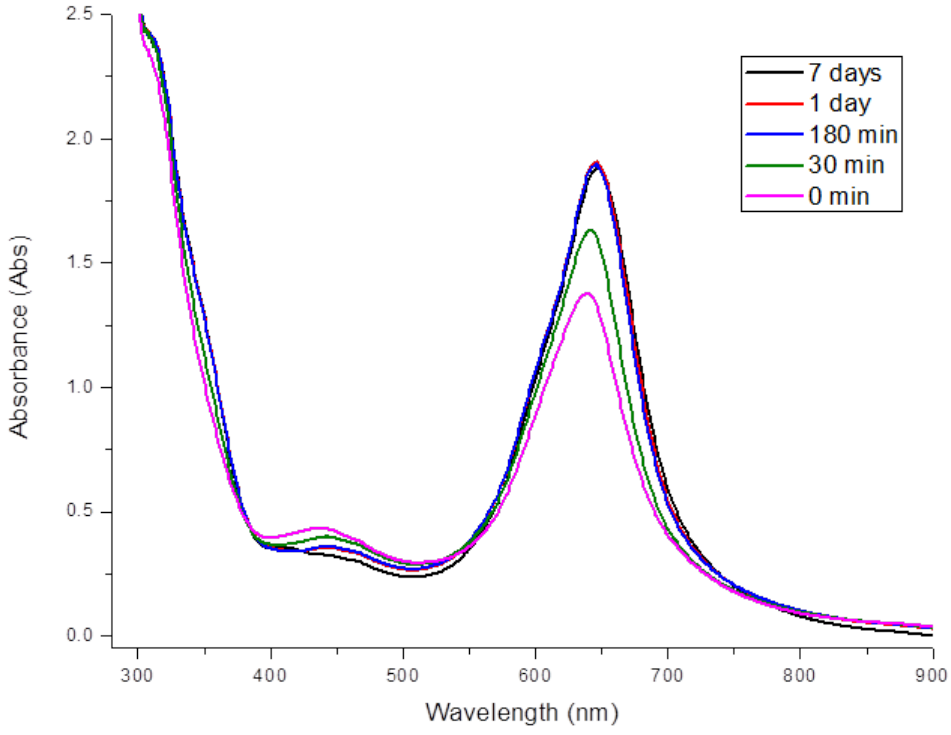

Figure 5.7: Electronic absorption of 0.1% v/v (0.3 mL pyridine) added into 3 mL $CoPcF_{16}$, $3.5x10^{-5}$ mol/L *via* time.

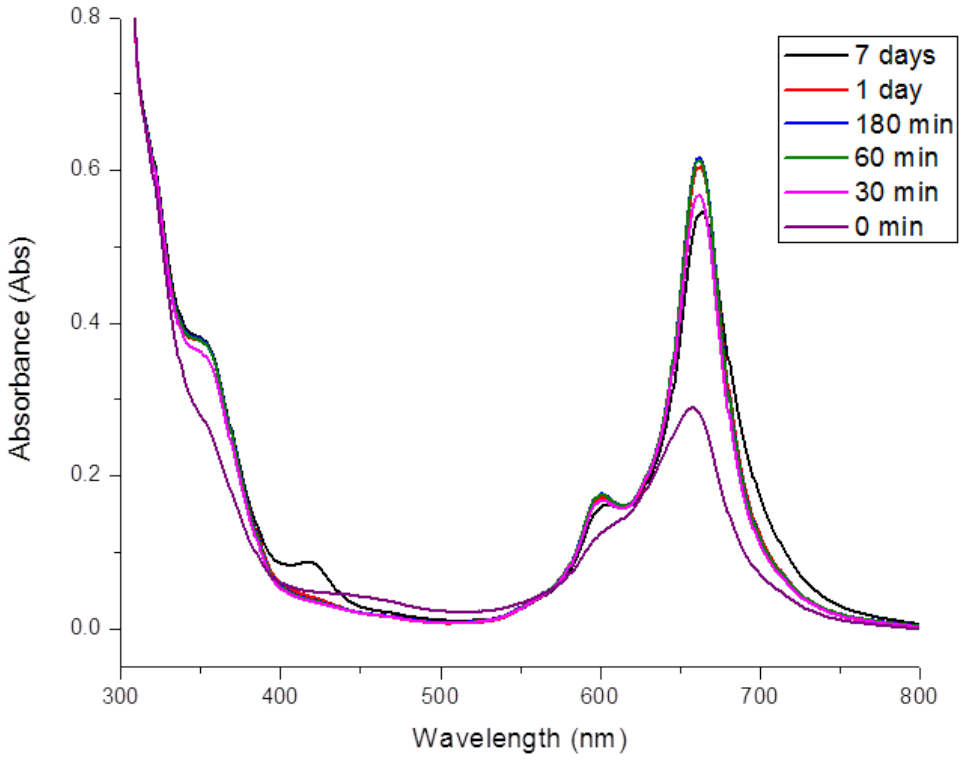

Figure 5.8: Electronic absorption of 0.1% v/v (0.3 mL $CoPcF_{16}$, $3.5x10^{-5}$ mol/L) added into 3 mL pyridine solution *via* time.

Table 5.4: Electronic spectra of Q band for $CoPcF_{16}$ and Co(II)Pc at different solvents.

Compounds	**Solvent**	**Q λ_{max} (nm)**	**Ref**
$CoPcF_{16}$	DMF	628	this work
	Pyridine	662	this work
Co(II)Pc	DMSO	657	38
	Pyridine	674 (film)	34
		700 (solution)	
	DMF	670 (solution)	40

CoPc complexes containing pyridine in axial position have been reported.[38,41] Nyokong reported the stepwise substitution of axial dimethylsulphoxide (DMSO) ligands by pyridine in $CoPc(DMSO)_2$ as in equation (1) and (2).[38] Axial ligand substitution reaction in phthalocyanine complexes are dissociative and occur in a

stepwise manner. The replacement of the first DMSO ligand is faster than that of the second one.

$$\text{py} + [\text{CoPc(DMSO)}_2] \overset{K_1}{\rightleftharpoons} [\text{CoPc(DMSO)(py)}] + \text{DMSO} \quad \textbf{(1)}$$

$$[\text{CoPc(DMSO)(py)}] + \text{DMSO} \overset{K_2}{\rightleftharpoons} [\text{CoPc(py)}_2] + \text{DMSO} \quad \textbf{(2)}$$

Substitution of the first ligand in MPc complexes is normally accompanied by a small wavelength change.[42]

Comparison of the spectra obtained from solutions containing pyridine and those containing P4VP (Figure 5.5) show that, while in polymer containing solution, the spectra are showing considerable changes with time, whilst the pyridine containing solutions are more stable. Also important is that the absorption maxima shifts from 635 nm in DMF to 650 nm in dilute pyridine to 665 nm in pure pyridine. These observations are in agreement with the above model and suggest that, in the presence of low pyridine concentrations, one pyridine is coordinated to the metal centre while in concentrated pyridine solution two pyridines are bound. Although further detailed studies are needed to fully confirm this it seems that in the presence of high pyridine concentrations less aggregation is found. This behaviour is not unlike that observed in the P4VP containing solutions. In the presence of P4VP, aggregation is observed in the beginning but with time more coordination of $CoPcF_{16}$ to the polymer backbone is taking place. Figure 5.5 shows that the broad Q feature observed at about 650 nm, that is mostly associated with aggregation, is reduced with time and a new band at about 670 nm is formed. The latter band is most likely related to the increasing coordination of $CoPcF_{16}$ to the polymer backbone as shown in **Error! Reference source not found.**Figure 5.6 Whether the coordination is to one or two polymer units is unclear. The small variations observed in the different "pyridine coordinated compounds" is explained by solvent and matrix (polymer) effects.

From these spectroscopic studies a picture emerges that indicates that solutions containing both polymer and phthalocyanine will change with time. The amount of coordinated $CoPcF_{16}$ tends to increase this binding process is a function of the pyridine concentration. This has two consequences one that the age of the solution used needs to

be considered and secondly that the aggregation taking place may affect the amount of electroactive material in the layer. This later issues will be discussed below. The results also suggest that coordination of the electrocatalysts is favoured by the presence of a high concentration of 4VP.

5.3.2 Electrochemical Properties of $CoPcF_{16}$ and P4VP/$CoPcF_{16}$

As already discussed in the last section the compound $CoPcF_{16}$ was investigated for its capacity to act as an electrocatalyst for hydrogen reduction. Phthalocyanines (Pcs) are of interest in this respect since they possess reduction potentials that are not wouldly negative so that they can be utilised for hydrogen generation at relatively low overpotentials. Detailed studies carried out on a range of such compounds suggest that in Pc type compounds the first reduction process occurs at the metal-centre, provided the metal centre is redox active and further reductions occur on the Pc ring and/or at different substituents on the Pc ring.[26,27,34,43] The cyclic voltammogram (CV) of the $CoPcF_{16}$ when immobilised on an glassy carbon (GC) electrode surface by drop casting solution is shown in Figure 5.9. The dependence of the CVs on the scan rate used is shown in Figure 5.9a over the scan rate 5-500 mV/s, analysis shows that the peak currents obtained were proportional to the scan rate, in agreement with the behaviour expected for a surface bound species. When the potential was scanned to more negative regions, another redox peak was observed at -0.80 V vs Ag/AgCl. The curves obtained show that when only the first redox couple is scanned a well behaved electrochemistry is observed (Figure 5.9a), however when the scan also includes the second redox couple, a less clear redox behaviour was obseved. This was likely at least partly caused by the onset of hydrogen production, at the second redox couple.

The first reduction process for $CoPcF_{16}$ was observed at -0.46 V vs Ag/AgCl. The formal electrode potential of the first redox process observed is calculated as -0.41 V vs SCE and the difference between the anodic and cathodic peak currents is 100 mV. Compared to the CV of CoPc of 0.56 V (Ag/AgCl) the first reduction potential has shifted to positive potential upon the introduction of the fluoro atoms which were electron withdrawing. [44]

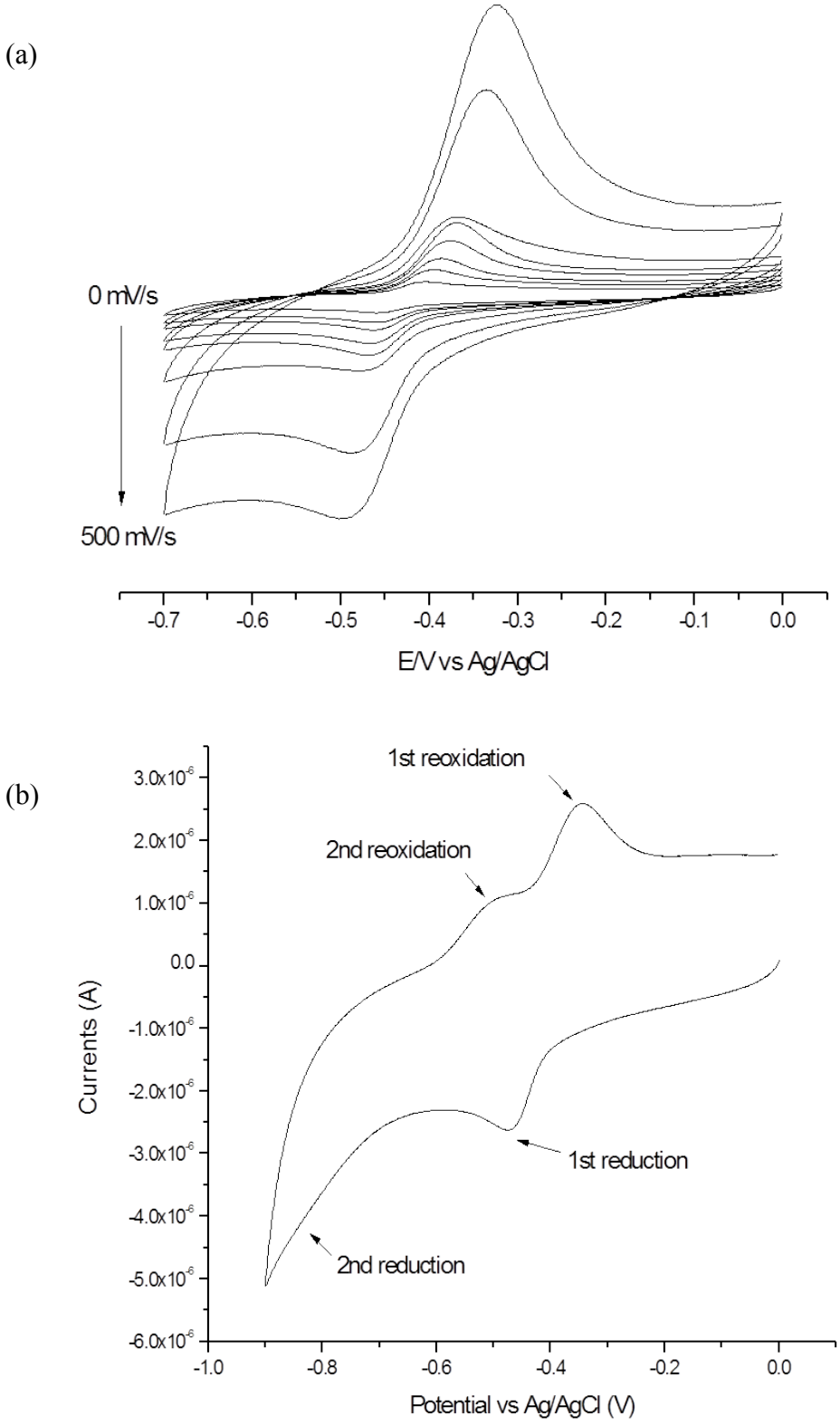

Figure 5.9: Cyclic voltammogram of GC electrode (effective area: 0.07 cm^2) coated with $CoPcF_{16}$ ($6.4x10^{-10}$ mol cm^{-2}) at pH 2 (0.1 M phosphate buffer solution) under Ar: (a) Scan rate from 5 to 500 mV/s; (b) Potential scan over the range 0 to -0.9 V with scan rate 100 mV/s.

For electrode immobilised **P4VP-1**/$CoPcF_{16}$, the first redox wave was observed at -0.55 V and a second peak at -0.78 V vs Ag/AgCl (Figure 5.10a). For **P4VP-2** similar results was obtained. The first reduction was 70 mV more negative than the same process observed for the $CoPcF_{16}$ monolayer (Figure 5.9 and Figure 5.10) at the same pH, however, the second reduction was slightly more positive by 20 mV. Meanwhile, **P4VP-3**/$CoPcF_{16}$ showed two reductions processes at -0.46 V and -0.78 V vs Ag/AgCl. (Figure 5.10b). The solvent and in this case also the matrix in which the redox active specieses were immobilised can have a great influence on the redox processes observed. For example, in pyridine solution where CoPc was expected to be coordinated by up to two pyridine ligands, the first redox potential observed at -0.57 V (vs SEC) compare to a value of -0.37 V (vs SEC) in DMF, a solvent that does not bind.[34] The more negative potential observed for $CoPcF_{16}$ in the polymer matrix may therefore be indicative for the presence of coordination by the metal centres to the polymer backbone.[34] It is unclear whether such coordination would be through one or two pyridine units.

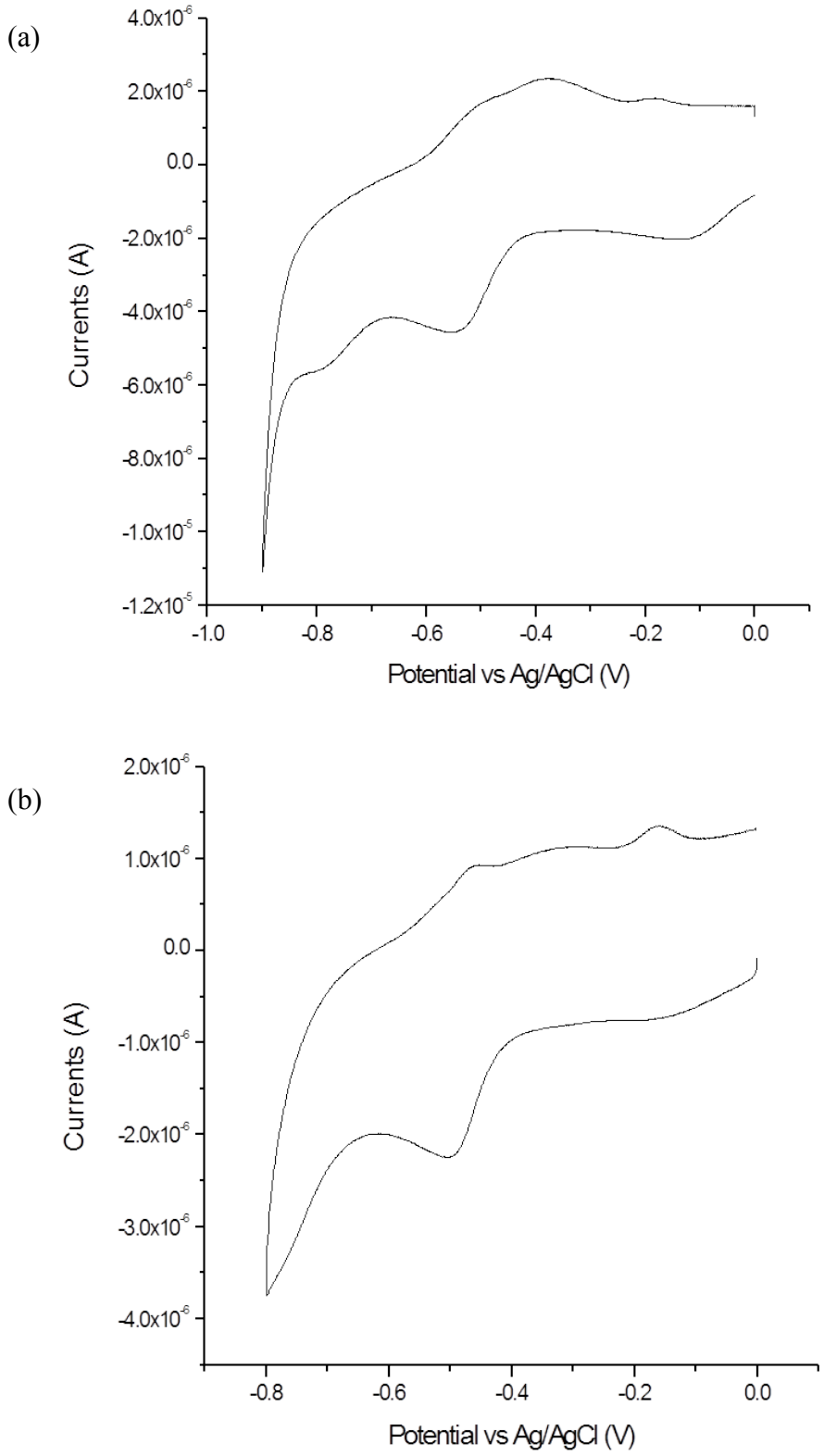

Figure 5.10: Cyclic voltammograms of $CoPcF_{16}$ incorporated in polymer matrixes at scan rate 200 mV/s (a) **P4VP-1**/$CoPcF_{16}$ (24 μM), (b) block copolymer **P4VP-3**/$CoPcF_{16}$ (15 μM).

5.3.3 Hydrogen evolution by $CoPcF_{16}$ and P4VP/$CoPcF_{16}$

The aim of the electrocatalytic approach investigated here for hydrogen production is to decrease the overpotential of the working electrode and to gain high current densities at this potential while at the same time using cheap and abundant metals such as cobalt and using polymer matrices to improve electrode stability and the amount of electroactive material that can be attached to the surface.

Electrochemical processes in polymer matrices such as hydrogen evolution, are mostly controlled by two different processes; the reduction of the complex by electron propagation through the polymer matrix and proton reduction by the reduced complex.[27,43] For Co based Pc compounds the second reduction which is generally assumed to be based on the ring is the one that catalyses the hydrogen generation is solution. It is not expected that this will be different when the compounds are immobilised in a polymer matrix. One mechanism proposed for proton reduction proposed is shown in Scheme 5.1.

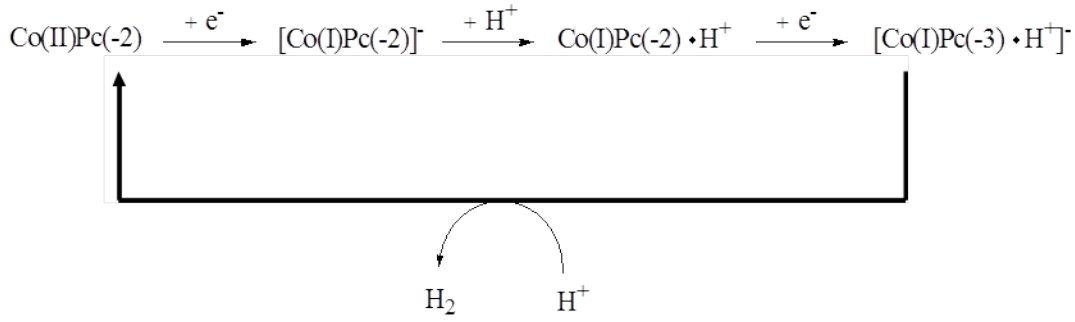

Scheme 5.1:Electrocatalytic mechanism of proton reduction by the CoPc incorporated in a P4VP matrix.[27,34]

To determine the efficiency of the electrocatalytical process, the amount of $CoPcF_{16}$ that is active in the catalytic process needs to be determined. This is generally carried out by measuring the area under the reduction wave of the first reduction wave, for example the first reduction wave shown in Figure 5.10a at about -0.5 V vs Ag/AgCl. The area under the wave is determined after subtraction of the background current. This

value is then compared with the amount of electrocatalytic material that was originally deposited on the electrode surface. The amount of electroactive material on the surface is important in order to be able to estimate the effectiveness of the electrocatalyst. In the first instance it is a measure for the effectiveness in which the catalytic process is carried out. However, not all material deposited by a syringe will stay attached to the surface. Another important factor is however the well-known aggregation of Pc type compounds, which may result in the formation of electroinactive compounds. The presence of aggregates will more than likely limit electrocatalytic behaviour and needs therefore to be limited. At this stage it is however not possible to differentiate between these two factors.

The electroactive fraction in $CoPcF_{16}$ and P4VP/$CoPcF_{16}$ films was determined from the peak area of first reduction, Co(II)Pc(-2)F_{16}/Co(I)Pc(-2)F_{16}^- couple as obtained from the cyclic voltammogram of the modified GC electrode at low scan rate. For neat $CoPcF_{16}$, layers the coating applied was estimated to be about $6x10^{-10}$ mol/cm^2. However, only $0.8x10^{-10}$ mol/cm^2, just over 10%, is electroactive. For, P4VP/$CoPcF_{16}$ coatings of **P4VP-1** and **P4VP-2** the electroactive fraction obtained on the surface were around 10 to 40% of the amount of material applied to the electrode is shown in Table 5.5. The values obtained were dependent on the polymer matrix used. Similar results obtained by Ouyang for $CoPcF_{16}$ films deposited on graphite.[44]

Table 5.5: Surface coverage and current density of for $CoPcF_{16}$ (Co), **P4VP-1**/$CoPcF_{16}$ and **P4VP-2**/$CoPcF_{16}$.

	Theoretical [a]				**Experiment**						
	Co	**P4VP/$CoPcF_{16}$**			**Co**	**P4VP-1/$CoPcF_{16}$**			**P4VP-2/$CoPcF_{16}$**		
Ratio 4VP:Co in volume (mL)	0:5	1:4	1:1	4:1	0:5	1:4	1:1	4:1	1:4	1:1	4:1
$CoPcF_{16}$ concentration (μM)[b]	30	24	15	6	30	24	15	6	24	15	6
Surface coverage (x 10^{-10} mol/cm^2) [c]	6.4	5.1	3.2	1.3	0.8	0.7	0.4	0.2	1.3	0.5	0.5
Current density (mA/cm^2)[d]	-	-	-	-	1.2	13.0	7.8	12.1	10.9	0.7	9.8
Current density (mA/cm^2)[e]	-	-	-	-	0.7	0.5	1.1	49.0	0.9	5.6	14.1
Ratio (%)[f]					13	14	13	15	25	16	38

[a] Theoretical values calculated based on the 1.5 μL coated on the GCE electrode surface (0.07 cm^2); [b] Concentration of $CoPcF_{16}$ after mixing with P4VP solution with total volume are 5 mL; [c] Surface coverage calculated through peak area of CV at low scan rate; [d] Current density measured obtained from Cyclicvoltametry measurements at -1.1 V; [e] Current density of bulk electrolysis measured at -1.1 V for 60 minutes; [f] Ratio electroactive species to the total amount of catalyst on the electrode.

The electrocatalytic parameters such as the onset of the catalytic process and the catalytic current produced were studied using CVs as shown in **Error! Reference source not found.**. This figure showed the CVs of P4PV/$CoPcF_{16}$ modified GC electrodes in pH 2.2 phosphate buffer solution at scan rates of 200 mV/s. The overpotential of modified electrode was shifted positively compare to the overpotential obtained for the bare electrode, -1.08 V under the same conditions -1.1 V, with a value of -0.93 V for the $CoPcF_{16}$ monolayer, -0.90 V for **P4VP-1** and -0.92 V for **P4VP-2**. Since high overpotential results in increasing economic costs for the electrolysis process, they need to be reduced as much as possible. The results obtained for the PVP coatings showed that the overpotential was reduced by about 200 mV compared to the bare electrode, but they were still more negative than potential on Ni and Pt

electrode.[21] At a potential of -1.1 V vs Ag/AgCl, the catalytic ccurrent of the **P4VP-1** modified GC electrode was $8.4x10^{-5}$ A, which three times higher than **P4VP-2** ($3.1x10^{-5}$ A), while the monolayer of $CoPcF_{16}$ electrode showed similar current flow to **P4VP-1**. The potentials at which these cathodic currents were observed suggest that the catalytic reaction for hydrogen generation was controlled by the Co(I)Pc(-3) species as shown in Scheme 5.1.

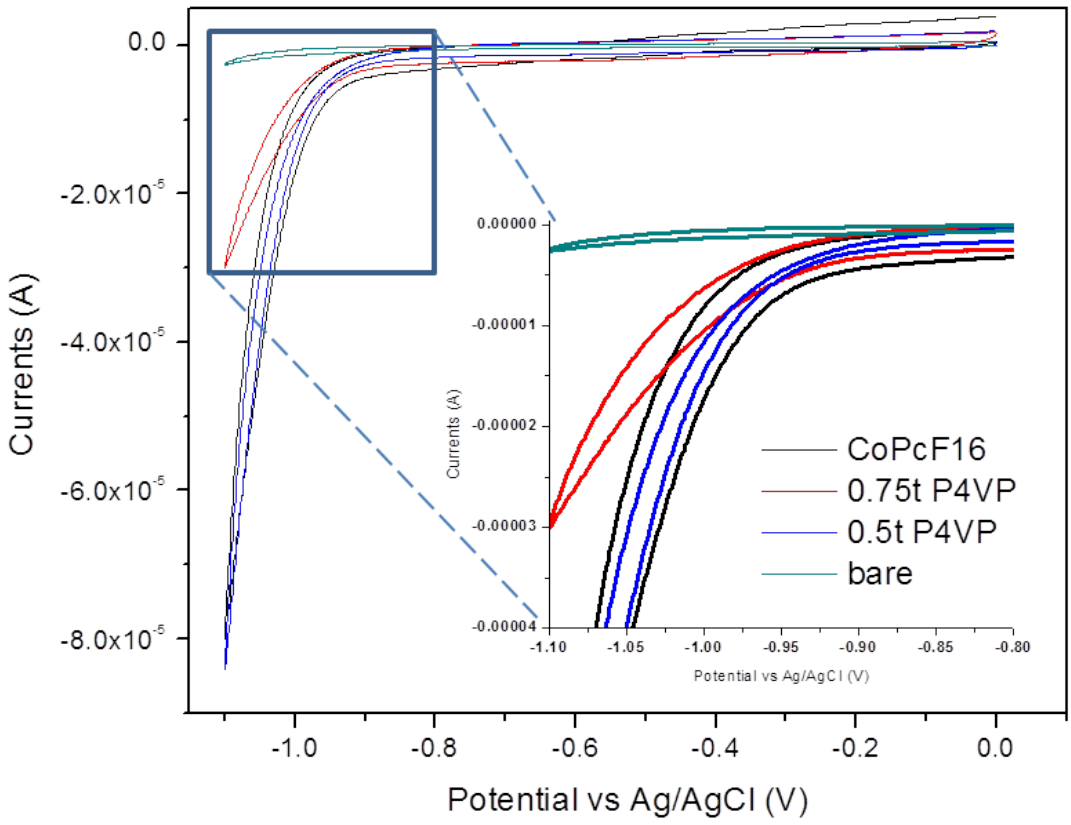

Figure 5.11: Cyclic voltammograms at a GC electrode (effective are 0.07 cm^2) coated with monolayer CoPcF16, P4VP-1 (Mw=5000g/mol) and P4VP-2 (Mw=160000 g/mol) in a 0.1 M phosphate buffer solution pH 2.2 under saturated argon at scan rate, 200 mV/s. Inset: The overpotential of modified electrode compare to the overpotetnial of bare electrode.

As outlined in the experimental part for the polymer/$CoPcF_{16}$ system, the concentration of $CoPcF_{16}$ in the P4VP polymer mixtures varied from 6-24 μM. For example, **P4VP-1**/$CoPcF_{16}$ (24 μM) was the mixture of 4 mL of $3x10^{-5}$ M $CoPcF_{16}$ added into 1 mL of **P4VP-1** solution resulting new concentration of $CoPcF_{16}$, 24 μM. On the other hand, **P4VP-1**/$CoPcF_{16}$ (6 μM) was prepared with addition of 1 mL of $CoPcF_{16}$ into 4 mL of a **P4VP-1** solution, the $CoPcF_{16}$ was five times diluted to 6 μM from the original concentration (*N.B*. the concentration of $CoPcF_{16}$ after mixed with P4VP solution shown in the bracket). Generally in the polymer/$CoPcF_{16}$ system, the overpotential shifted positively about 40 to 100 mV from the neat P4VP modified electrode. For instance in **P4VP-1**/$CoPcF_{16}$, the overpotential obtained at -0.83 V (6 μM), -0.84 V (15 μM) and -0.86 V (24 μM) compare to -0.9 V (Ag/AgCl) for monolayer **P4VP-1** and -1.08 V for the bare electrode. Similar results also obtained for **P4VP-2**/$CoPcF_{16}$ system. Figure 5.12 shows the current flows for P4VP/$CoPcF_{16}$ systems at different concentration of $CoPcF_{16}$. **P4VP-1**/$CoPcF_{16}$ (6 μM) and **P4VP-1**/$CoPcF_{16}$ (24 μM) indicated similar current flows of around $8.5x10^{-4}$ A, while the **P4VP-1**/$CoPcF_{16}$ (15 μM) only produces half of the current at potential -1.1 V vs Ag/AgCl (Figure 5.12**Error! Reference source not found.**a). At similar potential -1.1 V, the cyclicvoltammogram of **P4VP-2**/$CoPcF_{16}$ (6 μM) exhibited a sharp increase in cathodic currents to $9x10^{-4}$ A and the current was reduced by around 0.2 mA ($7x10^{-4}$ A) with the high concentration of $CoPcF_{16}$ as shown in Figure 5.12b. This behaviour confirmed that currents produce in the system depends on the type of reactive coverage on the electrode and that the overpotential for hydrogen generation can be reduced by polymer modification.

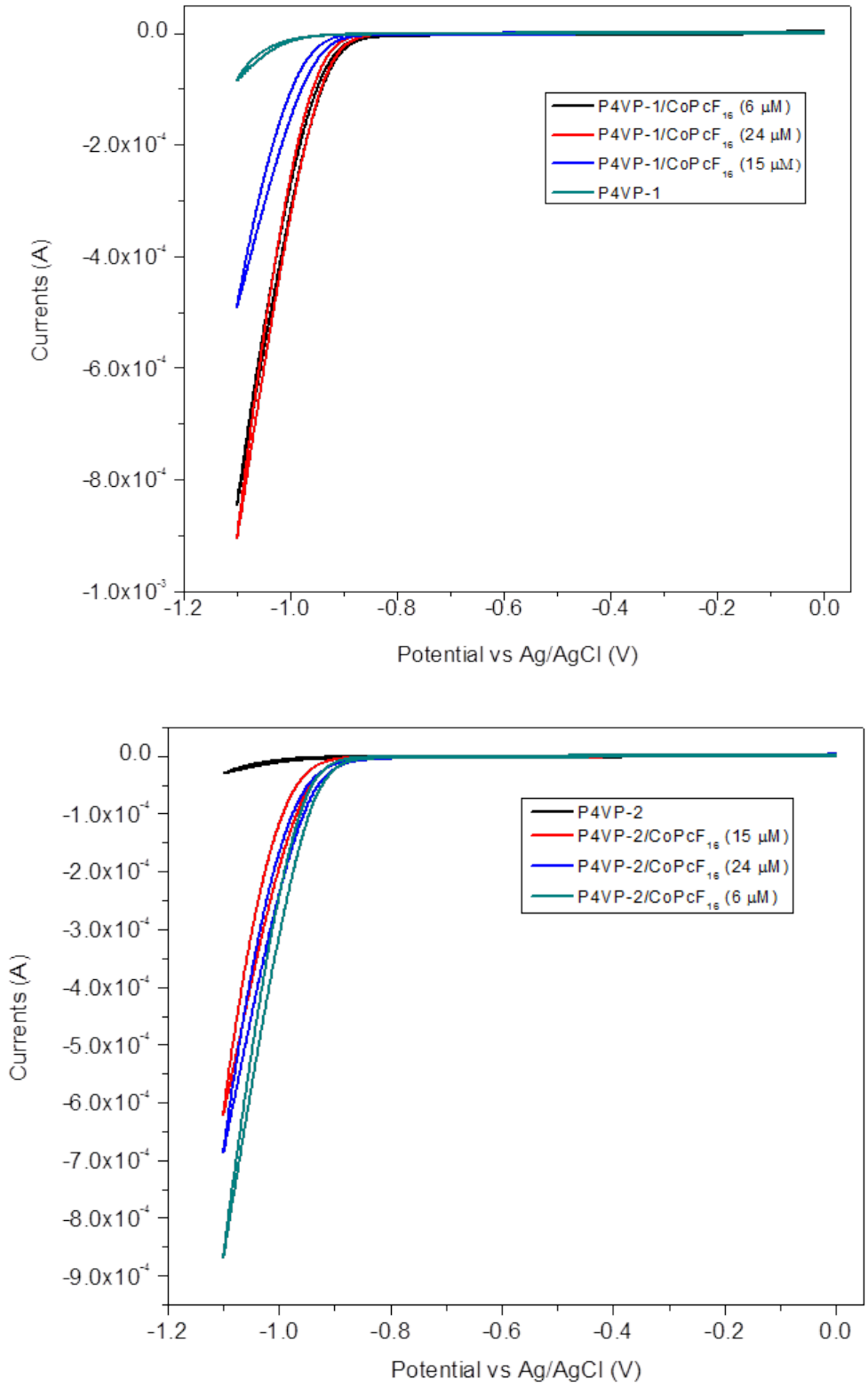

Figure 5.12: Cyclic voltammograms at a GC electrode (effective are 0.07 cm^2) coated with (a) **P4VP-1**/$CoPcF_{16}$ and (b) **P4VP-2**/ $CoPcF_{16}$ in 0.1 M phosphate buffer solution, pH 2.2 under saturated argon (Ar) at scan rate, 200 mV/s.

The electrocatalytic properties of the block copolymer **P4VP-3**/$CoPcF_{16}$ system which has a molar ratio 9:1 of 4VP to methyl methacrylate (MMA) was investigated. CVs of two different **P4VP-3**/$CoPcF_{16}$ ratios immobilised on GC electrode shown in Figure 5.13. When the potential applied was lower than -0.90 V, the cathodic currents exhibits a sharper increase due to the proton reduction than observed for the bare and **P4VP-2** modified electrode showing that the matrix works as a catalyst for proton reduction. The catalytic current of **P4VP-3**/$CoPcF_{16}$ (15 µM) and **P4VP-3**/$CoPcF_{16}$ (6 µM) were $6x10^{-4}$ A and $7.5x10^{-4}$ A, respectively which 20 times higher than the catalytic current observed for **P4VP-2** matrices.

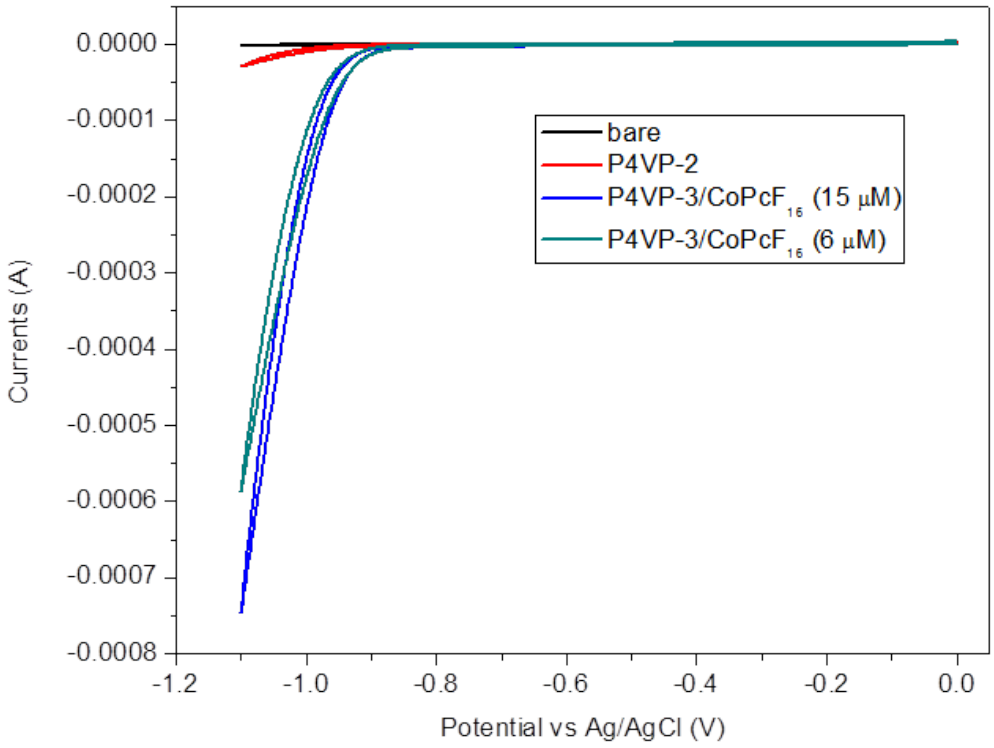

Figure 5.13: Cyclic voltammetry at GC electrode (effective are 0.07 mol/cm^2) coated with 0.5wt% **P4VP-3**/$CoPcF_{16}$ in 0.1 M phosphate buffer solution pH 2.2 under saturated argon at scan rate, 200 mV/s.

From the above cyclovoltametric experiments, it can be concluded that the overpotential for proton reduction for P4VP/$CoPcF_{16}$ based compounds was reduced compared with the bare GC electrode. Based on earlier work it seemed likely that the electrocatalytic process started at the second reduction step where one electron was added to the ring of complex to form $[Co(I)Pc(-3).H^{+}]^{-}$, a species that later forms hydrogen by interaction with a second proton as shown in Scheme 5.1. Therefore, although the Co compound had an earlier metal based reduction, this process is not directly involved in the electrocatalytic reaction and hydrogen generation only occurs after reduction of the Pc ring. As outlined above, the mechanism for electron transport in polymer matrices can be *via* diffusion (weak interaction between redox centre and the polymer) of the reactive centres or electron hopping (strong interaction).[27] On the basis of the results obtained, no definite conclusion concerning the mechanism can be reached for these electrode systems.

To further investigate the efficiency of the electrocatalytic process, bulk electrolysis of $CoPcF_{16}$ and its polymer complexes at potentials varying from -0.9 to -1.2 V was carried out for 1 h. In all experiments, electrode generated hydrogen was confirmed by the observation of bubles produced during the process and by subsequent GC analysis of the headspace (Figure 5.14). The turnover number (*TN*) is the parameter to express the activity of the catalyst to produce hydrogen. Meanwhile, the current density (J) shows the amount of current that flows at a specific surface area, typical 1 cm^2, calculated from equation **(3)**, where *I* is the current (A) and *A* is surface area (0.07 cm^2 for GC electrode). Table 5.6 shows the summary results for *TN* and current density (*J*) of $CoPcF_{16}$ and P4VP/$CoPcF_{16}$ complexes in this study, where the *TN* and *J* value are depends on the potential.

$$J = \frac{I}{A} \qquad \textbf{(3)}$$

For monolayers of $CoPcF_{16}$, *TN* and *J* increased with the potential applied as shown in Figure 5.15. *TN* at -1.0 V is $1.3x10^5$ h^{-1} and the value increased to $2.1x10^5$ h^{-1} at -1.1 V (Ag/AgCl), while the current density shows an increase from 0.26 mA/cm^2 at -1.0 V (Ag/AgCl) to 0.64 mA/cm^2 at -1.1 V (Ag/AgCl). The similar pattern is obtained for the $CoPcF_{16}$ complexes immobilised in the different polymer matrixes.

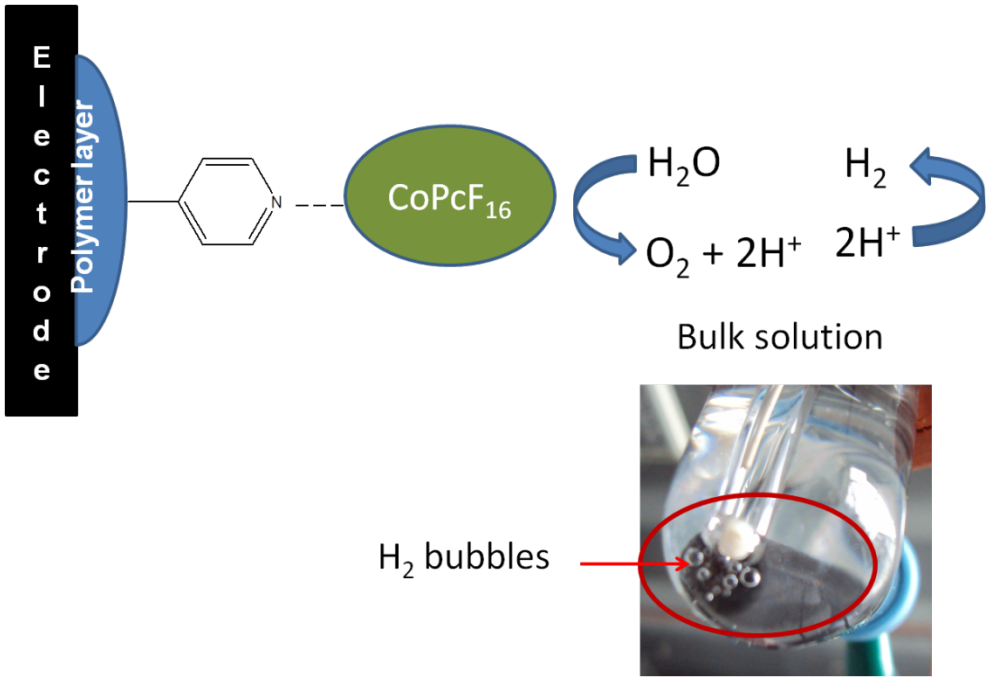

Figure 5.14: Schematic process of hydrogen evolution at electrode surface. Bubbles indicate the formation of H_2.

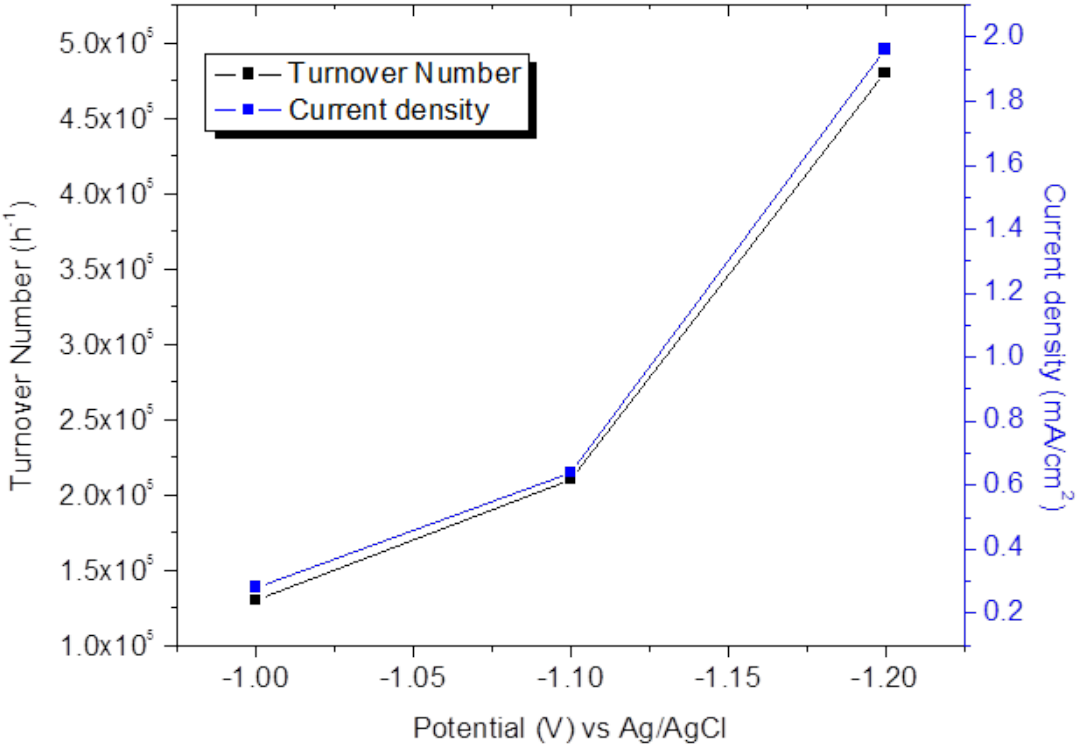

Figure 5.15: Turnover number and current density of monolayer $CoPcF_{16}$ coated on GC electrode versus different potential apply during electrolysis in phosphate buffer solution, pH 2.2.

Table 5.6: Potentiostatic electrolyses of $CoPcF_{16}$ and P4VP/$CoPcF_{16}$ matrices for 1 h in 0.1 M phosphate buffer solution, pH 2.2.

System[(a)]	**Potential (V) vs. Ag/AgCl**	**Turn Over Number, *TN* ($x10^5$)h^{-1}**		**Efficiency, %**	**Current density, *J* (mA/cm^2)**[(d)]
		Echem[(b)]	**GC calc.**[(c)]		
$CoPcF_{16}$	-1.0	1.3	-	-	0.3
	-1.1	2.1	-	-	0.6
	-1.2	4.8	-	-	2.0
P4VP-1/$CoPcF_{16}$	-0.9	0.1	-	-	0.1
(24 µM)	-1.0	0.8	-	-	0.4
	-1.1	1.4	-	-	0.5
P4VP-2/$CoPcF_{16}$	-0.9	6.9	3.4	49	0.9
(6 µM)	-1.0	39.7	26.7	65	4.9
	-1.1	66.5	9.8	22	14.1
	-1.2	78.9	25.1	33	16.2
P4VP-2/$CoPcF_{16}$	-0.9	0.8	-	-	0.3
(24 µM)	-1.0	0.9	-	-	0.3
	-1.1	2.1	-	-	0.9
	-1.2	44.0	-	-	1.3
P4VP-3/$CoPcF_{16}$	-1.0	2.7	2.6	99	1.5
(15 µM)	-1.1	3.6	1.1	22	2.3
	-1.2	8.8	3.6	40	2.2
P4VP-3/$CoPcF_{16}$	-1.2	20.1	19.6	91	4.9
(6 µM)					

[(a)]The concentration of $CoPcF_{16}$ after mixed with P4VP solution shows in the bracket. **P4VP-1** (P4VP, M_w=5000 g/mol), **P4VP-2** (P4VP, M_w=160000 g/mol), **P4VP-3** (P(4VP-*b*-MMA), M_w=54000 g/mol); ([b])Turnover number, based on the electroactive species present on the electrode estimated under the peak area at slow scan rate; [(c)]Turnover number, based on gas chromatography.

For the polymer/$CoPcF_{16}$ system, *TN* and *J* values increased compared to the neat $CoPcF_{16}$ system and the highest values were observed for the **P4VP-2**/$CoPcF_{16}$ system (Table 5.6). The *TN* value at -1.0 V (Ag/AgCl) calculated by electrochemical methods for **P4VP-2**/$CoPcF_{16}$ (6 μM) is 30 times higher compared to $CoPcF_{16}$. The *TN* value calculated by GC varies with a highest value obtained at -1.0 V is $26.7x10^5$ h^{-1} with 65% efficiency and a *J* of 4.9 mA/cm^2. The lowest efficiency is 22% obtained at a potential -1.1 V. *TN* values for **P4VP-2**/$CoPcF_{16}$ (24 μM) gradually increase from -0.9 V ($0.8x10^5$ h^{-1}) to -1.1 V ($2.1x10^5$ h^{-1}) followed by a sharp increase to $44.0x10^5$ h^{-1} (-1.2 V) as shown in Figure 5.16. The current density for both polymer matrices increased gradually over the potential range.

The block copolymer **P4VP-3**/$CoPcF_{16}$ with ratio 1:1 yields *TN* values from $2.7x10^5$ h^{-1} to $8.8x10^5$ h^{-1} at applied potentials of -1.0 to -1.2 V. Meanwhile, the GC results obtained show *TN* values with the lowest is 1.1 $x10^5$ h^{-1} at -1.1 V with 22% efficiency. We also investigated the block copolymer **P4VP-3**/CoPcF16 at low concentration, 6 μM, at an applied potential -1.2 V (Ag/AgCl). The results yield *TN* and *J* values of $20.1x10^5$ h^{-1} and 4.89 mA/cm^2, respectively with the 91% efficiency.

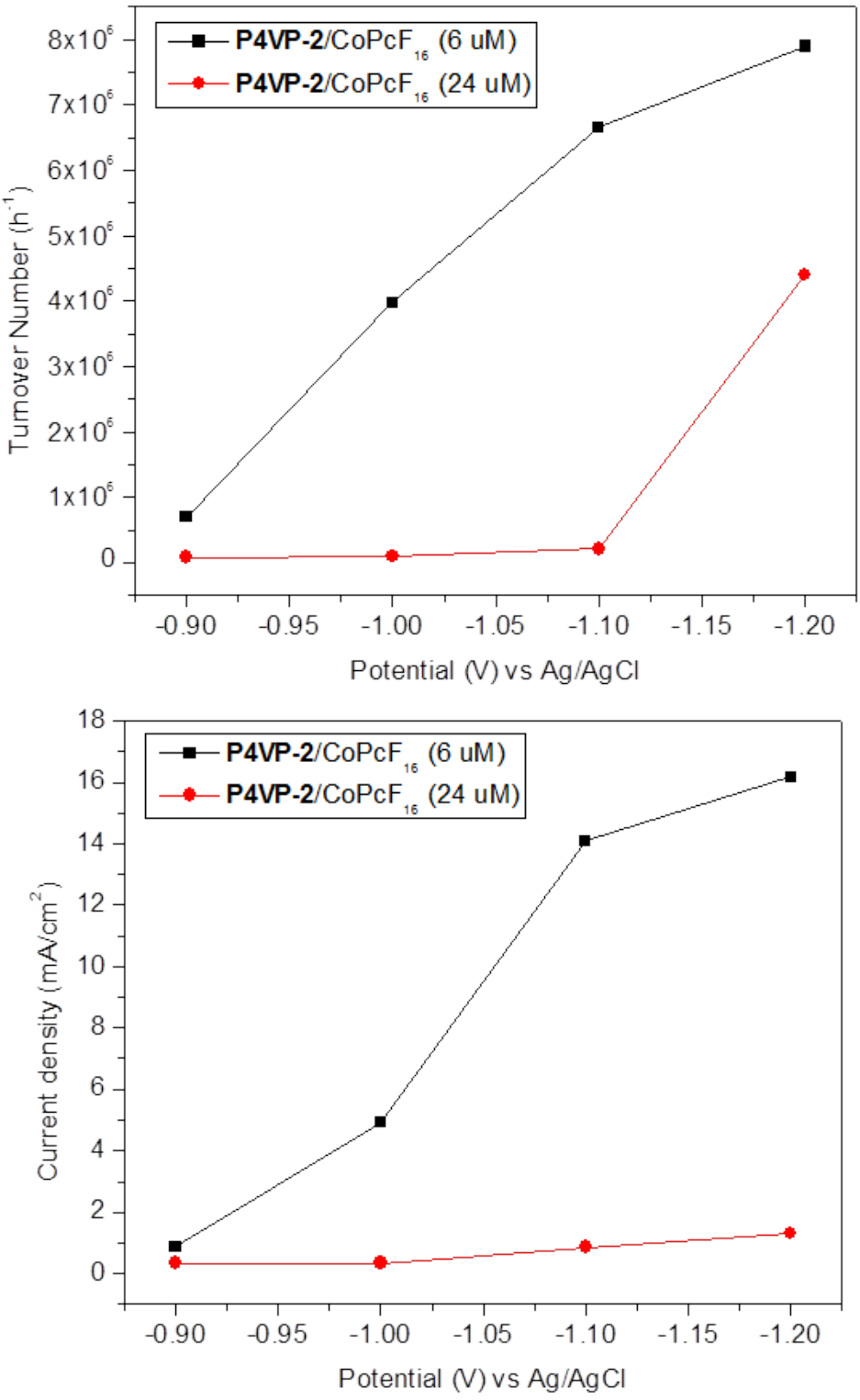

Figure 5.16: Turnover number (a) and current density (b) of **P4VP-2**/$CoPcF_{16}$ coated on GC electrode at different potential applied during electrolysis in 0.1 M phosphate buffer solution, pH 2.2 under saturated Ar.

Overall, immobilisation of $CoPcF_{16}$ in polymer matrices increases the current density and reduces the overpotential as shown by the CV experiments. Bulk electrolysis shows that the highest *TN* and current density are obtained when cobalt is combined with high molecular weight **P4VP-2**. Importantly under the electrocatalytic conditions used the P4VP backbone is protonated and this yields a very high local proton concentration. Therefore, this interaction between polymer and electrocatalyst may play an important role in controlling the electron transfer rate and catalytic activity. For **P4VP-3**/$CoPcF_{16}$, the *TN* value are also higher compare to monolayer $CoPcF_{16}$. Overall these results are similar to the *TN* value obtained by Zhao *et al*. at GC electrode coated by P(4VP-Styrene)/CoPc. [27] The proton migration from the solution into the polymer matrix is expected to be more rapid than the migration of the larger $H_2PO_4^-$ ion from the matrix into the solution and will therefore control the rate of the catalytic process.[45] Other similar systems have also been reported (Table 5.7). For example, Cheboratova and Nyokong reported that GC modified CoPc improved the catalytic activity for water electrolysis for H_2 evolution with 100% efficiency compare to unmodified electrode when conducted in 0.1 M KOH at -2.0 V vs Ag/AgCl for 1 hour. They also claimed that CoPc gaves better catalytic activity for water splitting compare to other transition metals (CoPc > NiPc > FePc > ZnPc, MnPc > H_2Pc).[21] Koca obtained the highest *TN* value for ITO electrode coated with Nf/CoPc in phosphate buffer solution at pH 2.2.[43].

Table 5.7: Summary results of hydrogen production based on cobalt phthalocyanine and its derivatives.[17]

Metal	Electrode	Potential	Solvent system	Gas	Turn Over Number (*TN*)
CoPc	P(4VP-St)/BPG	-0.90	pH 1.0, 0.1 M aq. NaH_2PO_4/H_3PO_4	Ar	$2x10^5$ h^{-1}
$CoPc(CN)_8$	P(4VP-St)/BPG	-0.90	pH 1.0, 0.1 M aq. NaH_2PO_4/H_3PO_4	Ar	$5x10^4$ h^{-1}
$CoPc(SO_3H)_4$	P(4VP-St)/BPG	-0.90	pH 1.0, 0.1 M aq. NaH_2PO_4/H_3PO_4	Ar	~ $1.2x10^3$ h^{-1}
CoPc substituted tetra-tricarbethoxyethyl	Nf/ITO	-0.45	pH 1.4, 0.1 M aq. NaCl/ NaH_2PO_4/H_3PO_4	Ar	20.1
	Nf/ITO	-0.50	pH 2.2, 0.1 M aq. NaCl/ NaH_2PO_4/H_3PO	Ar	39.9
	Nf/ITO	-0.54	pH 4.0, 0.1 M aq. NaCl/ NaH_2PO_4/H_3PO	Ar	31.5
	Nf/ITO	-0.58	pH 7.2, 0.1 M aq. NaCl/ NaH_2PO_4/H_3PO	Ar	6.18
	Nf/ITO	-0.60	pH 10.3, 0.1 M aq. NaCl/ NaH_2PO_4/H_3PO	Ar	34.2
CoPc	BPG	-1.06	pH 2.3, 0.1 M aq. Phosphate buffer	CO_2	$6.01x10^4$ (2 h)
	P(4VP-St)/BPG	-1.06	pH 2.3, 0.1 M aq. Phosphate buffer	CO_2	$1.31x10^6$ (2 h)
	BPG	-1.16	pH 4.4, 0.1 M aq. Phosphate buffer	CO_2	$1.27x10^4$ (2 h)
	P(4VP-St)/BPG	-1.16	pH 4.4, 0.1 M aq. Phosphate buffer	CO_2	$2.94x10^5$ (2 h)
	BPG	-1.26	pH 6.8, 0.1 M aq. Phosphate buffer	CO_2	$3.07x10^4$ (2 h)
	P(4VP-St)/BPG	-1.26	pH 6.8, 0.1 M aq. Phosphate buffer	CO_2	$3.66x10^5$ (2 h)
$CoPc(CN)_8$	BPG	-1.20	pH 9.3, 0.1 M aq. Phosphate buffer	CO_2	$6.0x10^4$ (1h)

5.3.4 Reduction of carbon dioxide (CO_2) by Poly 4-vinylpyridine (P4VP)

The electrocatalytic reduction of CO_2 in aqueous solution has been investigated extensively in the last number of years as climate change because of increasing carbon dioxide concentrations is becoming evident.(Table 5.7 and ref 17) Since CO_2 has a stable structure and, therefore, direct activation of CO_2 is difficult with a highly negative potential -1.9 V vs standard hydrogen electrode (SHE). However, in the presence of protons can bring CO_2 reduction to lower potentials to form a range of different products as shown in Table 5.8. All these reduction process involve H^+ consumption, showing that the product formed is strongly dependent to pH. The main reduction products formed are CO, formic acid, methanol, hydrocarbons and oxalic acid.

Sakata *et al*.[46] recently reported a number of reduction products with a Faradaic efficiency of 44% for CO and HCOOH (30%). Hydrocarbons such as methane, ethane, ethylene, propane and butane were also obtained. The presence of cations and anions in the electrolyte effect the current efficiency and Faradaic yield.[47] For example for the formation of HCOOH, the current efficiency with respect to the anion increased in order $PO_4^{3-} < SO_4^{2-} < CO_3^{2-} < HCO_3^-$. This phenomenon is related to the adsorption of the hydrate ion to the electrode surface. Small cations such as Na^+ and Li^+ have a strong hydration and carry a large number of water molecules, and thus supply protons for the reduction. Depending on the nature of cation present in the supporting electrolyte the current efficiency of the process increased as followed $Rb^+ < K^+ < Na^+ < Li^+$. Furthermore, $(NH_4COO)_2$ and $NaClO_4$ favour production of CO and hydrocarbons. [48] Innocent reported that the formation of formate depends on the pH, electrode potential and temperature. The optimal results are obtained at pH 7-9 and at a potential -1.6 V vs saturated calomel electrode (SCE) at a Pb electrode which 65% Faradaic efficiency. The Faradaic efficiency increased to 90% at 4°C when applied current density set at -2.5 mA cm^{-2}.[49] Conversion of CO_2 to formate was higher in bicarbonate solution than carbonate solution in alkaline polymer electrolyte membrane cells. [50]

Table 5.8: Formal potentials for multi-electron reduction of CO_2.[2]

Reaction	**E/V vs SHE (pH 7)**
$CO_2 + e^- \longrightarrow CO_2^{*-}$	-1.90
$2CO_2 + 2H^+ + 2e^- \longrightarrow H_2C_2O_4$	-0.90
$CO_2 + 2H^+ + 2e^- \longrightarrow HCOOH$	- 0.61
$CO_2 + 2H^+ + 2e^- \longrightarrow CO + H_2O$	-0.52
$CO_2 + 4H^+ + 4e^- \longrightarrow HCHO + H_2O$	-0.48
$CO_2 + 6H^+ + 6e^- \longrightarrow CH_3OH + H_2O$	-0.38
$CO_2 + 8H^+ + 8e^- \longrightarrow CH_4 + 2H_2O$	-0.24

Recently, Bocarsly's research group reported [51,52] high Faradaic efficiency for reduction CO_2 to MeOH around 20-30% with the low overpotentials at -0.55 V vs SCE at hydrogenated Pd electrodes in aqueous solution, pH 5.4 in the presence of the pyridinium ion. Formaldehyde was also obtained as a reduction product.[53] In addition, they reported that with p-GaP semiconductor electrodes under radiation, the Faradaic efficiency for production of methanol is close to 100%. However, Faradaic efficiency was reduced when more negative potentials were applied due to the competitions with evolution of hydrogen.[54] Bocarsly *et al*. proposed a mechanism involving multiple electron transfer steps in the reduction of CO_2 by the pyridinium ion at Pt electrode as shown in Scheme 5.2.[45] The authors suggest that the cathodic current increase linearly with pyridinium concentration in the range from 1 to 6 mM. However, the rate turns to plateau at higher pyridinium concentration when greater than 8 mM, showing that CO_2 is the limiting reagent in the process. Besides that, pyridinium ion and the pyridinyl radical ion were proposed as rate-determining for reduction of CO_2.[51] In the proposed process, under Ar, pyridine **(1)** is a weak base due to the N atom's lone pair, easy to quaternise in acidic solution by accepting a proton to form the pyridinium ion **(2)**. Then, **(2)** accepts an electron to form the pyridinyl radical **(3)**, following further reduction of **(3)** to form H_2. In the presence of CO_2, **(3)** yields a radical carbamate **(4)** species. These radicals are the key intermediates that allow reduction of CO_2 to formic acid **(5)**, formaldehyde **(6)** and methanol **(7)**.

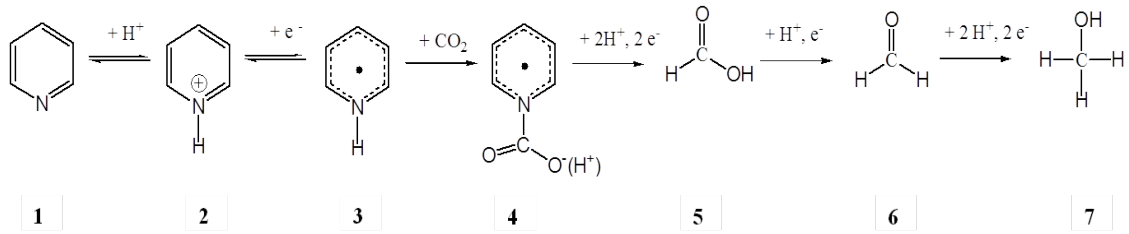

Scheme 5.2: Proposed mechanism for pyridinium-catalysed reduction of CO_2 to the various products of formic acid, formaldehyde and methanol.[51]

In order to investigate whether this observation could be reproduced when pyridine is attached to an electrode surface, the reduced capability of immobilised P4VP on GC under CO_2 and Ar atmosphere in an acidic phosphate buffer solution has been conducted. 6.70×10^{-11} mol of **P4VP-2** was deposited on the electrode surface by methods as described earlier and dried overnight at room temperature. Cyclic voltammograms for such modified electrodes at the different pHs and both under argon and CO_2 were recorded and are shown in Figure 5.17. In acidic solution, the CVs show the irreversible broad feature at -0.60 V vs SCE (Figure 5.17**Error! Reference source not found.**). Bocarsly reported that reduction of pyridine to pyridinium ion occurs at -0.58 V vs SCE at pH 5.3.[51] In contrast, pyridine reduction is obtained at -2.76 V vs Ag/AgCl in DMF solution.[52] Under Ar the current flow of the **P4VP-2** modified electrode in pH 2.17 is 2.5×10^{-6} A at -0.9V higher than observed under CO_2 (1.5×10^{-6} A). This current is possibly explained by the formation of hydrogen. Considerable reduced currents are observed at pH 4.41 and no clear catalytic current is observed.

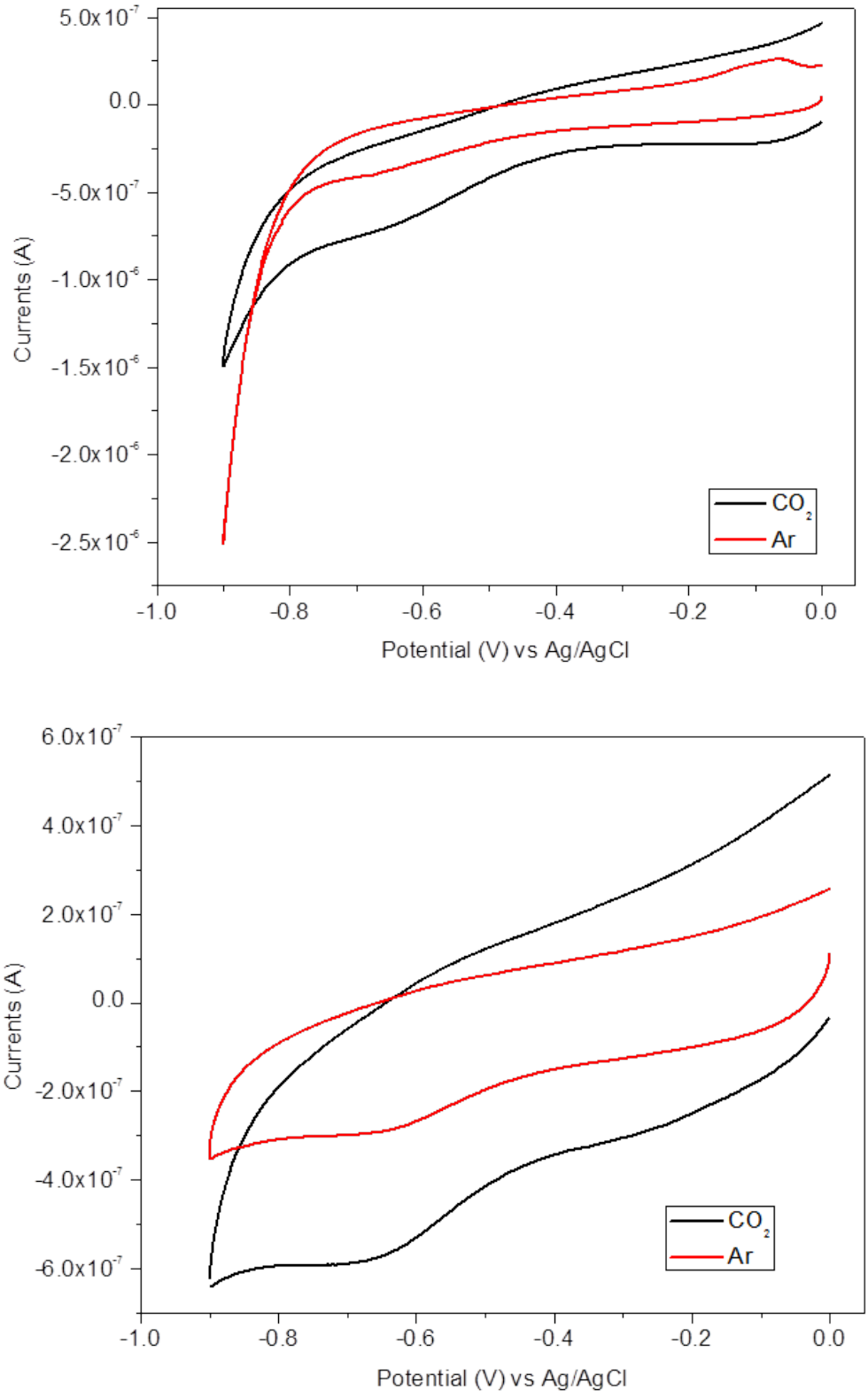

Figure 5.17: Cyclic voltammograms of **P4VP-2** in 0.1 M phosphate buffer solution under an Ar (red) and a CO_2 (black) at pH 2.17 (a) and pH 4.41 (b). Both scans were recorded at 20 mV/s.

After 1 hour electrolysis, the aqueous phosphate buffer solution was investigated for the presence of formate ions by ionic chromatography. A trace amount of formate ion was obtained at a retention time 3.3 min for pH 2.17 when a potential -1.2 V applied to the system as shown in Figure 5.18. There was no significant different in the amount of formate ion with a reaction time of 5 hours at -1.2 V. Using a potential of -1.4 V and 1 hour of reaction, it was obtained less formate ion compare to -1.2 V. No formate ion was obtained at pH 4.41. Electrolysis under CO_2 at -0.6 V as reported by Bocarsly was not investigated because no catalytic current was obtained during the CV experiments. These results indicate that under the conditions used in these experiments no significant amounts of CO_2 reduction products are obtained. The reduction of CO_2 is favoured over hydrogen generation at pH 4.41 but no products or electrochemical currents are observed. Furthermore, no catalytic processes were observed upon at of -0.60 V as observed by Bocarsly. It would be possible that the immobilisation of the pyridine groups leads to their deactivation as electrocatalysts. However, recent reported by Keith and Carter suggest otherwise. They reported that the pyridinium ion and radical pyridinyl are not active participants in CO_2 reduction based on a computational theoretical study.[55,56] Two factors leading to this conclusion are: (a) the pKa value of calculated radical pyridinyl is times greater than reported in the Bocarsly paper; (b) the reduction potentials are both ~1 V more negative than the experimental value (-1.37 V [50] in acetonitrile, or -1.44 V[57] in aqueous solution vs -0.58 V [45], all vs SCE). Their conclusion, in agreement with our observations, was that the electrocatalytic process as reported by Bocarsly and co-workers is highly problematic and unlikely to occur.

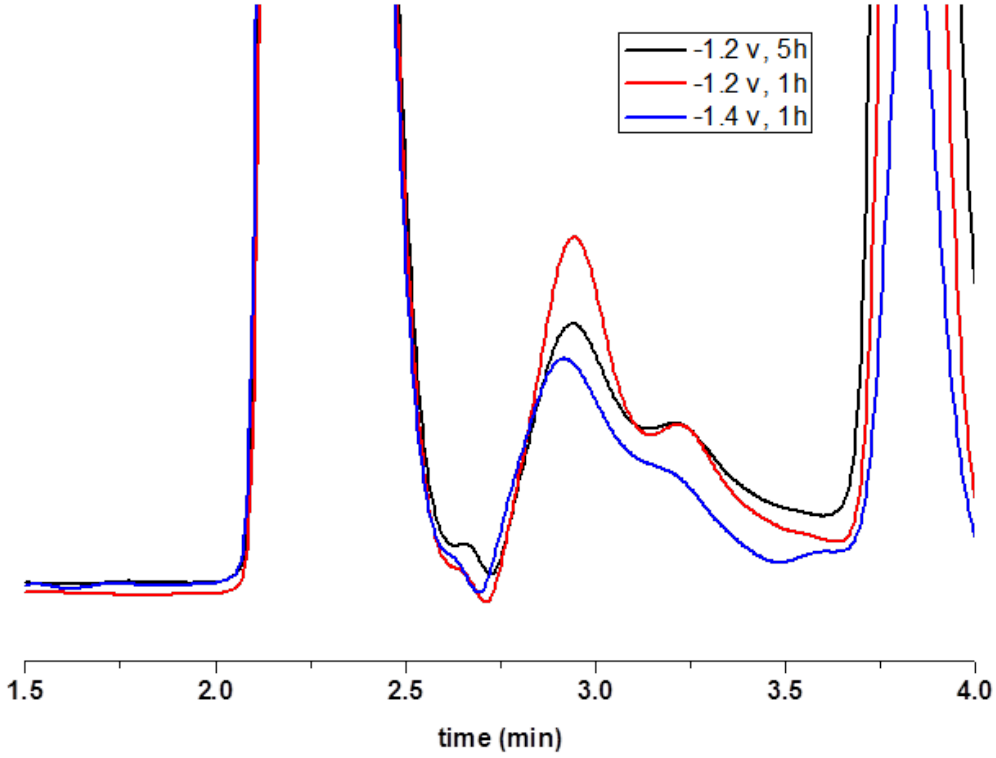

Figure 5.18: Ionic chromatogram of formate ion of aqueous phosphate buffer solution at pH 2.17.

5.4 Conclusion

The results obtained in this chapter show that electrodes modified with $CoPcF_{16}$/P4VP matrices are attractive ways of electro catalytically producing hydrogen from water. Compared to electrodes coated with monolayers of the CoPc catalysts higher current densities can be obtained with very good turnover numbers at reduced overpotentials compared to bare carbon electrodes. The electrochemical analysis shows that the electrocatalytic process is taking place at the second, ring based, reduction process; a hydrogen molecule is only formed when the reduced complex $[Co(I)Pc(-3)*H^{+}]^{-}$ accepts a second proton. The electrocatalytic parameters depend on the composition of the electrocatalytic polymer matrix, with issues such as molecular weight and the amount of $CoPcF_{16}$ present in the layer being important. One of the problems is the low solubility of $CoPcF_{16}$ and its tendency to form aggregates. As the UV/Vis spectral investigations have shown solutions of this compound can change their composition with time and an equilibrium between free and aggregated molecules is most likely present. When the Pc

catalyst is in a P4VP polymer matrix coordination of the species with the polymer backbone is taking place on a slow timescale, this leads to less aggregation and a higher fraction of electroactive species. A better understanding and a better control of these parameters is needed to allow for a further improvement of the electrocatalytic system. The results so far suggest that high molecular weight, P4VP gives the best results. Turn over number and current densities are found to increase with increasing the potential and low concentration of $CoPcF_{16}$. Higher concentrations probable lead to increases aggregation, but without further studies on the solution behaviour of the catalyst this cannot be certain. Finally, as with all polymer modified electrodes more well defined methods for the immobilisation of the layers and the solubilising of the electrocatalyst need to be developed.

The investigation on the potential of P4VP as an electrocatalytic membrane was not successful. A report by Cole *et al*.[51] suggest in agreement with our results that the pyridinium ion and radical pyridinyl are not involved in the reaction. Therefore, formate ion is an impossible product in acidic pH because hydrogen is more favourable product. The use of pyridine as an electrocatalysts is therefore not possible and the papers suggesting this approach are in error.

References

1. U.S. Energy Information Administration, International Energy Outlook 2011.

2. Abe T, Kaneko M, Prog Polym Sci 2003; 28:1441.

3. Olah GA, Prakash GKS, Goeppert A. J Am Chem Soc 2011; 133:12881.

4. Moomaw W, Yamba F, Kamimoto M, Maurice L, Nyboer J, Urama K, Weir T, 2011: Introduction. In IPCC Special Report on Renewable Energy Sources and Climate Change Mitigation [Edenhofer O, Pichs-Madruga R, Sokona Y, Seyboth K, Matschoss P, Kadner S, Zwickel T, Eickemeier P, Hansen G, Schlömer S, von Stechow C. (eds)], Cambridge University Press, Cambridge, United Kingdom and New York, NY, USA.

5. Gust D, Moore TA, Moore AL. Acct Chem Res 2009; 42:1890**.**

6. Centi G, Perathoner S. ChemSusChem 2010; 3:195.

7. Roy SC, Varghese OK, Paulose M, Grimes CA. ACS Nano 2010; 4:1259.

8. Ursu´a A, Gandı´a LM, Sanchis P. Proceedings of the IEEE | Vol. 100, No. 2, February 2012.

9. Dunn S. Int J Hydrogen Energy 2002; 27:235.

10. Momirlan M, Veziroglu TN. Int J Hydrogen Energy 2005; 30:795.

11. Jitaru M. J Univ Chem Tech Metall 2007; 42:333.

12. Leznoff CC, Lever ABP. editors. 1989 Phthalocyanines properties and applications, vol 1-4 New York VCH Publischers Inc

13. Claessens CG, Hahn U, Torres T. The Chem Rec 2008; 8:75.

14. Gregory P. J Porphyr Phthalocyan 2000; 4:432.

15. O'Malley S, Schazmann B, Diamond D, Nolan K. Tetrahedron Lett 2007; 48:9003.

16. Guillaud G, Simon J, Germain JP. Coord Chem Rev 1998; 180:1433.

17. Inglis JL, MacLean BJ, Pryce MT, Vos JG. Coord Chem Rev 2012; 256:2571.

18. Koca A. Int J Hydrogen Energy 2009; 342:2107.

19. Artero V, Kerlidou MC, Fontecave M. Angew Chem Int Ed 2011; 50:7238.

20. Zagal JH, Griveau S, Silva JF, Nyokong T, Bedioui F. Coord Chem Rev 2010; 254:2755.

21. Chebotareva N, Nyokong T. Electrochim Acta 1997; 42:3519.

22. Koca A, Özkaya AR, Selçukoğlu M, Hamuryudan E. Electrochim Acta 2007; 52:2683.

23. Koca A, Kalkan A, Bayir ZA. Electrochim acta 2011; 56:5513.

24. Koca A, Özçeşmeci M, Hamuryudan E. Electroanalysis 2012; 22:1623.

25. Selçukoğlu M, Hamuryudan E. Dyes Pigments 2007; 74:17.

26. Koca A. Int J Hydrogen Energ 2008; 33:3281.

27. Zhao F, Zhang J, Abe T, Wöhrle D, Kaneko M. J Mol Catal A: Chem 1999; 145:245.

28. Yin HS, Zhou YL, Ai SY. J Electroanal Chem 2009; 626:80.

29. Loose S, Vos JG, Rau S. Coord Chem Rev 2010; 254:2492.

30. Ogata H, Higashi R, Kobayashi N. J Porphy Phthalocyan 2003; 7:551.

31. Snow AW, Jarvis NL. J Am Chem Soc 1984;106:4706.

32. Dodsworth ES, Lever ABP, Seymour P, and Leznoff CC. J Phys Chem 1985; 89:5698.

33. Suchan R, Nackiewicz J, Hnatejko Z, Waclaweka W, Lis S. Dyes Pigments 2009; 80:239.

34. Yoshida T, Kamato K, Tsukamoto M, Iida T, Schlettwein D, Whohrle D, Kaneko M. J Electroanal Chem 1995; 385:209.

35. Man F, Wang S, Li X. J Phys Chem Solids 2012;73:589.

36. Nevin WA, Liu W, Lever ABP. Can J Chem 1987; 65:855 and reference therein.

37. Zheng Y, Gupts S, Huang H, Yeager EB. J Appl Electrochem 1991; 21:973.

38. Nyokong T. Polyhedron 1995; 14:2325 and reference therein.

39. Zeng ZY, Gupta SL, Huang H, Yeager EB. J Appl Electrochem 1991; 21:973.

40. Ghani F, Kristen J, Riegler H. J Chem Eng Data 2012; 57:439.

41. Cariati F, Galizzioli D, Morazzoni F, Busetto C. J Chem Soc Dalton Trans 1975; 556.

42. Pennesi G, Ercolani C, Ascenzi P, Brunori M, Monaceli F. J Chem Soc Dalton Trans 1985; 1107.

43. Koca A, Şener MK, Koçak MB, Gül A. Int J Hydrogen Energy 2006; 31:2211.

44. Ouyang J, Shigehara K, Yamada A, Anson FC. J Electroanal Chem 1991; 297:489.

45. Zhao F, Zhang J, Wöhrle D, Kaneko M. J Porphy Phthalocyan 2000; 4:31.

46. Hara K, Kudo A, Sakata T. J Electroanal Chem 1997; 421:1.

47. Jitaru M, Lowy D, Toma M, Toma B, Oniciu L. J Appl Electrochem 1997; 27:875.

48. Hernández RM, Márquez J, Márquez OP, Choy M, Ovalles C. J Electrochem Soc 1999; 146:4131.

49. Innocent B, Liaigre D, Pasquier D, Ropital F, Le´ger JM, Kokoh KB. J Appl Electrochem 2009; 39:227.

50. Narayanan SR, Haines B, Soler J, Valde TI. J Electrochem Soc 2011; 158:167.

51. Cole EB, Lakkaraju PS, Rampulla DM, Morris AJ, Abelev E, Bocarsly AB. J Am Chem Soc 2010; 132:11539.

52. Morris AJ, McGibbon RT, Bocarsly AB. ChemSusChem 2011; 4:191.

53. Seshadri G, Lin C, Bocarsly AB. J Electroanal Chem 1994; 372:145.

54. Barton EE, Rampula DM, Bocarsly AB. J Am Chem Soc 2008; 130:6342.

55. Keith JA, Carter EA. J Am Chem Soc 2012; 134:7580.

56. Keith JA, Carter EA. J Chem Theo Compt 2012; 8:3187.

57. Tossell JA. Comp Theor Chem 2011; 977:123.

6 Conclusion and future works

6.1 Conclusion

Controlled radical polymerisation is very attractive for the synthesis of polymer due to the possibility to control molecular weight and molecular weight distribution. In this study, ATRP and NMP were investigated in the synthesis of amphiphilic block copolymers poly(4 vinylpyridine-*b*-methyl methacrylate), poly(4VP-*b*-MMA). It is well known that 4VP is a challenging monomer in ATRP because it can compete with the ATRP ligand for the binding of the catalytic metal. On the other hand, MMA is a difficult monomer for NMP due to the frequency of termination reaction.

For the ATRP approach (Chapter 2), PMMA-Cl was synthesised as first segment followed by chain extension with the 4VP monomer. The kinetic study indicated that PMMA followed first-order reaction in the synthesis of linear polymers. Introducing 30% of Cu(II) in the beginning of the PMMA polymerisation resulted in a slow initiation process. Further extension with 4VP works better with Cu/HMTETA than with Cu/Me_6TREN as the combination of catalyst/ligand for block copolymer. The results of the synthesis of star PMMA showed that termination reactions are the critical issues in this polymerisation. However, termination reactions can be reduced when conducted in diluted condition and keep the conversion below 60%.

Well-defined P4VP with low dispersity at high conversion (99%) was synthesised using BlocBuilder MAMA-SG1. P4VP-SG1 was used as a macroinitiator that was further extended with MMA to form poly(4VP-*b*-MMA). The M_n obtained for the block copolymers was higher than the theoretical value resulting probably from termination reaction. Therefore, a small amount of styrene was introduced in the early stage of the polymerisation to reduce the polymerisation rate. Self assembly of poly(4VP-*b*-MMA) in THF solution formed inverse micelles with P4VP as a core and PMMA as a corona. The particles size of $P4VP_{190}$-*b*-$PMMA_{91}$ and $P4VP_{190}$-*b*-($PMMA_{57}$-*co*-PS_{18})) was 70 and 130 nm, respectively. Then, the core micelles were loaded with copper. Star P4VP were synthesised using two new star initiators proposed in this study. The NHS

functionalised MAMA-SG1 was grafted to the JEFFAMINE® and PPI dendrimer expecting 3 and 8 arms, respectively.

In summary, poly(4VP-*b*-MMA) was successfully synthesised by ATRP and NMP as discussed in Chapter 2 and 3, respectively. However, NMP provided a cleaner block copolymer synthesis due to the absence of a metal catalyst. P4VP micelles also showed promise as a template for nanoparticles as shown in Chapter 3 and can act to bind catalysts in electrocatalysis to enhance the hydrogen evolution as discussed in Chapter 5.

In electrocatalyst, P4VP was used to immobilise the catalyst, cobalt(II) hexadecafluorophthalocyanine ($CoPcF_{16}$). The investigation by UV-Vis spectroscopy revealed that the mixed solution of P4VP and $CoPcF_{16}$ in DMF tends to aggregate at the beginning, but more $CoPcF_{16}$ immobilised to the polymer backbone with time. This aggregation may be affected by the amount of electroactive materials in the layer. The P4VP/$CoPcF_{16}$ solutions were coated on the surface of a glassy carbon electrode and hydrogen generation in phosphate buffer aqueous solution at pH 2 was studied. From cyclic voltammograms, it was observed that the film of P4VP/$CoPcF_{16}$ reduced the overpotential of neat $CoPcF_{16}$ films. This turnover number value of the P4VP/$CoPcF_{16}$ complexes was dependent on the concentration of $CoPcF_{16}$ in the polymer matrices, molecular weight of P4VP and the potential applied for electrolysis. At high polymer molecular weight, the layer obtained is more stable and strongly adsorbed at the surface.

6.2 Future work

Well-defined polymer of P4VP and poly(4VP-*b*-MMA) can be obtained when considering all this condition such as concentration of initiator and monomer, time of reaction, temperature and polymerisation method. In our study, NMP appeared to be the more promising method compare to ATRP for preparing the clean block copolymer in control molecular weight and dispersity. We also showed that the linear block copolymer can used as nanocarriers with 4VP bind the copper inside the core of micelles. Further investigation is needed to understand how many 4VP unit bind to the metal and the protonation effect of 4VP in the size and organisation of micelles. Besides

that, the metal loading of star polymers is also interesting to study due to their multiple chains and high molecular weight. It provided more space for metal binding and probably forming a different organisation than the micelles. However, the condition of synthesis the star polymer proposed in Chapter 4 need to improve.

In chapter 5, many parameters need to be considered and manipulated such as solvent, temperature and concentration for achieving maximum results for electrocatalysis of $CoPcF_{16}$. Based on UV studies, the mixture of P4VP and $CoPcF_{16}$ will age with time. The investigation of using the fresh sample is highly recommend for understand the affect of aggregation to the CV and hydrogen evolution. On top of that, deposition method of catalyst on the surface is important for highly electroactivity materials. The stability of the film could be improved with multilayer coated or quarternised P4VP in-situ on the surface by crosslink agent.

APPENDIX 1 –ATRP

Calculation for poly methyl methacrylate (PMMA)

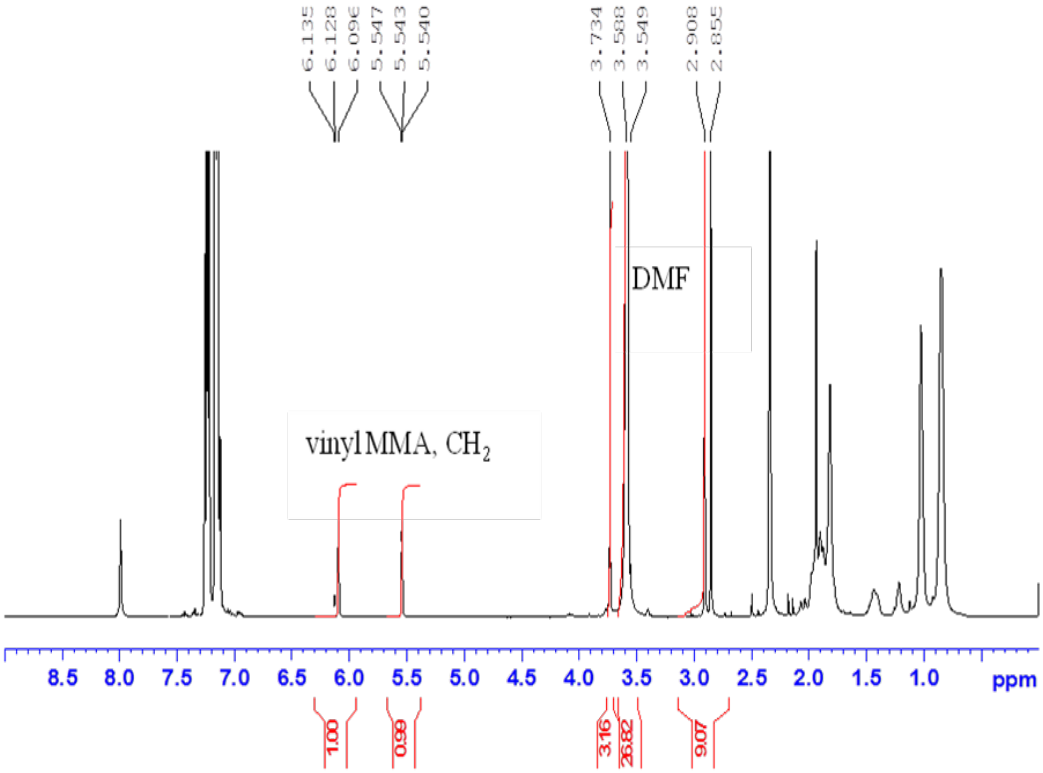

Figure 1: ^{1}H NMR polymerisation of poly(methyl methacrylate).

Conversion was calculated by the integration of vinyl monomer MMA (2H, 6.1 and 5.5ppm) with integration of methyl peak DMF (6H, 2.9 and 2.8ppm) as references peak using equation (1).

$$x = 1 - \frac{[M]\,time}{[M]\,initial} \ldots\ldots\ldots\ldots\ldots\ldots\ldots\ldots (eq.1)$$

where,

$$\frac{[M]time}{[M]initial} = \frac{\int monomer\ peak\ time / \int DMF\ peak\ \ time}{\int monomer\ peak\ initial\ / \int DMF\ peak\ initial}$$

At initial experiment,

Integration of MMA peaks are 1 and 1.01 while integration of DMF peaks are 0.92. Therefore, [MMA] initial/ [DMF] initial is 6.55.

After 6 hours of reaction,

$$Integration\ of\ 1H\ MMA = \frac{1 + 0.99}{2} = 0.995$$

$$Integration\ of\ 1H\ DMF = \frac{9.07}{6} = 1.512$$

So, $[MMA]_t$ / [DMF]t is 0.658

Using the equation 1,

$$x = 1 - \frac{0.658}{6.55} = 0.9$$

Thus, the conversion for PMMA- is 90%.

Calculation for poly (methyl methacrylate-*b*-4-vinylpyridine)

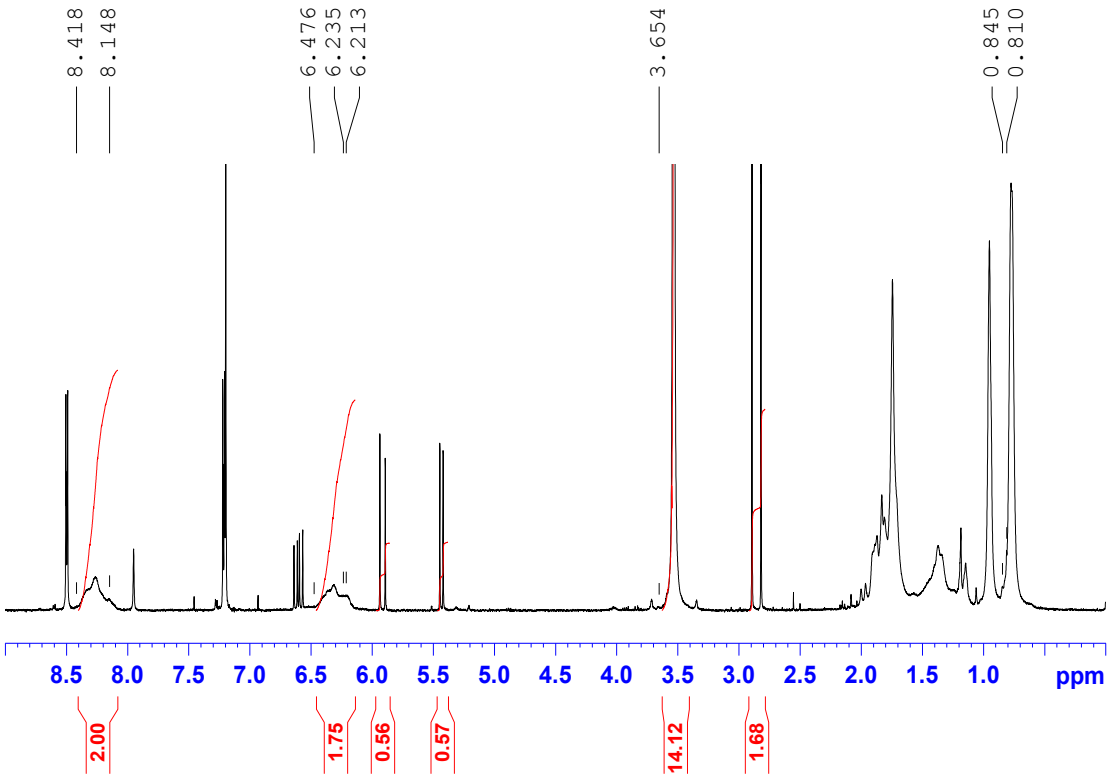

Figure 2: ^{1}H NMR polymerisation of poly(MMA-*b*-4VP) block copolymer.

Block copolymer conversion was calculated by the integration of methoxyl peak MMA (3H, 3.65 ppm) with integration of pyridine peak 4VP (2H, 8.14 and 6.21 ppm).

An example,

$$Integration\ of\ 1H\ MMA = \frac{14.12}{3} = 4.7$$

$$Integration\ of\ 1H\ 4VP = \frac{1.75}{2} = 0.9$$

Thus, $1H\ MMA = 4.7 \rightarrow 200\ units,$

$$1H\ 4VP = 0.9\ \rightarrow x\ unit$$

So, *x* is 37 units

As the ratio $[M]_0/[I]_0$ is 192,

$$\frac{37}{192} \times 100 = 19.27\%$$

Therefore, conversion of 4VP as second segment is 19.27%.

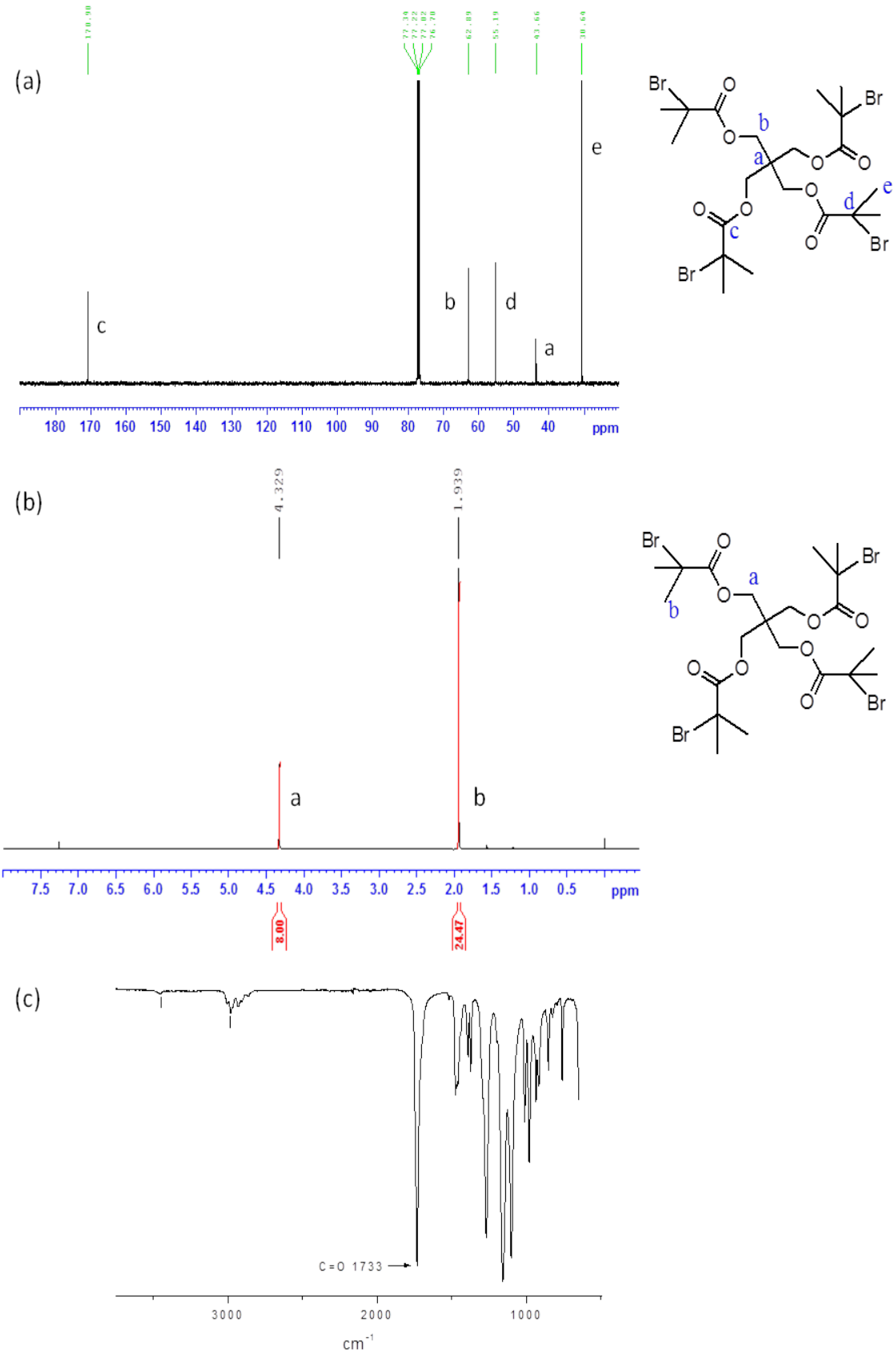

Figure 3: Characterisation of PT-Br; (a) ^{13}C NMR, (b) ^{1}H NMR, (c) IR spectra.

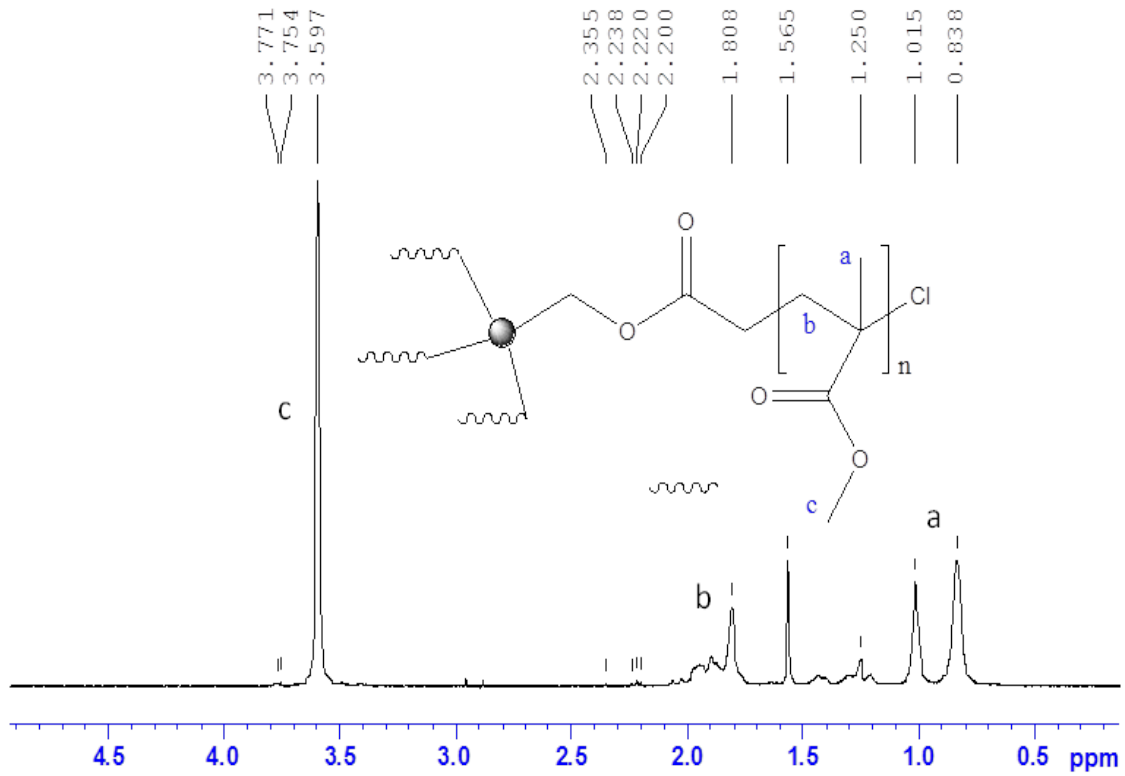

Figure 4: ^{1}H NMR spectra of 4 arms star PMMA.

APPENDIX 2 – NMP

Calculation for poly 4-vinylpyridine (P4VP)

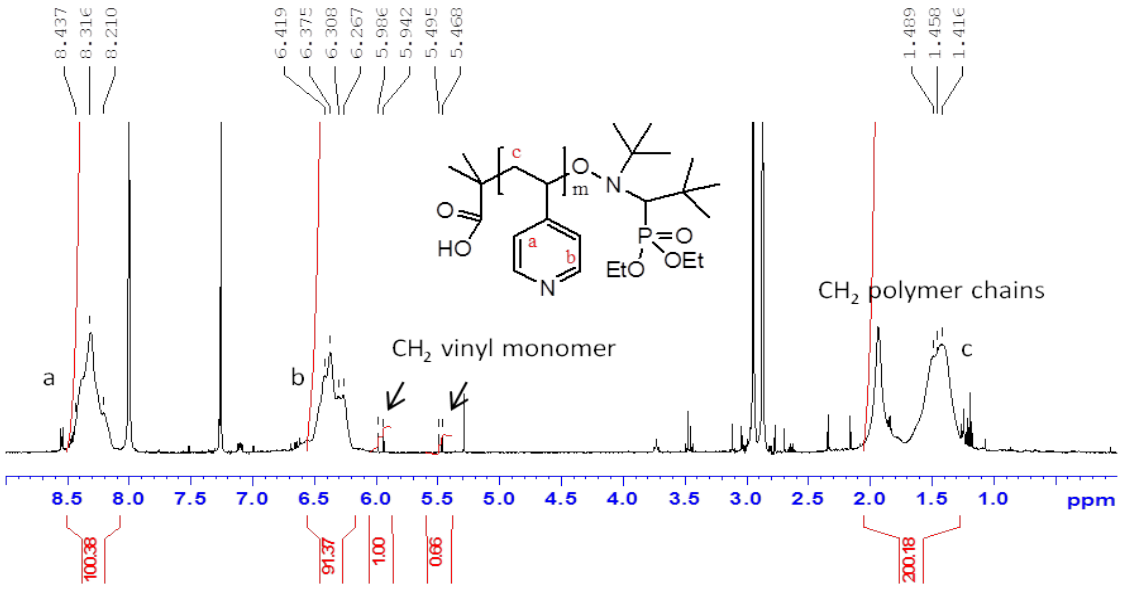

Figure 1: ^{1}H NMR spectra of poly(4-vinylpyridine)

Conversion was calculated by the integration of vinyl monomer 4VP (CH_2, 5.9 and 5.4ppm) with integration of polymer peak 4VP (CH_2, 1.5ppm).

$$Conversion = \frac{\int CH2\ 4VP\ polymers}{\int CH2\ 4VP\ polymers + \int CH2\ 4VP\ monomer}$$

For monomer 4VP,

$$1H = \frac{1 + 0.66}{2} = 0.8$$

For polymer 4VP,

$$1H = \frac{200.18}{2} = 100$$

Therefore,

$$Conversion = \frac{100}{100 + 0.8} = 99\%$$

Calculation for block poly(4-vinylpyridine-*b*-methyl methacrylate)

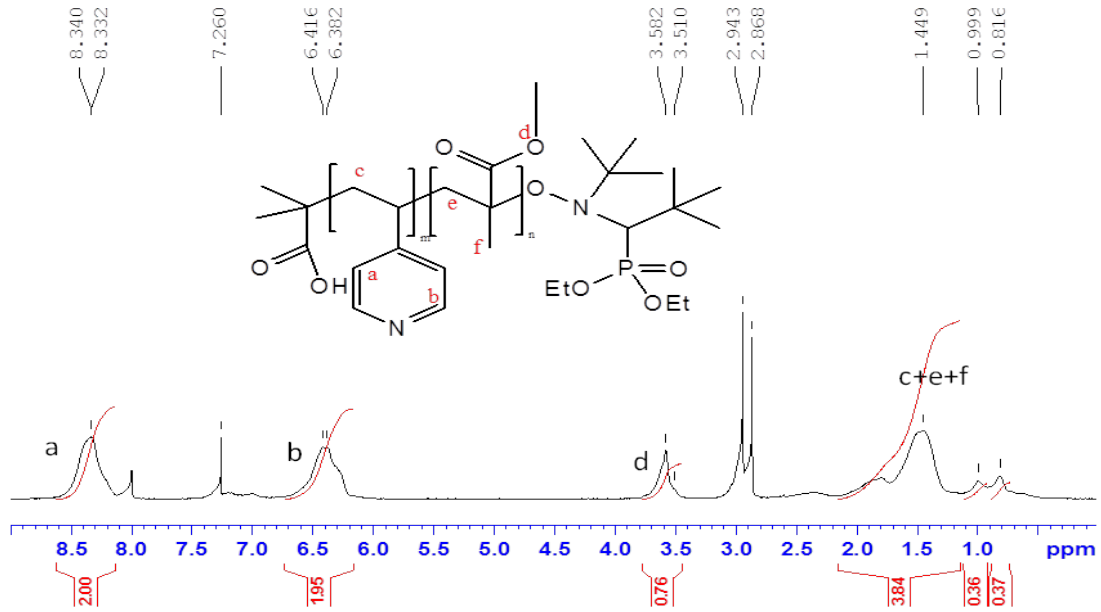

Figure 2: ^{1}H NMR of poly(4VP-*b*-PMMA) block copolymer.

Block copolymer conversion was calculated by the integration of methoxyl peak MMA (3H, 3.58ppm) with integration of pyridine peak 4VP (2H, 8.3 and 6.4ppm).

$$Integration\ of\ 1H\ MMA = \frac{0.76}{3} = 0.253$$

$$Integration\ of\ 1H\ 4VP = \frac{1.95}{2} = 0.975$$

Thus, $1H\ 4VP = 0.975 \rightarrow 192\ units,$

$$1H\ MMA = 0.253\ \rightarrow x\ unit$$

So, *x* is 50 units

As the ratio $[M]_0/[I]_0$ is 200. Therefore, conversion of MMA as second segment,

$$\frac{50}{200} \times 100 = 26\%$$

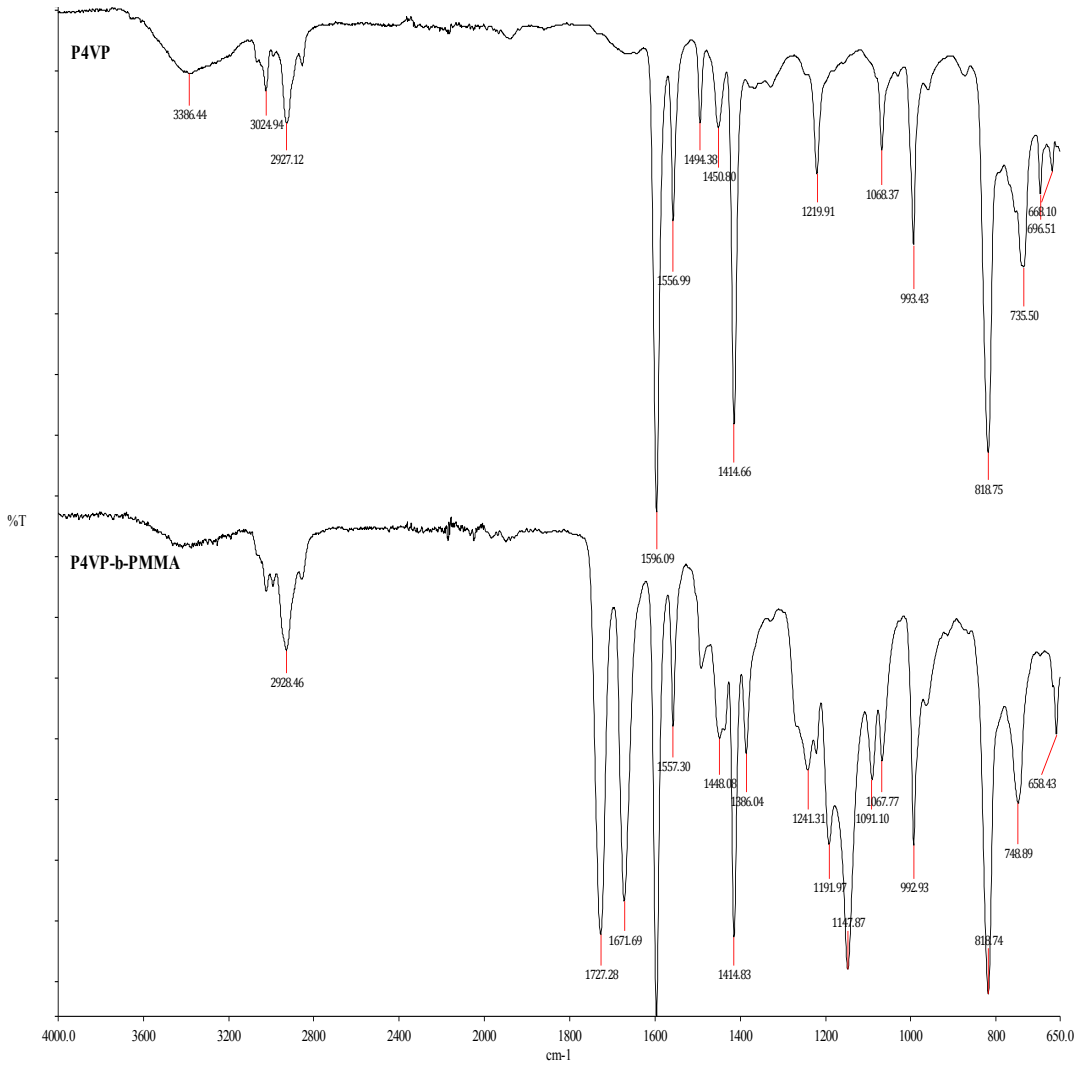

Figure 3: IR spectrum of P4VP and P4VP-*b*-PMMA.

APPENDIX 3 – Electrocatalytic study

Polymer used in Chapter 5

a) P4VP 0.5% w/w (Mw= 5,000 g/mol, 4VP units per mol=50) called as **P4VP-1**
b) P4VP 0.75% w/w (Mw=160,000g/mol, 4VP units per mol=1500) called as **P4VP-2**
c) P(4VP-b-MMA) 0.5% w/w (Mw=54 000 g/mol, composition=10% MMA and 90% 4VP, 4VP units per mol=170) called as **P4VP-3**

Polymer	Concentration prepared in 25 mL (mM)	Mol of polymer (mol)	Active polymer in 1.5 µL (mol)	Mol of 4VP unit (mol)	Active 4VP unit in 1.5 µL (mol)
P4VP-1	0.94	$2.35x10^{-9}$	$1.41x10^{-9}$	$1.17x10^{-3}$	$7.02x10^{-8}$
P4VP-2	0.045	$1.12x10^{-6}$	$6.68x10^{-11}$	$1.67x10^{-3}$	$1.0x10^{-7}$
P4VP-3	0.088	$2.20x10^{-6}$	$1.32x10^{-10}$	$3.74x10^{-4}$	$2.24x10^{-8}$

Calculation methods:

DMF – density = 0.945 g/mL; 23.625 g in 25 mL

Dilution factor = 1000 mL / 25 mL= 40

P4VP-1

a) Mass = (0.5% x 23.625 g)/99.5% = 0.118 g
b) No of mol of **P4VP-1** = 0.118 g/5000 g/mol = $2.35x10^{-5}$ mol
c) Concentration = $2.35x10^{-5}$ mol x 40 = $9.4x10^{-4}$ mol/L
d) Active species on surface = $9.4x10^{-4}$ mol/L x (1.5 µL/1000000) = $1.41x10^{-9}$ mol
e) No of 4VP unit = $2.35x10^{-5}$ mol x 50 unit = $1.17x10^{-3}$ mol
f) Concentration = = $1.17x10^{-3}$ mol x (25/1000)L = 0.047 mol/L
g) Active species on surface = 0.047 mol/L x (1.5 µL /1000000) = $7.02x10^{-8}$ mol

P4VP-2

a) mass = (0.75% x 23.625 g)/99.25% = 0.178 g
b) No of mol = 0.178 g/160000 g/mol = 1.12×10^{-6} mol
c) Concentration = 1.12×10^{-6} mol x (25/1000)L = 4.45×10^{-5} mol/L
d) Active species on surface = 4.45×10^{-5} mol x (1.5 µL /1000000) = 6.68×10^{-11}mol
e) No of 4VP unit = 1.12×10^{-6} mol x 1500 unit = 1. 67×10^{-3} mol
f) Concentration = 1.67×10^{-3} mol x (25/1000)L = 0.067 mol/L
g) Active species on surface = 0.067 mol/L x (1.5 µL /1000000) = 1.0×10^{-7} mol

P4VP-3

a) mass = (0.5% x 23.625 g)/99.5% = 0.118 g
b) No of mol = 0.118 g/54000 g/mol = 2.20×10^{-6} mol
c) Concentration = 2.20×10^{-5} mol x (25/1000)L = 8.8×10^{-5} mol/L
d) Active species on surface = 8.8×10^{-5} mol/L x (1.5 µL /1000000) = 1.32×10^{-10} mol
e) No of 4VP unit = 2.20×10^{-6} mol x 170 unit = 3.74×10^{-4} mol
f) Concentration = 3.74×10^{-4} mol x (25/1000)L = 0.015 mol/L
g) Active species on surface = 0.015 mol/L x (1.5 µL /1000000) = 2.24×10^{-8} mol